R.A. 1175

UNAVAILABLE

~~CONFIDENTIAL~~

RM No. L6J15

NACA

RESEARCH MEMORANDUM

for the

Bureau of Aeronautics, Navy Department

WIND-TUNNEL TESTS OF A $\frac{1}{4}$-SCALE MODEL OF THE NAVAL AIRCRAFT FACTORY FLOAT-WING CONVOY INTERCEPTOR

TED NO. NACA 2314

By

Evalyn G. Wells and Elizabeth G. McKinney

Langley Memorial Aeronautical Laboratory
Langley Field, Va.

Made Unavailable by Admin. Action per Hqs. Let. dtd. 6-8-59 / BAM

CLASSIFICATION CANCELLED

NACA Form #453 12-12-50

MHG 1-23-51

Library

NATIONAL ADVISORY COMMITTEE FOR AERONAUTICS

UNAVAILABLE

WASHINGTON

Jan. 16, 1947

~~CONFIDENTIAL~~

NACA RM No. L6J15

NATIONAL ADVISORY COMMITTEE FOR AERONAUTICS

RESEARCH MEMORANDUM

for the

Bureau of Aeronautics, Navy Department

WIND-TUNNEL TESTS OF A $\frac{1}{4}$-SCALE MODEL OF THE NAVAL AIRCRAFT FACTORY FLOAT-WING CONVOY INTERCEPTOR

TED NO. NACA 2314

By Evalyn G. Wells and Elizabeth G. McKinney

SUMMARY

A $\frac{1}{4}$-scale model of the Naval Aircraft Factory float-wing convoy interceptor was tested in the Langley 7- by 10-foot tunnel to determine the longitudinal and lateral stability characteristics. The model was tested in the presence of a ground board to determine the effect of simulating the ground on the longitudinal characteristics.

The hull had excessive drag because of the type of propeller installation. Neutral points were calculated which show a positive static margin exists for all conditions investigated. Power had a large stabilizing effect.

An elevator deflection range of -5° to 2° for propeller windmilling and -10° to 2° with power is sufficient to trim through the speed range tested. In the presence of the ground board, a range of -10.5° to 1° with propeller windmilling or with take-off power is required for trim in the landing configuration with the stabilizer set at 3.5°.

Tuft tests indicated that the wing stalled early in the vicinity of the propeller. At higher lift coefficients the wing tended to stall at the ailerons, with power accentuating the tendency of the left wing panel to stall. The extreme wing tips remained unstalled.

The effective dihedral, lateral force characteristics, and directional stability with controls fixed were satisfactory.

Rudder lock did not occur for the range of yaw angles tested. Freeing the rudder caused oscillation and severe shaking of the model. Power caused only small changes in directional trim.

INTRODUCTION

At the request of the Bureau of Aeronautics, Navy Department, a general series of tests has been made of a $\frac{1}{4}$-scale powered model of the Naval Aircraft Factory float-wing convoy interceptor. The purpose of the tests was to determine the longitudinal and lateral stability characteristics of the model with power on and off and wing flaps up and down and to determine the effect of simulating the ground on the longitudinal characteristics. Also included are the results of miscellaneous propeller-off tests and of tests of the isolated horizontal tail. Tuft surveys were made to determine the stalling characteristics of the model.

COEFFICIENTS AND SYMBOLS

The results of the tests are presented as standard NACA coefficients of forces and moments. Rolling-, yawing-, and pitching-moment coefficients are given about the center-of-gravity location shown in figure 1 (24.7 percent of the mean aerodynamic chord). The data are referred to the stability axes, which are a system of axes having their origin at the center of gravity and in which the Z-axis is in the plane of symmetry and perpendicular to the relative wind, the X-axis is in the plane of symmetry and perpendicular to the Z-axis, and the Y-axis is perpendicular to the plane of symmetry. The positive directions of the stability axes, of angular displacements of the airplane and control surfaces, and of hinge moments are shown in figure 2.

The coefficients and symbols are defined as follows:

C_L lift coefficient (Lift/qS)

C_X longitudinal-force coefficient (X/qS)

C_Y lateral-force coefficient (Y/qS)

C_l rolling-moment coefficient (L/qSb)

C_m pitching-moment coefficient (M/qSc')

C_n yawing-moment coefficient (N/qSb)

C_{h_e} elevator hinge-moment coefficient ($H_e/qb_e\bar{c}^2$)

C_{h_r} rudder hinge-moment coefficient ($H_r/qb_r\bar{c}^2$)

T_c' effective thrust coefficient based on wing area (T_{eff}/qS)

Q_c torque coefficient $\left(\frac{Q}{\rho V^2 D^3}\right)$

nD/V propeller diameter-advance ratio

η propulsive efficiency ($T_{eff}V/2\pi nQ$)

Lift = -Z

$\left.\begin{matrix}X\\Y\\Z\end{matrix}\right\}$ forces along axes, pounds

$\left.\begin{matrix}L\\M\\N\end{matrix}\right\}$ moments about axes, pound-feet

H_e hinge moment of one elevator, pound-feet

H_r hinge moment of rudder, pound-feet

T_{eff} propeller effective thrust, pounds

Q propeller torque, pound-feet

q free-stream dynamic pressure, pounds per square foot $\left(\frac{\rho V^2}{2}\right)$

q_t effective dynamic pressure at tail, pounds per square foot

S wing area (10.00 square feet on model)

S_t horizontal-tail area (1.91 square feet on model)

c' wing mean aerodynamic chord (M.A.C.)(1.494 feet on model)

$\bar{c}$ root-mean-square chord of a control surface back of hinge line, feet

[redacted]

b	wing span (7.458 feet on model)
b_e	span of one elevator along hinge line, feet
b_r	span of rudder along hinge line, feet
V	air velocity, feet per second
D	propeller diameter (1.862 feet on model)
n	propeller speed, revolutions per second

and

ρ	mass density of air, slugs per cubic foot
α	angle of attack of horizontal base line, degrees
α_t	angle of attack of tail chord line
ψ	angle of yaw, degrees
ϵ	angle of downwash, degrees
i_t	angle of stabilizer with respect to horizontal base line, degrees; positive when trailing edge is down
δ	control-surface deflection, degrees
β	propeller blade angle at 0.75 radius (27 degrees on model)
n_o	tail-off aerodynamic-center location, percent wing mean aerodynamic chord
Γ_{eff}	effective dihedral, degrees

Subscripts:

a	aileron (a_R, a_L, right and left aileron)
e	elevator (e_R, e_L, right and left elevator)
r	rudder
f	flap
t	horizontal tail

[redacted]

ψ denotes partial derivatives of a coefficient with respect to yaw (example: $C_{l_\psi} = \partial C_l / \partial \psi$)

Abbreviations:

TA	thrust axis
Wm	propeller windmilling
HRT	half-thrust of take-off power
TOP	take-off power

MODEL AND APPARATUS

The low-wing seaplane fighter model was supplied by the Naval Aircraft Factory. A three-view drawing and photographs of the model are shown in figures 1 and 3. The airplane is a float-wing type seaplane with a three-blade right-hand propeller set in the hull above the wing trailing edge. Plan-form and blade-form curves for the propeller used on the model are shown in figure 4. The physical characteristics of the airplane are tabulated in tables I, II, III, and IV.

The test program was originally begun with the thrust axis tilted 3° (top of propeller moved back) about the center line of the propeller; but as a result of mechanical difficulties, the remainder of the tests were made with the thrust axis horizontal. A fillet formed of plasticene was added to the horizontal tail where it joined the fuselage. (See fig. 3(a).) For one propeller-off test the opening in the hull for the propeller was sealed and faired thus forming a smooth hull contour with no breaks or gaps. For all tests the cooling-air scoops on the sides of the hull were removed from the model and the openings sealed so that there was no flow through the cooling-air exhaust opening immediately in front of the propeller. The engine exhaust ports in the float step do not exist on the model. A drawing of the $\frac{1}{4}$-scale model of the horizontal tail, on which isolated tail tests were made in the Langley 4- by 6-foot tunnel, is shown in figure 5. An electrical strain gage was used in each elevator and in the rudder for measuring hinge moments. The elevator and rudder gaps on the model were 0.017 and 0.026 inches, respectively; because of inaccuracies in the construction of the model, the aileron and flap gaps were variable and therefore were not measured. Plain flaps were used, and the elevator and rudder had a radius leading edge with minimum balance. There were no tabs on the control surfaces.

[redacted]

In order to simulate ground effect for some tests, the model was mounted in the tunnel above a ground board which completely spanned the tunnel and extended about 40 inches ahead of and 80 inches behind the pivot point. The ground board was placed 12.75 inches below the normal center of gravity at 0° angle of attack, which allowed about 1/2-inch clearance under the model at $\alpha = 12°$. (See fig. 6.)

Photographs of tufts to determine the stall progression of the wing were made from the top of the tunnel. The photographs were taken at 1/25 of a second exposure. For this timing condition, a tuft that appears as a point or is pointed upstream indicates stall, while a blurred tuft indicates unsteady flow.

The model propeller was driven by a 56-horsepower electric motor, the speed of which was determined from an electric tachometer whose error is within ±0.2 percent.

The model was tested in both cruising and landing configurations away from the ground and in landing and take-off configurations near the ground board. The flaps were set at 0° deflection for the cruising and take-off configurations and at 60° for the landing configuration. The flap deflection was the only variation of the model in the different configurations.

TESTS AND RESULTS

Test Conditions

Langley 7- by 10-foot tunnel.- The tests were made at dynamic pressures of 16.37, 9.21, 4.09, and 1.02 pounds per square foot, which corresponded to airspeeds of about 80, 60, 40, and 20 miles per hour. The test Reynolds numbers were about 1,120,000, 840,000, 560,000, and 280,000 based on the wing mean aerodynamic chord of 1.494 feet. The dynamic pressures of 16.37 and 9.21 were used for propeller windmilling and power on, respectively. Because of the turbulence factor of 1.6 for the tunnel, the effective Reynolds numbers (for maximum lift coefficients) were about 1,790,000, 1,340,000, 890,000, and 440,000.

Langley 4- by 6-foot tunnel.- The tests were made at a dynamic pressure of 13 pounds per square foot, which corresponds to an airspeed of about 72 miles per hour. The test Reynolds number was about 450,000 based on the tail average chord of 0.679 feet. Because of the turbulence factor of 1.93 for the tunnel, the effective Reynolds number (for maximum lift coefficients) was about 880,000.

[redacted]

Corrections

Langley 7- by 10-foot tunnel.- The data obtained with the ground board in place were not corrected for tares caused by the model support strut because of the impracticability of obtaining tares. Jet-boundary corrections were not applied because they have been shown to be negligible for the ground-board test installation. All other data have been corrected for tares caused by the model support strut; and jet-boundary corrections have been applied to the angles of attack, the drag coefficients, and the tail-on pitching-moment coefficients. The corrections were computed as follows by use of reference 1:

$$\Delta\alpha = 1.156C_L$$

$$\Delta C_X = -0.0165C_L^2$$

$$\Delta C_m = -8.23C_L\left(\frac{\delta_T}{\sqrt{q_t/q}} - \delta_w\right)\left(\frac{\partial C_m}{\partial i_t}\right)$$

where

$\Delta\alpha$ is in degrees

δ_w (0.1145) jet-boundary factor at the wing

δ_T (0.204 to 0.214) total jet-boundary correction at the tail

All jet-boundary corrections were added to the test data.

Langley 4- by 6-foot tunnel.- The data have been corrected for tares caused by the model support strut. A jet-boundary correction was applied as follows:

$$\Delta\alpha = 1.161C_L$$

The jet-boundary corrections to the hinge moment were not applied since they were negligible.

Test Procedure

A propeller calibration was made by measuring the longitudinal force of the model with flaps retracted and horizontal tail off at an angle of attack of 0° for a range of propeller speeds. Thrust

[redacted]

coefficients were determined from the relation

$$T_C' = C_{X(\text{propeller operating})} - C_{X(\text{propeller removed})}$$

The torque coefficients were computed by use of a calibration of motor torque as a function of minimum current. The results of the model propeller calibration are presented in figure 7.

The variations of thrust and torque coefficient with lift coefficient for the full-scale airplane and the model are shown in figures 8 and 9. The data for the full-scale airplane were obtained from full-scale propeller data. The thrust coefficients of the airplane were reproduced during power-on tests by the use of figures 7 and 8 to match the propeller speed and lift coefficient of the model. The value of T_C' for the tests with propeller windmilling was about -0.022. In general, the torque coefficients for the model were not the same as the airplane coefficients. (See fig. 9.)

At each angle of attack for power-on yaw tests the propeller speed was held constant throughout the yaw range. Since the lift and thrust coefficients vary with yaw when the propeller speed and angle of attack are held constant, the thrust coefficient is strictly correct only at zero yaw.

Lateral-stability derivatives were obtained from pitch tests at angles of yaw of $\pm 5^\circ$ by assuming a straight-line variation between these points. The large-symbol points on the plots of lateral-stability derivatives were obtained by measuring slopes through zero yaw from yaw tests.

Because previous tests indicated that propeller operation had little effect on the flow over the ailerons, all the aileron tests were made with the propeller windmilling.

Presentation of Results

An outline of the figures presenting the results is given below. (Figs. 1 through 9 are model drawings, photographs, and power charts.)

	Figure
A. Miscellaneous propeller-off tests	
I. Effect of stabilizer setting	10
II. Effect of Reynolds number	11

[redacted]

[redacted]

[redacted]

DISCUSSION

Propeller-Off Tests

A comparison of propeller-off and propeller-windmilling data (figs. 10 and 17), shows that the propeller causes C_m to be slightly more negative. The $\frac{dC_m}{dC_L}$ of the different stabilizer settings appear to be almost the same with propeller-off and propeller windmilling.

With an increase in Reynolds number from 280,000 to 1,120,000 (fig. 11), $C_{L_{max}}$ increased 20 percent, C_X became 27 percent less negative at zero lift, and the static longitudinal stability $\frac{\partial C_m}{\partial C_L}$ increased from -0.122 to -0.162. All the increase in $\frac{\partial C_m}{\partial C_L}$ occurred between the Reynolds numbers of 280,000 and 560,000.

Figure 12 gives a value of elevator effectiveness $\frac{\partial C_m}{\partial \delta_e}$ of -0.0161. This value compared with the value of -0.0147 for the propeller windmilling (fig. 23(a)) shows that the propeller when windmilling reduces the elevator effectiveness about 9 percent.

The only measurable effect of the tail fillet (fig. 13) occurs in the longitudinal force coefficient; removing the tail fillet made C_X slightly less negative throughout most of the lift range.

The drag of the hull is large because the propeller is located in an opening in the middle of the hull. Figure 14 shows that the hull propeller opening caused the minimum drag to be about 46 percent higher than when the cut-out was covered with a simple fairing. The opening also caused a small decrease in the slope of the lift curve, and increased the static longitudinal stability $\frac{dC_m}{dC_L}$ about 0.01.

Isolated Tail Characteristics

A series of tests was made on the horizontal tail to investigate the lift and hinge-moment characteristics over a complete range of elevator deflections with the elevator hinge gap open and sealed. (See figs. 15 and 16.) The isolated tail hinge-moment coefficients are based on the average of the right and left elevator hinge moments. The values of the various parameters which were read over ranges of $\pm 4^\circ\alpha$ and $\pm 5^\circ\delta_e$, respectively, are summarized in the following table:

	Gap sealed	Gap open	Gap sealed and faired
C_{L_α}	0.050	0.049	0.052
C_{L_δ}	.036	.034	-----
α_δ	-.68	-.67	-----
C_{h_α}	-.002	-.003	-----
C_{h_δ}	-.0066	-.0063	-----

Longitudinal Stability

Neutral point.- Figure 21 presents the variation of neutral-point position and the effective tail-off aerodynamic center location calculated from stabilizer and elevator data. A positive static margin exists for all conditions investigated for the normal center-of-gravity location. Power has a large stabilizing effect while flap deflection and inclination of the thrust axis (with windmilling propeller) have very little effect.

[redacted]

The stabilizing effect of power, particularly as shown by the shift of the tail-off aerodynamic center, is greater than would be caused by the thrust and normal force of the propeller. Part of the increased stability must be caused by change of air flow over the wing.

Effect of power on downwash and dynamic-pressure ratios.- An increase of $\frac{d(q_t/q)}{d\alpha}$ and $\frac{d\epsilon}{d\alpha}$ with power over the values for the windmilling condition is shown in figure 22 for the cruising and landing configurations. The values of $\frac{q_t}{q}$ and ϵ were calculated using isolated-tail data given in figure 15. For the windmilling propeller ϵ is about 1/2° to 1° less with the thrust axis tilted 3° than with the thrust axis horizontal. No power-on data are available with the thrust axis tilted.

Elevator deflection required for trim.- It appears (fig. 25) that an elevator deflection range of -5° to 2° for propeller windmilling and -10° to 2° with power is sufficient to trim through the speed range tested with the tab neutral, $i_t = 3.50°$, and center of gravity at 24.7 mean aerodynamic chord in either cruising or landing configuration.

Ground Effect

The results of stabilizer and elevator tests (figs. 26 through 29) with the model tested near the ground board shows that the presence of the ground board increased C_{L_α} 6 percent with the propeller windmilling and 17 percent with power over the values of C_{L_α} with the model away from the ground board (figs. 19, 20, 23, and 24). Near the ground board $C_{L_{max}}$ was slightly lower than when the model was tested away from the ground.

A comparison of figure 30, which presents the neutral points calculated from the ground-board data of figures 26 and 27, with figure 21 shows that the model is, in general, more stable near the ground.

Values of the downwash angle and dynamic-pressure ratios at the tail of the model near the ground were calculated using isolated-tail data (fig. 15) and are shown in figure 31. The presence of the ground reduced downwash angles and dynamic pressure ratios.

[redacted]

From figure 32 it appears that with $i_t = 3.5^\circ$ in the landing configuration a range of elevator deflection of -10.5° to 1° is required for trim with either the propeller windmilling or with take-off power.

Stalling Characteristics

The results of tuft tests of the model with propeller windmilling and with take-off power are presented in figure 33 for the cruising configuration and in figure 34 for the landing configuration.

For the windmilling propeller, cruising and landing configurations, the stall appears to start at the trailing edge of the root section in the region of the propeller at rather low lift coefficients. Application of power tends to increase the area near the propeller over which the flow is stalled, especially over the left wing. The application of power also accentuates the tendency of the left wing panel to stall in the region of the aileron before $C_{L_{max}}$ of the model is reached. The right wing panel tends to stall in the vicinity of the aileron, but the extreme tip of both wing panels remains unstalled.

Lateral Stability

Stability derivatives at small angles of yaw.- In the cruising configuration for both propeller windmilling, and take-off power (fig. 35), the effective dihedral varies between 6.5° and 8° over most of the lift range with the exception of a sudden drop in the effective dihedral for the propeller-windmilling condition at a lift coefficient of 0.94. This sudden change in dihedral effect is probably a result of unsymmetrical wing stall. The effective dihedral in landing configuration with propeller windmilling varies from 8° at a lift coefficient of 0.25 to 3.5° at a lift coefficient of 1.43; for the same configuration with take-off power it varies from 9.5° at a lift coefficient of 0.21 to 4.5° at a lift coefficient of 1.57.

Directional stability exists (C_{n_ψ} is negative) for all the conditions tested; C_{n_ψ} varies from approximately -0.0005 to -0.0050 over the lift range. Directional stability increases about 40 percent over the lift range for take-off power because of the increased slipstream velocity ratio. For untrimmed conditions the large

positive values of C_{Y_ψ} indicate that the lateral-force characteristics will be in the correct direction, that is, right bank will accompany right sideslip and vice versa.

Rudder characteristics.- Figure 37 shows the characteristics in yaw of the model for propeller windmilling with the rudder free. An undesirable reversal in the slope of the C_n curve occurs at about $\pm 20^\circ$ yaw. There are no rudder-free data for higher power conditions. Oscillations of the rudder occurred when the model was tested with the rudder free, causing the model to shake badly. At angles of attack above 5.4° in landing configuration and at any angle of attack in cruising configuration, this shaking became so severe that the model could not be yawed past about $\pm 20^\circ$, nor was it possible to read the scales at smaller angles of yaw. No rudder lock occurs within the range of yaw angles tested. Figure 38 shows a small negative value for C_{h_ψ} in each power condition tested in the cruising configuration. In the landing configuration (fig. 39) C_{h_ψ} is zero for propeller windmilling and take-off power and 0.0022 for half thrust of take-off power. $C_{h_{\delta_r}}$ (figs. 38 and 39) has large negative values increasing with T_C'. The rudder has sufficient effectiveness to trim at yaw angles of at least $\pm 20^\circ$ for all conditions tested.

Miscellaneous power effects.- This model was rather unusual for single-engine airplanes with single-rotating propellers in that the vertical tail seems to be so located in the propeller slipstream that power caused very small changes in the rudder deflection required for trim at $\psi = 0^\circ$. However, power did cause a large amount of asymmetry, particularly in the pitching-moment coefficient and rudder hinge-moment coefficient at large angles of yaw where for high power operation nearly 10° of elevator deflection is required to trim the change in C_m in 20° of yaw.

Aileron characteristics.- The results of the aileron tests are shown in figure 40. For both cruising and landing configurations $\frac{dC_l}{d\delta_a}$ at $\alpha = 0^\circ$ is about 0.0014. The yawing-moment coefficient is small throughout most of the angle-of-attack range in both configurations. At high angles of attack, however, there is a considerable reduction in aileron effectiveness for maximum aileron deflection.

[redacted]

SUMMARY OF RESULTS

Results of wind-tunnel tests of a $\frac{1}{4}$-scale model of the Naval Aircraft Factory float-wing convoy interceptor indicate that:

1. The drag of the hull is large because of the type of propeller installation. The propeller opening in the hull caused the minimum drag to be about 46 percent higher than when the cut-out was covered with a simple fairing.

2. The model had satisfactory longitudinal stability with the normal center-of-gravity location for all conditions tested. Power had a large stabilizing effect, while flap deflection had very little effect.

3. An elevator deflection range of -5° to 2° for propeller windmilling and -10° to 2° with power is sufficient to trim through the speed range tested. In the presence of the ground board, a range of -10.5° to 1° with propeller windmilling or with take-off power is required for trim in the landing configuration with the stabilizer set at 3.5°.

4. Stall tests made with tufts on the wing showed that the wing stalled early in the vicinity of the propeller. At higher lift coefficients the wing tended to stall at the ailerons, with power accentuating the tendency of the left wing panel to stall. The extreme wing tips remained unstalled.

5. The effective dihedral, lateral-force characteristics, and directional stability with controls fixed were satisfactory.

6. When the model was tested with the rudder free, the rudder oscillated and caused the model to shake. No rudder lock was indicated within the range of yaw angles tested.

[redacted]

7. Power caused only small changes in directional trim but did create asymmetry of the pitching-moment coefficient through the yaw range.

Langley Memorial Aeronautical Laboratory
National Advisory Committee for Aeronautics
Langley Field, Va.

Evalyn G. Wells
Engineering Aide

Elizabeth G. McKinney
Engineering Aide

Approved: Thomas A. Harris
for

Hartley A. Soulé
Chief of Stability Research Division

MEL

REFERENCE

1. Gillis, Clarence L., Polhamus, Edward C., and Gray, Joseph L., Jr.: Charts for Determining Jet-Boundary Corrections for Complete Models in 7- by 10-Foot Closed Rectangular Wind Tunnels. NACA ARR No. L5G31, 1945.

[redacted]

TABLE I.- PHYSICAL CHARACTERISTICS OF THE NAVAL AIRCRAFT

FACTORY FLOAT-WING AIRPLANE

Type	Float-wing seaplane interceptor
Engine:	
Manufacturer's designation	Ranger XV-770-9
Ratings:	
Normal power	565 bhp at 3200 rpm at sea level
	450 bhp at 3200 rpm at 27,000 ft
Military power	625 bhp at 3400 rpm at sea level
	500 bhp at 3400 rpm at 27,000 ft
Take-off power	625 bhp at 3400 rpm at sea level
Propeller gear ratio	17:11 (0.6471)
Propeller:	
Type	Aeroproducts
Diameter, ft	7.5
Blade design	C-20-144
Number of blades	3 blades
Landing gear:	
None (float-wing seaplane with catapult and retrieving hooks)	

NATIONAL ADVISORY
COMMITTEE FOR AERONAUTICS

[redacted]

TABLE II.- AIRPLANE WEIGHT-BALANCE SUMMARY

Condition	Gross weight (lb)	Center of gravity		
		(in. behind airplane nose)	(percent M.A.C.)	(in. above horizontal base line)
Fighter normal	4000	125.97	24.7	42.55
Fighter overload	4319	123.83	21.7	42.02

NATIONAL ADVISORY
COMMITTEE FOR AERONAUTICS

TABLE III.- AIRPLANE WING AND TAIL-SURFACE DATA

	Wing	Horizontal tail	Vertical tail
Area, sq ft	160	30.50	15.50
Span, ft	29.83	11.25	6.04
Aspect ratio	5.56	4.15	2.35
Taper ratio	0.40	0.45	
[a]Dihedral, deg	9	Upper surface maximum ordinates in same place	
Sweepback, quarter chord line, deg	0		
Root section	66-2-216	0009-64	-----
Tip section	66-(216)-212	0009-64	-----
[b]Angle of incidence at root, deg	6	Adjustable 0.1 to 9.5	0
[b]Angle of incidence at tip, deg	4	Adjustable 0.1 to 9.5	0
Mean aerodynamic chord, ft (starting 6.25 in. aft of leading edge at center line)	5.98		
Root chord, ft	8.00	3.48	
Theoretical tip chord, ft	3.18	1.56	

[a]Dihedral measured from bottom surface of wing.

[b]Angle of incidence measured with respect to horizontal base line.

NATIONAL ADVISORY
COMMITTEE FOR AERONAUTICS

TABLE IV.- AIRPLANE CONTROL-SURFACE DATA

	Ailerons	Elevators	Rudder	Flaps
Percent span	33.50	98.50	100.00	40.00
Area, behind hinge line, sq ft	7.91	12.08	9.70	15.30
Balance area, sq ft	Minimum balance	Minimum balance	Minimum balance	Minimum balance
Root-mean-square chord, behind hinge line, ft	0.80	1.16	1.39	
Distance to hinge line from normal center of gravity, ft		15.62	16.07	

Flap deflections, deg (corresponding powers)

For landing . . . . . 60(power off)
For cruising and take off . . . . . Flaps retracted

FIGURE LEGENDS

Figure 1.– Three-view drawing of the $\frac{1}{4}$-scale NAF seaplane model.

Figure 2.– System of axes and control-surface hinge moments and deflections. Positive values of forces, moments, and angles are indicated by arrows. Positive values of tab hinge moments and deflections are in the same directions as the positive values for the control surfaces to which the tabs are attached.

Figure 3a.–Phtograph of the $\frac{1}{4}$-scale NAF seaplane model with propeller off. Cruising configuration, tail fillet on.

Figure 3b.– Photograph of the $\frac{1}{4}$-scale NAF seaplane model with horizontal thrust axis. Landing configuration.

Figure 4.– Plan-form and blade-form curves for propeller used on the $\frac{1}{4}$-scale NAF seaplane model D, diameter; R, radius; r, station radius; b, section chord; h, section thickness; β, propeller blade angle.

Figure 5.– Horizontal tail of the $\frac{1}{4}$-scale NAF seaplane model.

Figure 6.– Position of the $\frac{1}{4}$-scale model of the NAF airplane and ground board in the tunnel, $\alpha = 0^\circ$.

Figure 7.– Characteristics of a 1.862-foot diameter three-bladed propeller on the $\frac{1}{4}$-scale NAF seaplane model $\alpha = 0^\circ$, $\beta = 27^\circ$, $q = 9.21$ pounds per square foot.

Figure 8.– Effective thrust coefficient available at any lift coefficient for the NAF seaplane.

Figure 9.– Comparison of torque coefficient values for the constant speed seaplane propeller (625 hp at 2200 rpm at sea level) and for a $\frac{1}{4}$-scale model propeller (fixed pitch, $\beta = 27^\circ$) delivering the same T_c'.

Figure 10.– Effect of stabilizer setting on the aerodynamic characteristics of the $\frac{1}{4}$-scale model of the NAF seaplane. Prop. off, $\delta_e = 0$; $q = 16.37$ pounds per square foot $\delta_f = 0^\circ$; thrust axis horizontal.

Figure 11.– Effect of Reynolds number on the aerodynamic characteristics of the $\frac{1}{4}$-scale model of the NAF seaplane. Prop. off; $\delta_e = 0$; $i_t = 9\frac{1}{2}^\circ$; $\delta_f = 0^\circ$; thrust axis horizontal.

[redacted]

FIGURE LEGENDS.- Continued

Figure 12.- Effect of elevator deflection on the aerodynamic characteristics of the $\frac{1}{4}$-scale model of the NAF seaplane. Prop. off; $i_t = 6\frac{1}{4}^\circ$; $q = 16.37$ pounds per square foot, $\delta = 0^\circ$; thrust axis horizontal.

Figure 12.- Concluded.

Figure 13.- Effect of tail fillet on the aerodynamic characteristics of the $\frac{1}{4}$-scale model of the NAF seaplane. Prop. off; $i_t = \frac{3}{4}^\circ$; $\delta_e = 0$; $q = 16.37$ pounds per square foot; $\delta_f = 0^\circ$; thrust axis horizontal.

Figure 13.- Concluded.

Figure 14.- Effect of sealing hull propeller opening on the $\frac{1}{4}$-scale model of the NAF seaplane. Prop. off; $i_t = \frac{3}{4}^\circ$; $\delta_e = 0$, $q = 16.37$ pounds per square foot; $\delta_f = 0^\circ$; thrust axis horizontal.

Figure 15.- Characteristics of the isolated horizontal tail of the $\frac{1}{4}$-scale model of the NAF float-wing seaplane with the hinge gap unsealed.

Figure 15.- Concluded.

Figure 16.- Characteristics of the isolated horizontal tail of the $\frac{1}{4}$-scale model of the NAF float-wing seaplane with the hinge gap unsealed.

Figure 16.- Concluded.

Figure 17.- Effect of stabilizer on the aerodynamic characteristics in pitch of the $\frac{1}{4}$-scale NAF seaplane model. Cruising configuration; prop. windmilling; $\delta_e = 0^\circ$; thrust axis inclined 3° to horizontal.

Figure 18.- Effect of stabilizer on the aerodynamic characteristics in pitch of the $\frac{1}{4}$-scale NAF seaplane model landing configurations; prop. windmilling; $\delta_e = 0^\circ$; thrust axis inclined 3° to horizontal.

Figure 19.- Effect of stabilizer on the aerodynamic characteristics in pitch of the $\frac{1}{4}$-scale NAF seaplane model. Cruising configuration. $\delta_e = 0^\circ$ Thrust axis horizontal.

(a) Windmilling.

[redacted]

FIGURE LEGEND.- Continued

Figure 19.- Concluded.

(b) Take-off power.

Figure 20.- Effect of stabilizer on the aerodynamic characteristics in pitch of the $\frac{1}{4}$-scale NAF seaplane model landing configuration, $\delta_e = 0^\circ$. Thrust axis horizontal.

(a) Windmilling.

Figure 20.- Concluded.

(b) Take-off power.

Figure 21.- Effect of power, model configuration, and thrust axis inclination on the elevator-fixed neutral point location and on the effective tail-off aerodynamic center location of $\frac{1}{4}$-scale model of the N.A.F. seaplane.

(a) Cruising configuration.
(b) Landing configuration.

Figure 21.- Concluded.

(c) Cruising configuration.
(d) Landing configuration.

Figure 22.- Dynamic-pressure ratios and average downwash angles at the tail of the $\frac{1}{4}$-scale model of the NAF seaplane.

(a) Cruising configuration.

Figure 22.- Concluded.

(b) Landing configuration.

Figure 23.- Effect of elevator deflection on the aerodynamic characteristics in pitch of the $\frac{1}{4}$-scale NAF seaplane model. Cruising configuration, $i_t = 3.50^\circ$. Thrust axis horizontal.

(a) Windmilling.

Figure 23.- Continued.

(a) Continued.

[redacted]

FIGURE LEGEND.- Continued

Figure 23.- Continued.

(a) Concluded.

Figure 23.- Continued.

(b) Take-off power

Figure 23.- Continued.

(b) Continued.

Figure 23.- Continued.

(b) Continued.

Figure 23.- Concluded.

(b) Concluded.

Figure 24.- Effect of elevator deflection on the aerodynamic characteristics in pitch of the $\frac{1}{4}$- scale NAF seaplane model. Landing configuration, $i_t = 3.50^\circ$. Thrust axis horizontal.

(a) Windmilling.

Figure 24.- Continued.

(a) Continued.

Figure 24.- Continued.

(a) Concluded.

Figure 24.- Continued.

(b) Half thrust of take-off power.

Figure 24.- Continued.

(b) Continued.

Figure 24.- Continued.

(b) Continued.

[redacted]

FIGURE LEGEND.- Continued

Figure 24.- Continued.

(b) Concluded.

Figure 24.- Continued.

(c) Take-off power

Figure 24.- Continued.

(c) Continued.

Figure 24.- Continued.

(c) Continued.

Figure 24.- Concluded.

(c) Concluded.

Figure 25.- Elevator deflection required for trim of the $\frac{1}{4}$-scale NAF seaplane model away from the ground; $i_t = 3.50^\circ$; thrust axis horizontal; sea level operation.

Figure 26.- Effect of stabilizer on the aerodynamic characteristics in pitch of the $\frac{1}{4}$-scale NAF seaplane model near the ground. Take-off configuration; $\delta_e = 0^\circ$; thrust axis horizontal.

(a) Windmilling

Figure 26.- Concluded.

(b) Take-off power.

Figure 27.- Effect of stabilizer on the aerodynamic characteristics in pitch of the $\frac{1}{4}$-scale NAF seaplane model near the ground. Landing configuration; $\delta_e = 0^\circ$; thrust axis horizontal.

(a) Windmilling

Figure 27.- Concluded.

(b) Take-off power.

[redacted]

FIGURE LEGEND.- Continued

Figure 28.- Effect of elevator deflection on the aerodynamic characteristics in pitch of the $\frac{1}{4}$-scale NAF seaplane model near the ground. Landing configuration; $i_t = 3.50°$; thrust axis horizontal.

(a) Windmilling.

Figure 28.- Continued.

(a) Concluded.

Figure 28.- Concluded.

(b) Take-off power.

Figure 29.- Effect of elevator deflection on the aerodynamic characteristics in pitch of the $\frac{1}{4}$-scale NAF seaplane model near the ground. Landing configuration; prop. windmilling; $i_t = 0.42°$; thrust axis horizontal.

Figure 29.- Concluded.

Figure 30.- Effect of power and model configuration on the elevator-fixed neutral point location of the $\frac{1}{4}$-scale model of the N.A.F. seaplane near the ground. Thrust axis horizontal.

(a) Take-off configuration.
(b) Landing configuration.

Figure 31.- Dynamic-pressure ratios and average downwash angles at the tail of the $\frac{1}{4}$-scale model of the NAF seaplane near the ground. Thrust axis horizontal.

(a) Take-off configuration.

Figure 31.- Concluded.

(b) Landing configuration.

Figure 32.- Elevator deflection required for trim of the $\frac{1}{4}$-scale NAF seaplane model near the ground. Landing configuration; thrust axis horizontal.

[redacted]

FIGURE LEGEND.- Continued

Figure 33.- Tuft studies of the $\frac{1}{4}$-scale NAF seaplane model. Cruising configuration.

(a) Windmilling.

Figure 33.- Continued.

(a) Concluded.

Figure 33.- Continued.

(b) Take-off power.

Figure 33.- Concluded.

(b) Concluded.

Figure 34.- Tuft studies of the $\frac{1}{4}$-scale NAF seaplane model. Landing configuration.

(a) Windmilling

Figure 34.- Continued.

(a) Concluded.

Figure 34.- Continued.

(b) Take-off power.

Figure 34.- Concluded.

(b) Concluded.

Figure 35.- Effect of flap setting on the lateral-stability characteristics of small angles of yaw. $\frac{1}{4}$-scale model of NAF seaplane. Thrust axis horizontal.

(a) Windmilling.

Figure 35.- Concluded.

(b) Take-off power.

[redacted]

FIGURE LEGEND.- Continued

Figure 36.- Aerodynamic characteristics in yaw of the $\frac{1}{4}$-scale model of the NAF seaplane. Propeller windmilling; $\delta_r = 0^\circ$; $i_t = 3.2^\circ$; $q = 16.37$ lbs/sq ft, thrust axis horizontal.

Figure 36.- Continued.

Figure 36.- Concluded.

Figure 37.- Aerodynamic characteristics in yaw of the $\frac{1}{4}$-scale model of the NAF seaplane. Propeller windmilling; rudder free; $i_t = 3.2^\circ$; $\alpha = 5.4^\circ$; $\delta_f = 60^\circ$; $q = 16.37$ lbs/sq ft; thrust axis horizontal.

Figure 37.- Concluded.

Figure 38.- Effect of rudder deflection on the aerodynamic characteristics in yaw of the $\frac{1}{4}$-scale model of the NAF seaplane. Cruising configuration; $i_t = 3.5^\circ$; $\delta_e = 0^\circ$; thrust axis horizontal.

(a) Windmilling; $\alpha = 0.54$.

Figure 38.- Continued.

(a) Continued.

Figure 38.- Continued.

(a) Continued.

Figure 38.- Continued.

(a) Concluded.

Figure 38.- Continued.

(b) Take-off power, $\alpha = 1.46$.

Figure 38.- Continued.

(b) Continued.

Figure 38.- Continued.

(b) Continued.

[redacted]

FIGURE LEGEND.- Continued

Figure 38.- Continued.

(b) Concluded.

Figure 38.- Continued.

(c) Windmilling; $\alpha = 5.94$.

Figure 38.- Continued.

(c) Continued.

Figure 38.- Continued.

(c) Continued.

Figure 38.- Continued.

(c) Continued.

Figure 38.- Continued.

(c) Concluded.

Figure 38.- Continued.

(d) Take-off power; $\alpha = 5.16$

Figure 38.- Continued.

(d) Continued.

Figure 38.- Continued.

(d) Continued.

Figure 38.- Concluded.

(d) Concluded.

Figure 39.- Effect of rudder deflection on the aerodynamic characteristics in yaw of the $\frac{1}{4}$-scale model of the NAF seaplane. Landing configuration; $i_t = 3.5^\circ$; $\delta_e = 0^\circ$; thrust axis horizontal.

(a) Windmilling; $\alpha = 3.26$.

[redacted]

FIGURE LEGEND.- Continued

Figure 39.- Continued.

(a) Continued.

Figure 39.- Continued.

(a) Continued.

Figure 39.- Continued.

(a) Concluded.

Figure 39.- Continued.

(b) Half thrust of take-off power, $\alpha = 2.89$.

Figure 39.- Continued.

(b) Continued.

Figure 39.- Continued.

(b) Continued.

Figure 39.- Continued.

(b) Concluded.

Figure 39.- Continued.

(c) Take-off power, $\alpha = 0.50$.

Figure 39.- Continued.

(c) Continued.

Figure 39.- Continued.

(c) Continued.

Figure 39.- Concluded.

(c) Concluded.

[redacted]

FIGURE LEGEND.- Concluded

Figure 40.- Aileron characteristics of the $\frac{1}{4}$-scale model of the NAF seaplane. Windmilling propeller; $\delta_{a_r} = 0^\circ$; thrust axis horizontal.

(a) Cruising configuration.

Figure 40.- Concluded.

(b) Landing configuration.

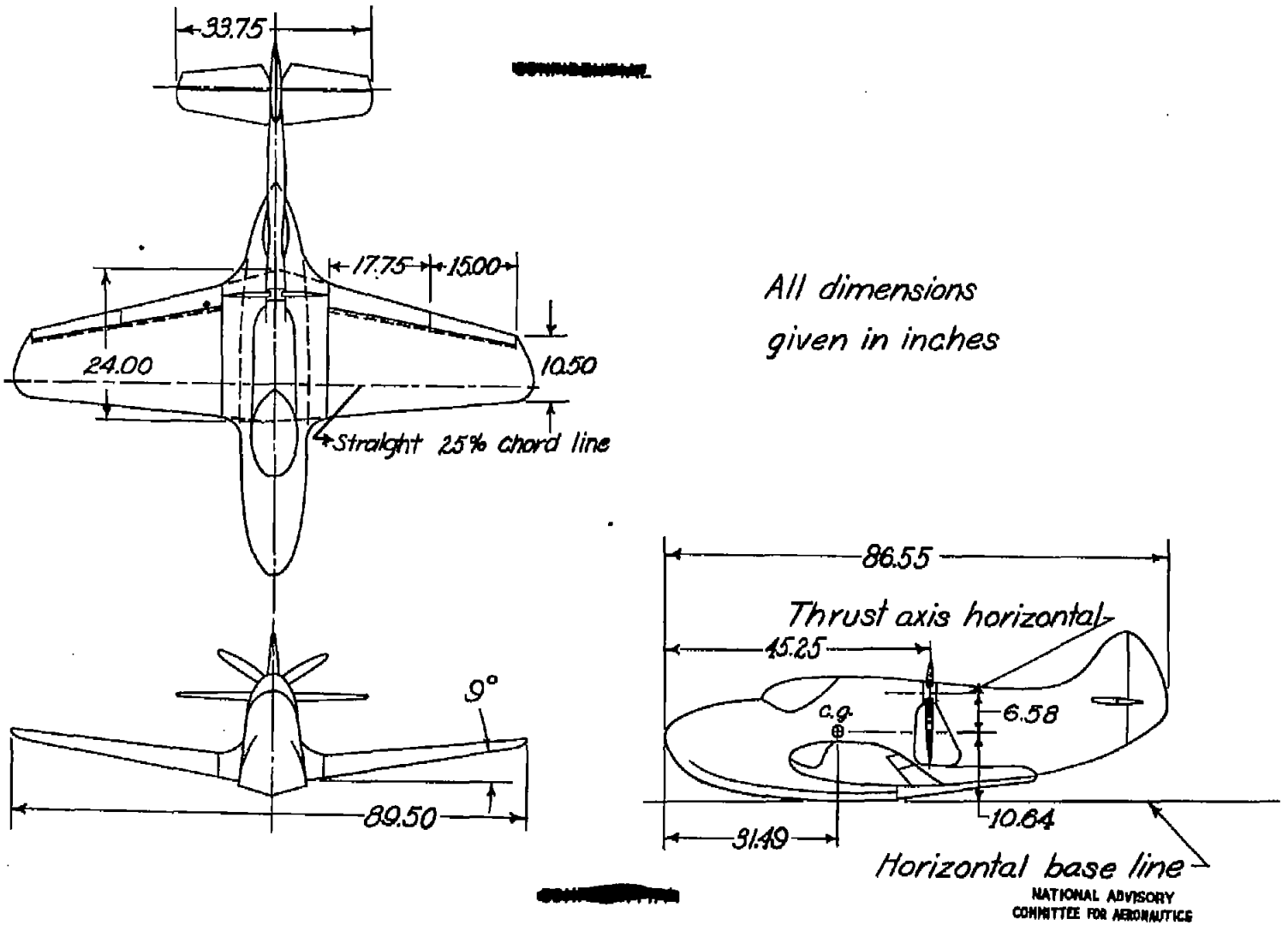

Figure 1. - Three-view drawing of the ¼-scale NAF seaplane model.

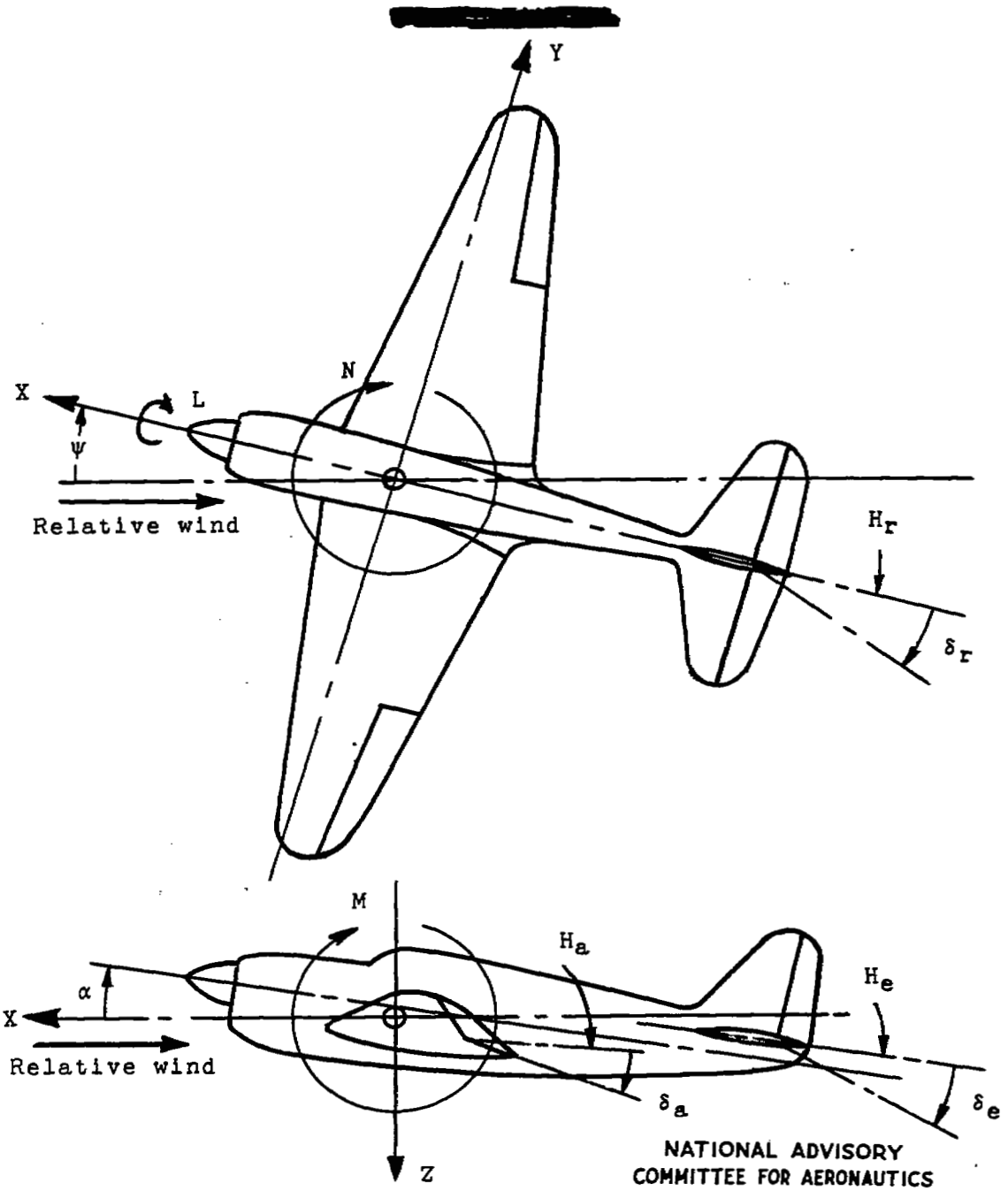

Figure 2 .- System of axes and control-surface hinge moments and deflections. Positive values of forces, moments, and angles are indicated by arrows. Positive values of tab hinge moments and deflections are in the same directions as the positive values for the control surfaces to which the tabs are attached.

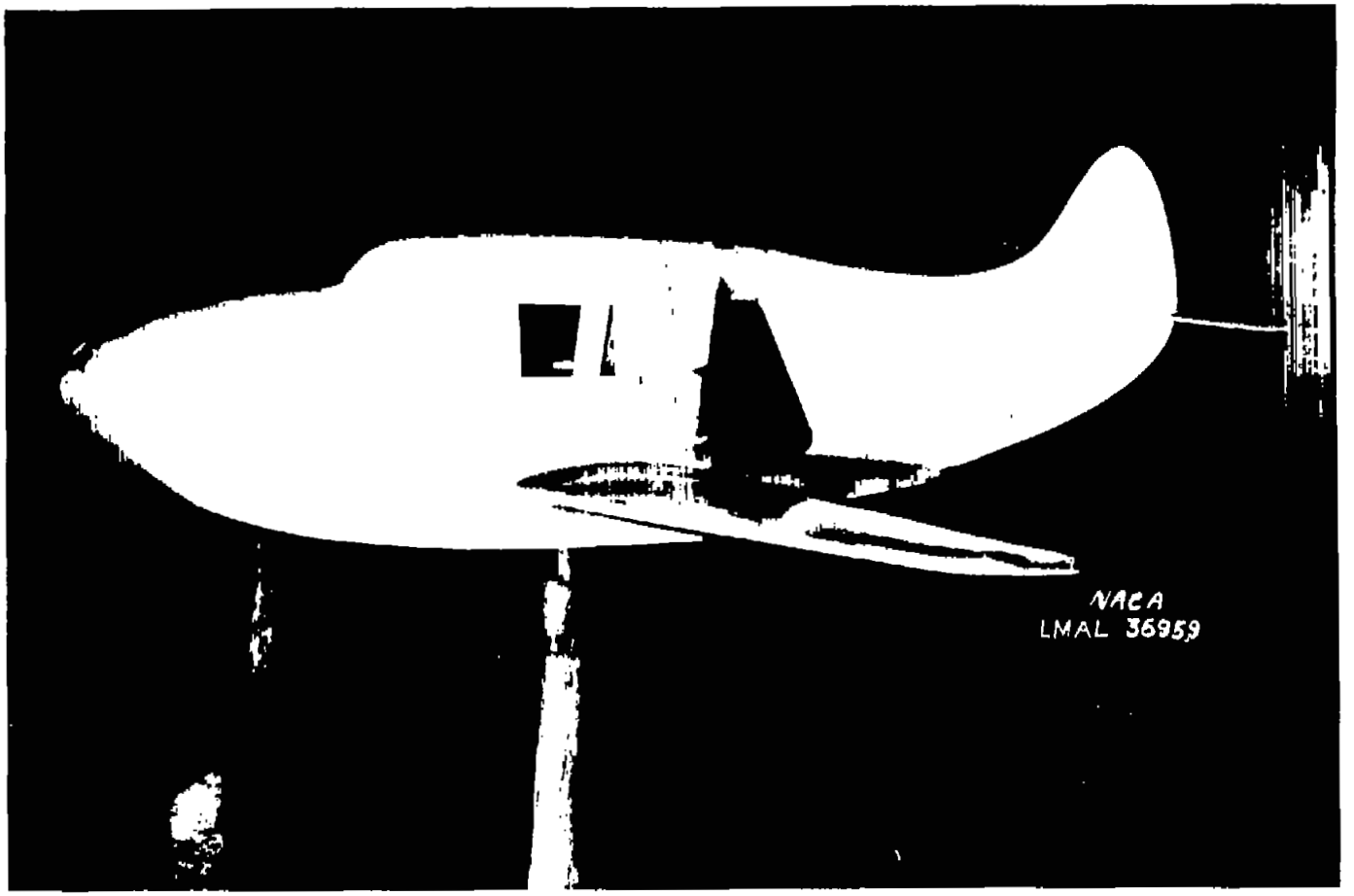

Figure 3a.- Photograph of the 1/4-scale NAF seaplane model with propeller off. Cruising configuration, tail fillet on.

NATIONAL ADVISORY COMMITTEE FOR AERONAUTICS
LANGLEY MEMORIAL AERONAUTICAL LABORATORY - LANGLEY FIELD, VA.

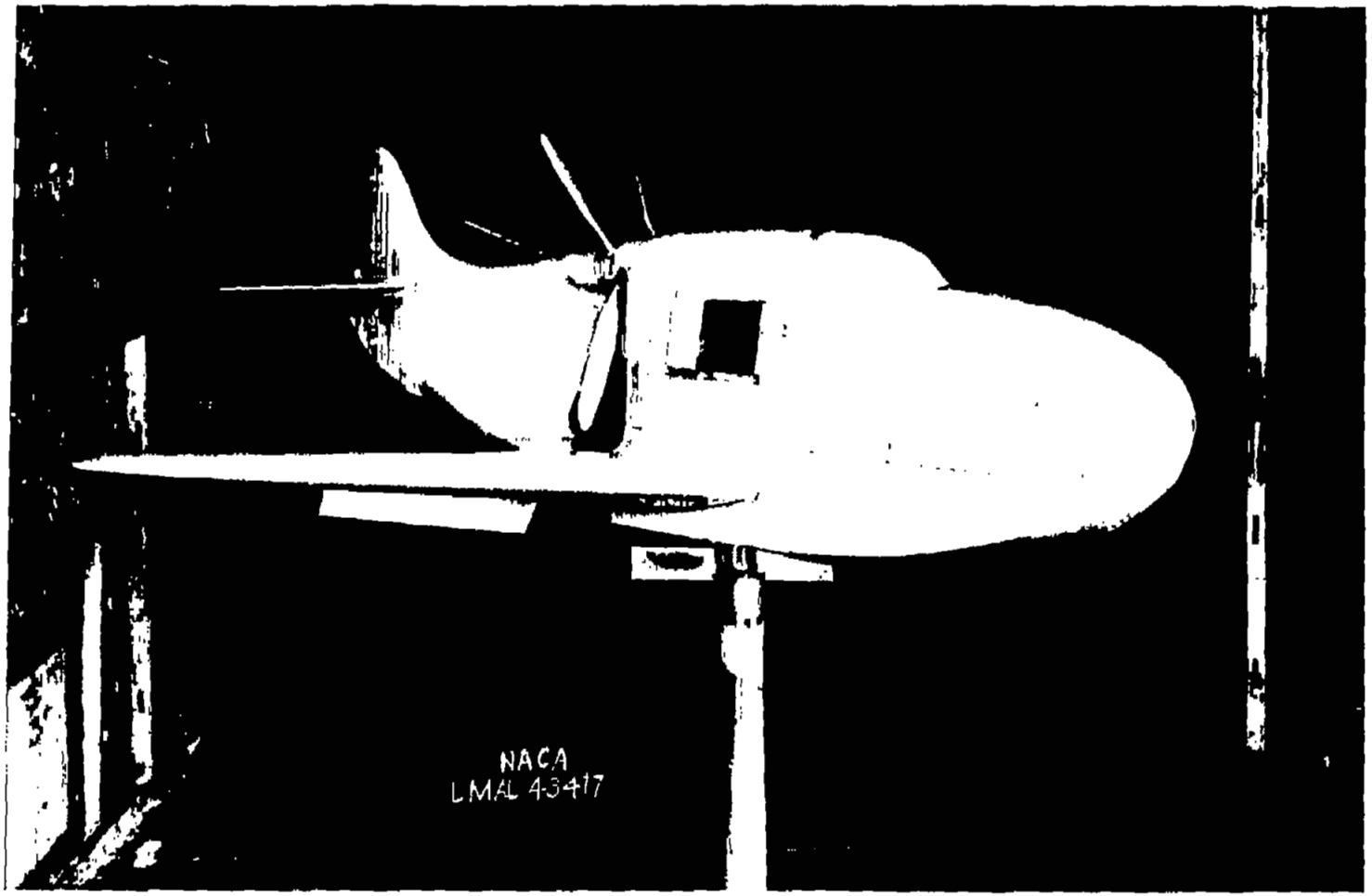

Figure 3b.- Photograph of the 1/4-scale NAF seaplane model with horizontal thrust axis. Landing configuration.

NATIONAL ADVISORY COMMITTEE FOR AERONAUTICS
LANGLEY MEMORIAL AERONAUTICAL LABORATORY - LANGLEY FIELD, VA.

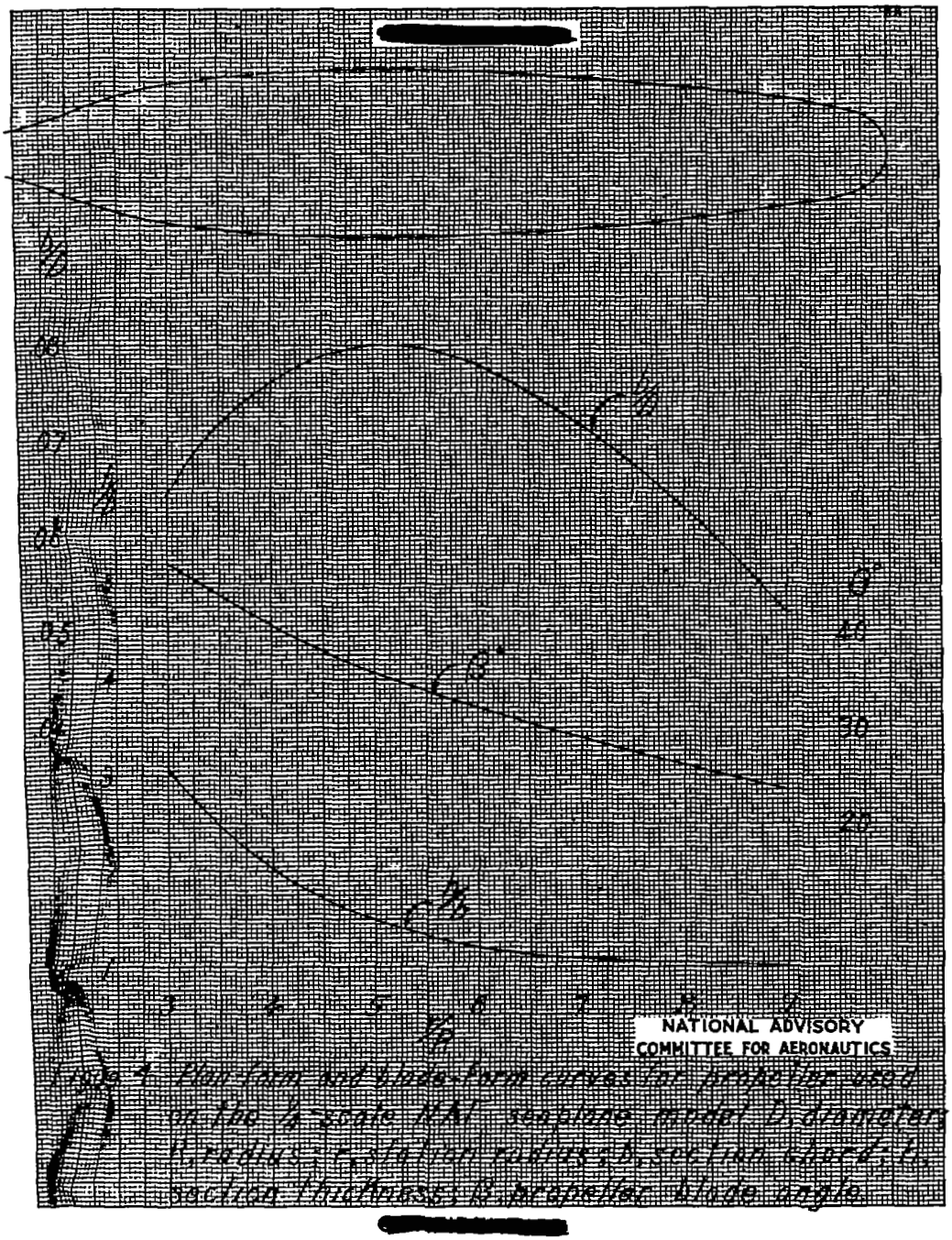

Figure 4.- Plan-form and blade-form curves for propeller used on the 1/4-scale NAI seaplane model. D, diameter; R, radius; r, station; $c_{0.75R}$, section chord; t, section thickness; β, propeller blade angle.

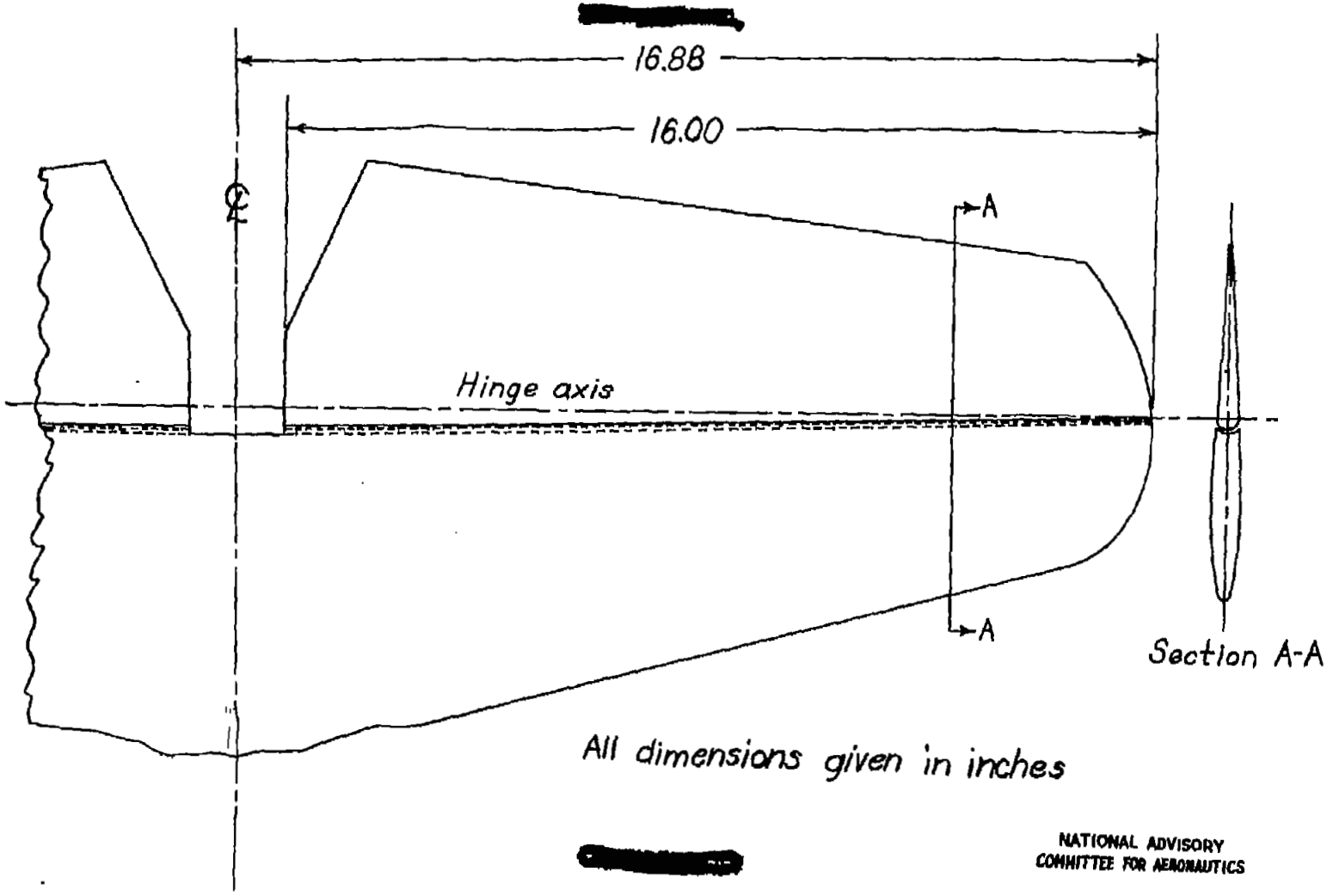

Figure 5.- Horizontal tail of the $\frac{1}{4}$-scale NAF seaplane model.

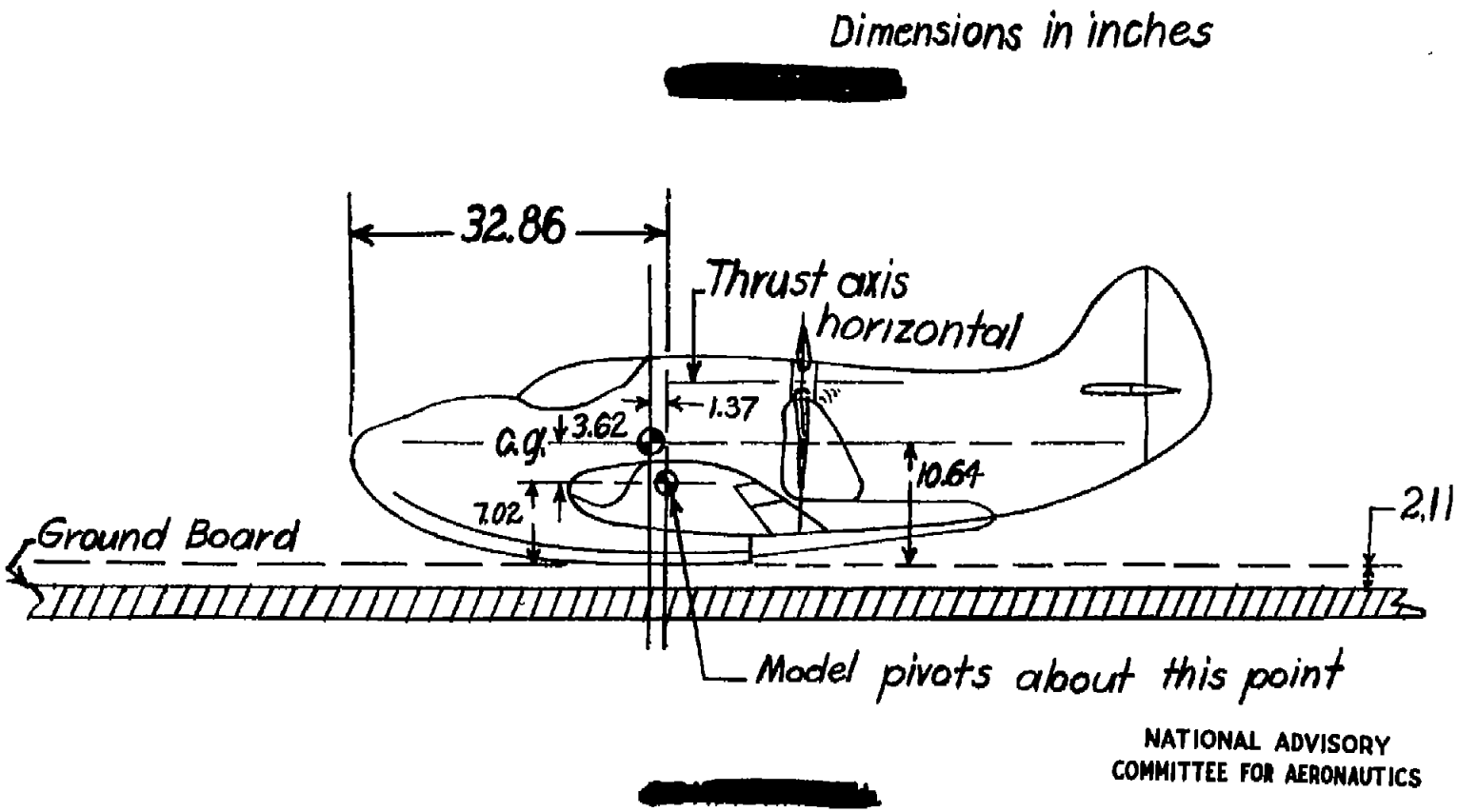

Figure 6.-Position of the 1/4-scale model of the NAF airplane and ground board in the tunnel, $\alpha = 0°$.

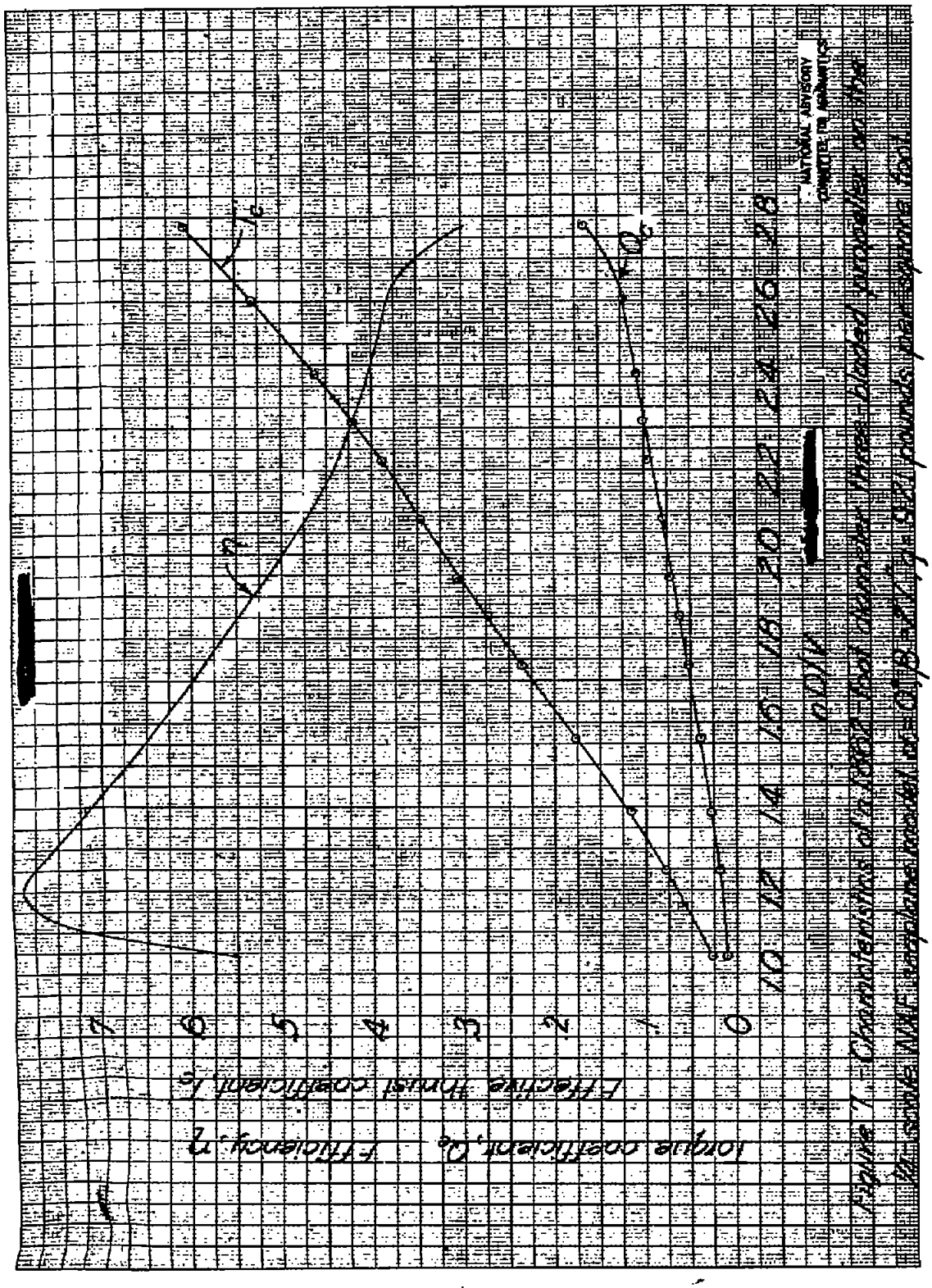
Torque coefficient, Q_e
Effective thrust coefficient, F_e
Efficiency, η
NATIONAL ADVISORY COMMITTEE FOR AERONAUTICS

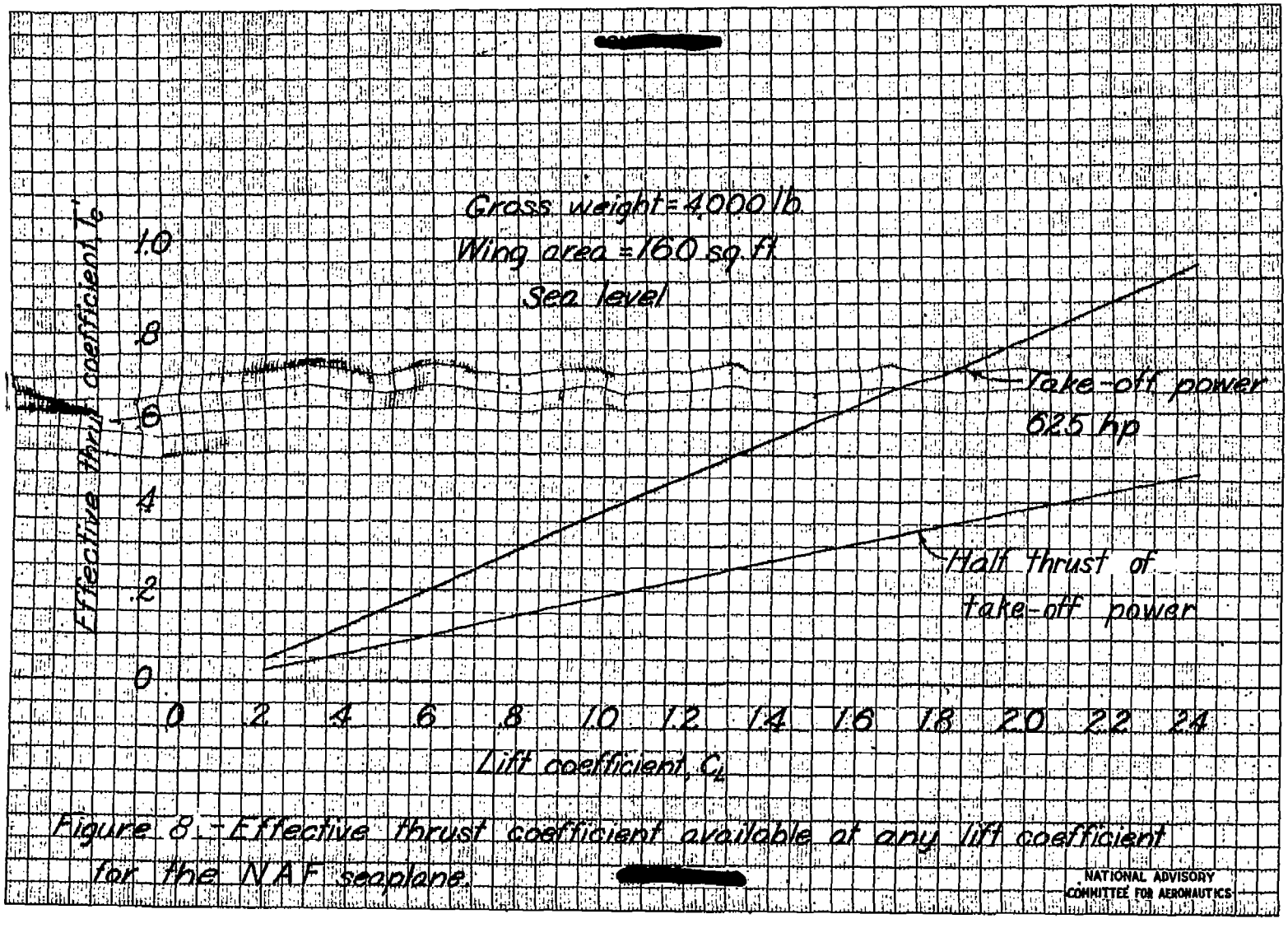

Figure 8.- Effective thrust coefficient available at any lift coefficient for the NAF seaplane.

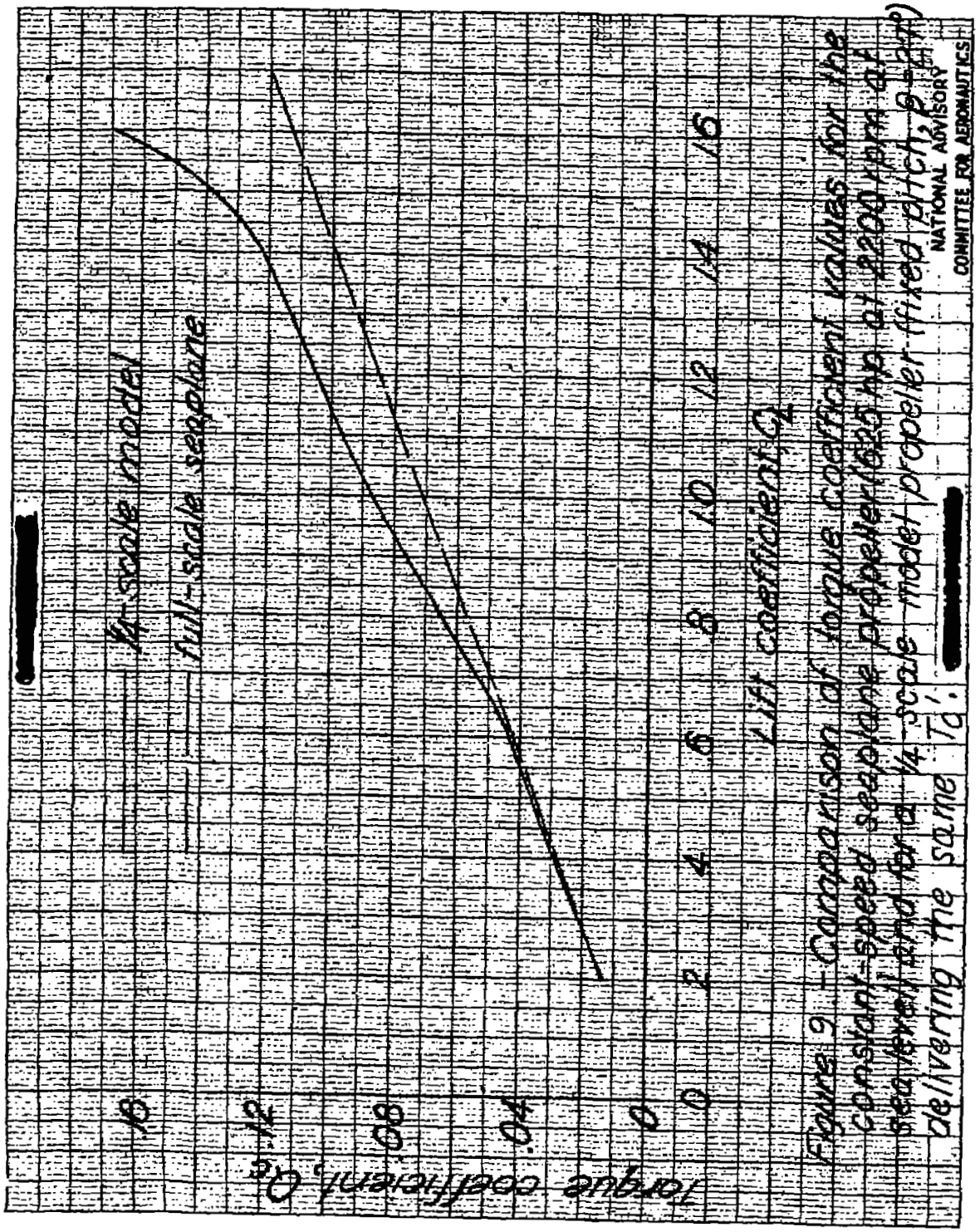

Figure 9.- Comparison of torque coefficient values for the constant-speed sequence propeller operating at 1200 rpm at several inflow conditions and ¼-scale model propeller (fixed pitch, 2-blade) delivering the same T_c'.

Figure 10.- Effect of stabilizer setting on the aerodynamic characteristics of the ¼ scale model of the NAF seaplane. Flap off; [illegible]

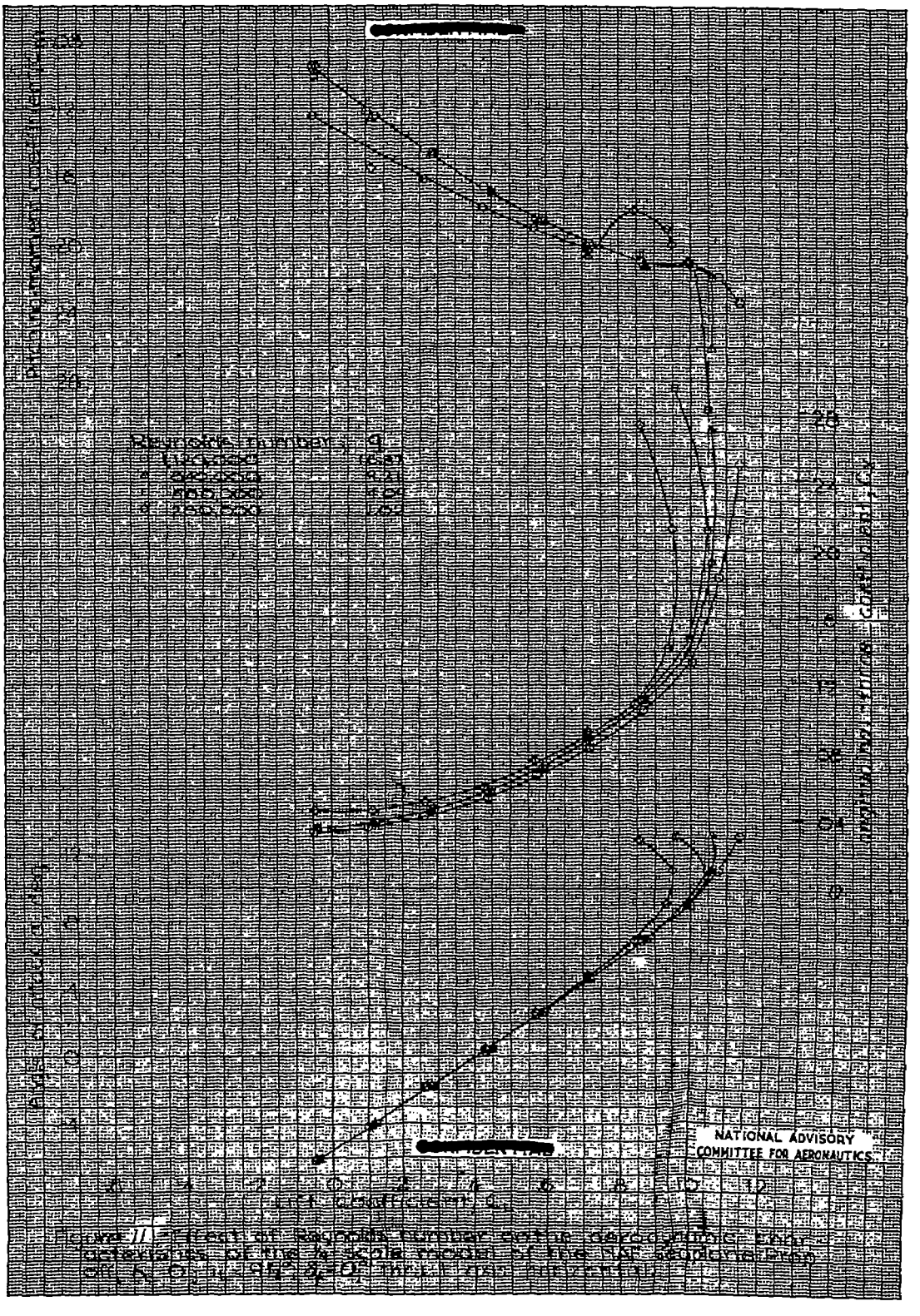

Figure 11.- Effect of Reynolds number on the aerodynamic characteristics of the ¼-scale model of the NAF sequoia from [illegible]

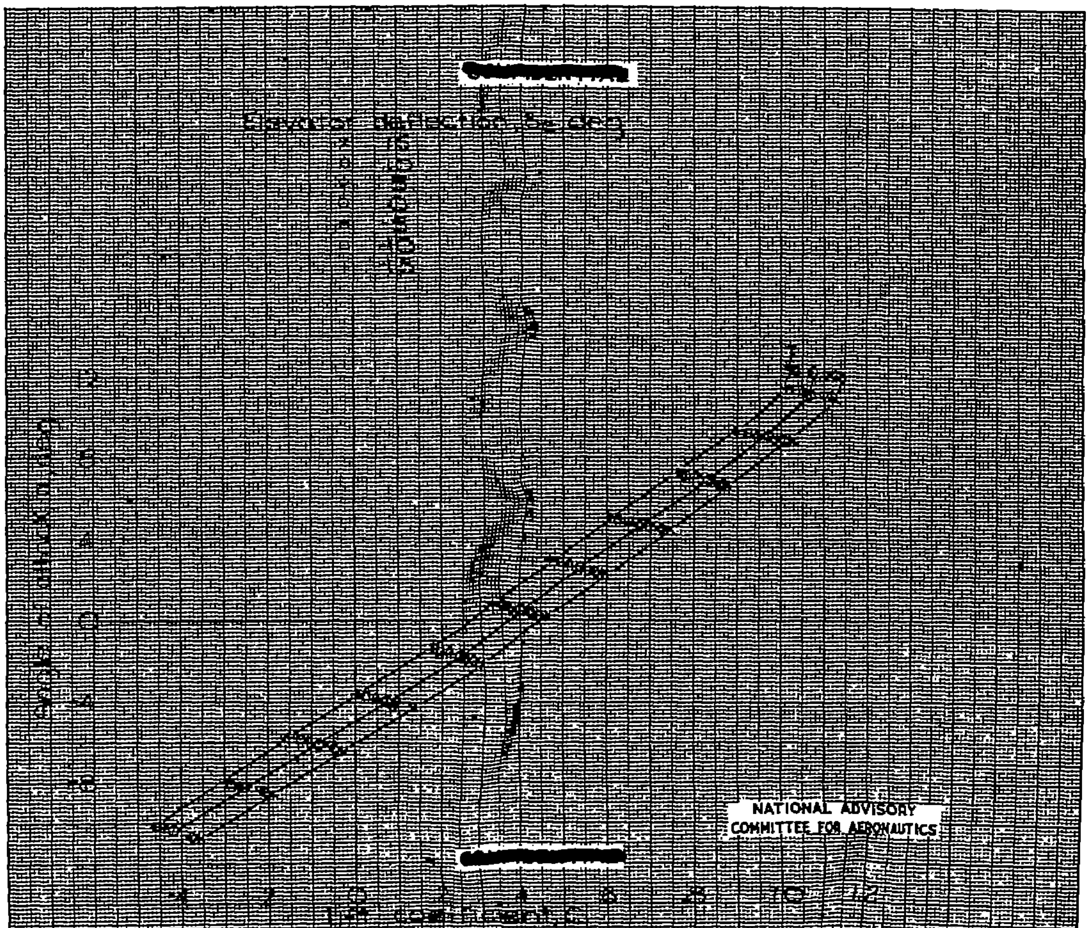

Figure 12.- Effect of elevator deflection on the aerodynamic characteristics of the [illegible]-scale model of the [illegible] airplane. [illegible] q, [illegible] pounds per square foot; [illegible] thrust axis horizontal.

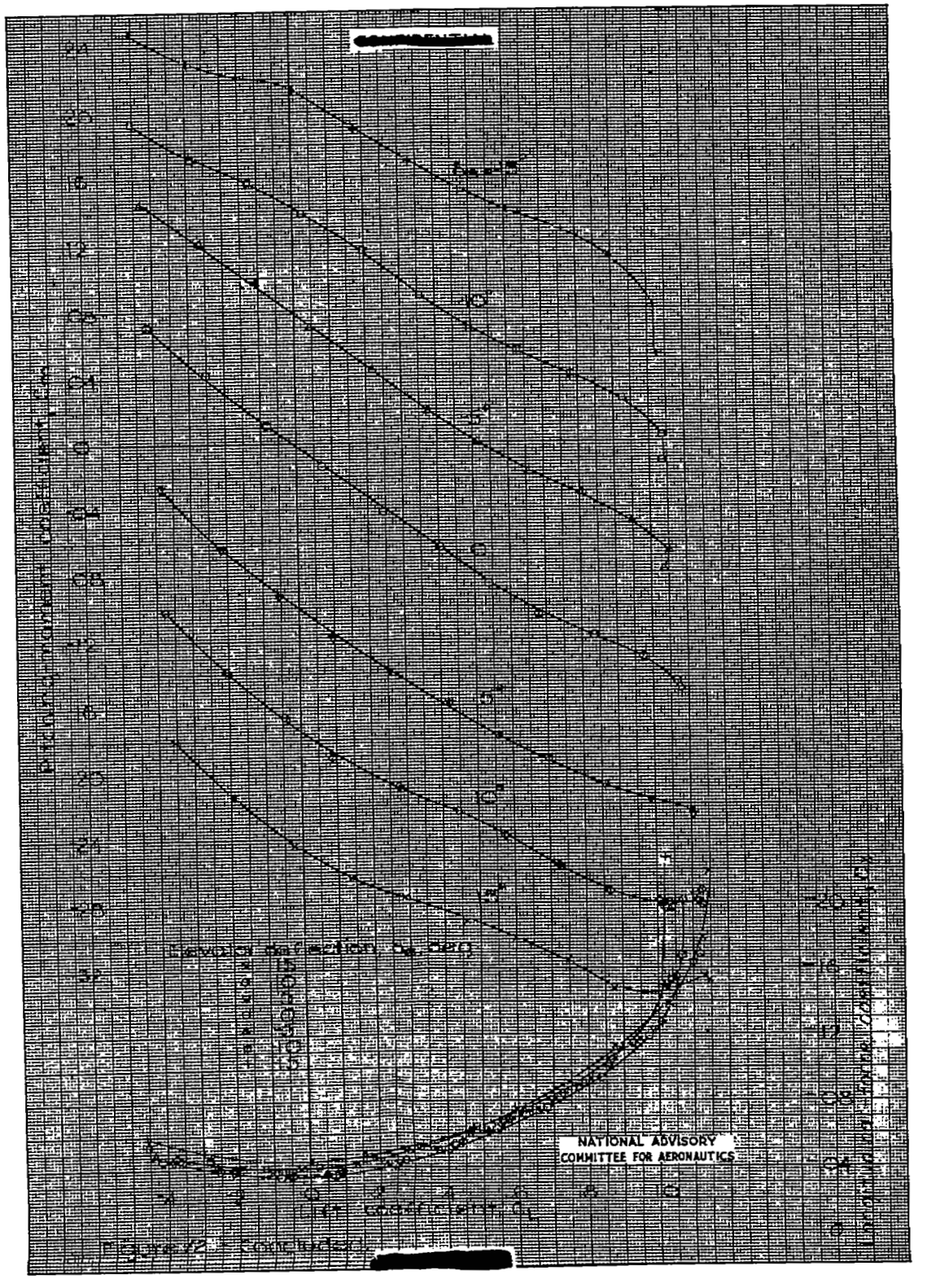

Figure 12.- Concluded.

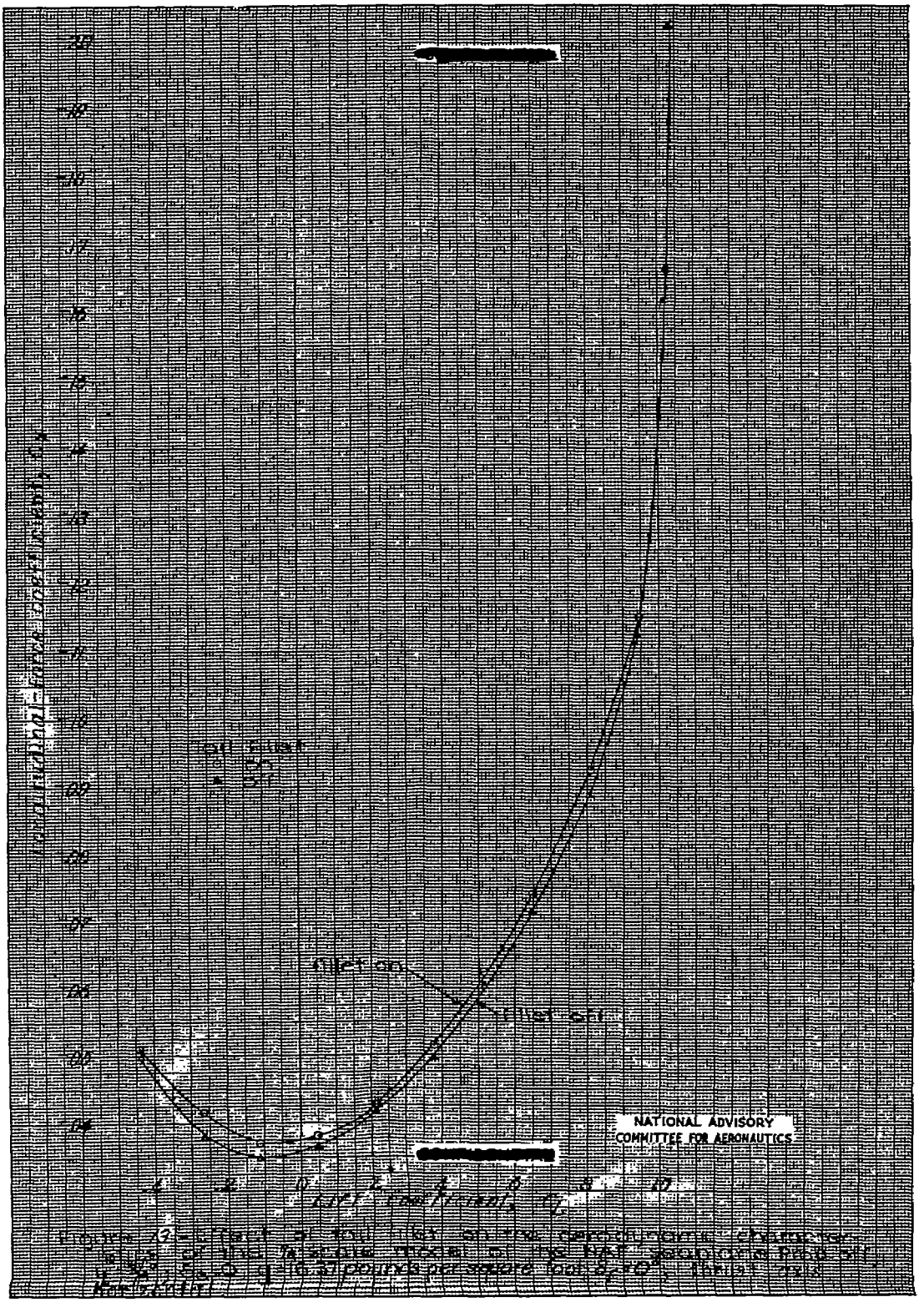
NATIONAL ADVISORY
COMMITTEE FOR AERONAUTICS

Fig. 13 conc.

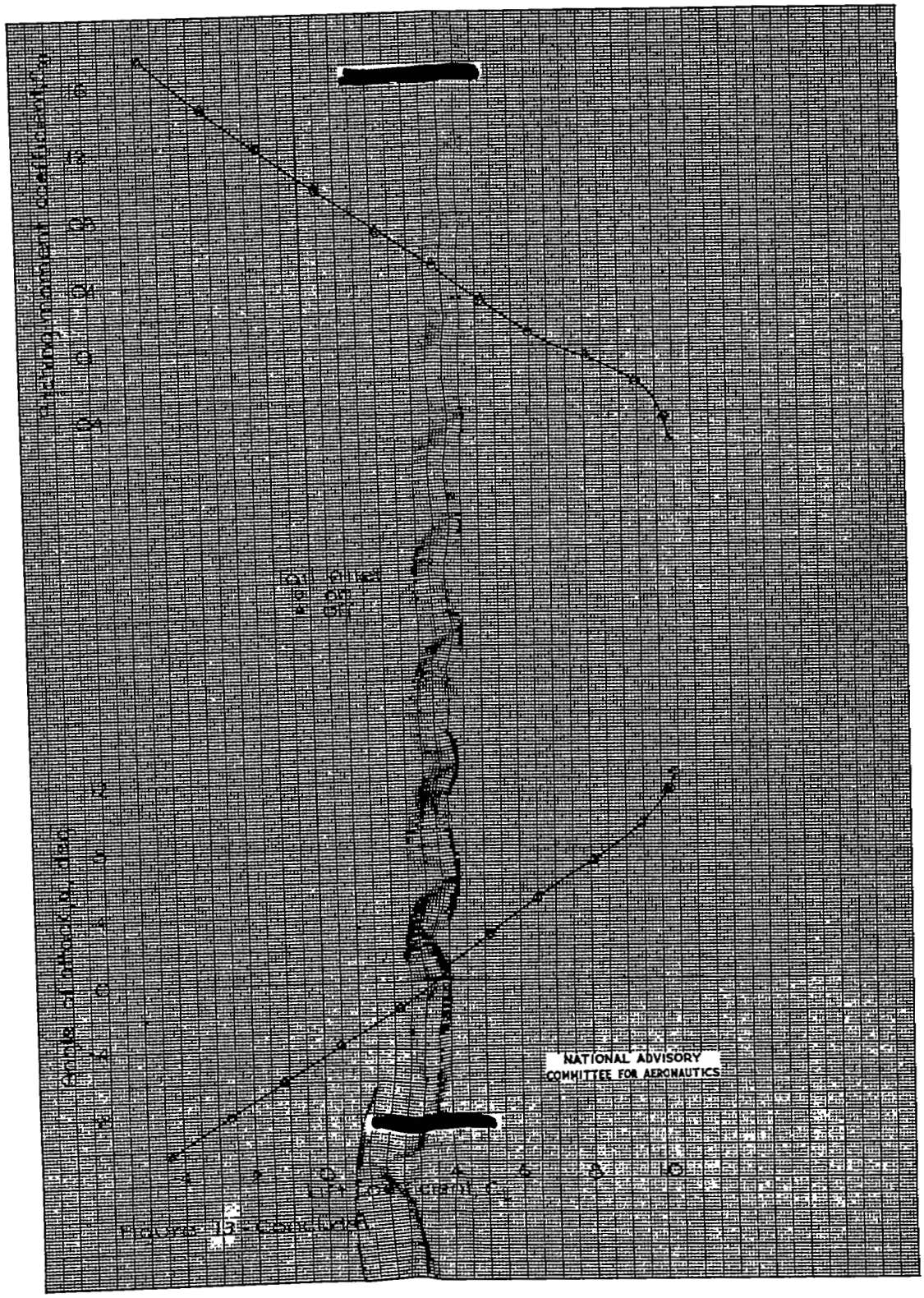

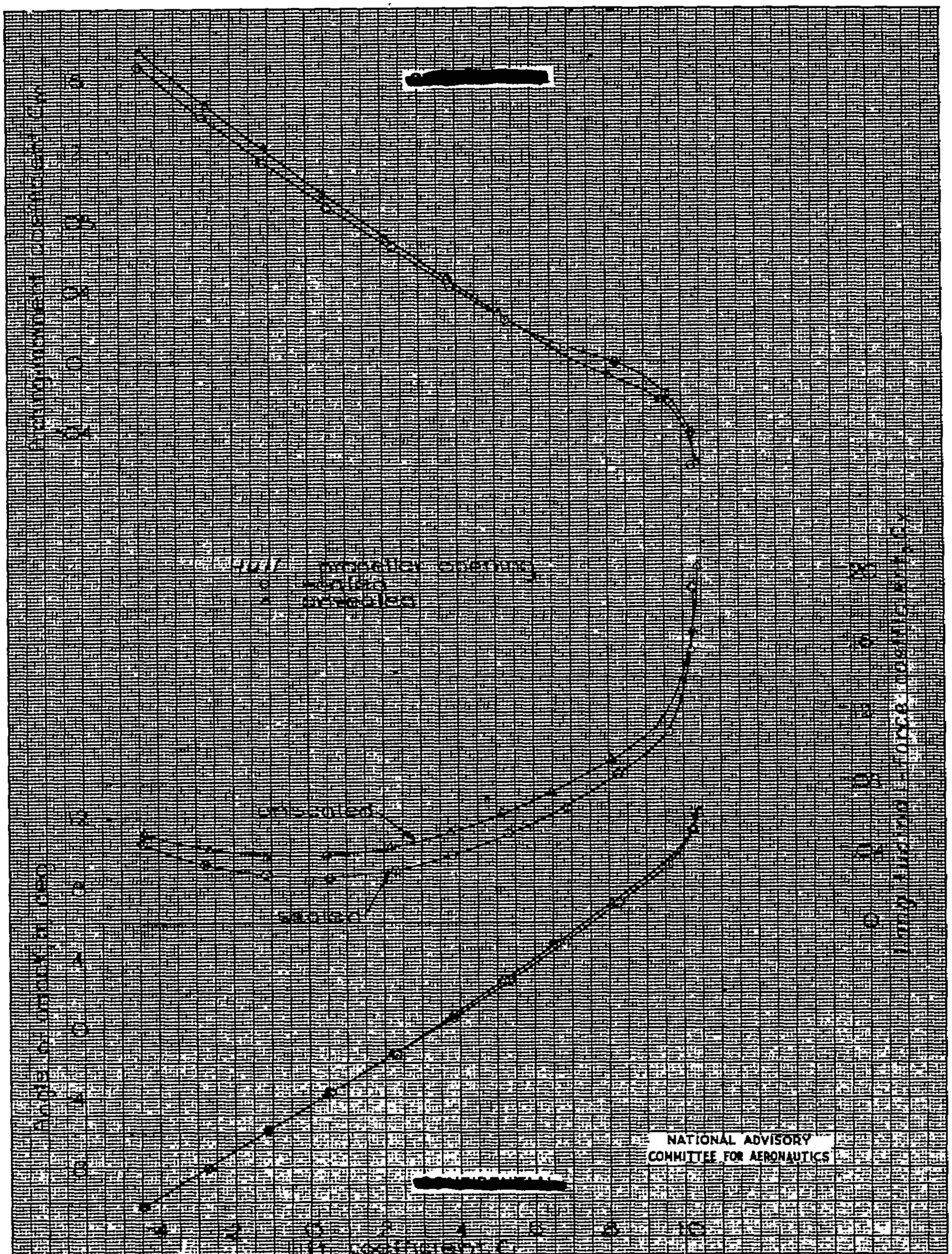

Figure 14- Effect of sealing hull propeller opening on the 1/6 scale model of the NAF Seaplane Prop off; $\delta_e = 0$; q 6.3 pounds per square foot, δ_f 0°; thrust axis horizontal.

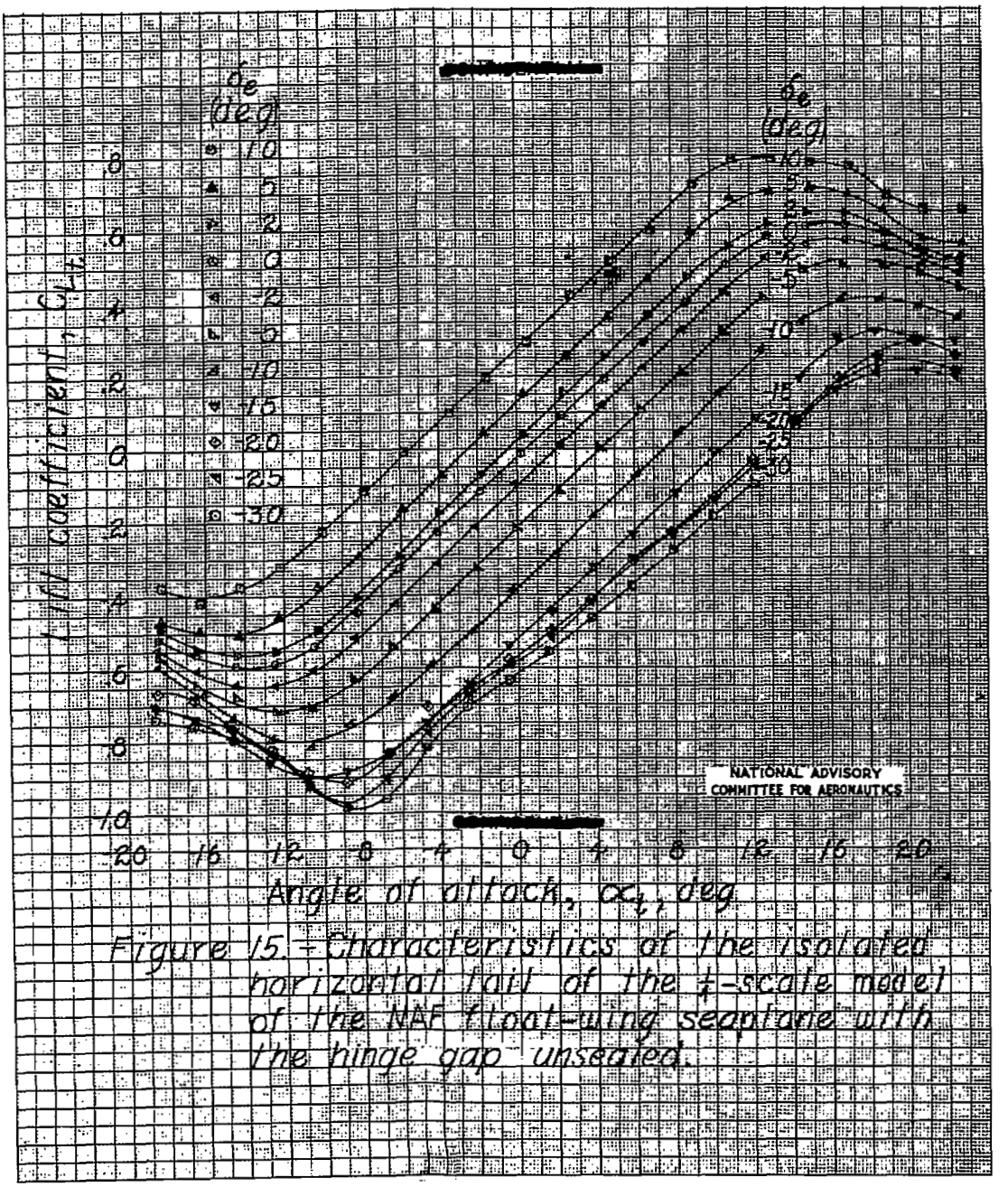

Figure 15.- Characteristics of the isolated horizontal tail of the 1/4-scale model of the NAF float-wing seaplane with the hinge gap unsealed.

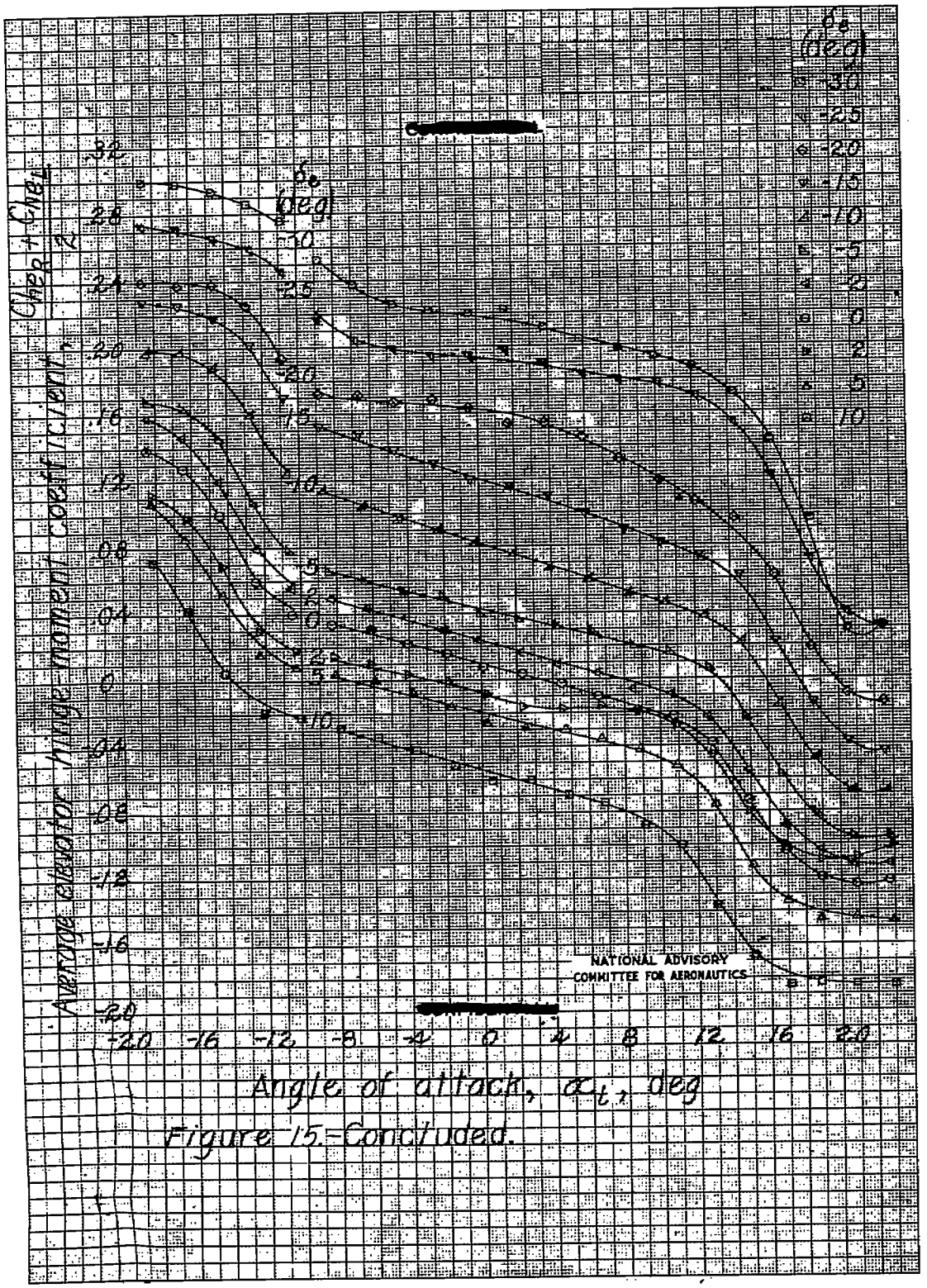

Figure 15.- Concluded.

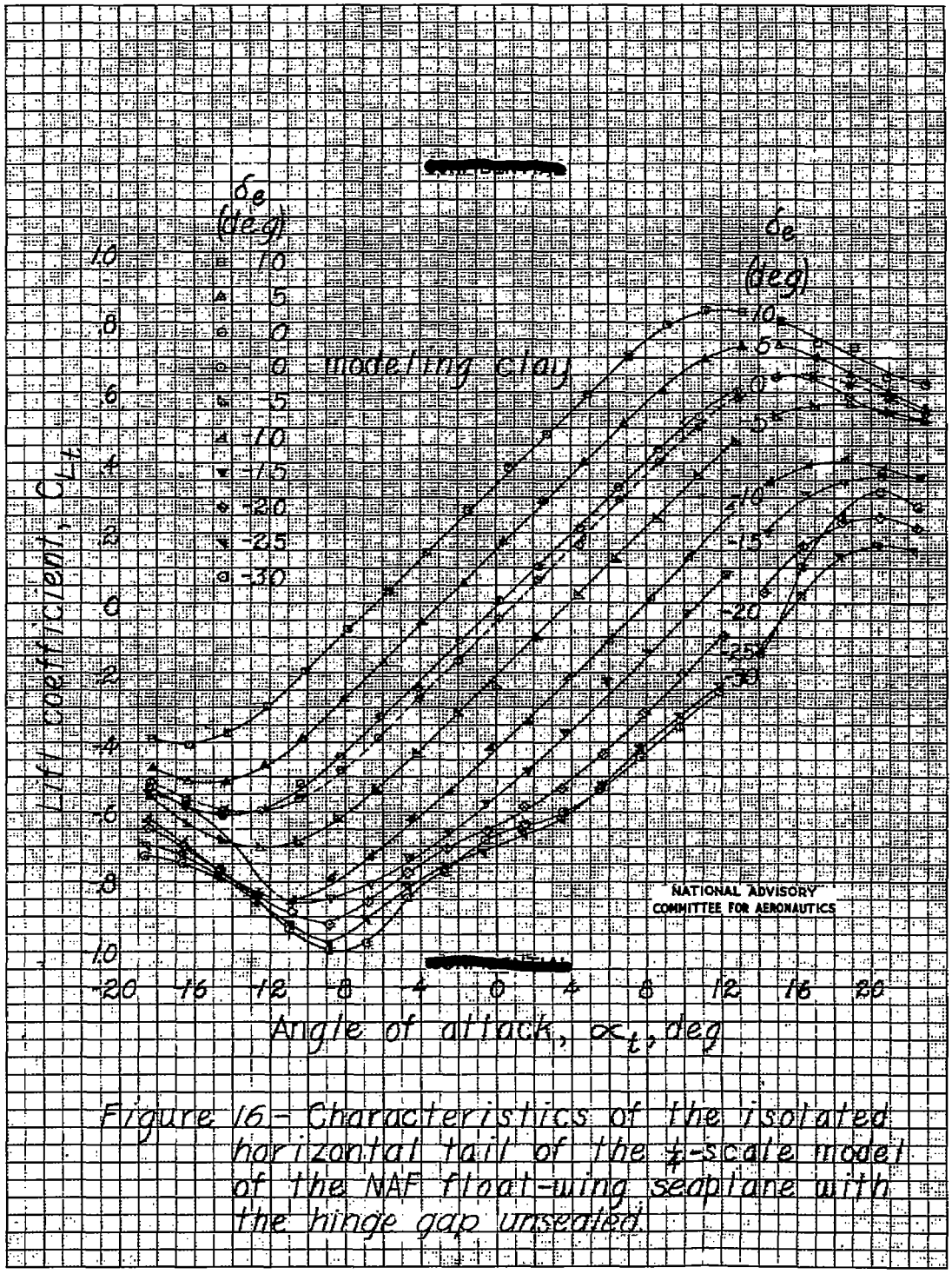

Figure 16 - Characteristics of the isolated horizontal tail of the $\frac{1}{4}$-scale model of the NAF float-wing seaplane with the hinge gap unsealed.

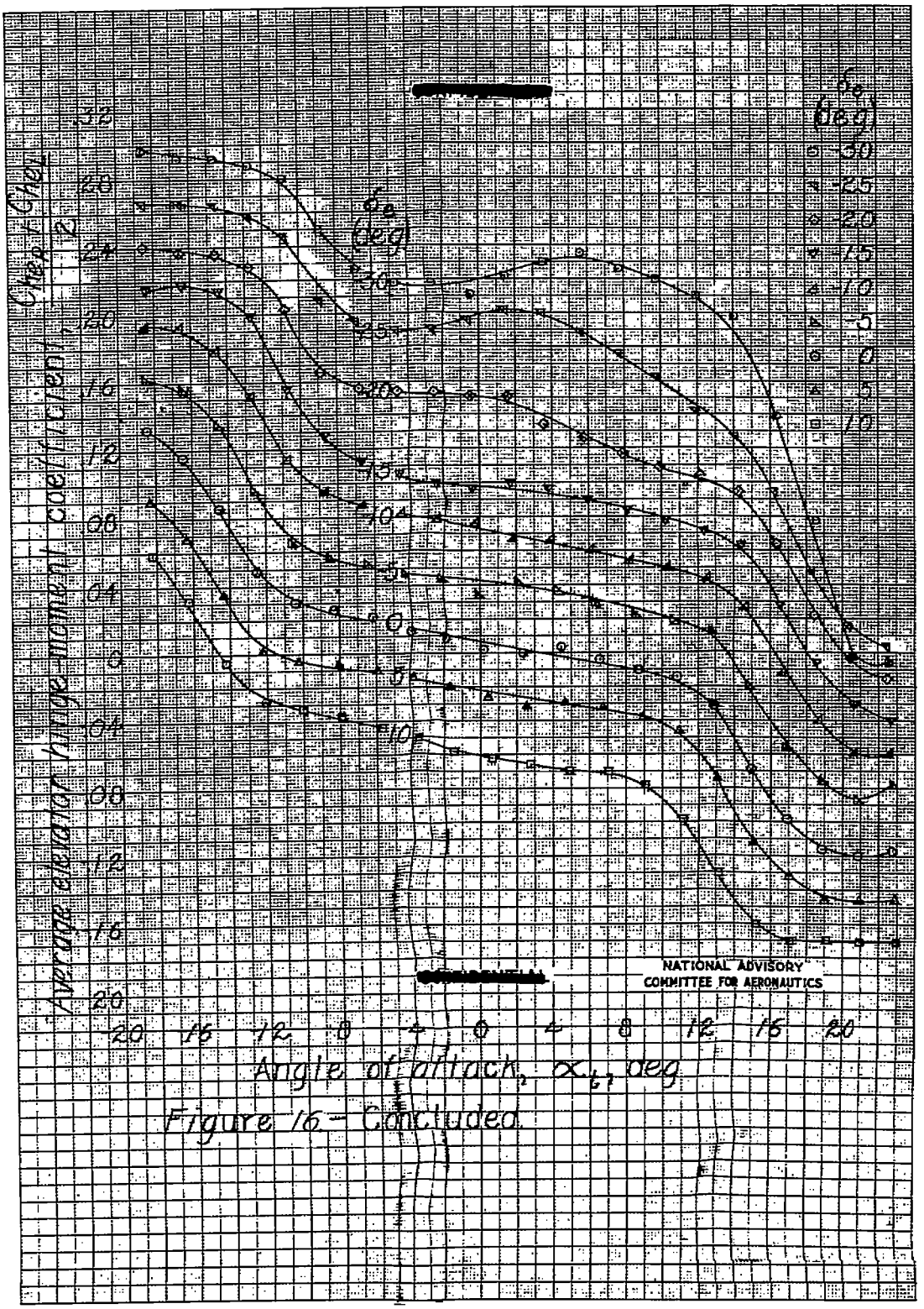

Figure 16 - Concluded

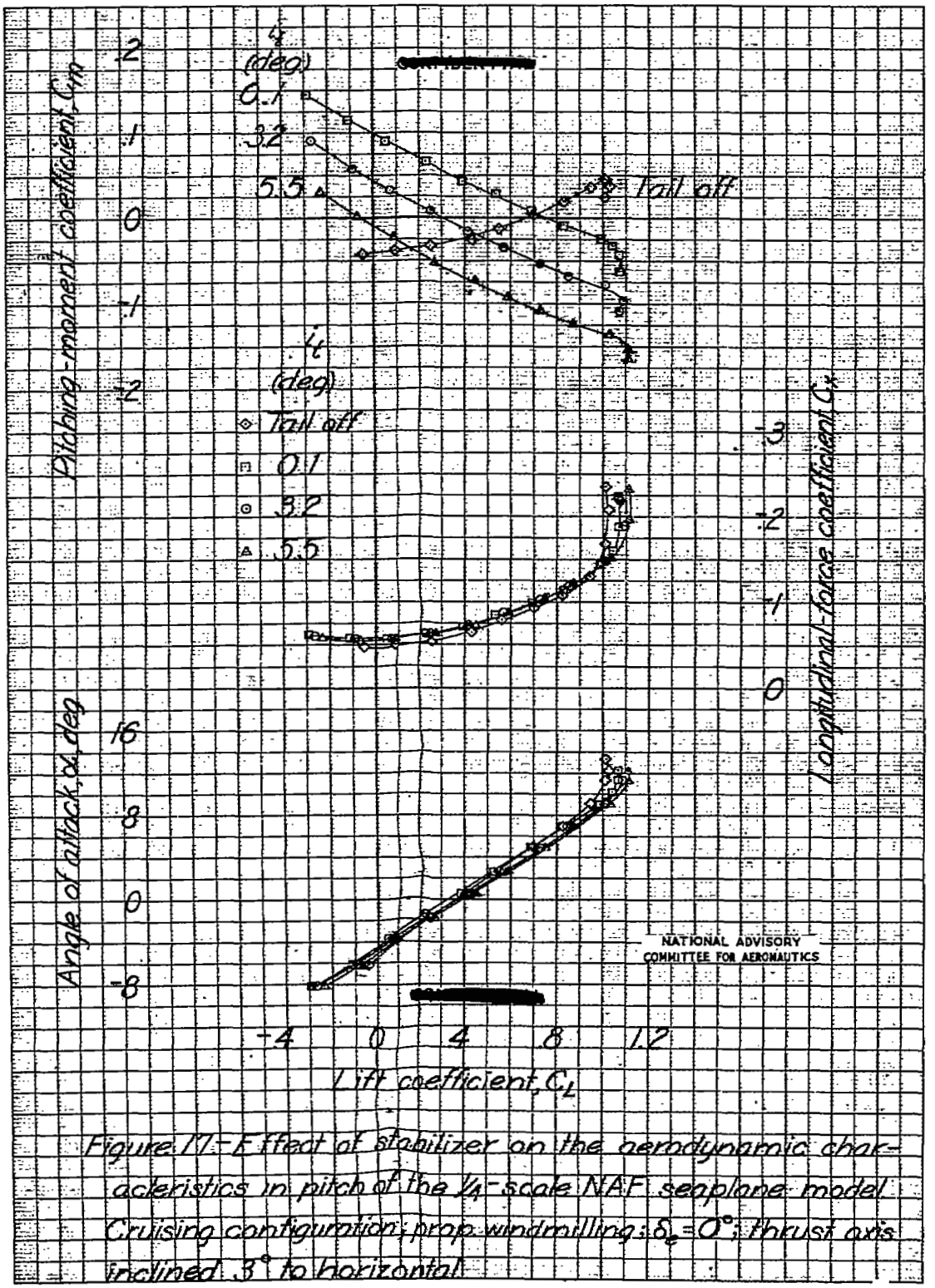

Figure 17.- Effect of stabilizer on the aerodynamic characteristics in pitch of the 1/4-scale NAF seaplane model. Cruising configuration; prop. windmilling; $\delta_e = 0°$; thrust axis inclined 3° to horizontal.

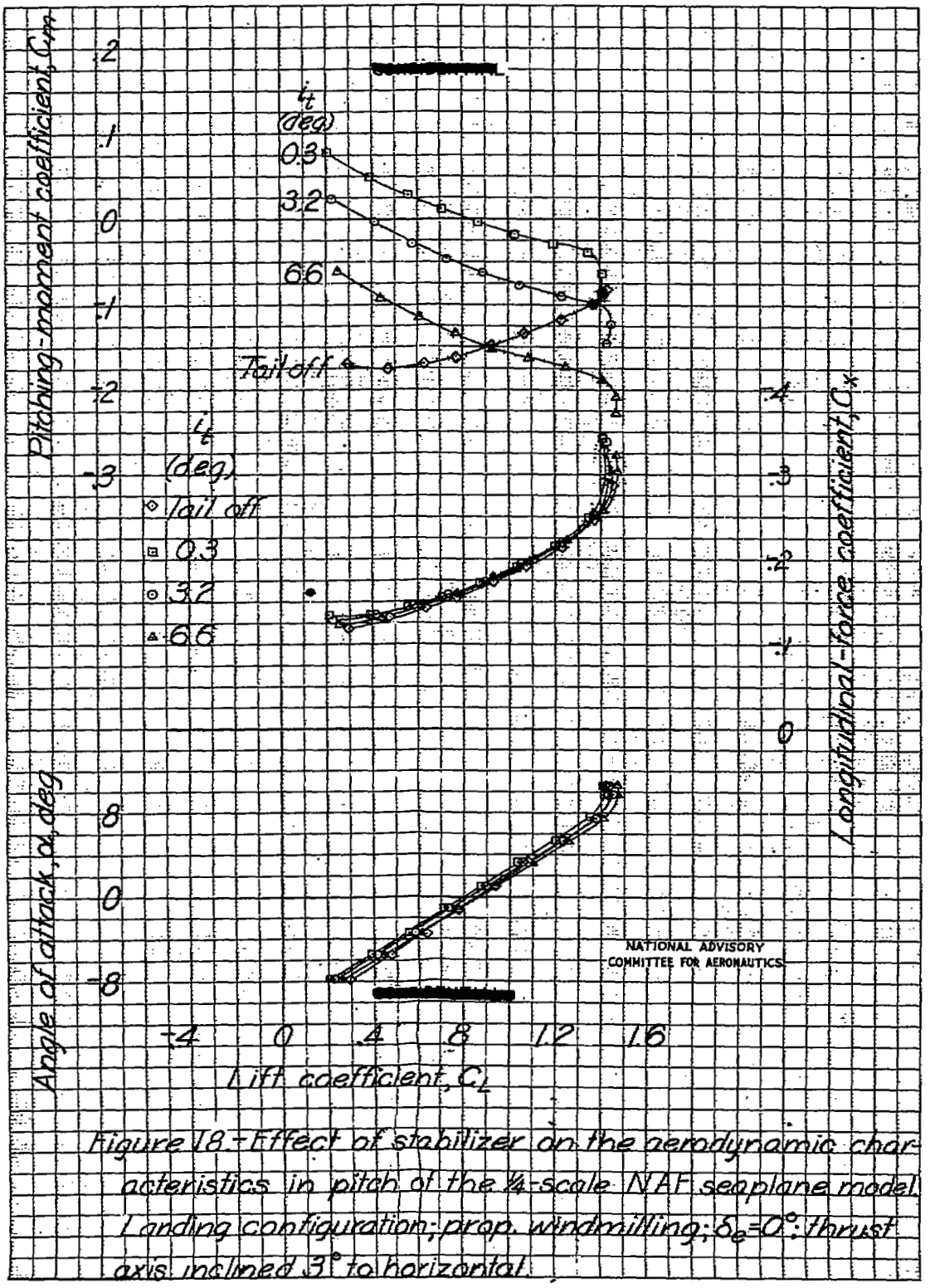

Figure 18.- Effect of stabilizer on the aerodynamic characteristics in pitch of the ¼-scale NAF seaplane model. Landing configuration; prop. windmilling; $\delta_e = 0°$; thrust axis inclined 3° to horizontal.

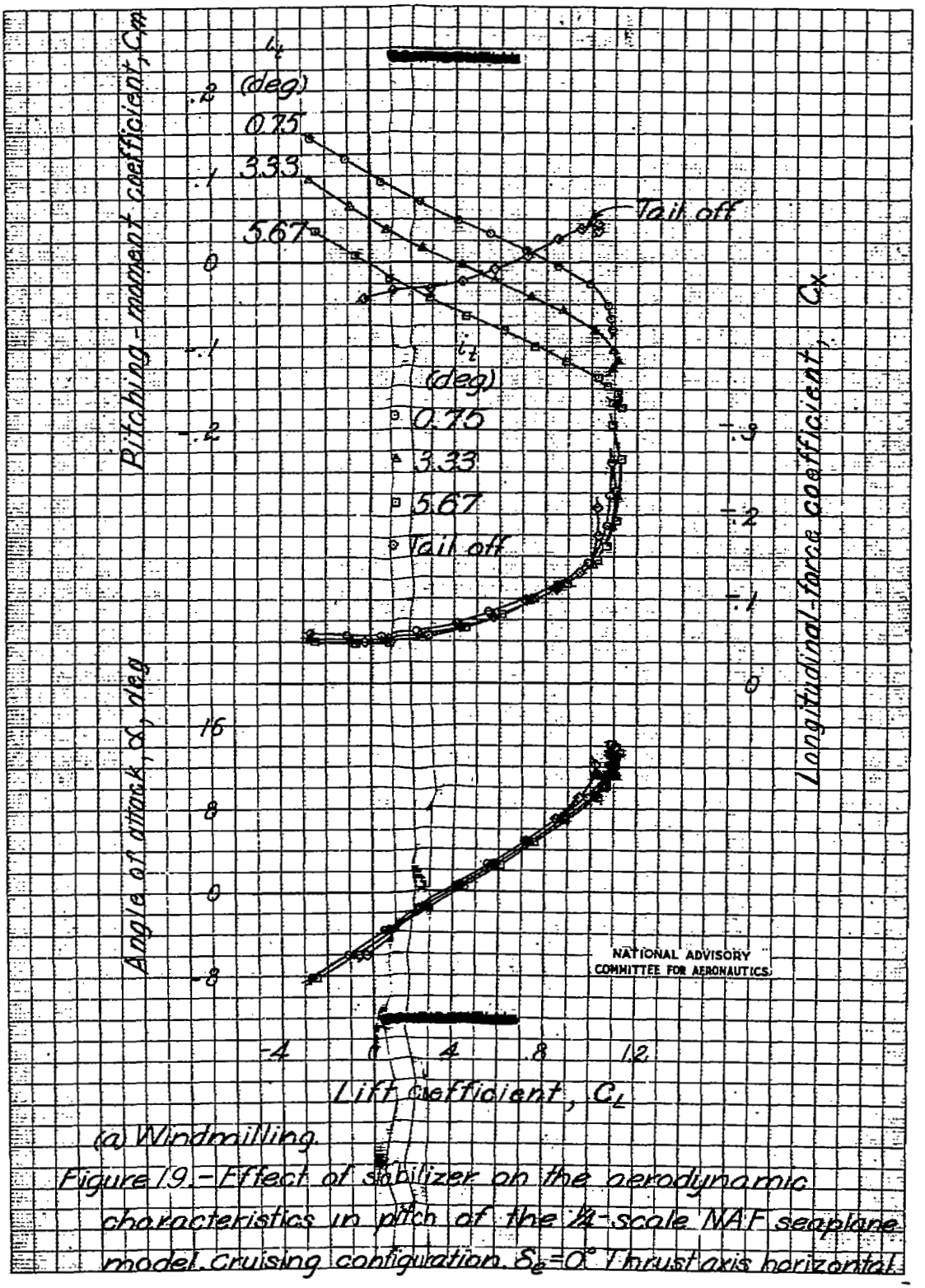

(a) Windmilling.

Figure 19.- Effect of stabilizer on the aerodynamic characteristics in pitch of the ¼-scale MAF seaplane model. Cruising configuration. $\delta_e=0°$ Thrust axis horizontal.

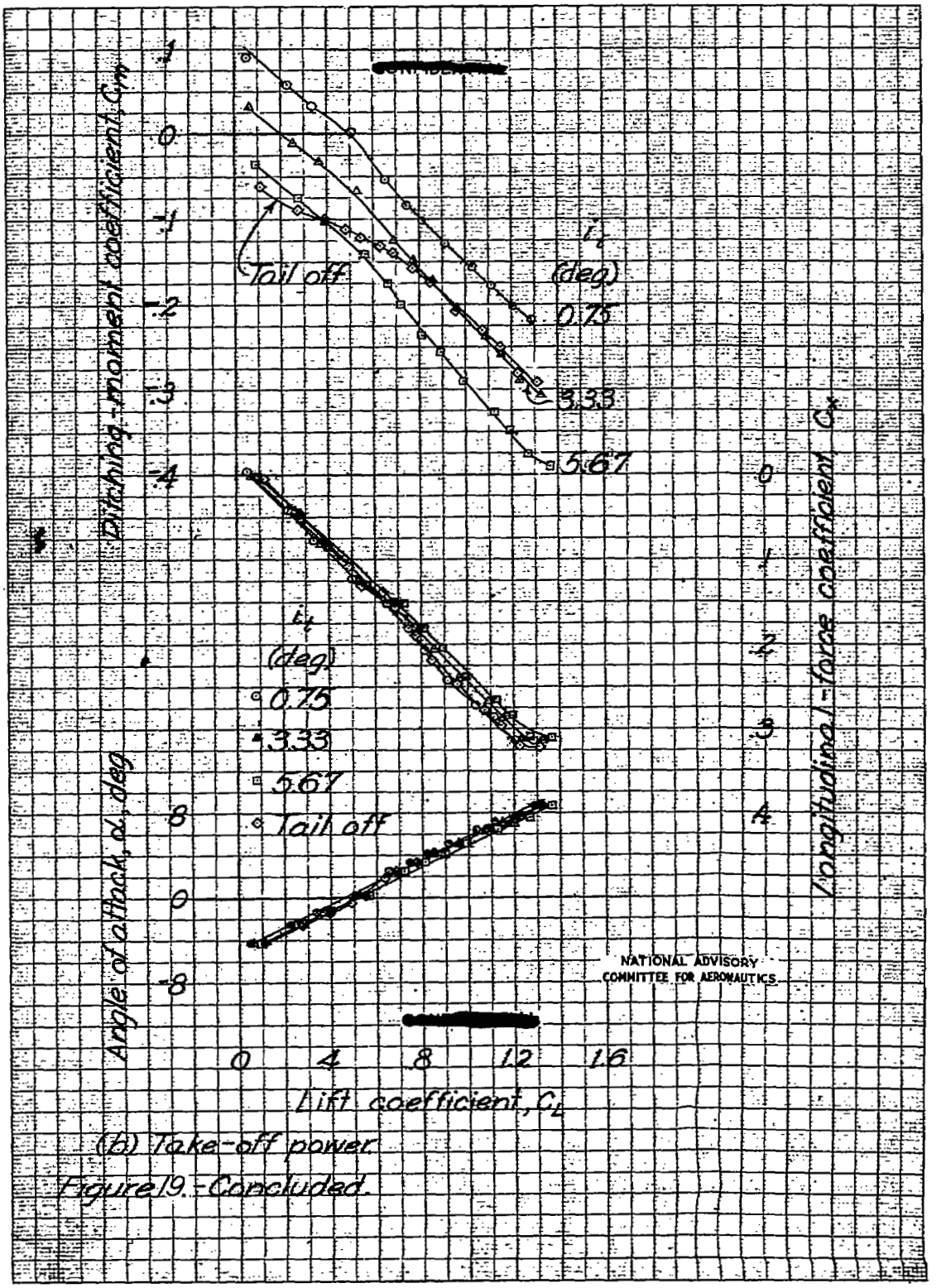

(b) Take-off power.

Figure 19.- Concluded.

Fig. 20a

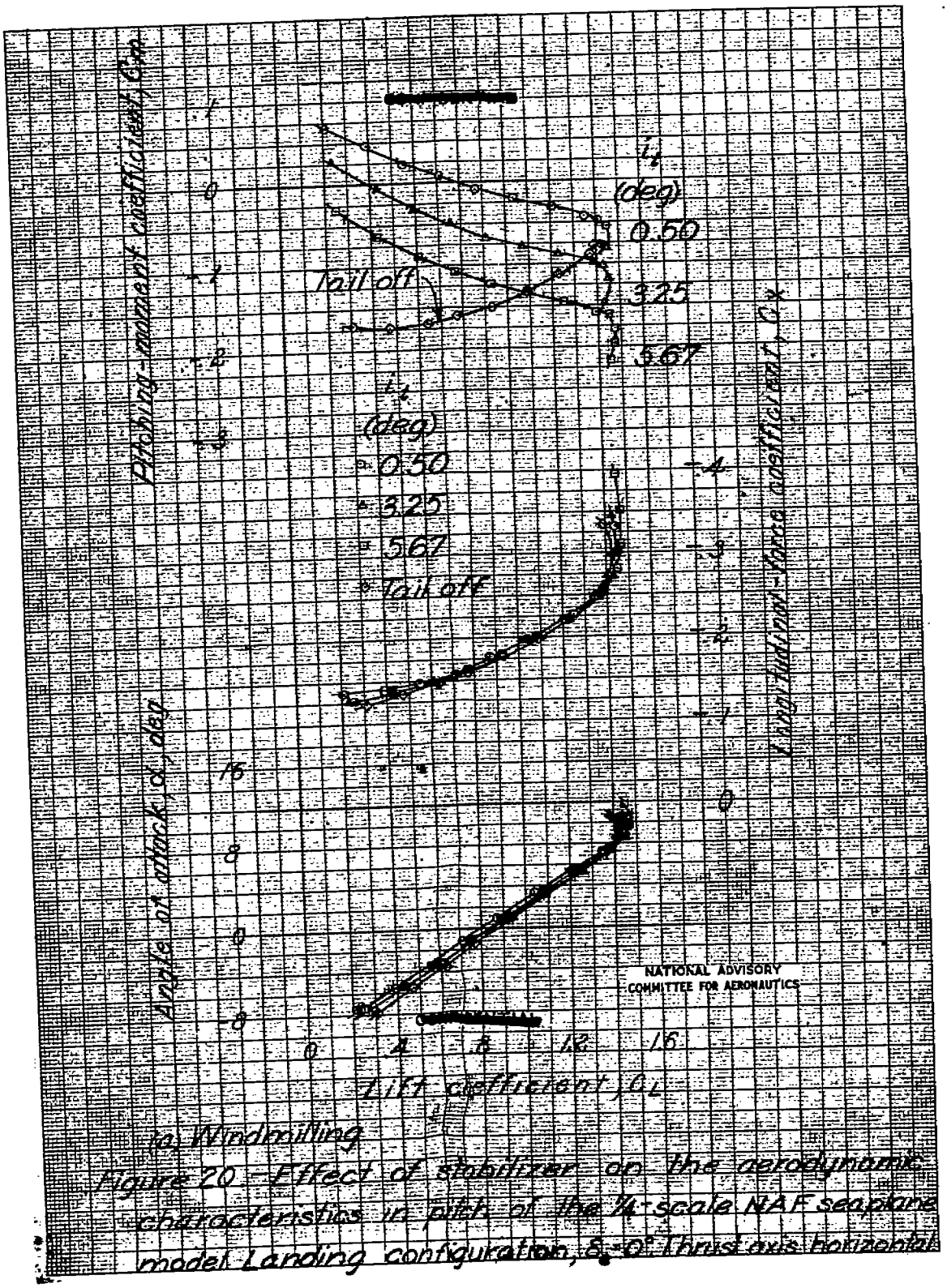

(a) Windmilling

Figure 20.- Effect of stabilizer on the aerodynamic characteristics in pitch of the ¼-scale NAF seaplane model. Landing configuration, $\delta_e = 0°$, thrust axis horizontal.

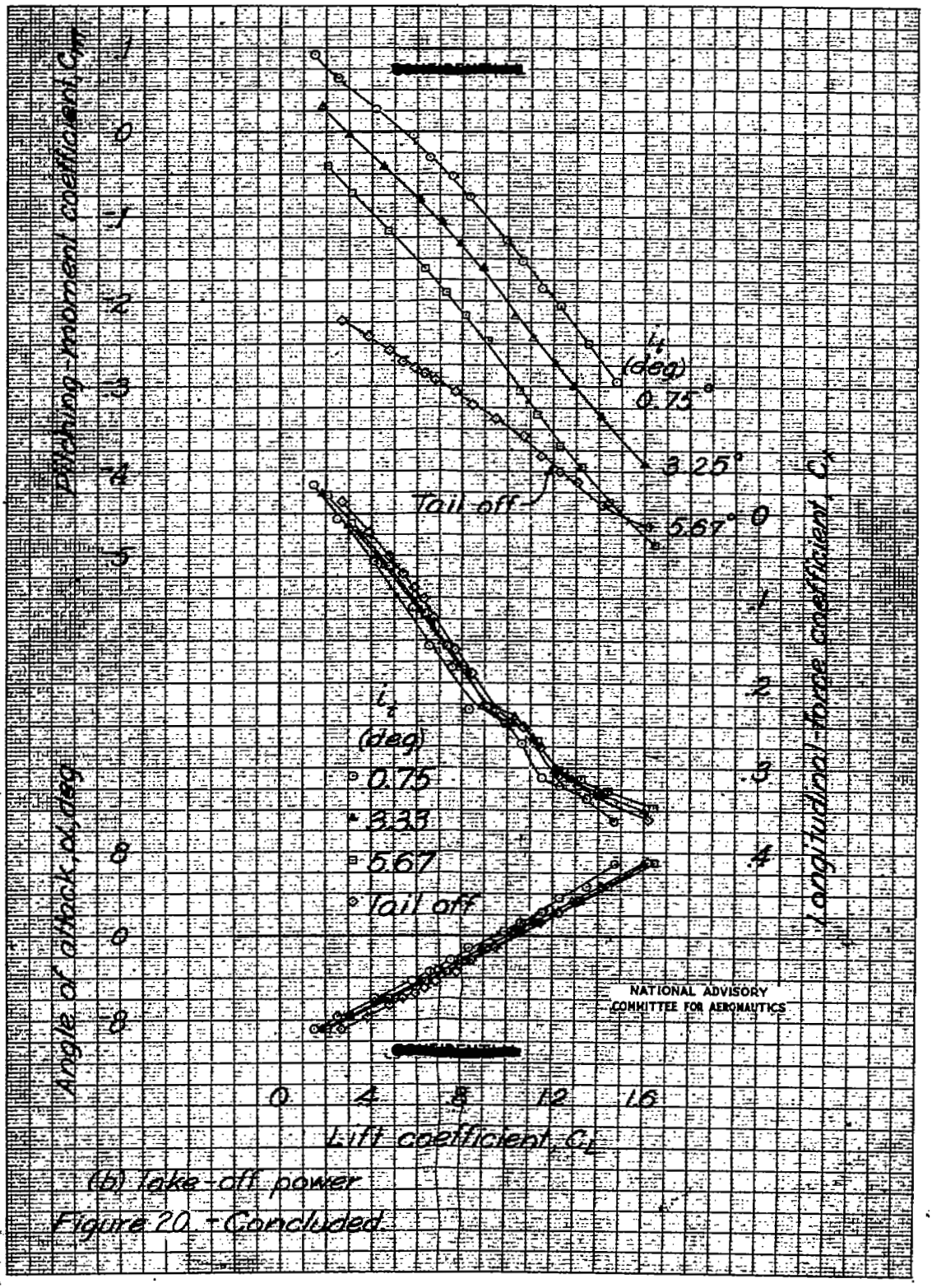

(b) Take-off power

Figure 20.- Concluded.

[redacted]

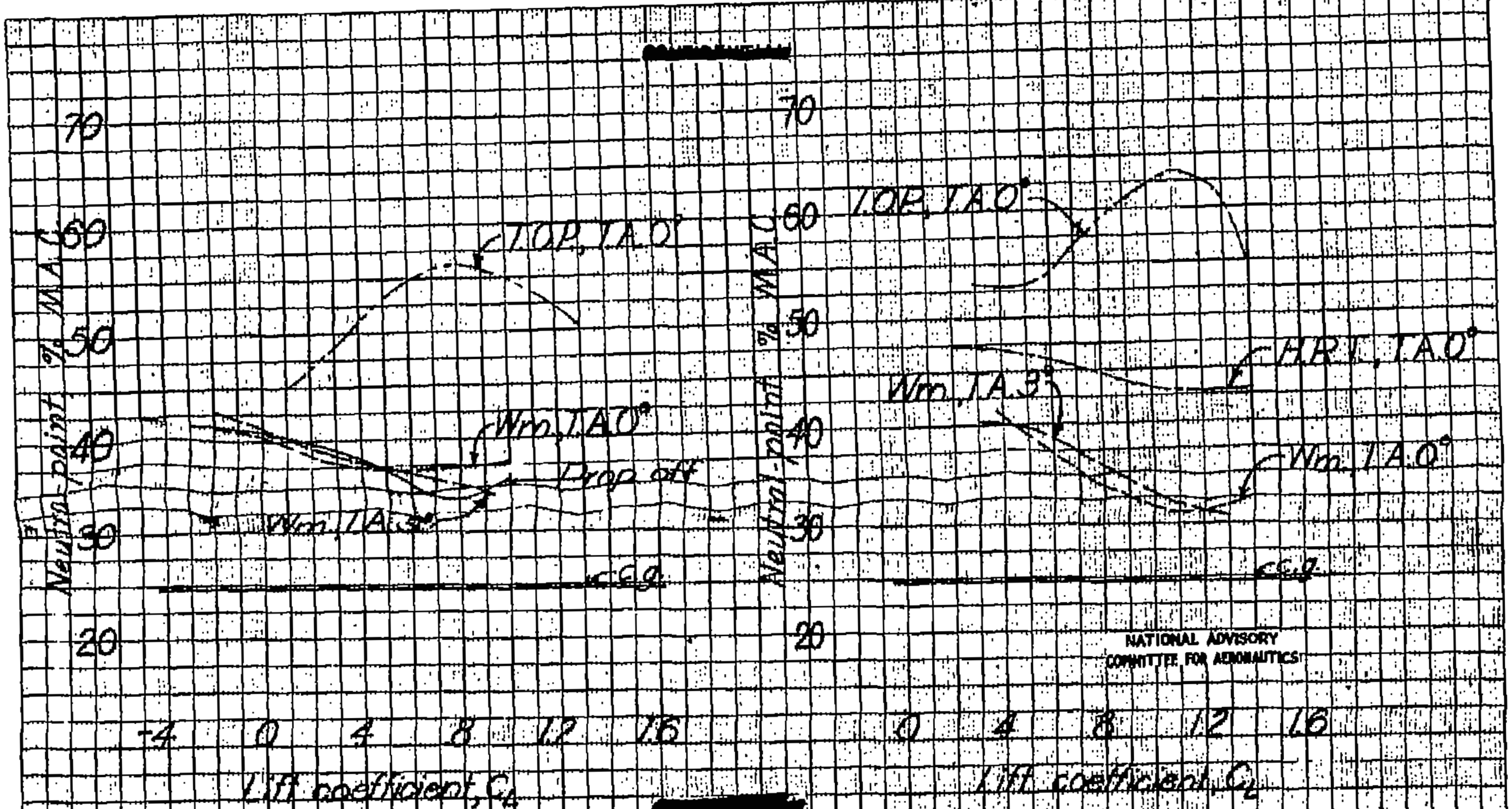

(a) Cruising configuration

(b) Landing configuration

[redacted]

Figure 21.- Effect of power, model configuration, and thrust axis inclination on the elevator fixed neutral point location and on the effective tail-off aerodynamic center location of 1/4-scale model of the N.A.F. seaplane.

19421

[redacted]

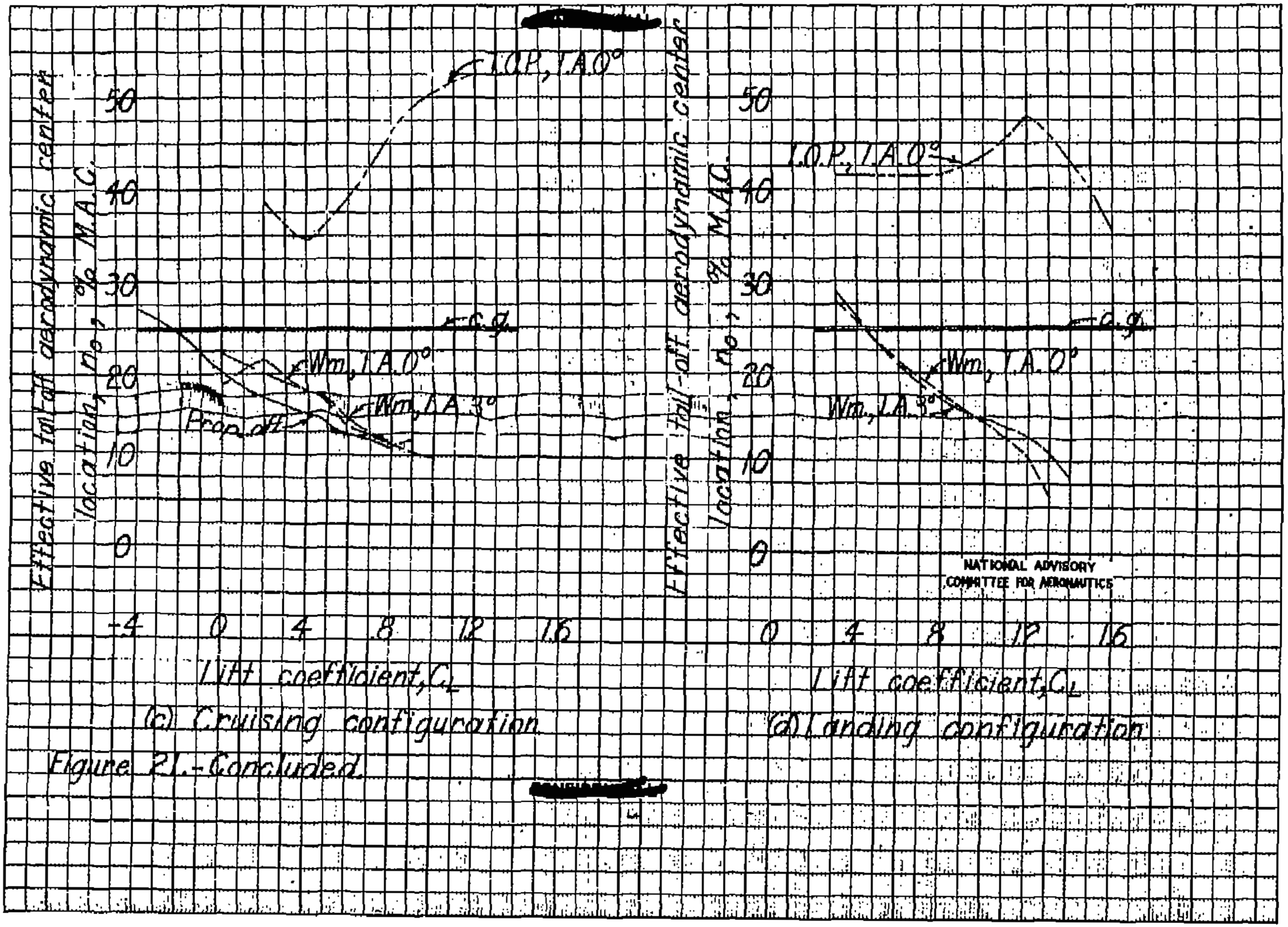

Figure 21.- Concluded.

[redacted]

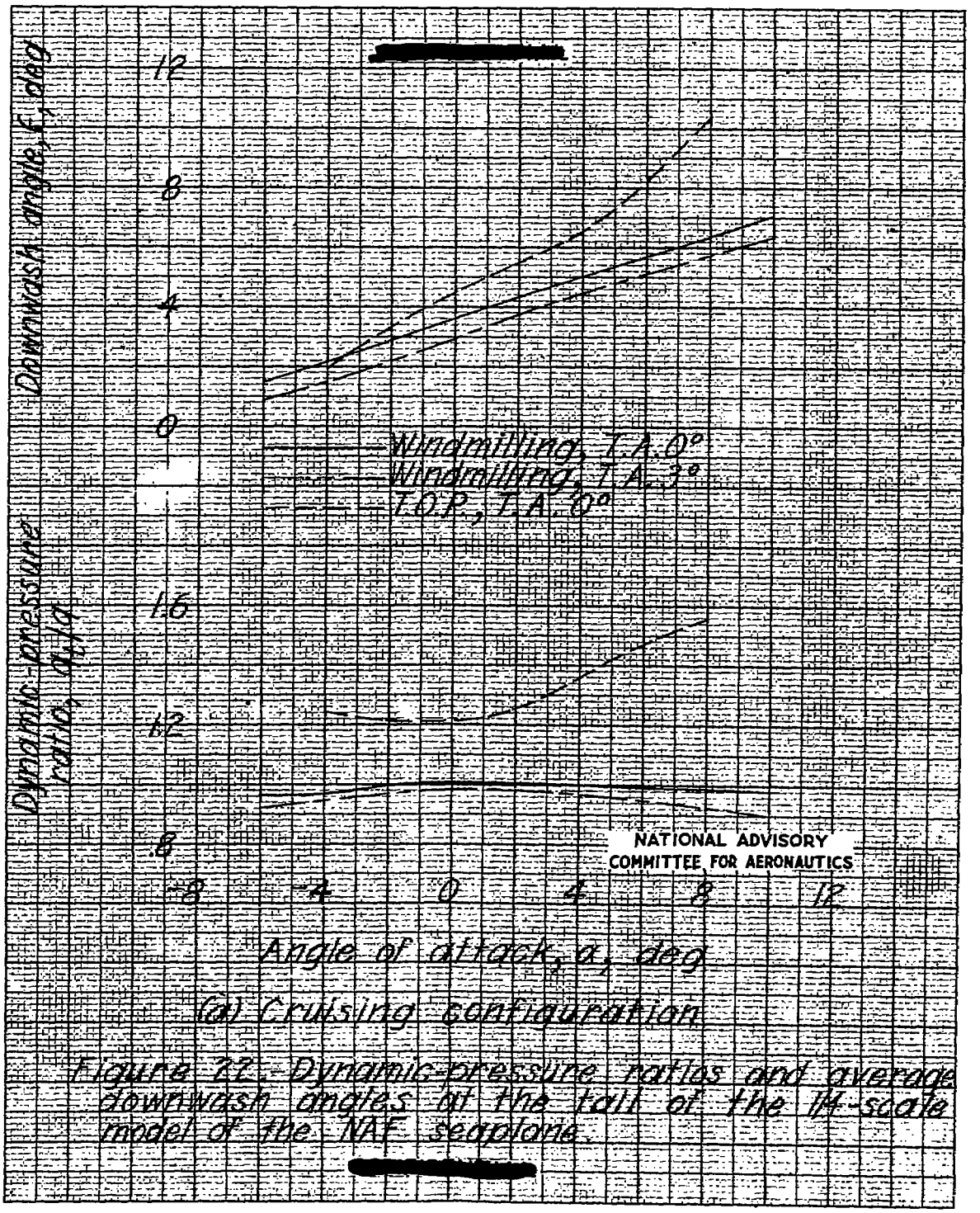

(a) Cruising configuration

Figure 22.- Dynamic-pressure ratios and average downwash angles at the tail of the 1/4-scale model of the NAF seaplane.

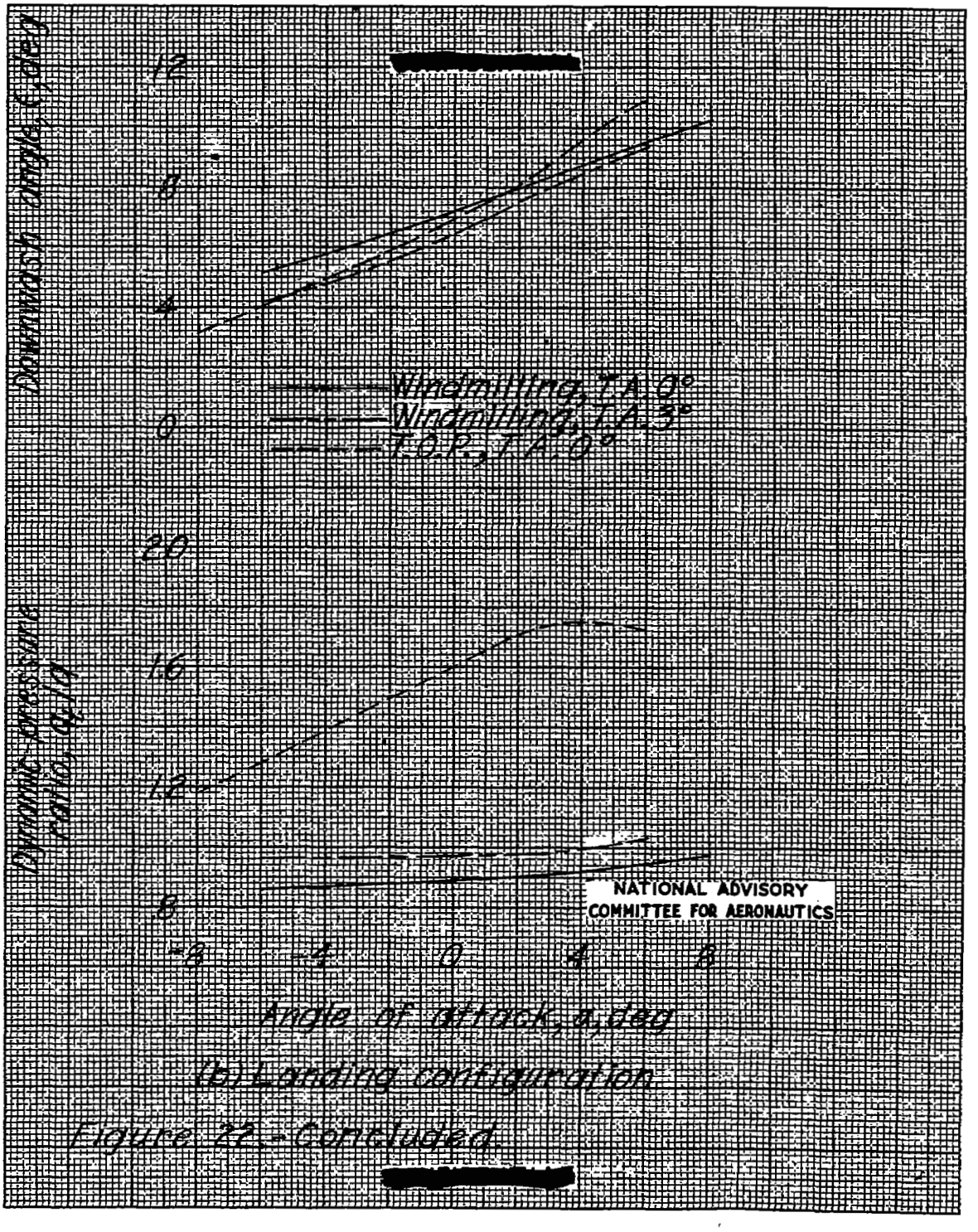

(b) Landing configuration

Figure 22.- Concluded.

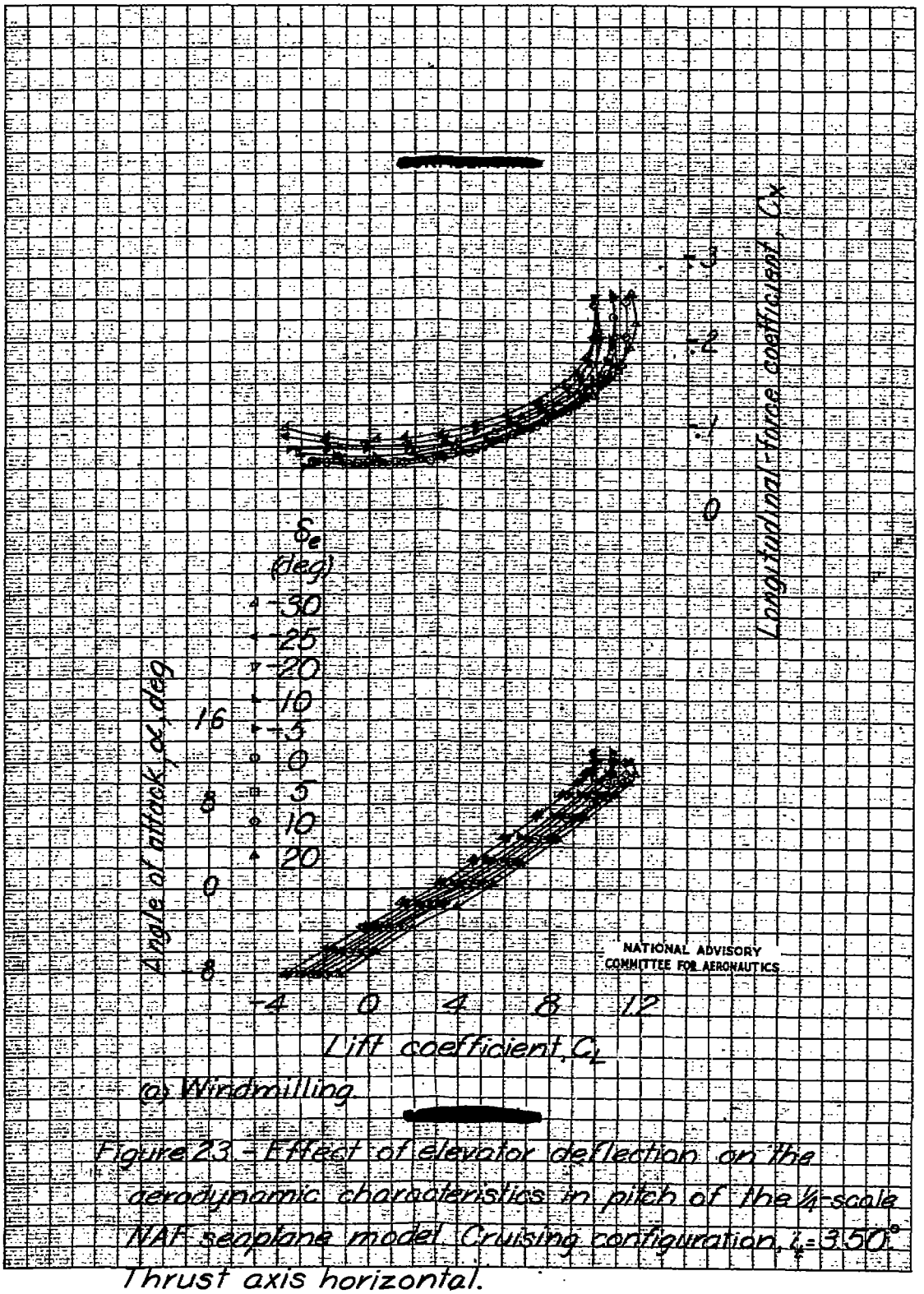

(a) Windmilling.

Figure 23.- Effect of elevator deflection on the aerodynamic characteristics in pitch of the ¼-scale NAF seaplane model. Cruising configuration, $i_t = 3.50°$. Thrust axis horizontal.

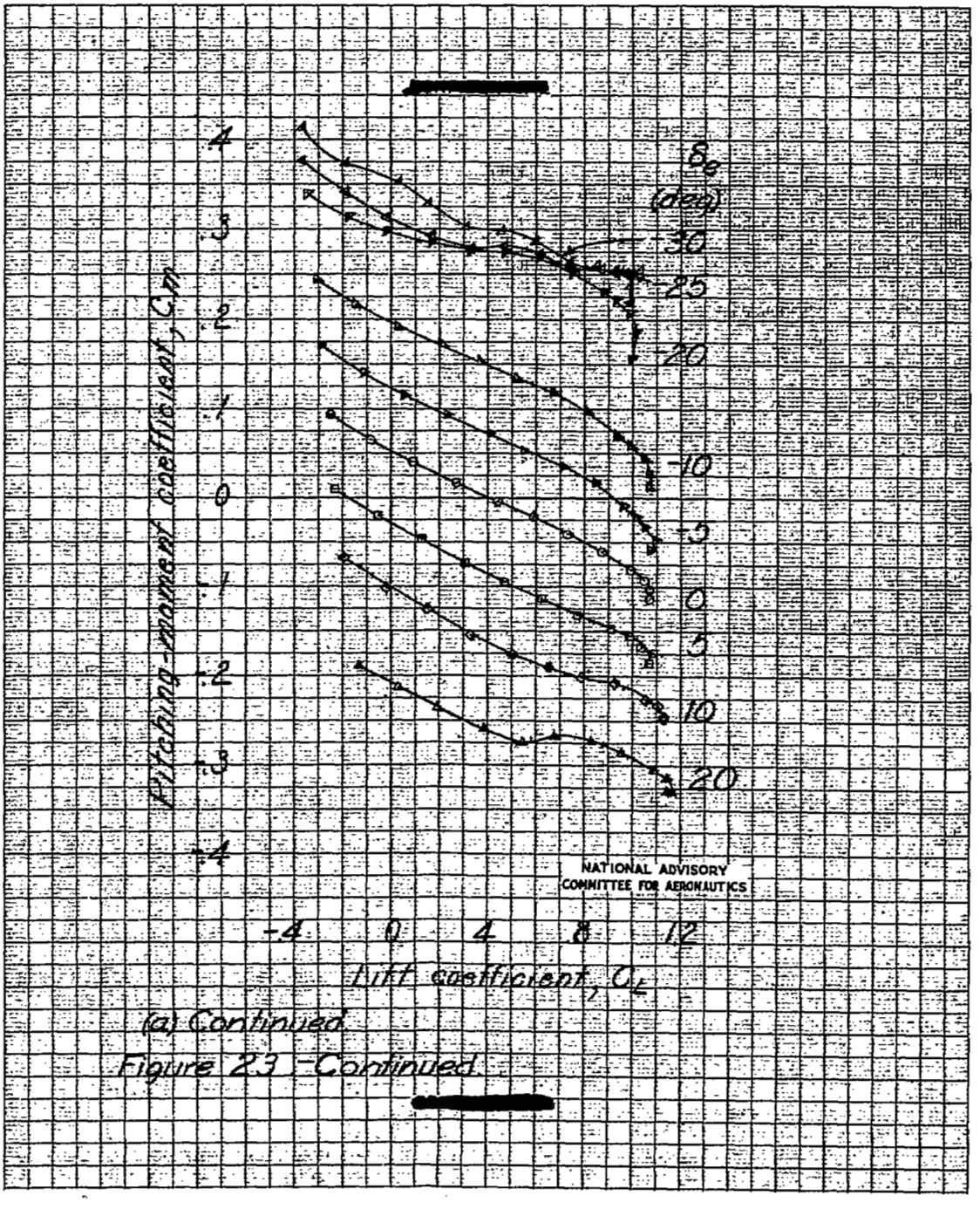

(a) Continued.

Figure 23 - Continued.

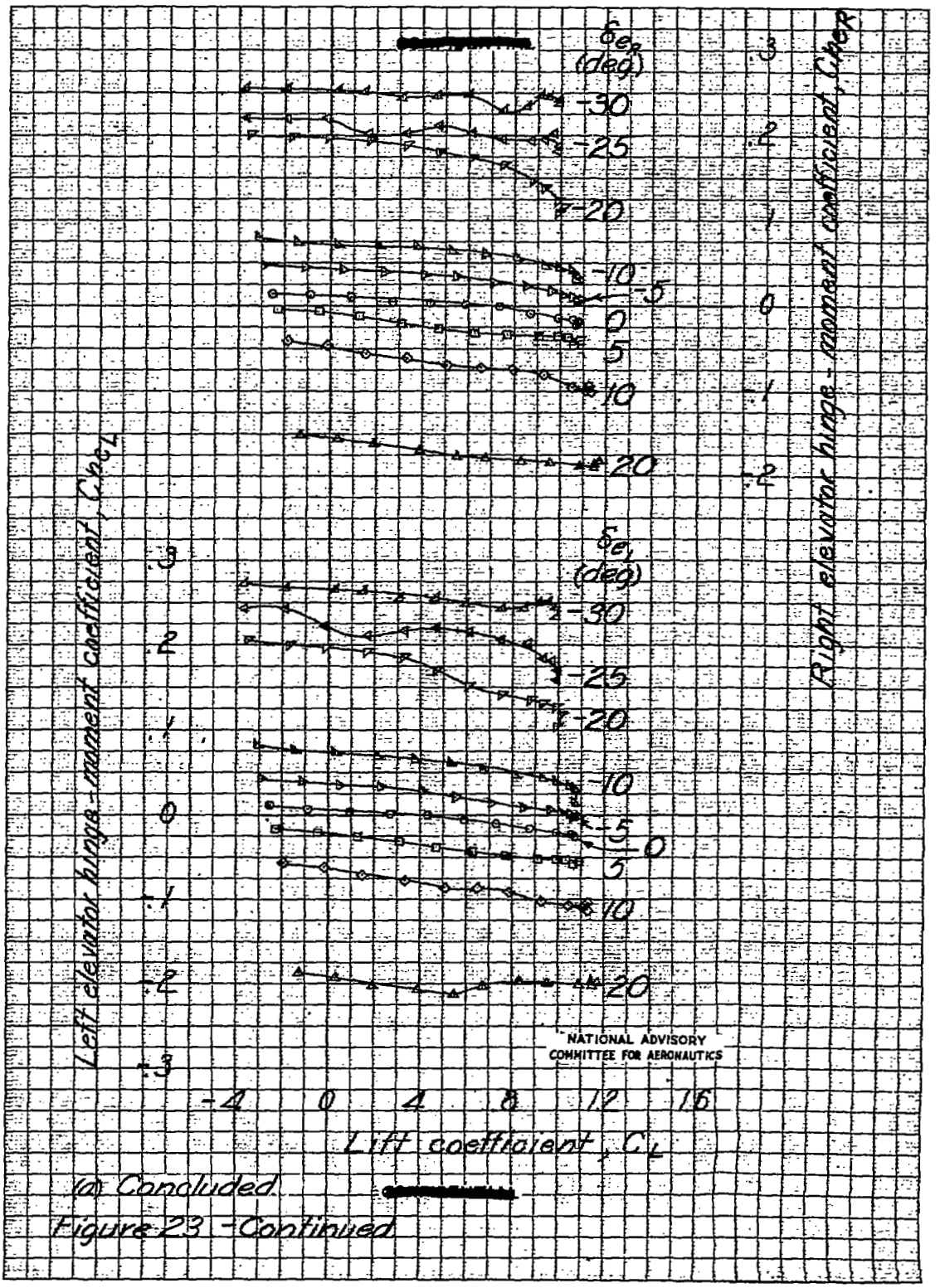

(a) Concluded.

Figure 23 - Continued

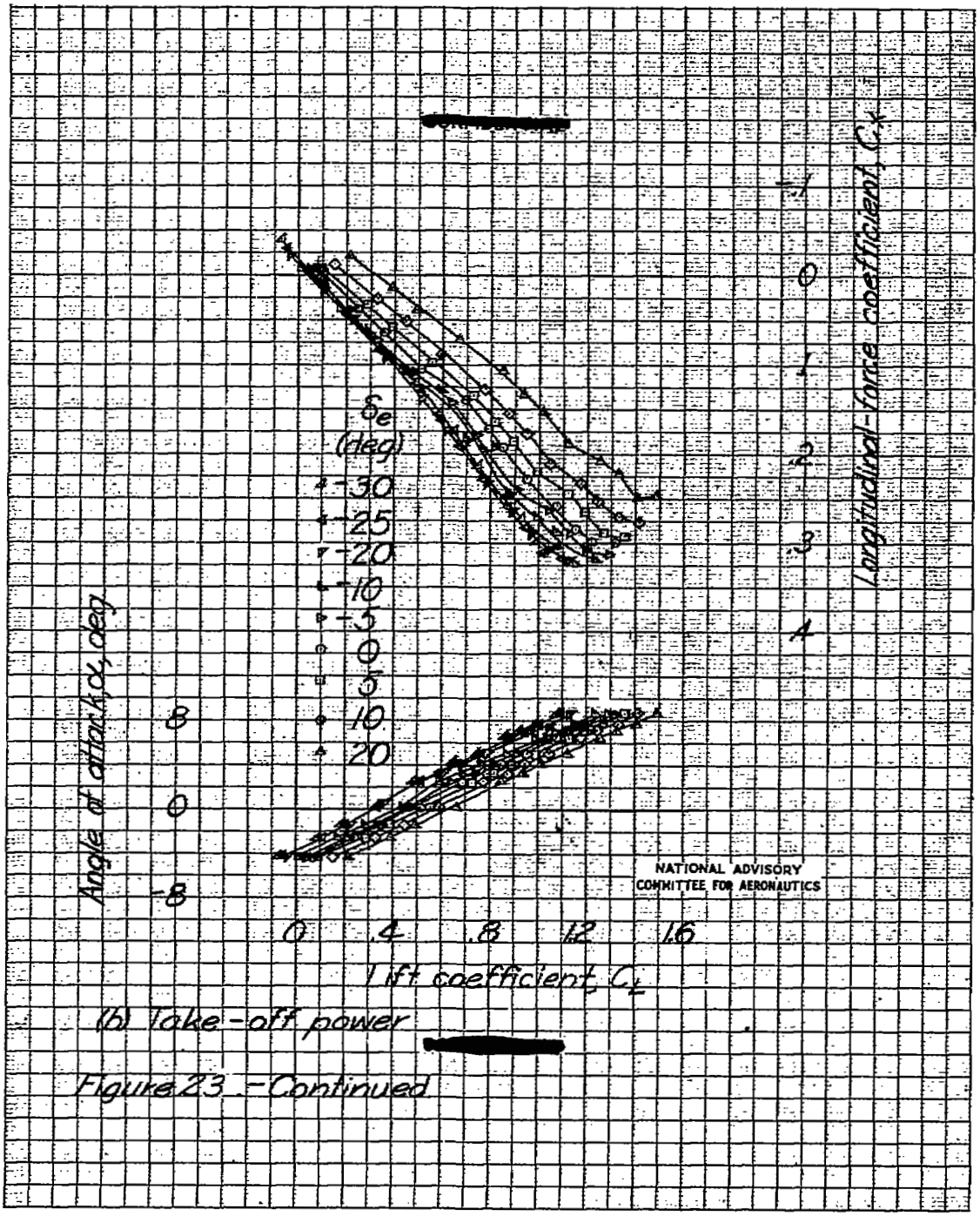

(b) Take-off power

Figure 23.- Continued

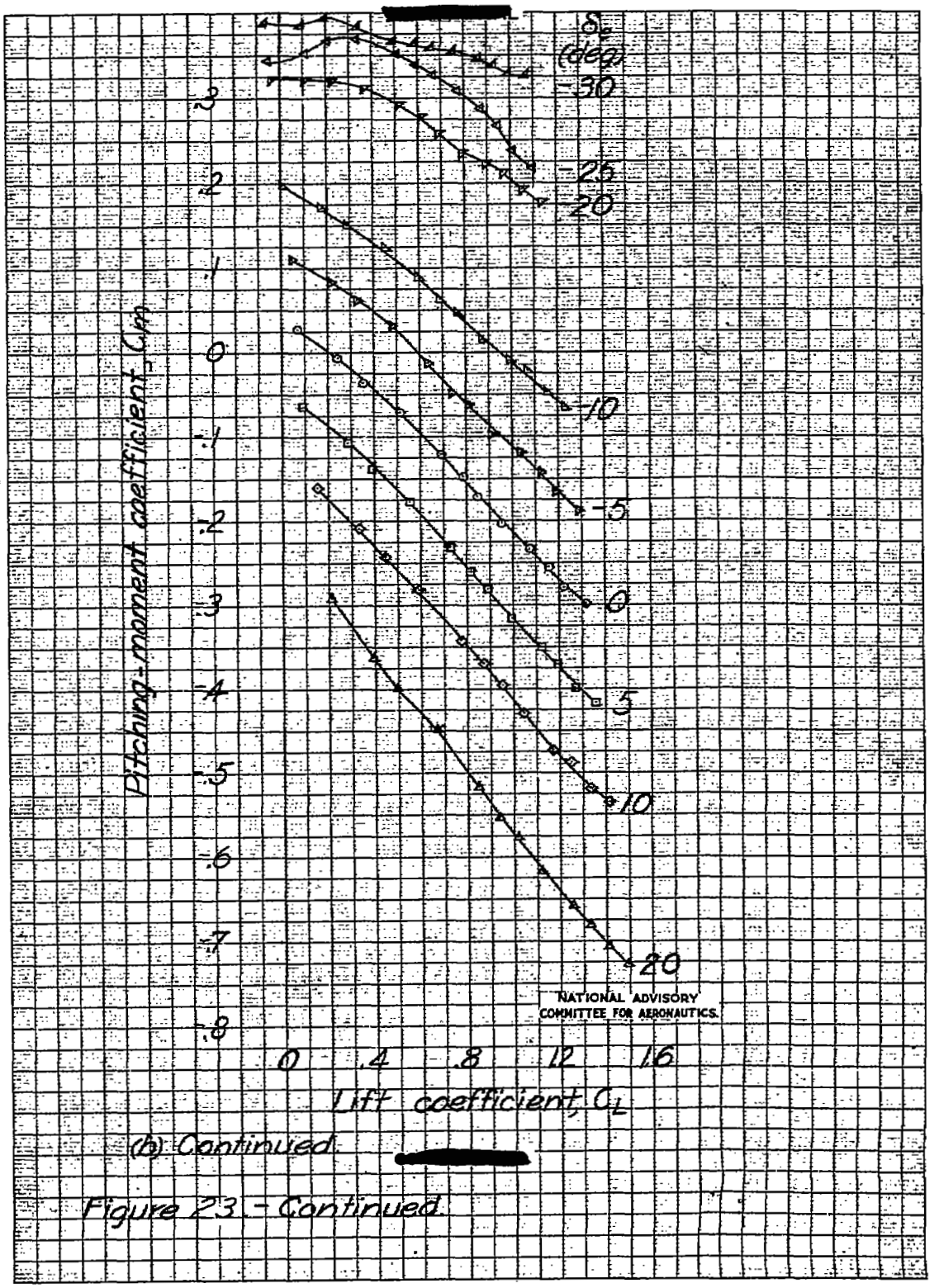

(b) Continued.

Figure 23.- Continued.

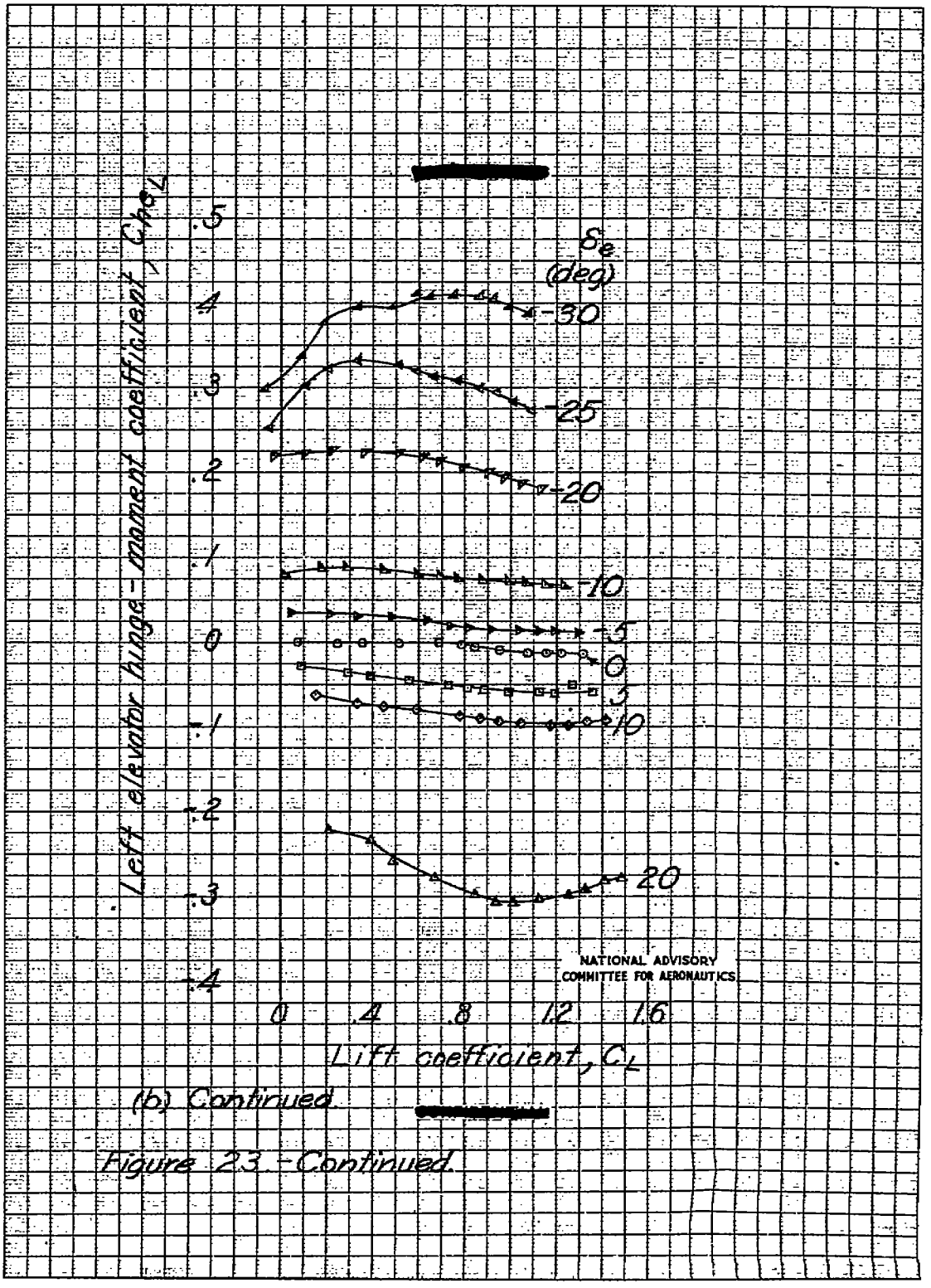

(b) Continued.

Figure 23.-Continued.

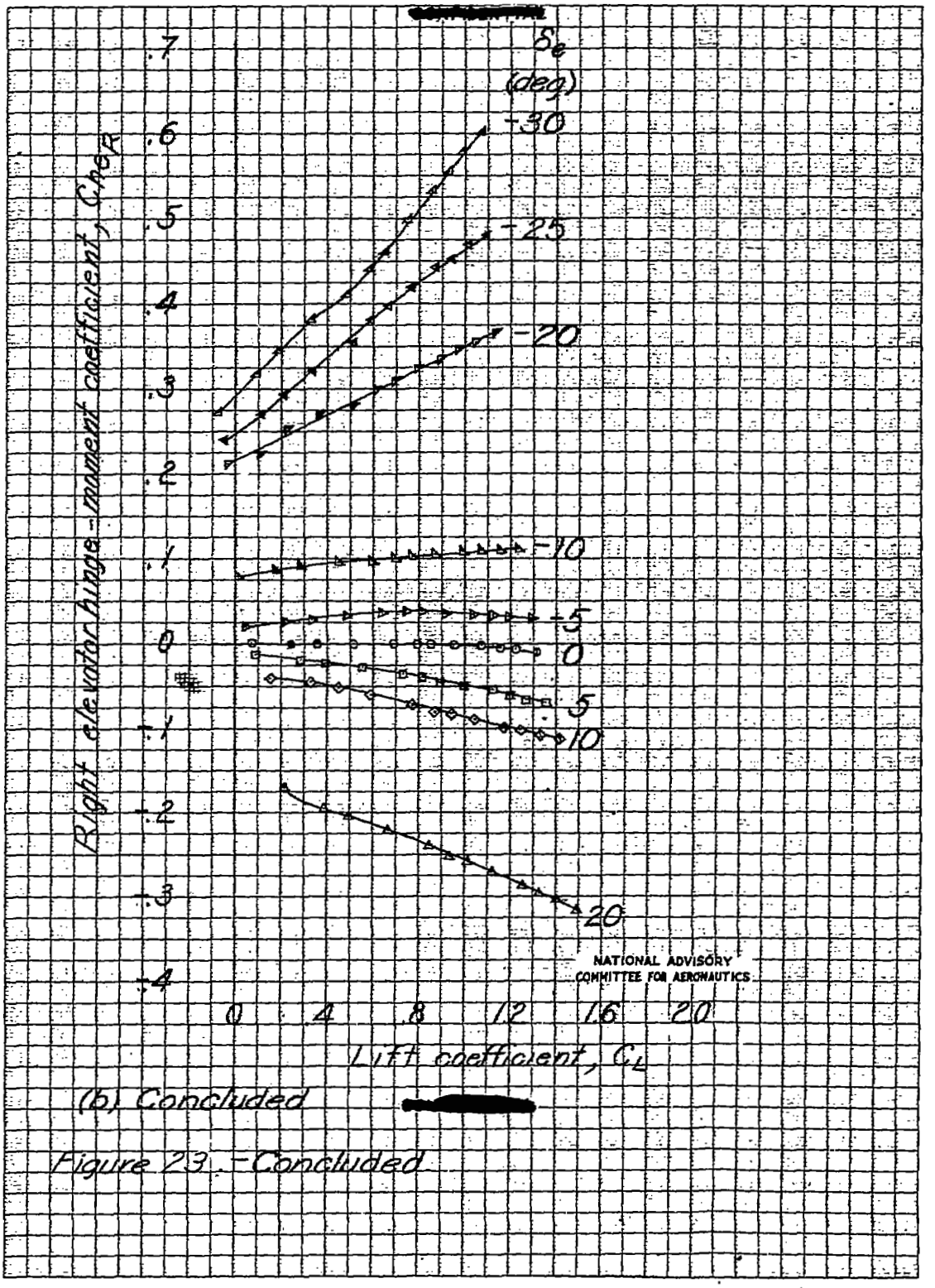

(b) Concluded

Figure 23.- Concluded

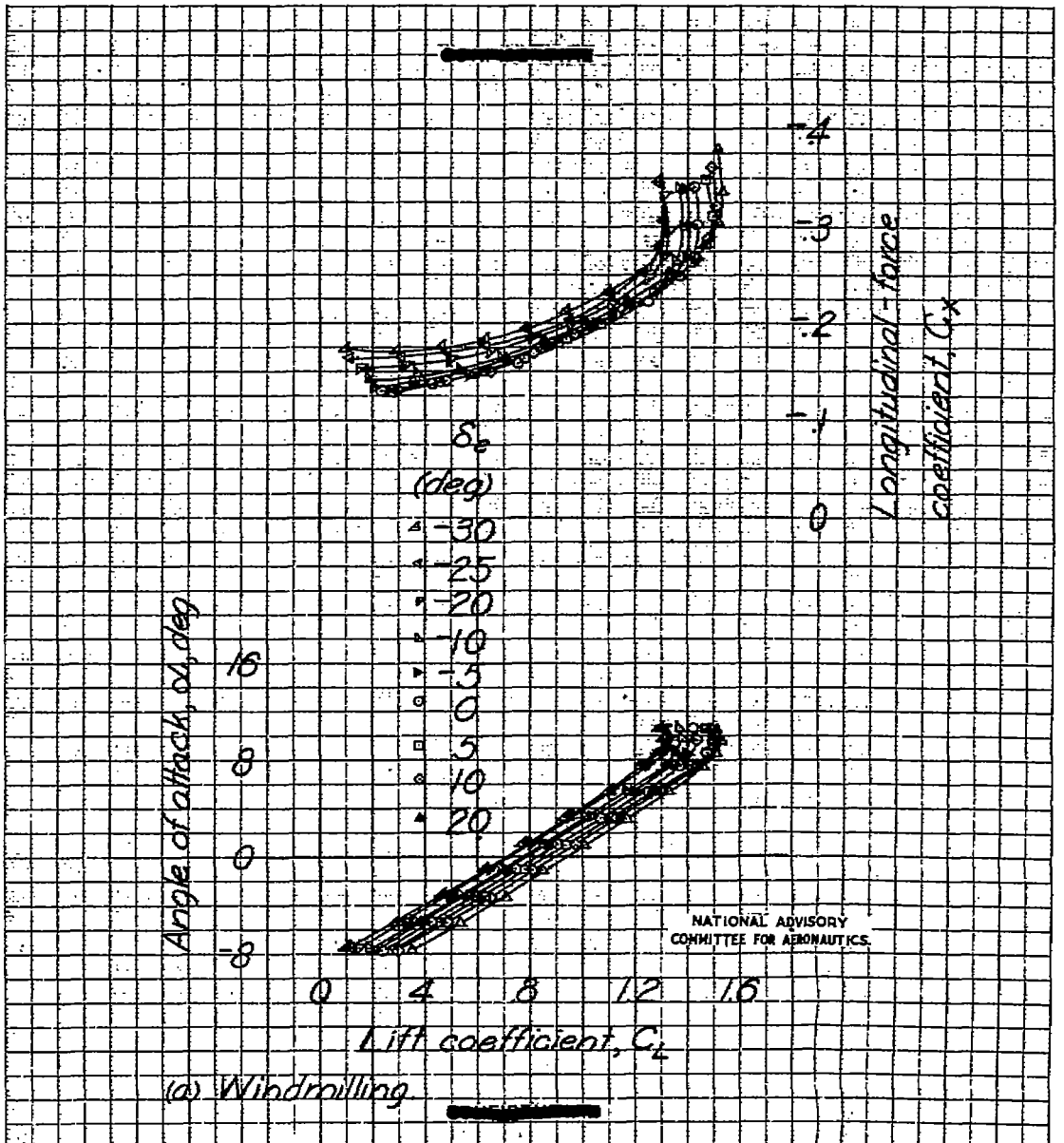

(a) Windmilling.

Figure 24.- Effect of elevator deflection on the aerodynamic characteristics in pitch of the 1/4-scale NAF seaplane model. Landing configuration, i_t=3.50°. Thrust axis horizontal.

Fig. 24a cont.

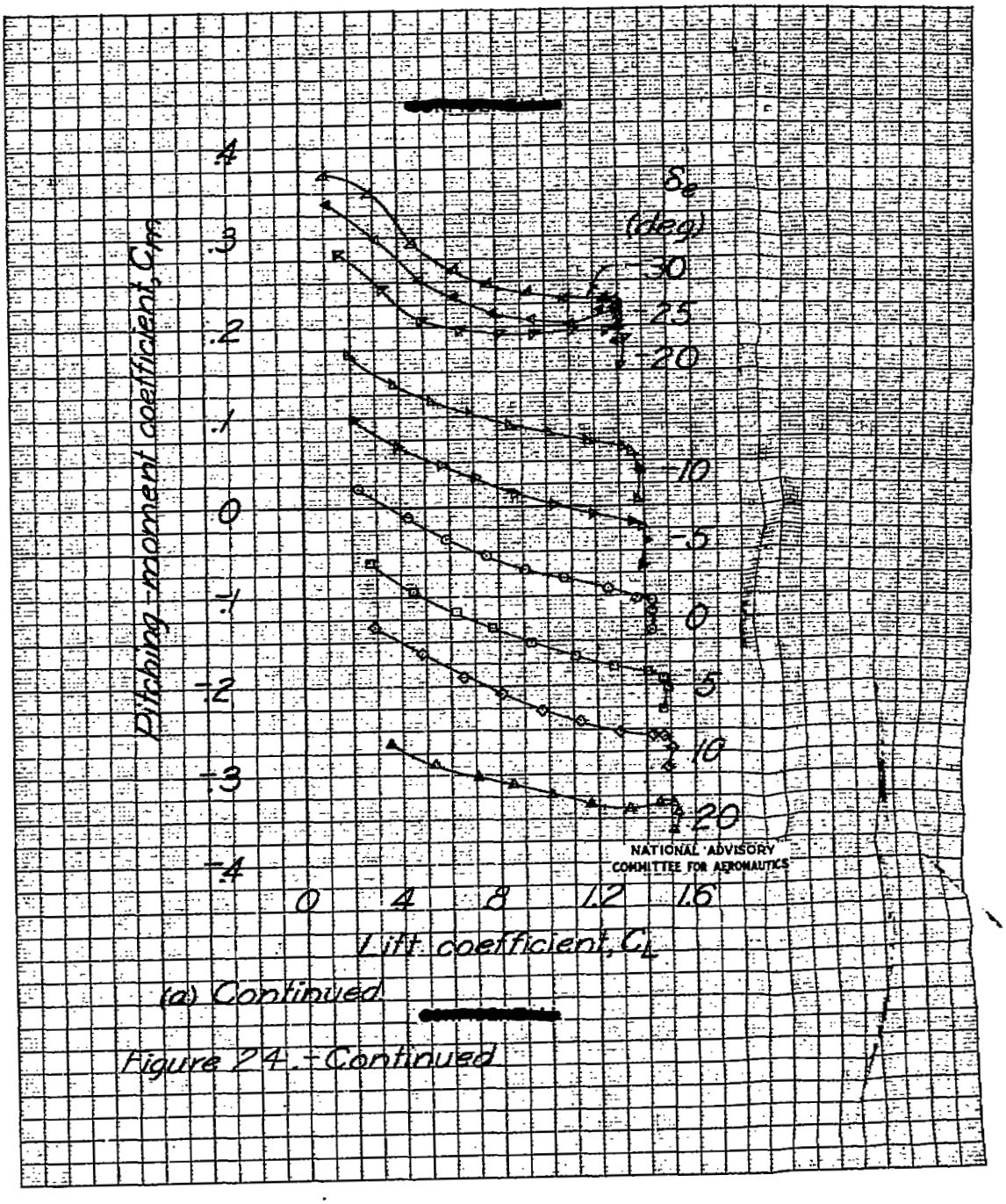

(a) Continued

Figure 24.- Continued

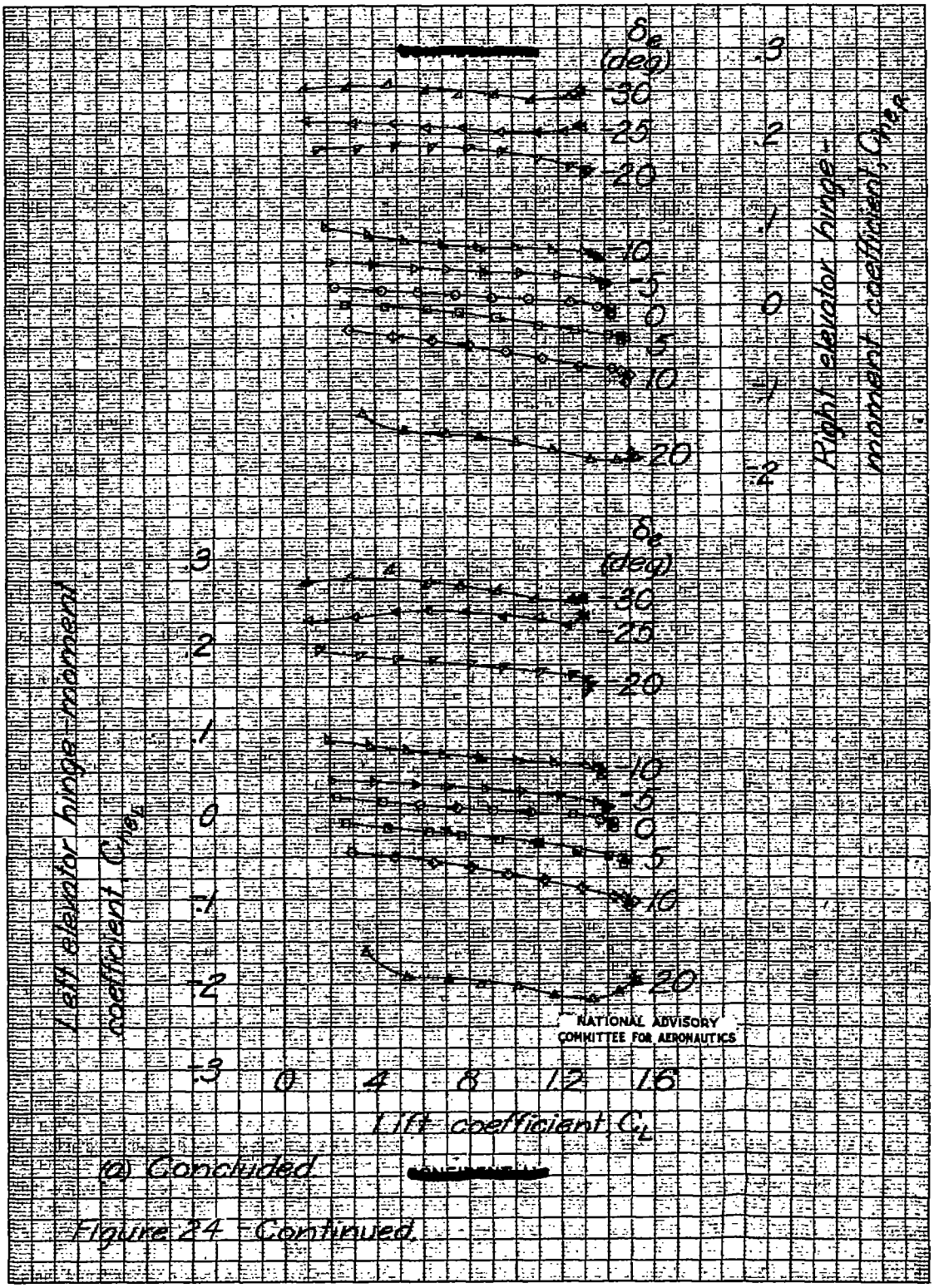

(d) Concluded

Figure 24 Continued.

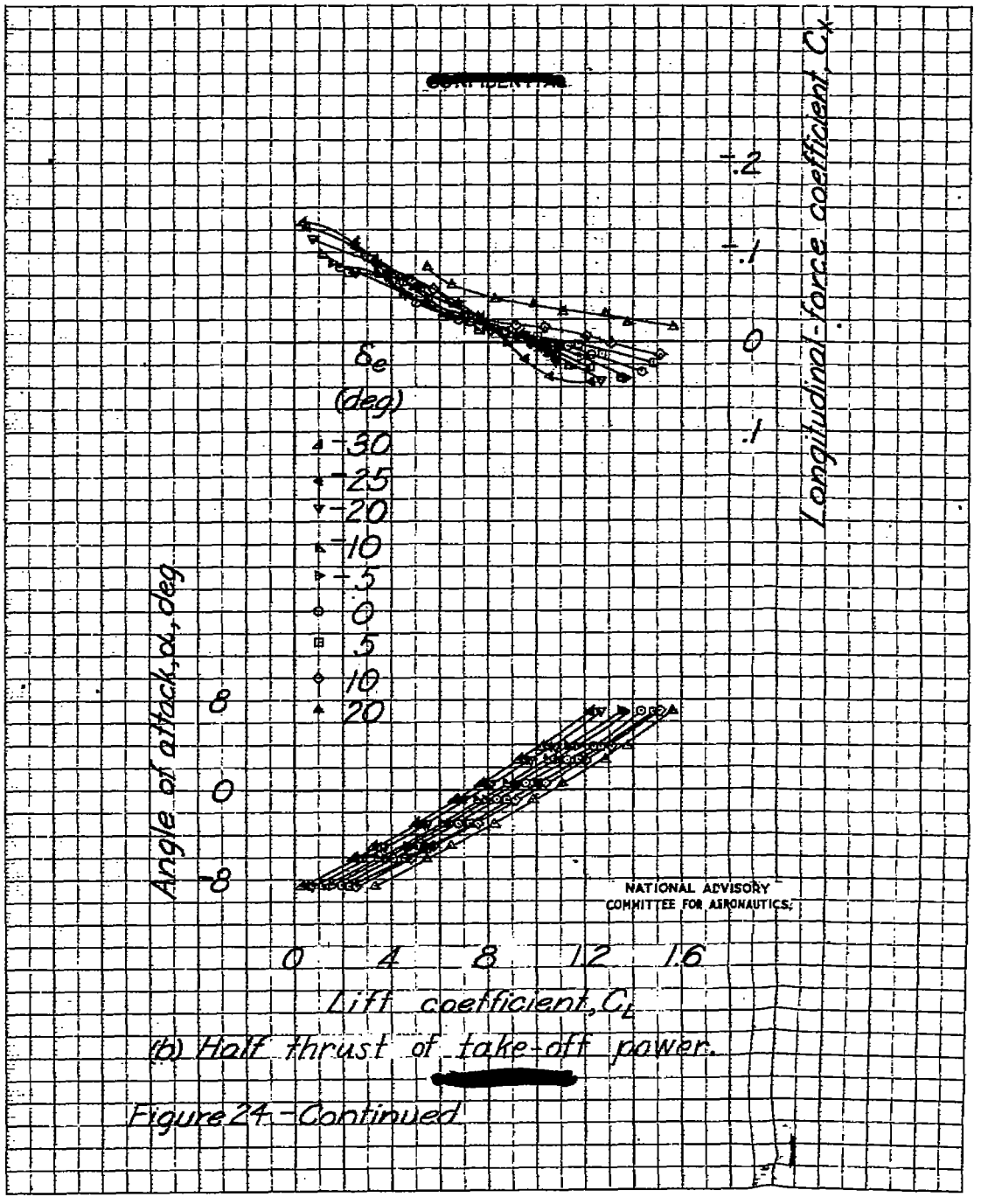

(b) Half thrust of take-off power.

Figure 24.- Continued.

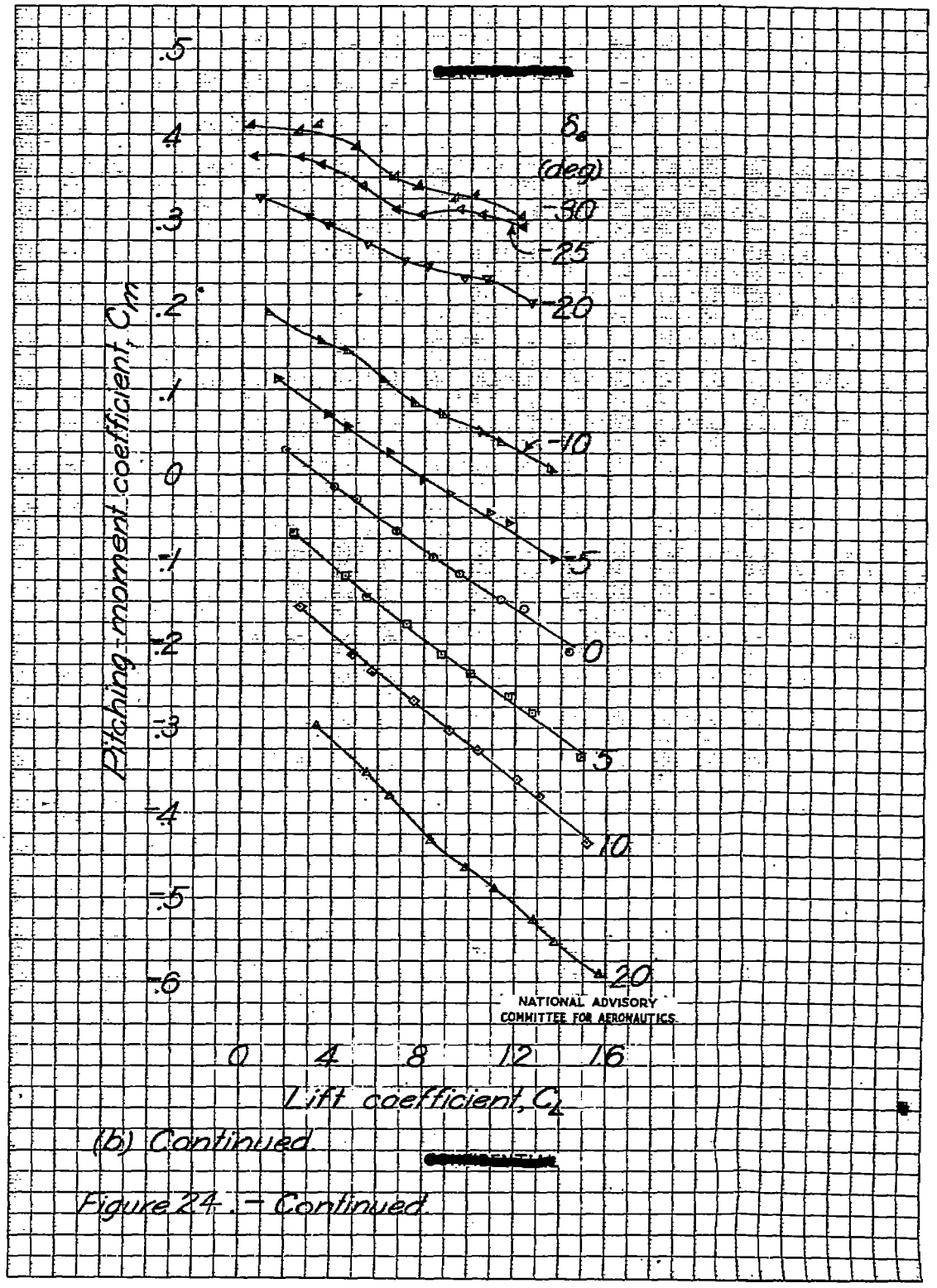

(b) Continued

Figure 24.- Continued.

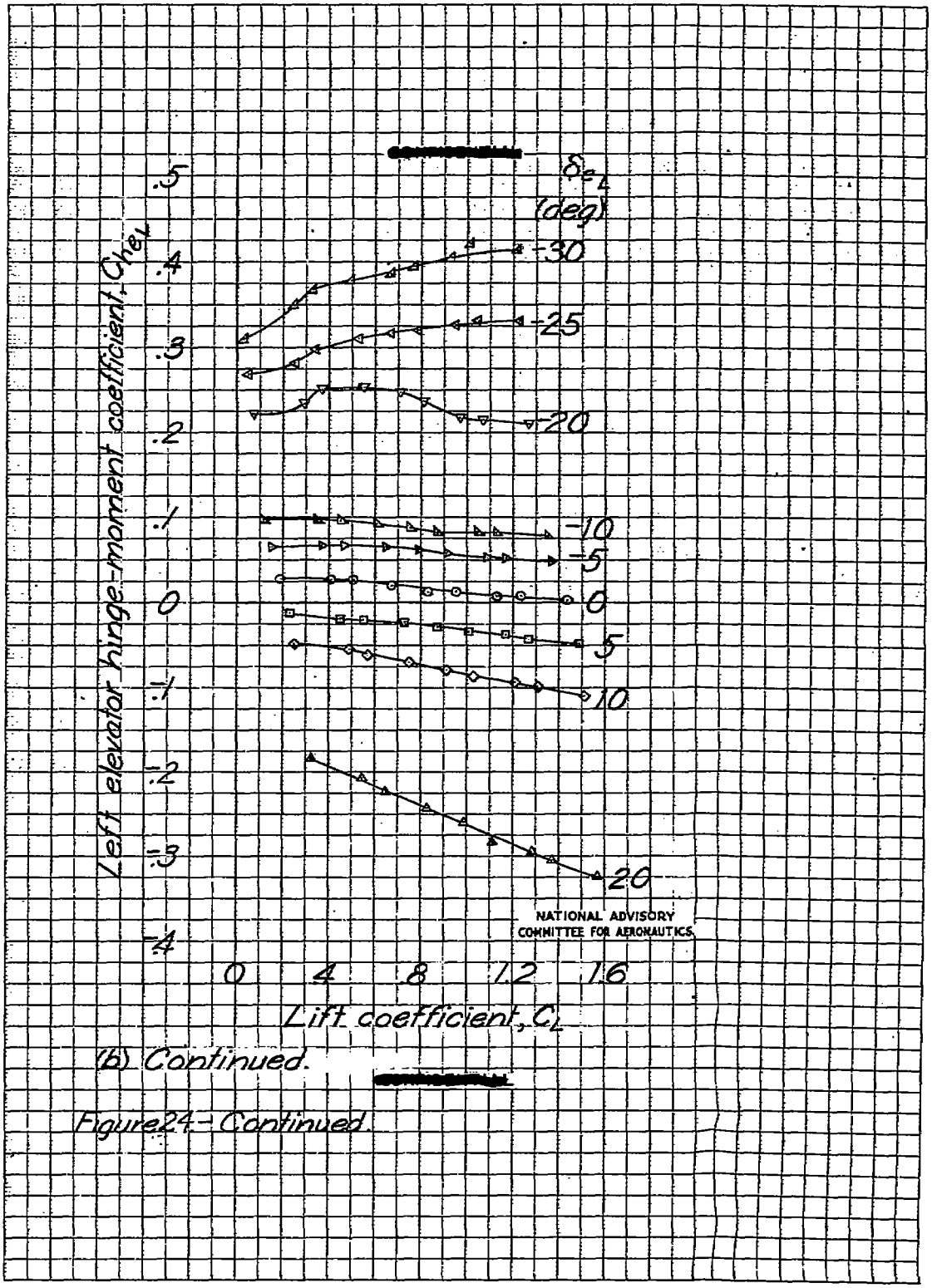

(b) Continued.

Figure 24.- Continued.

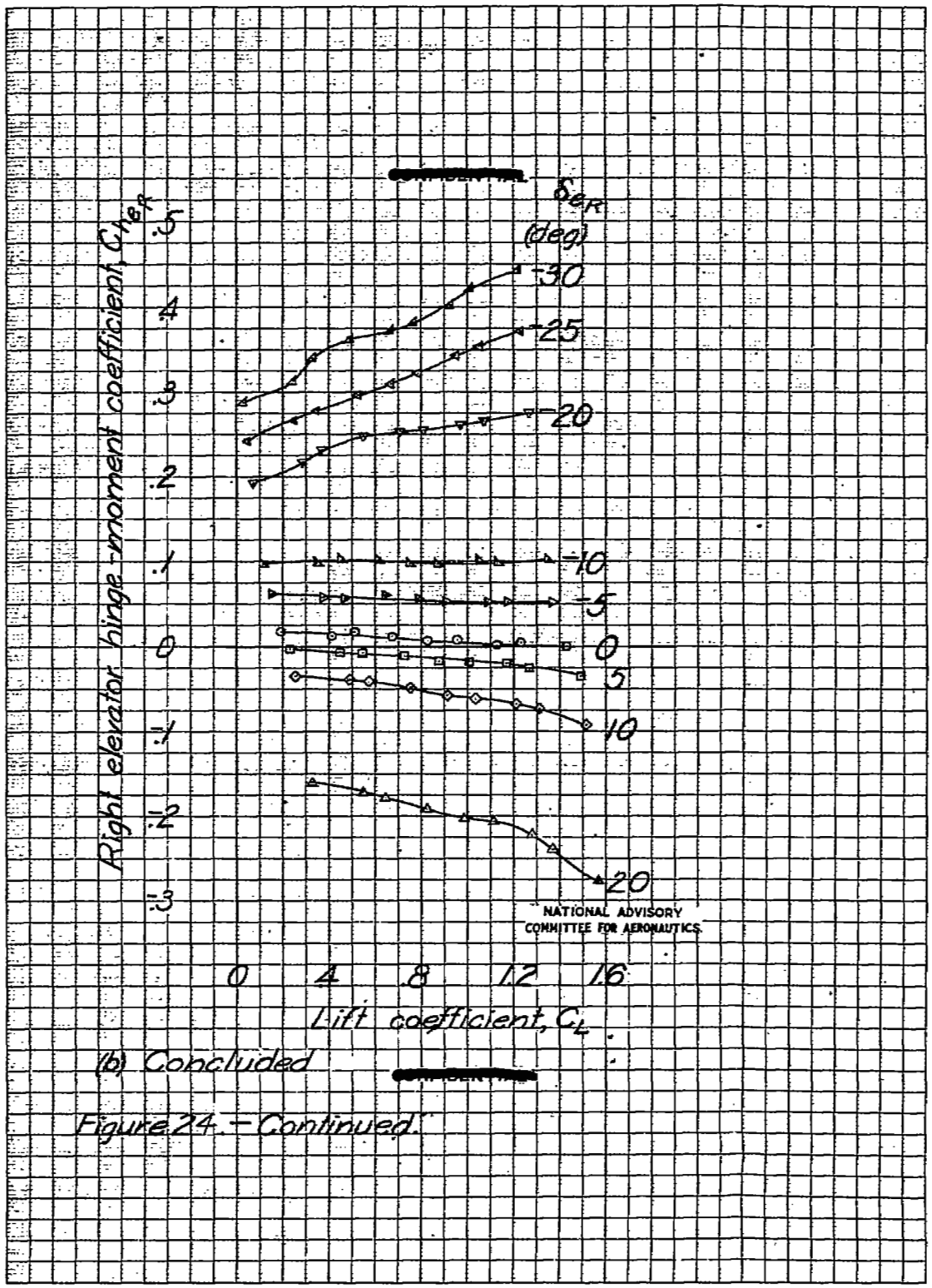

(b) Concluded

Figure 24.- Continued.

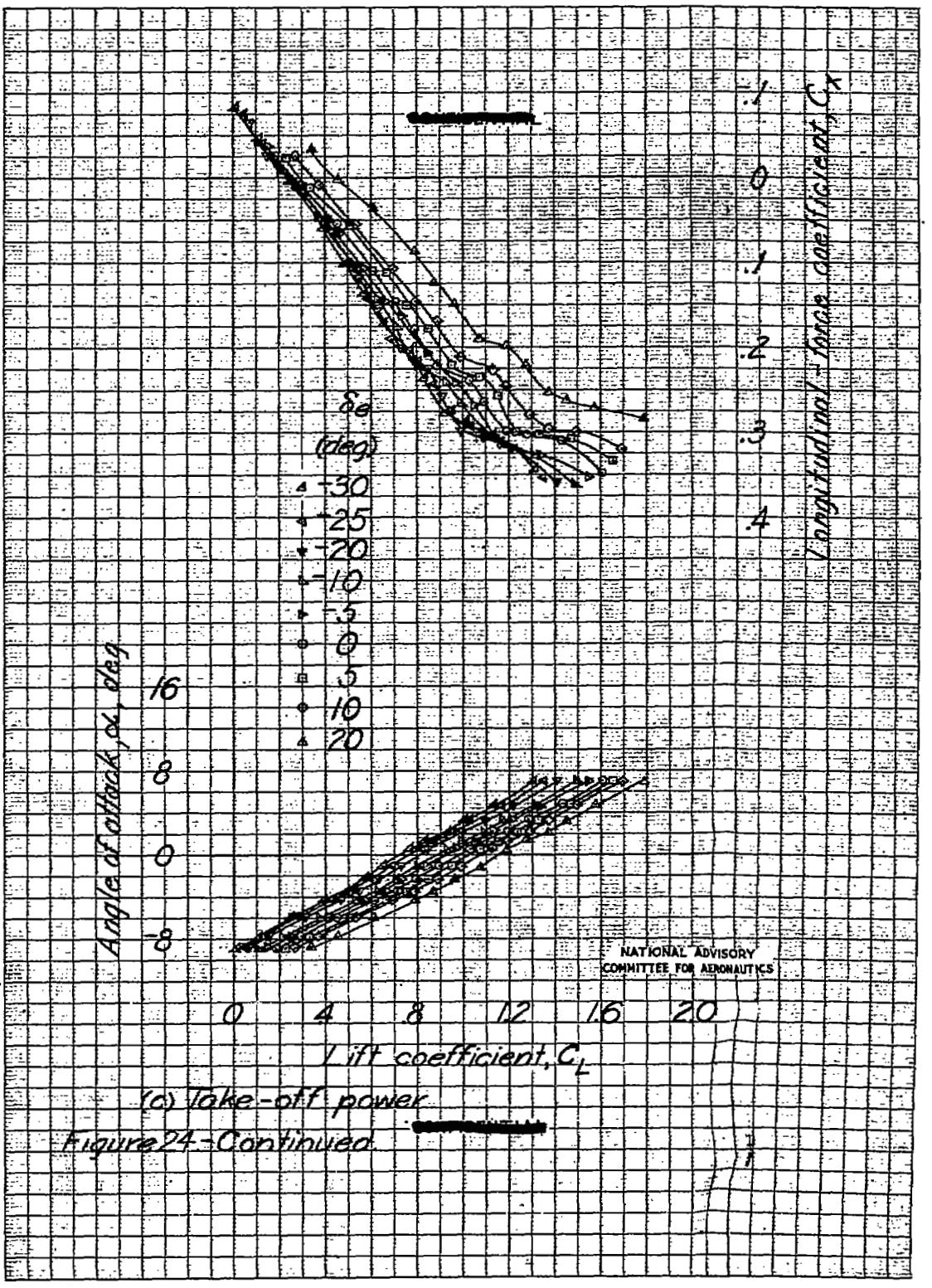

(c) Take-off power

Figure 24.- Continued

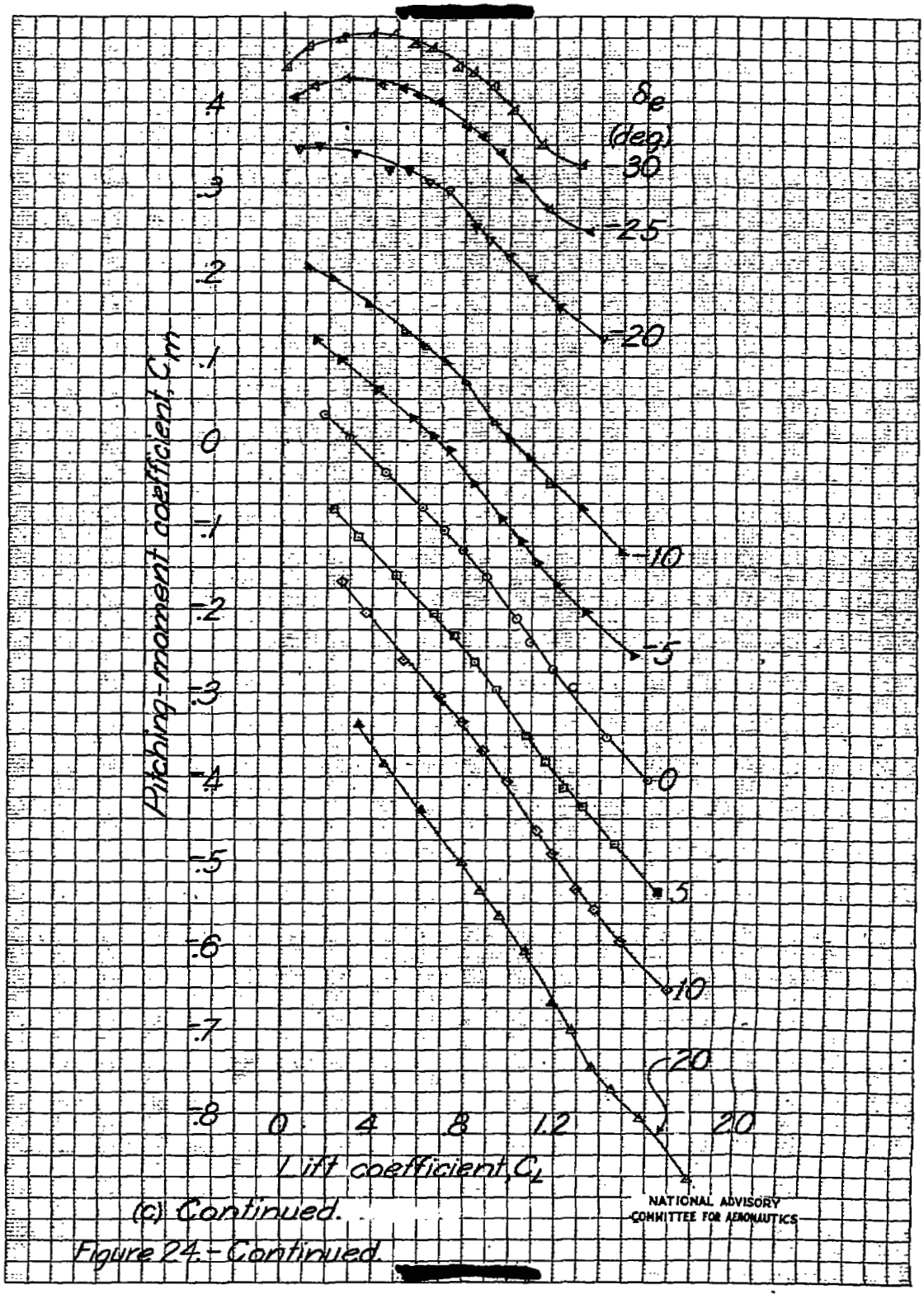

(c) Continued.

Figure 24.- Continued.

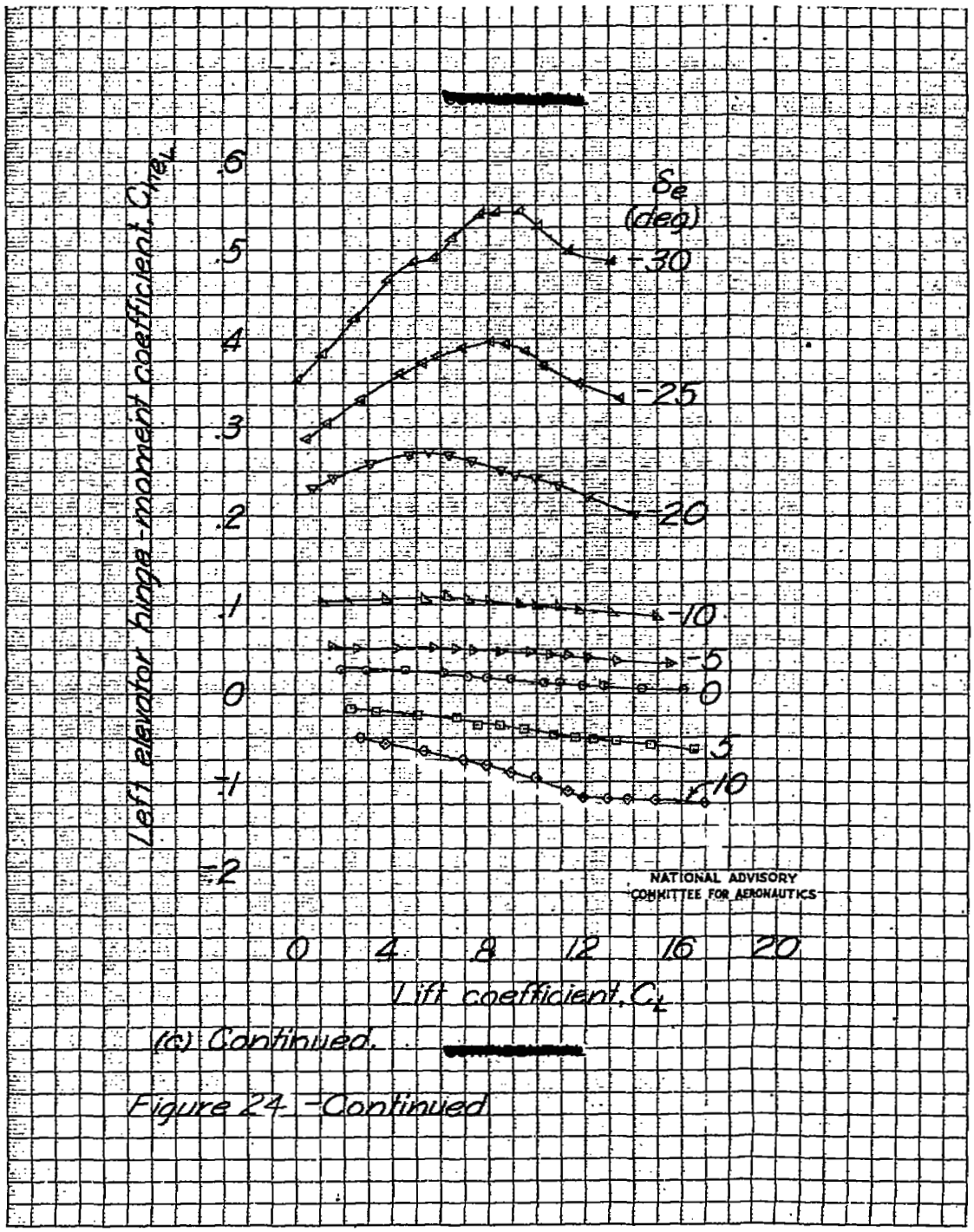

(c) Continued.

Figure 24.- Continued

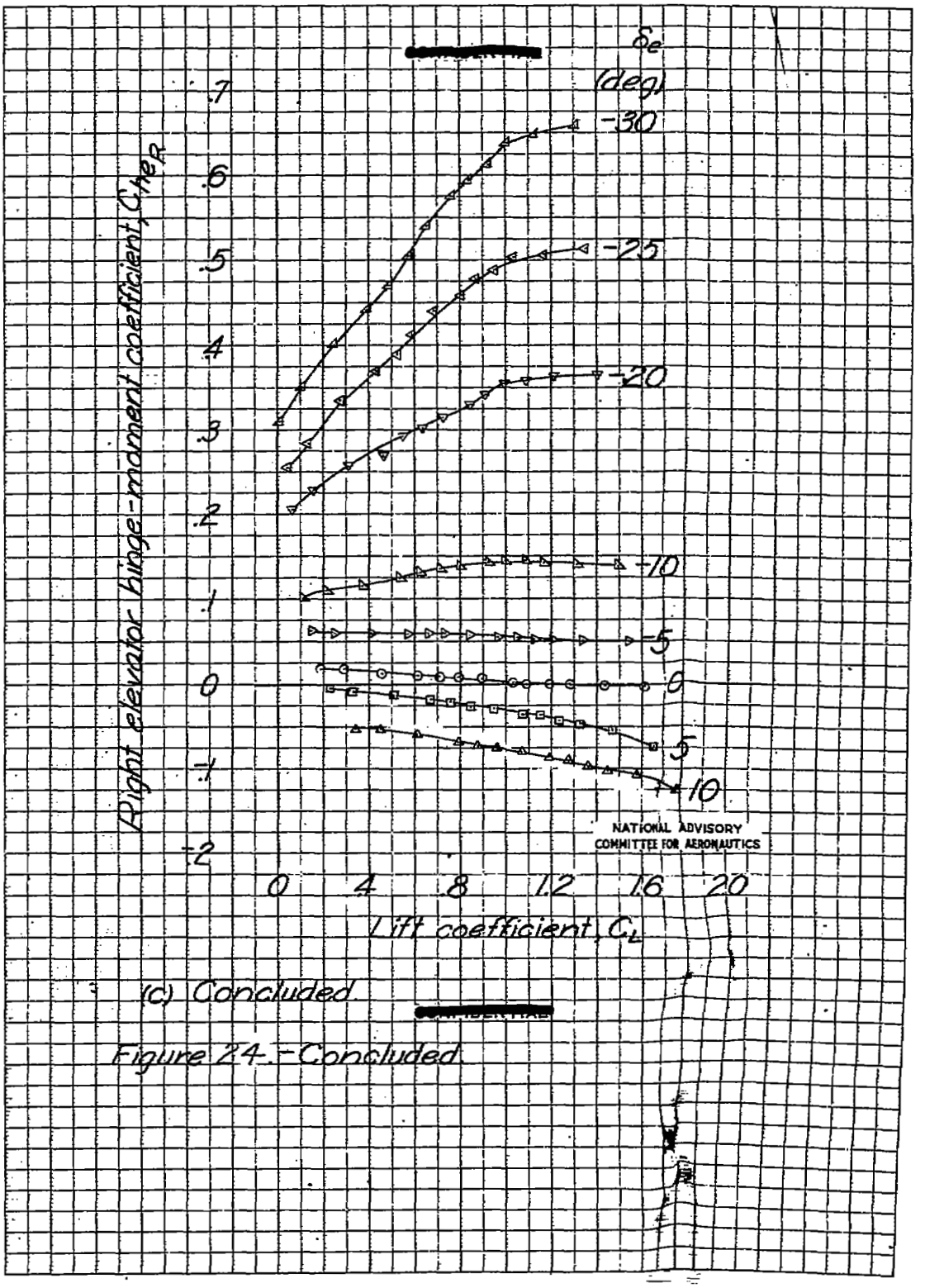

(c) Concluded

Figure 24.- Concluded.

Fig. 25

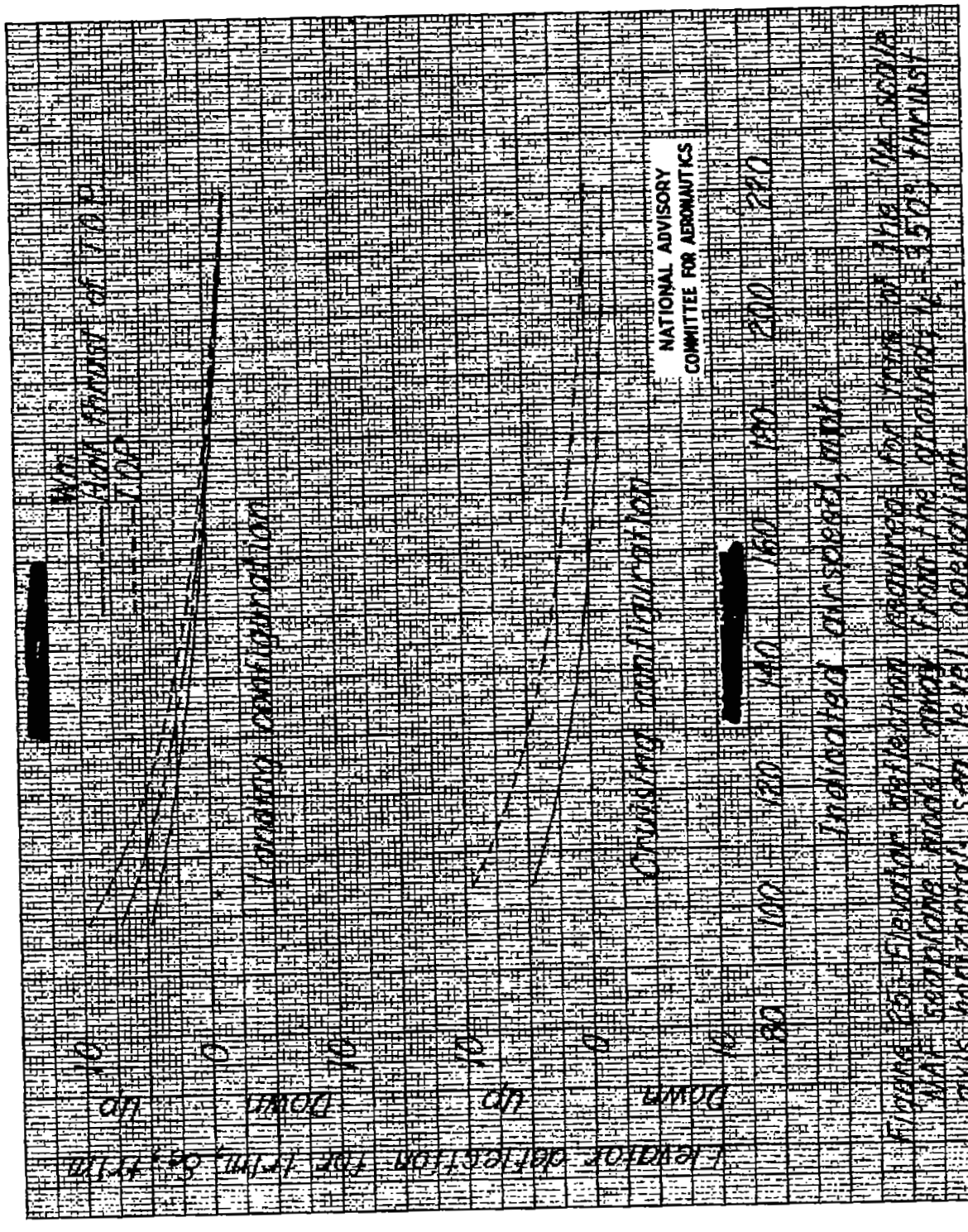

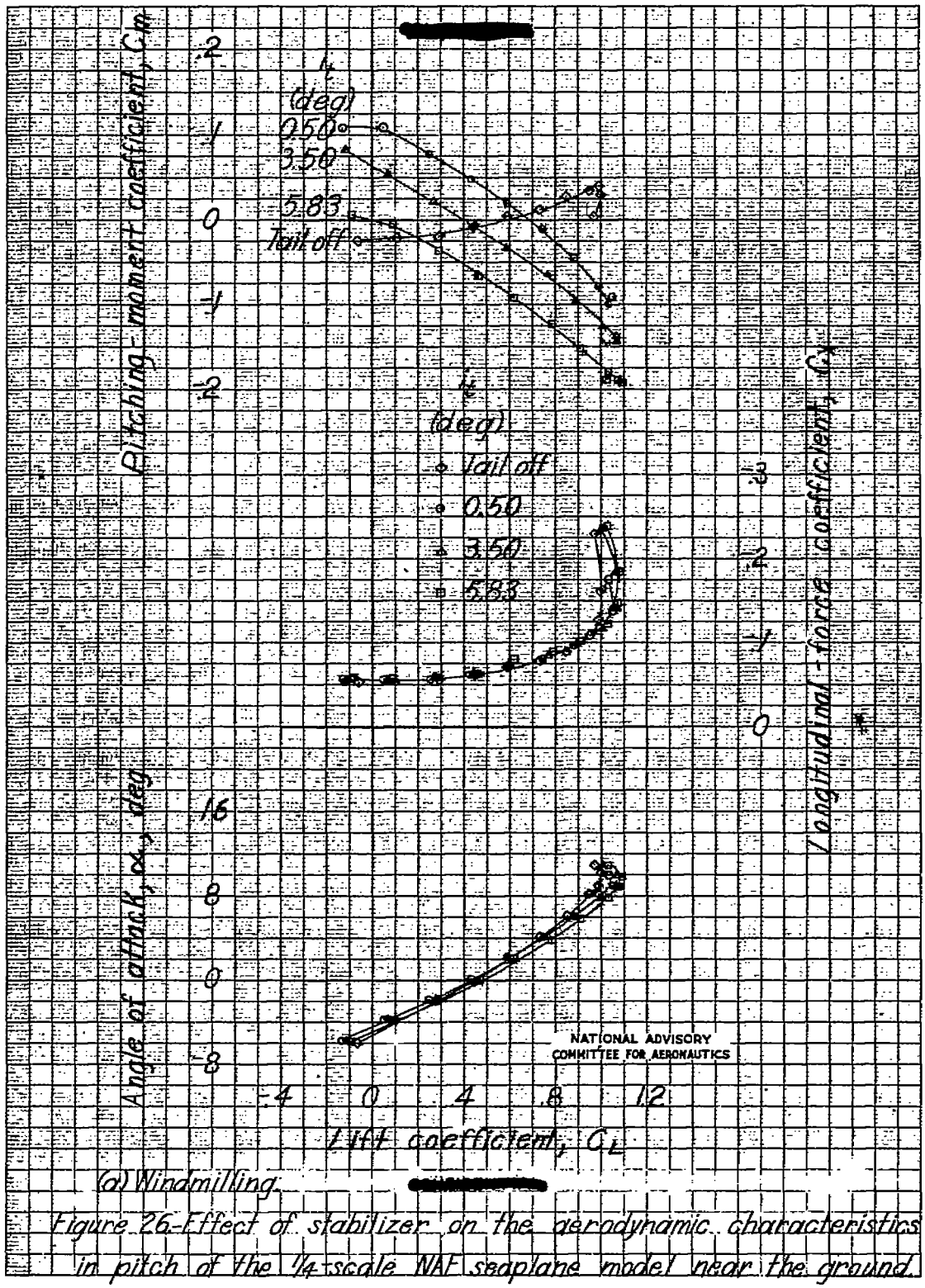

(a) Windmilling.

Figure 26.-Effect of stabilizer on the aerodynamic characteristics in pitch of the 1/4-scale NAF seaplane model near the ground. Take-off configuration; $\delta_e = 0°$; thrust axis horizontal.

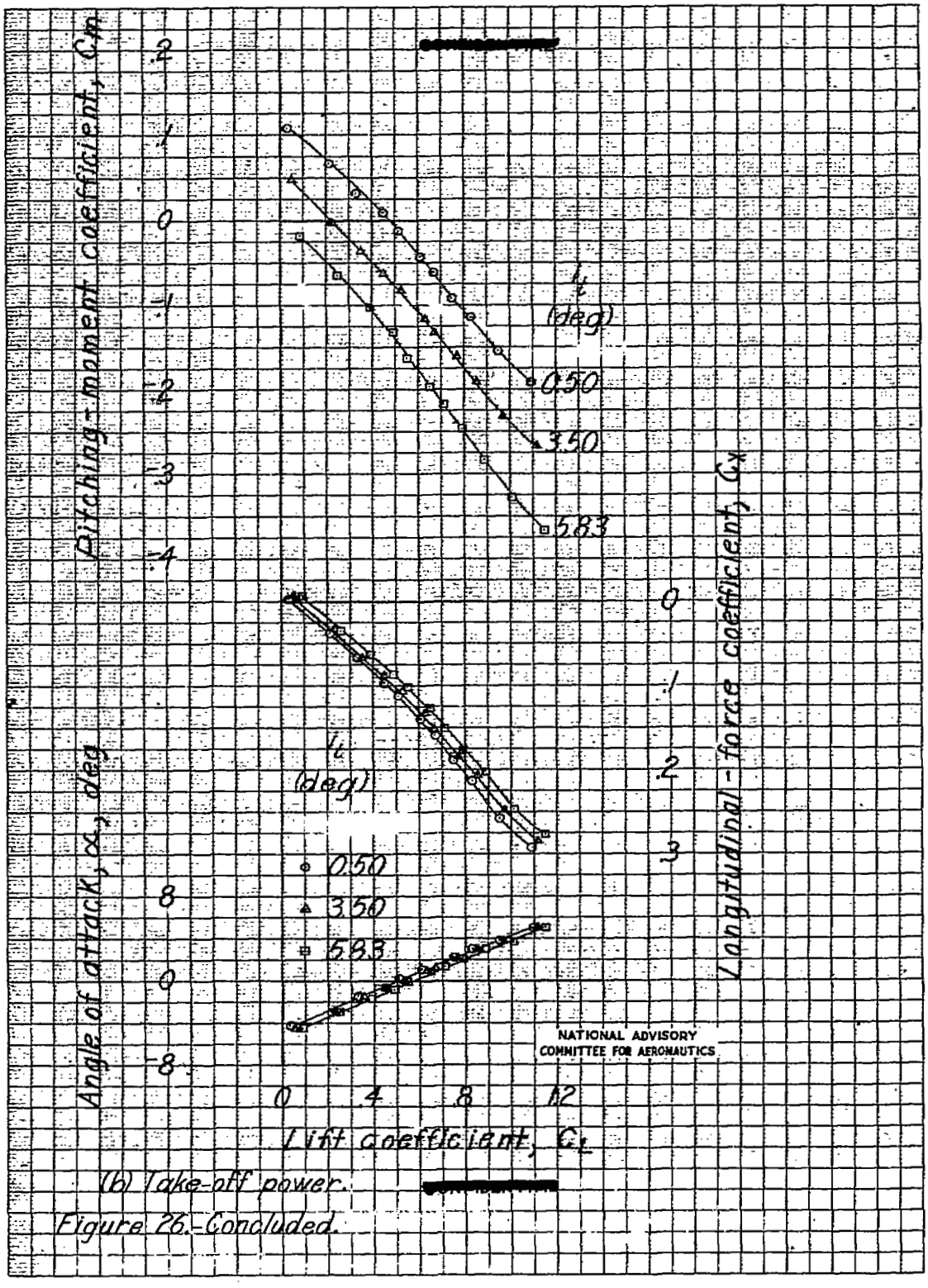

(b) Take-off power.

Figure 26.- Concluded.

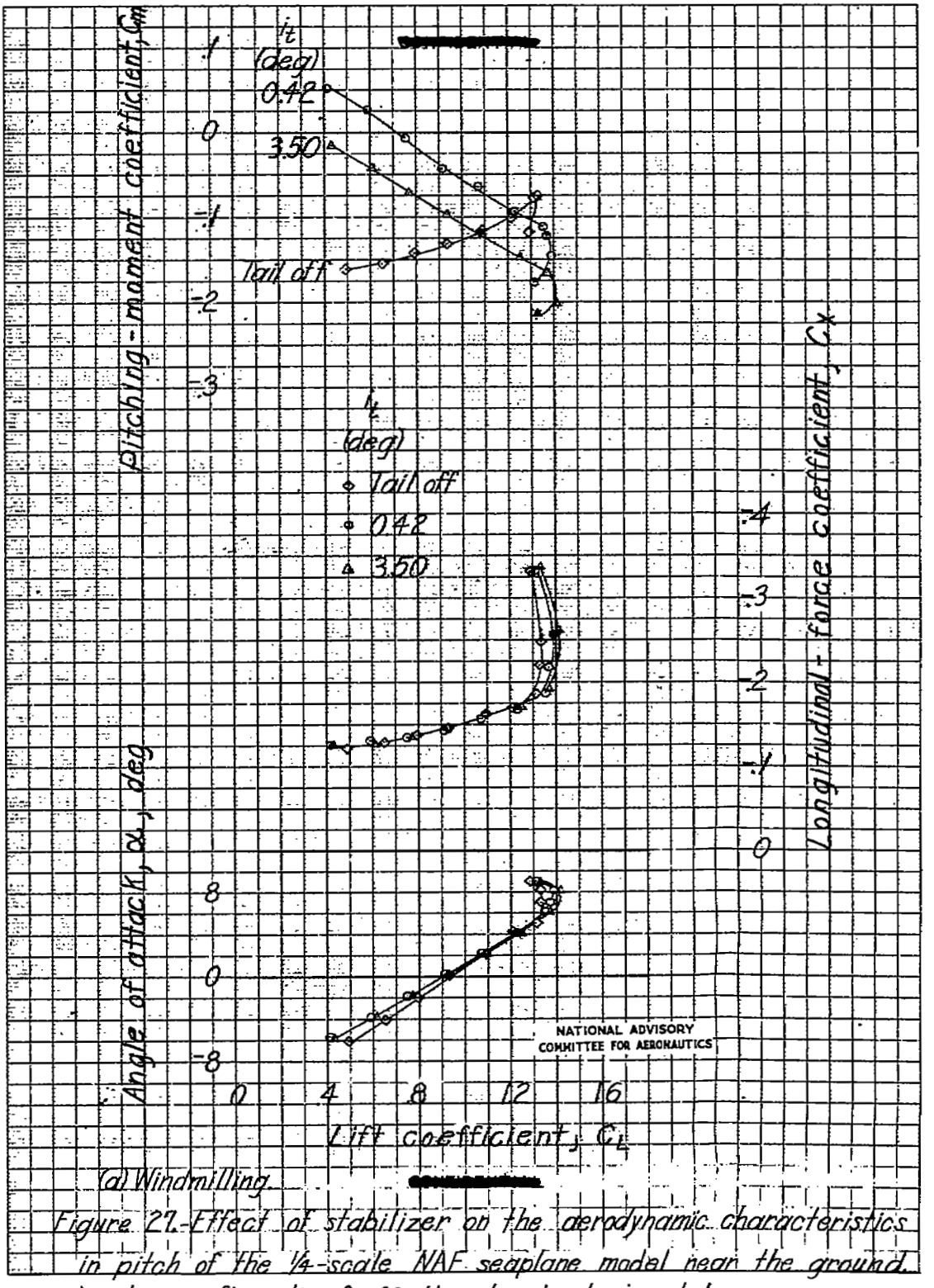

(a) Windmilling.

Figure 27.- Effect of stabilizer on the aerodynamic characteristics in pitch of the 1/4-scale NAF seaplane model near the ground. Landing configuration; $\delta_e = 0°$; thrust axis horizontal.

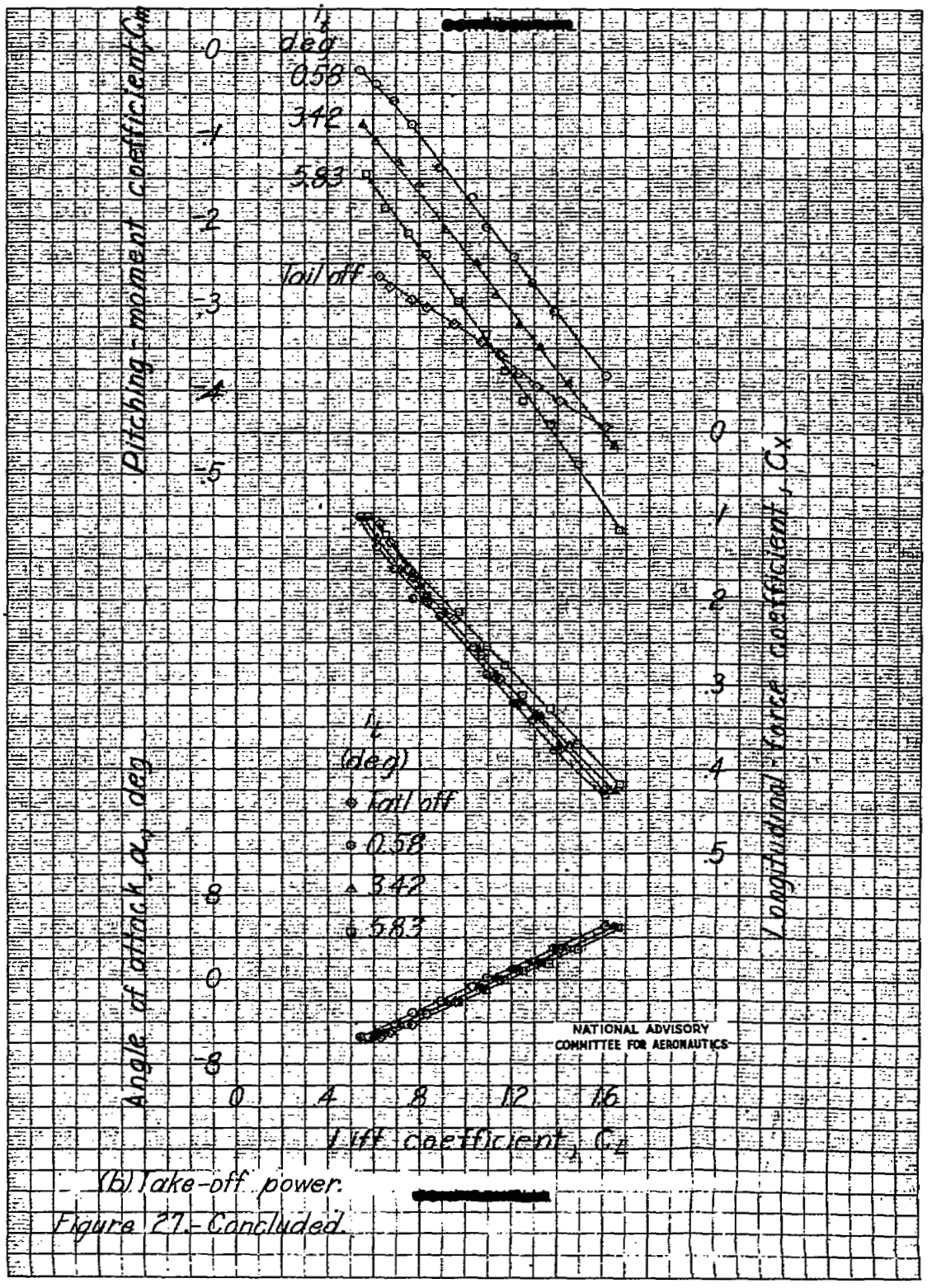

(b) Take-off power.

Figure 27.- Concluded.

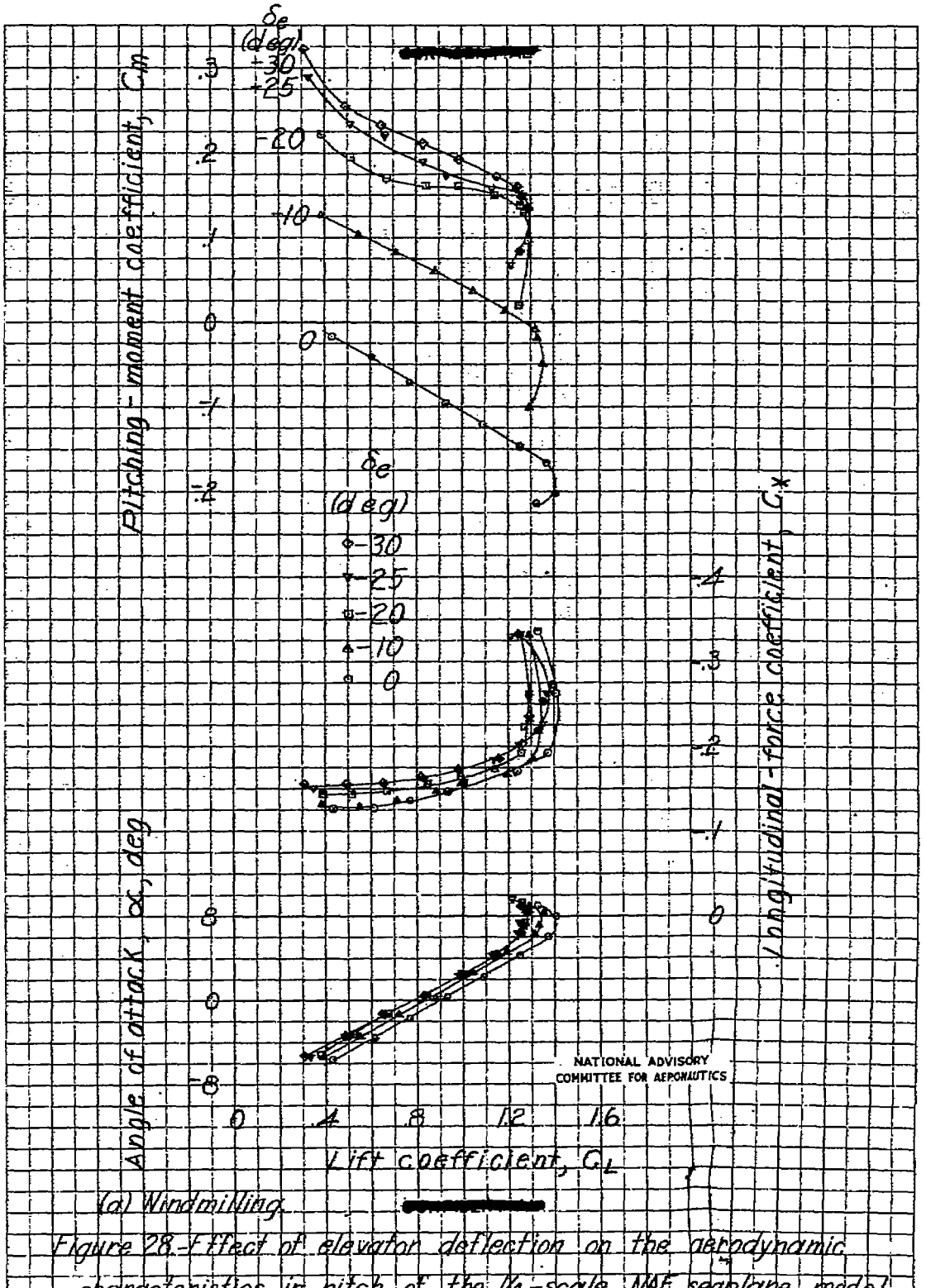

(a) Windmilling.

Figure 28.- Effect of elevator deflection on the aerodynamic characteristics in pitch of the 1/4-scale NAF seaplane model near the ground. Landing configuration; $i_t = 3.50°$; thrust axis horizontal.

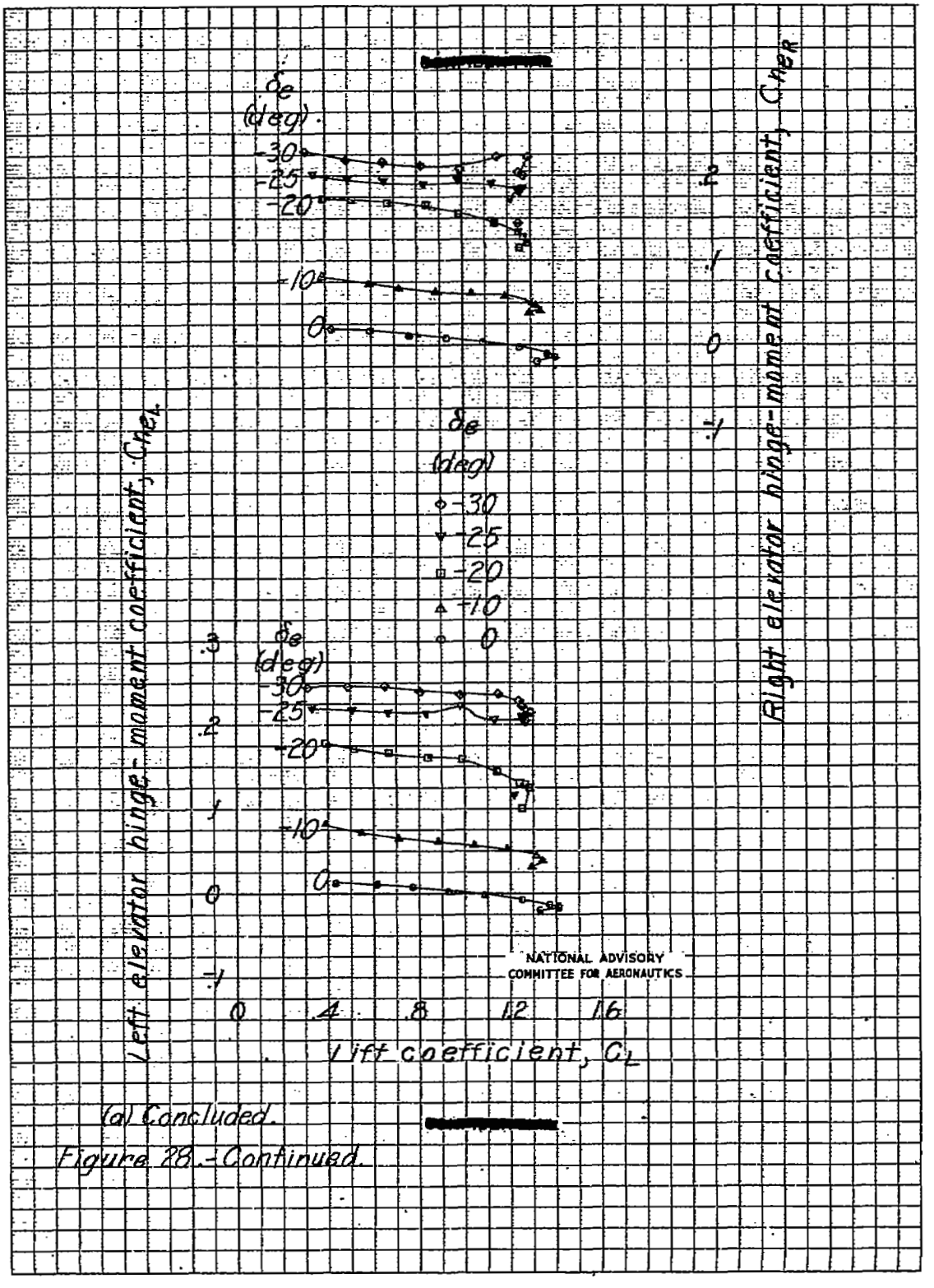

(a) Concluded.

Figure 28.- Continued.

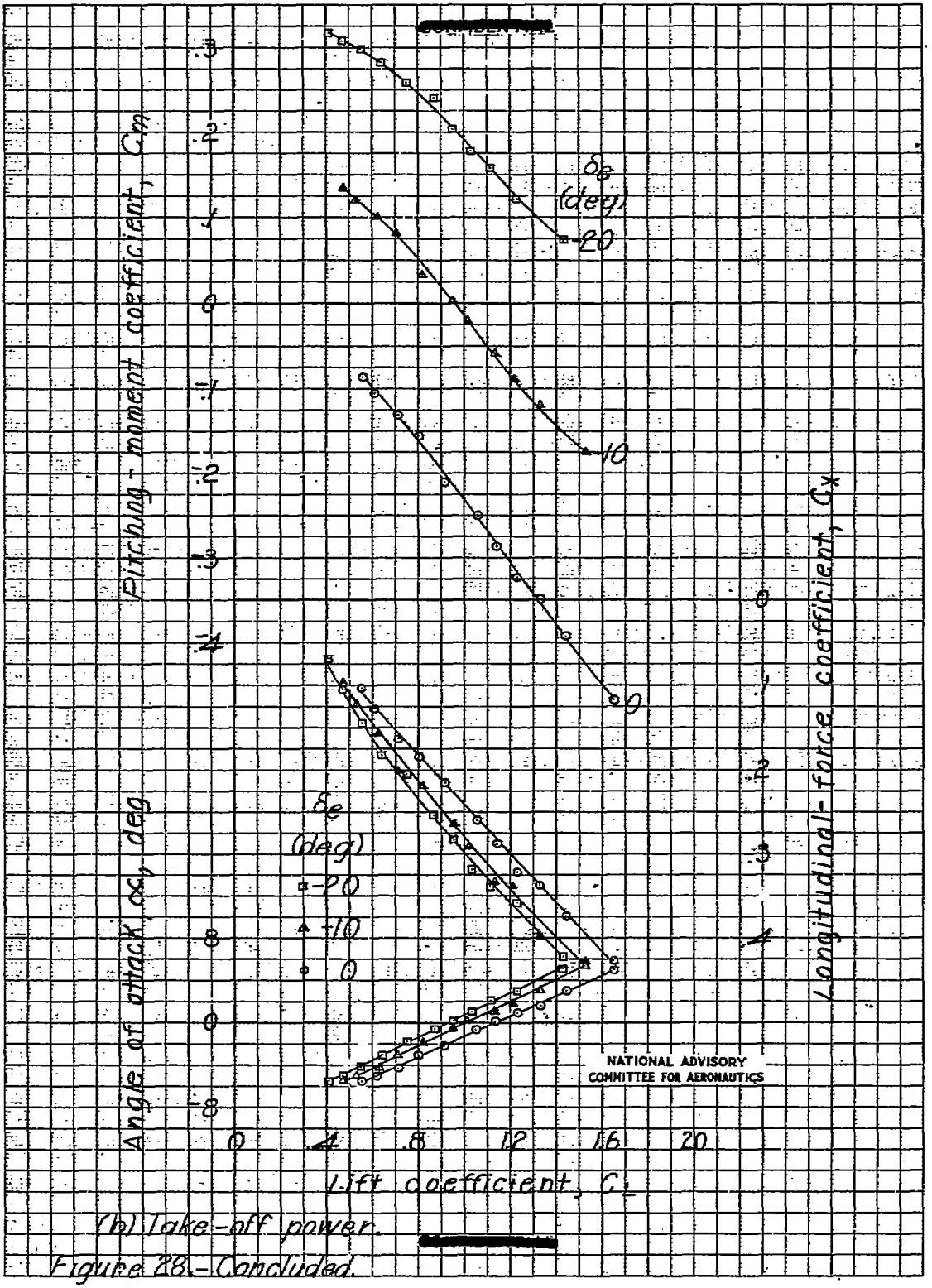

(b) Take-off power.

Figure 28.- Concluded.

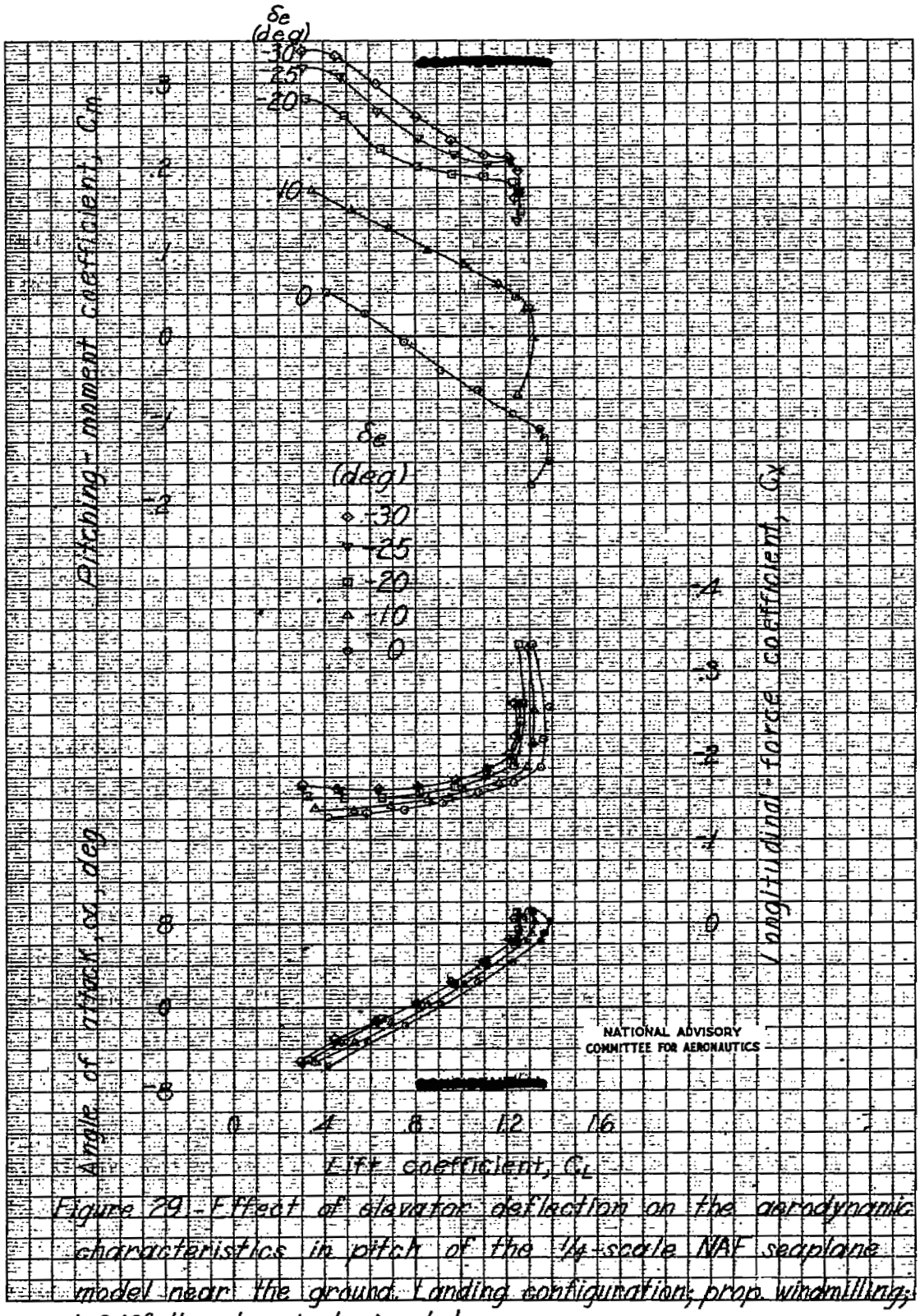

Figure 29.- Effect of elevator deflection on the aerodynamic characteristics in pitch of the 1/4-scale NAF seaplane model near the ground. Landing configuration; prop. windmilling; i_t=0.42°; thrust axis horizontal.

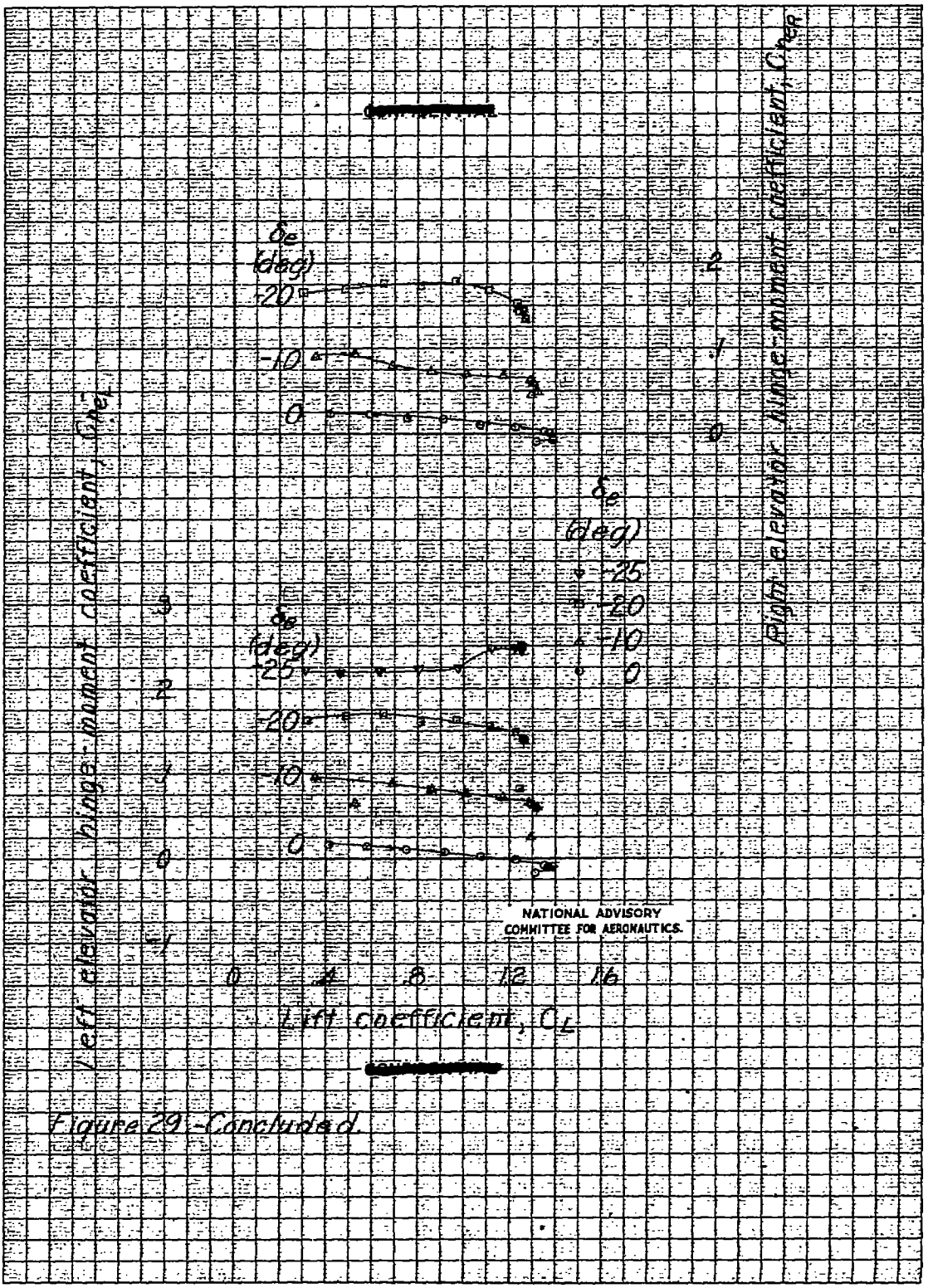

Figure 29.-Concluded.

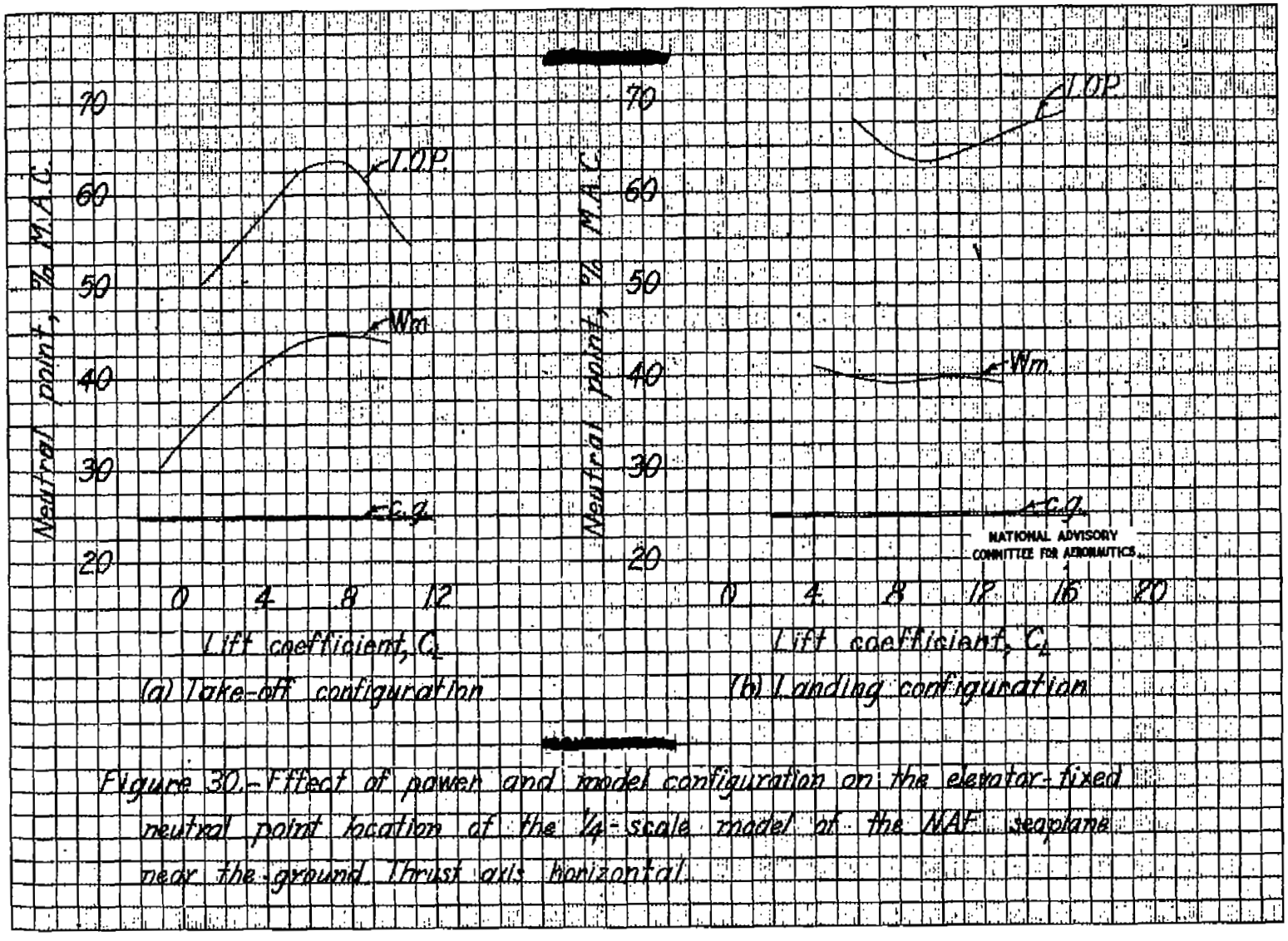

Figure 30.- Effect of power and model configuration on the elevator-fixed neutral point location of the 1/4-scale model of the NAF seaplane near the ground. Thrust axis horizontal.

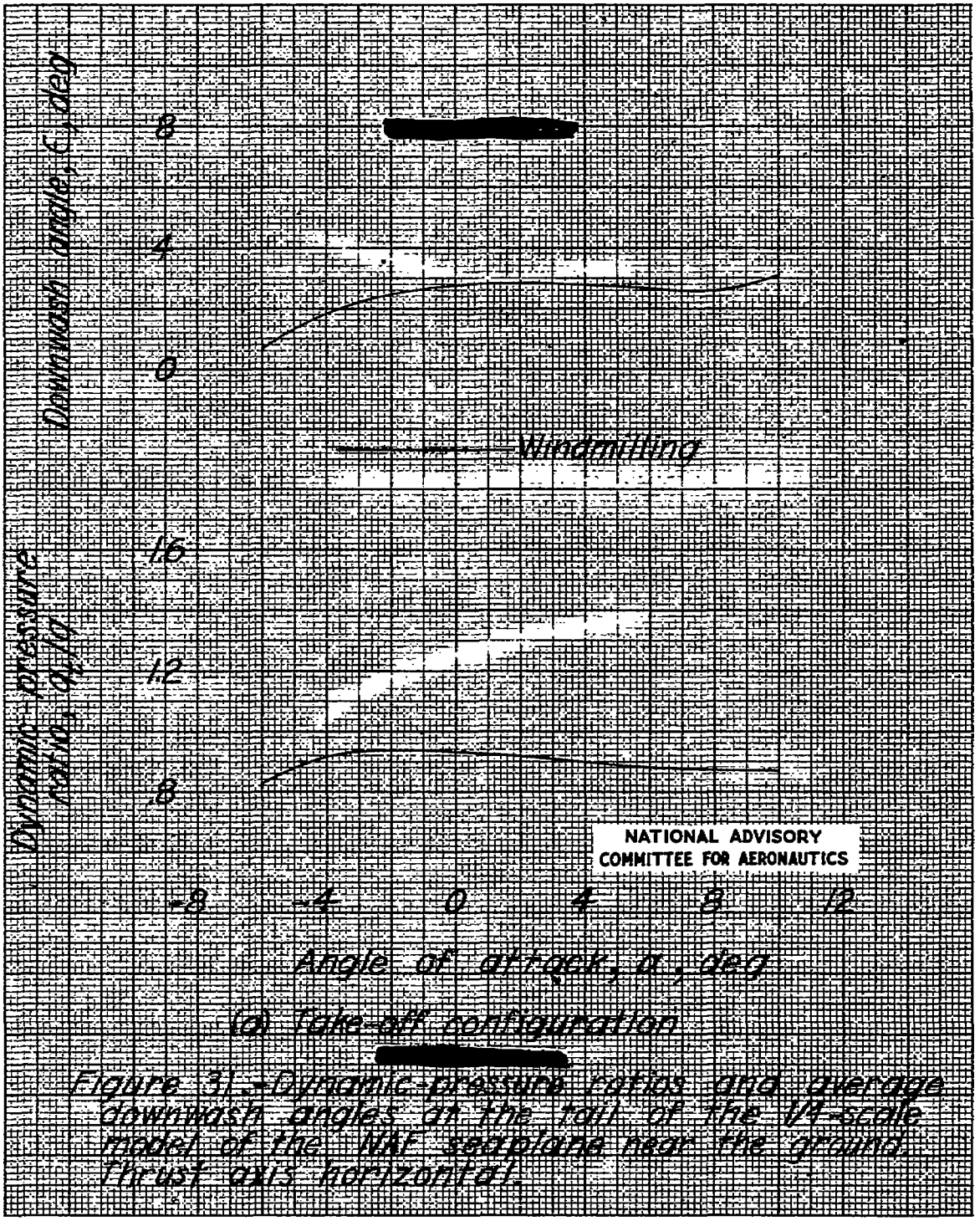

(a) Take-off configuration.

Figure 31.- Dynamic-pressure ratios and average downwash angles at the tail of the 1/4-scale model of the NAF seaplane near the ground. Thrust axis horizontal.

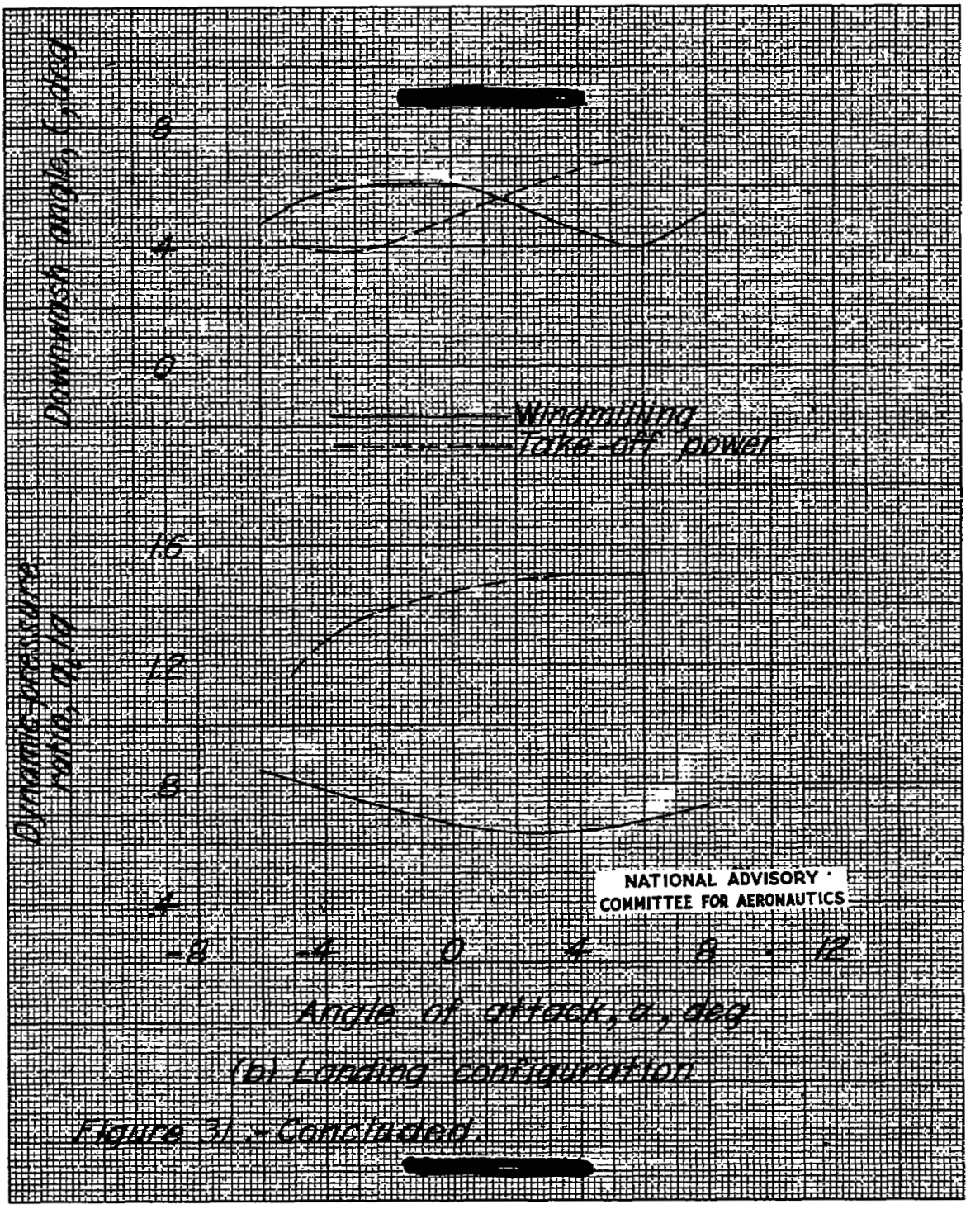

(b) Landing configuration

Figure 31.- Concluded.

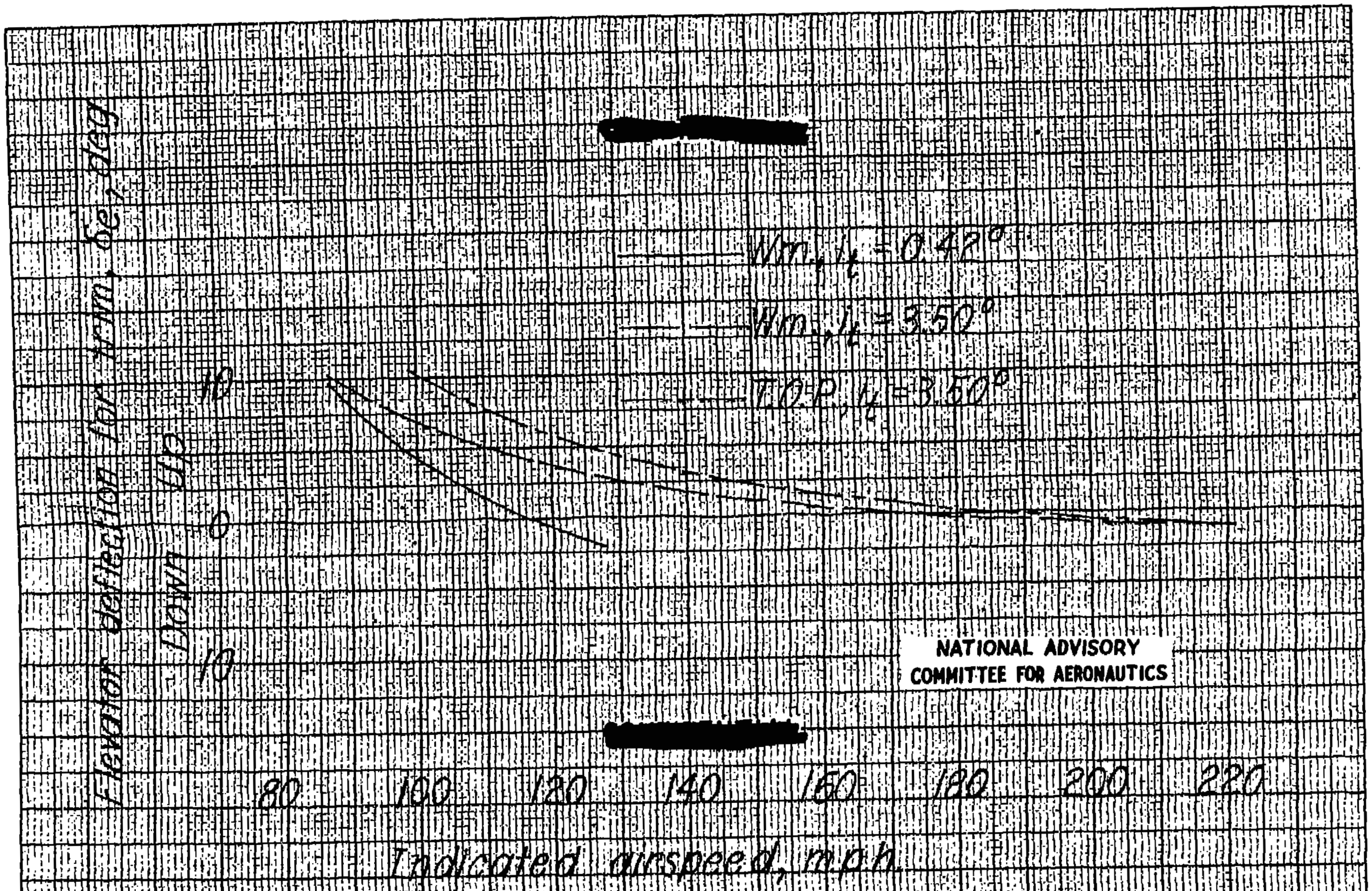

Figure 32.- Elevator deflection required for trim of the 1/4-scale NAF seaplane model near the ground. Landing configuration; thrust axis horizontal.

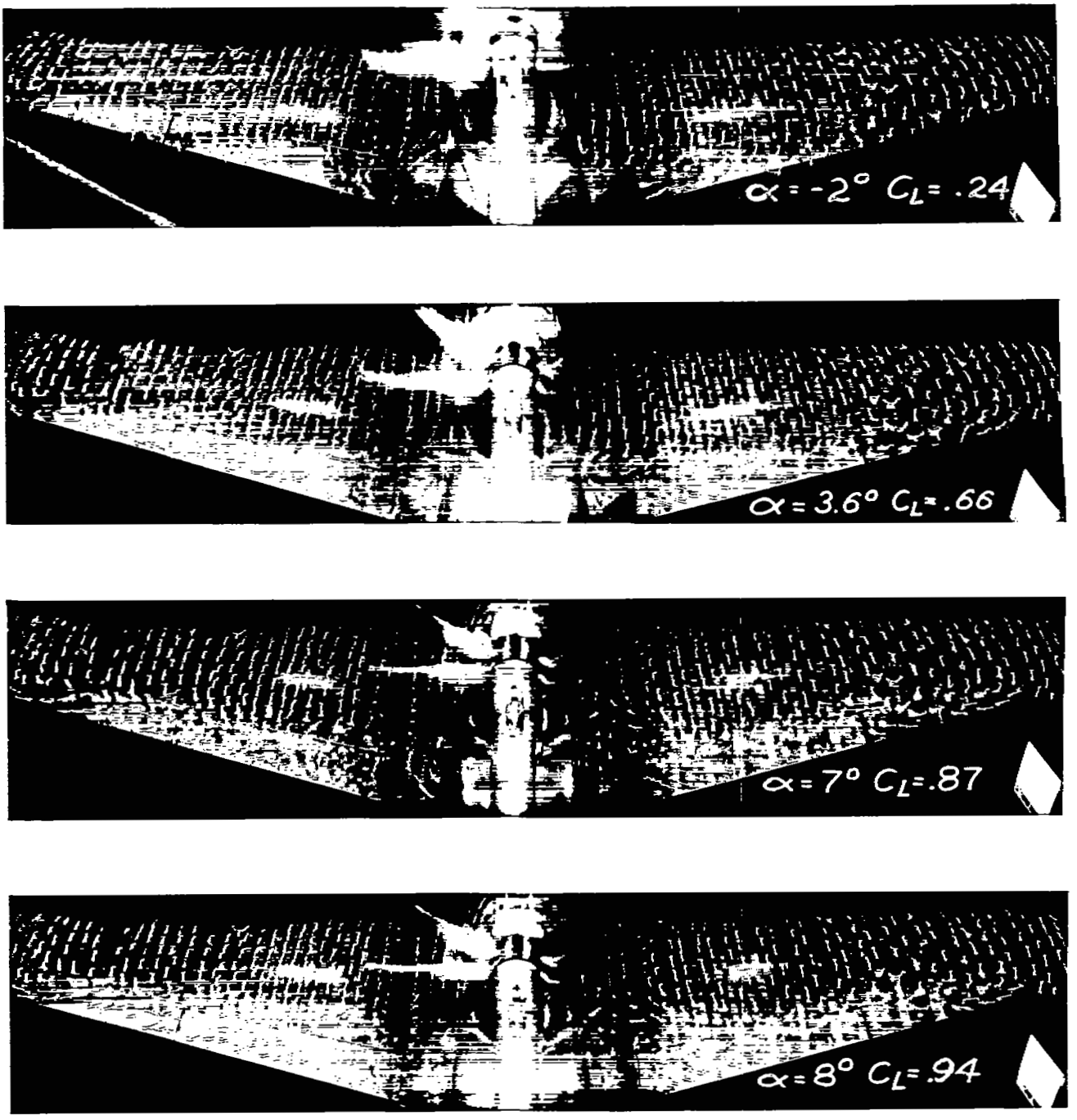

(a) Windmilling.

Figure 33.- Tuft studies of the 1/4-scale NAF seaplane model. Cruising configuration.

[redacted]

NATIONAL ADVISORY COMMITTEE FOR AERONAUTICS
LANGLEY MEMORIAL AERONAUTICAL LABORATORY – LANGLEY FIELD, VA.

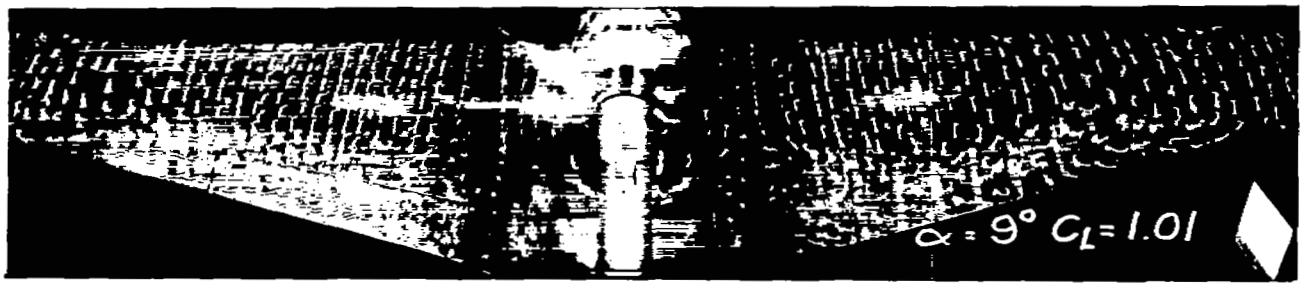

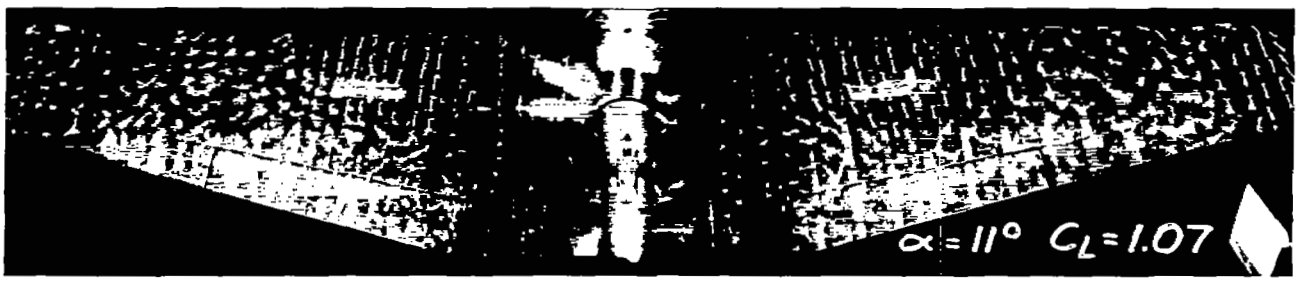

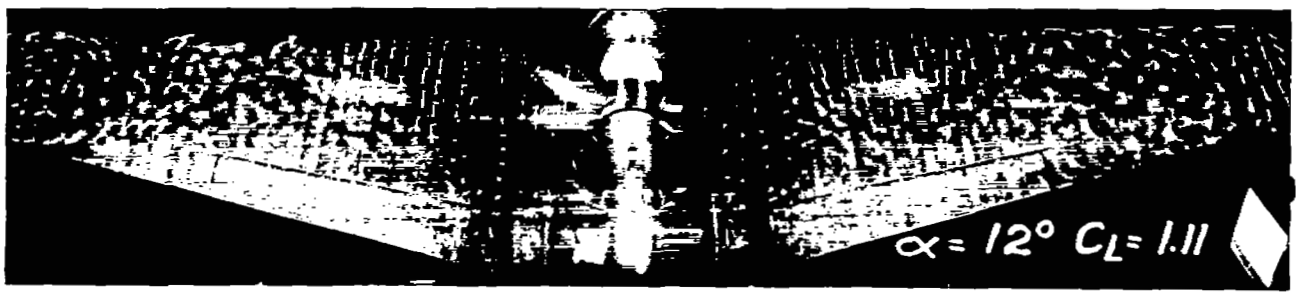

(a) Concluded.

Figure 33.- Continued.

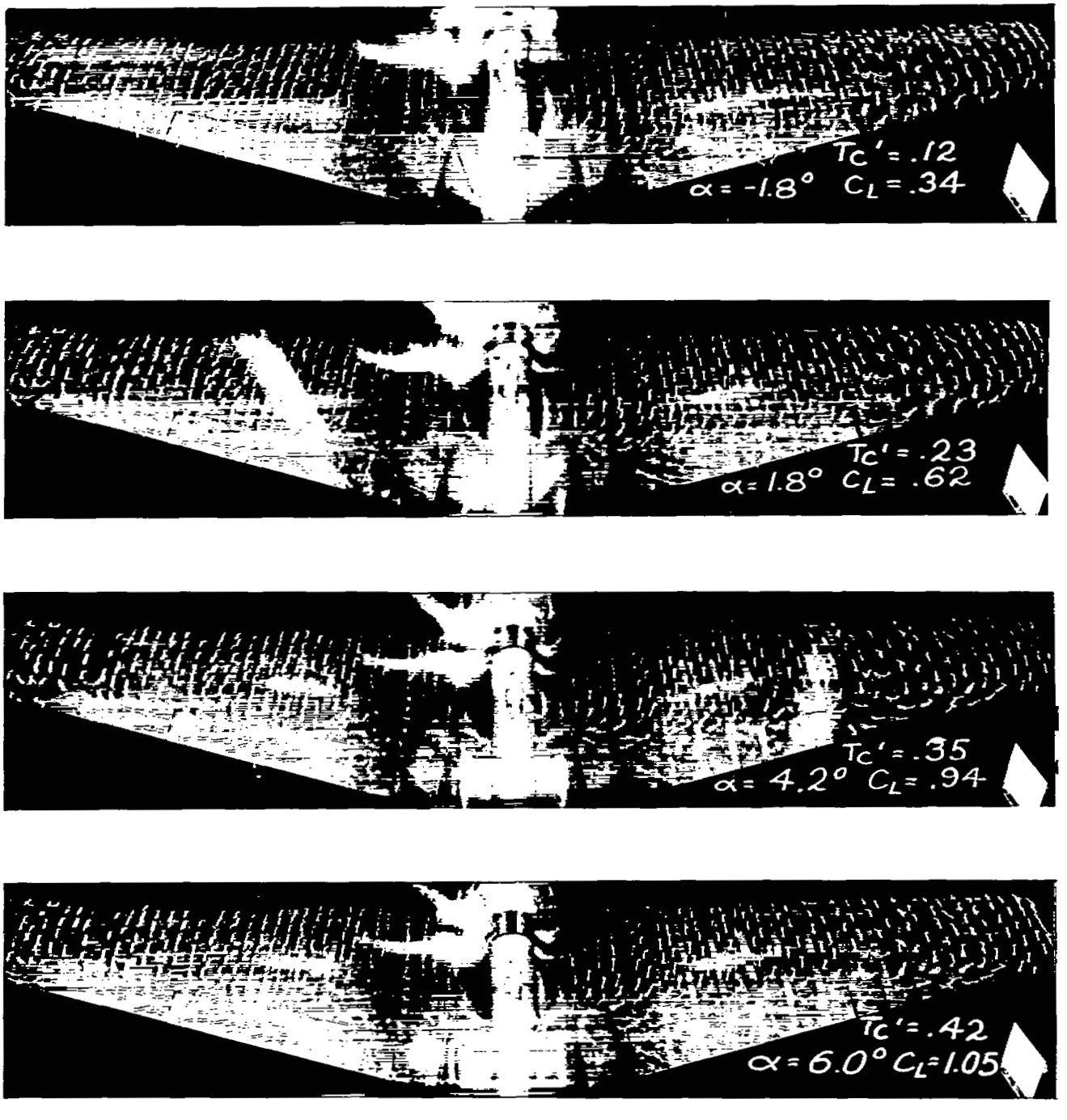

[redacted] (b) Take-off power.

Figure 33.- Continued.

NATIONAL ADVISORY COMMITTEE FOR AERONAUTICS
LANGLEY MEMORIAL AERONAUTICAL LABORATORY - LANGLEY FIELD, V

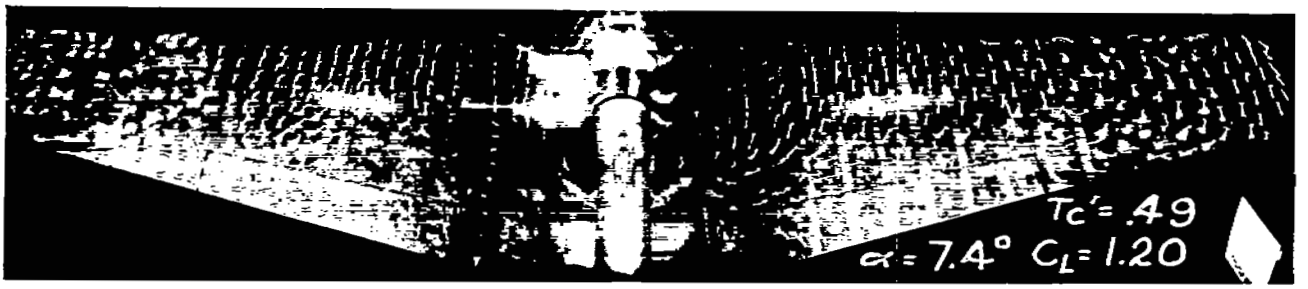

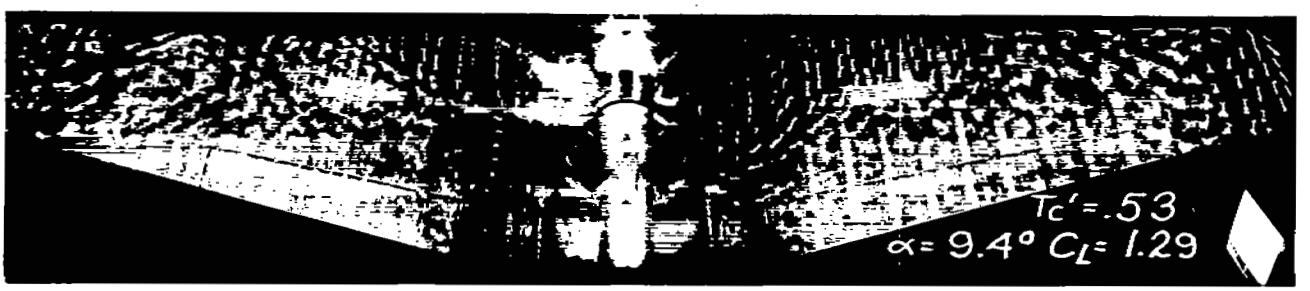

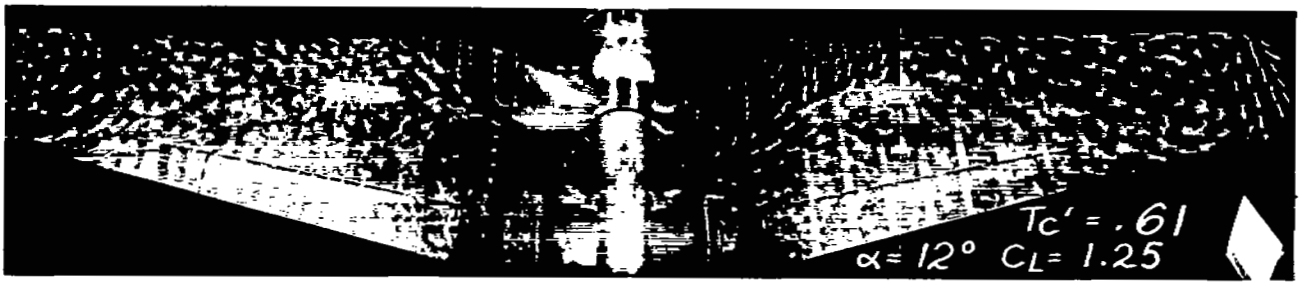

[redacted]

(b) Concluded.

Figure 33.- Concluded.

NATIONAL ADVISORY COMMITTEE FOR AERONAUTICS
LANGLEY MEMORIAL AERONAUTICAL LABORATORY – LANGLEY FIELD, VA.

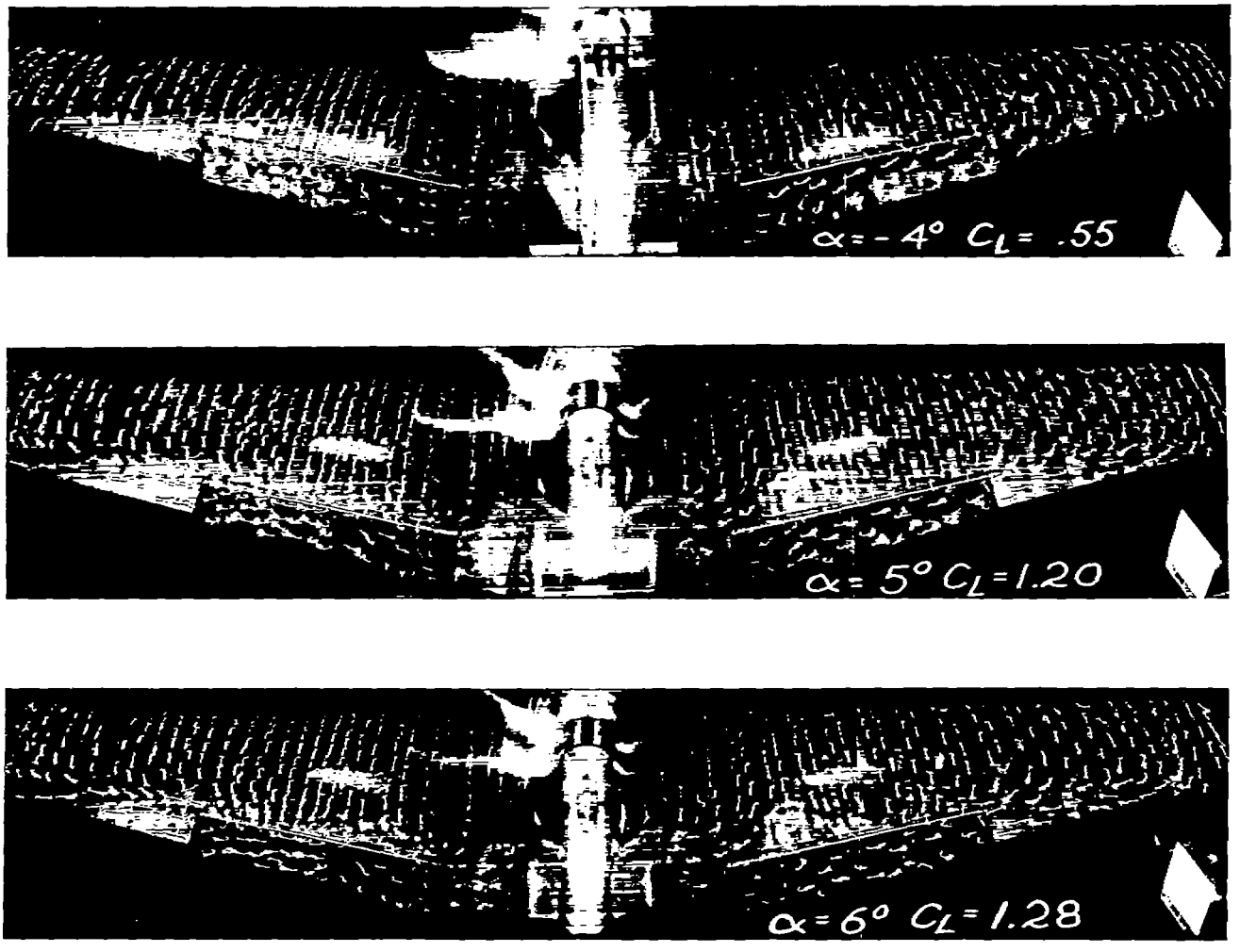

(a) Windmilling.

Figure 34.- Tuft studies of the 1/4-scale NAF seaplane model. Landing configuration.

[redacted]

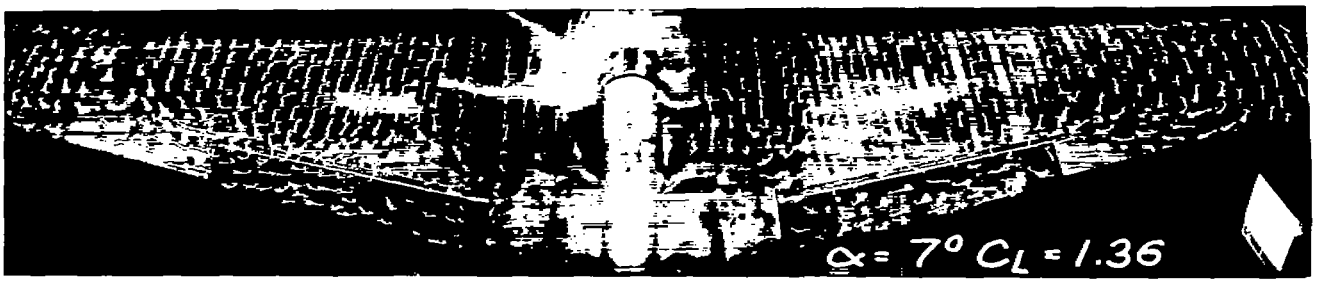

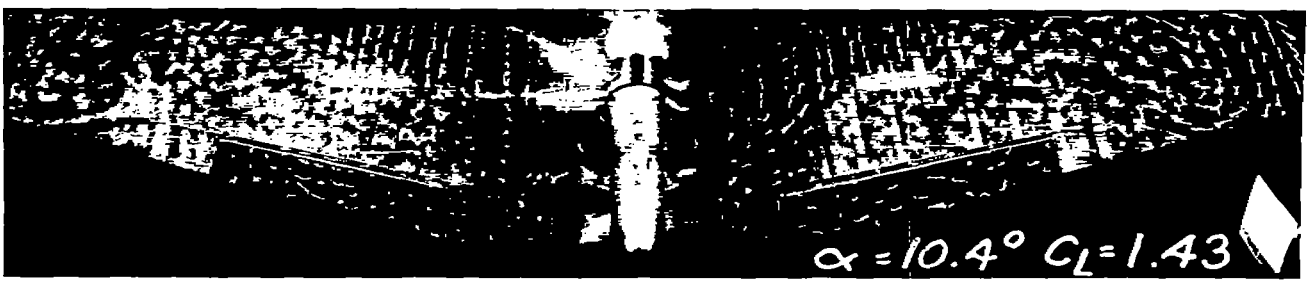

[redacted]

(a) Concluded.

Figure 34.- Continued.

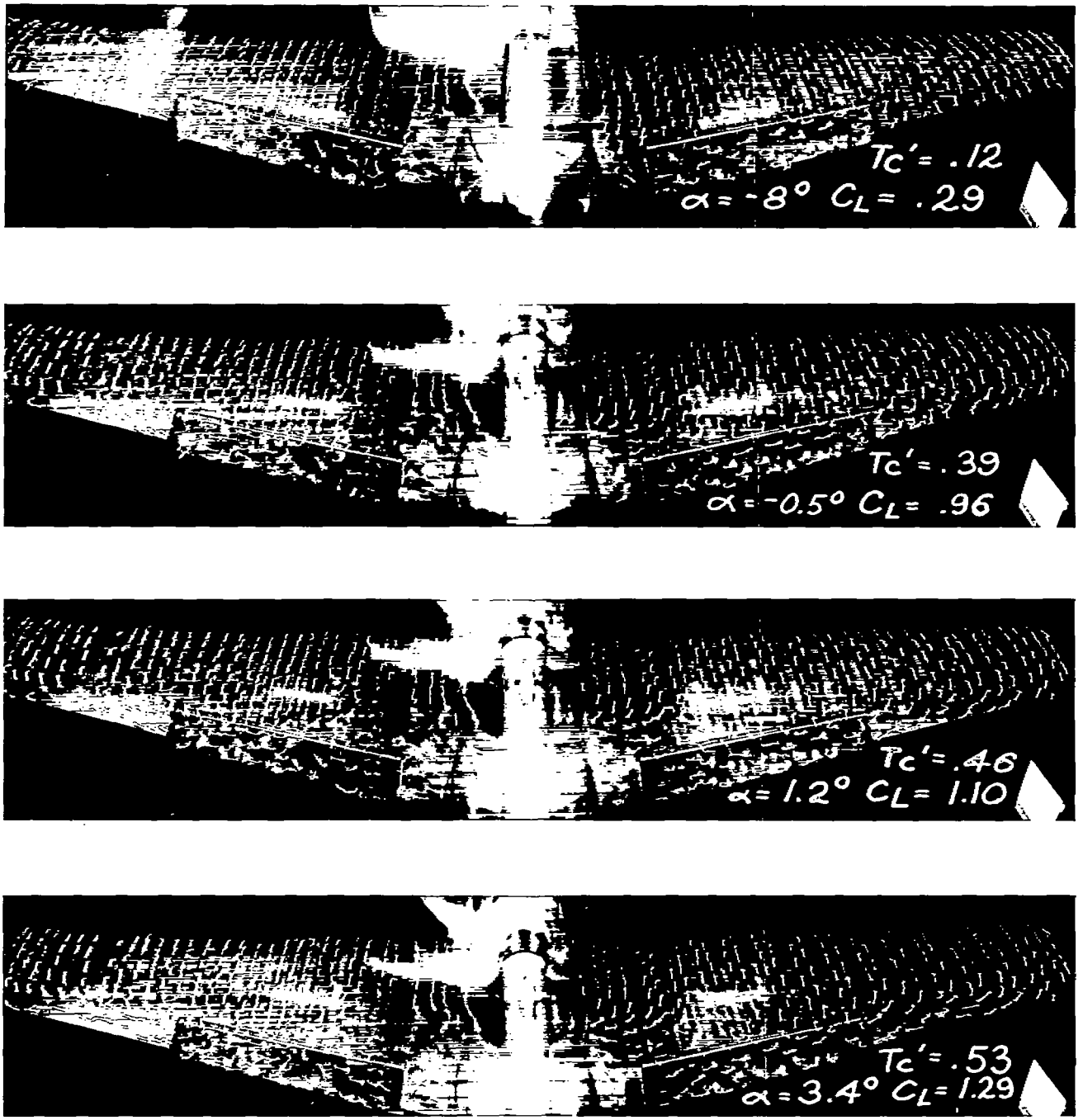

[redacted] (b) Take-off power.

Figure 34.- Continued.

NATIONAL ADVISORY COMMITTEE FOR AERONAUTICS
LANGLEY MEMORIAL AERONAUTICAL LABORATORY - LANGLEY FIELD, VA.

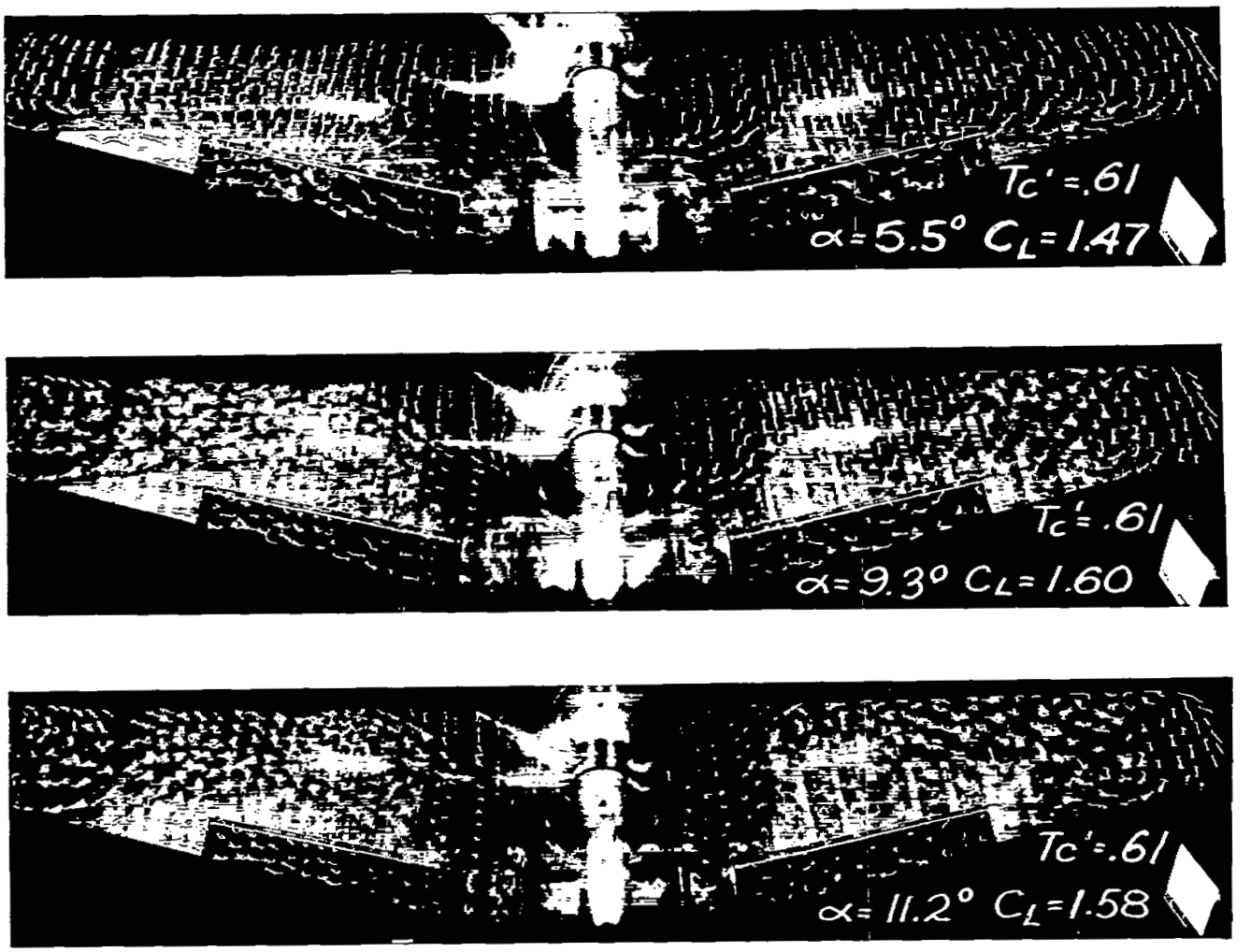

[redacted] (b) Concluded.

Figure 34.- Concluded.

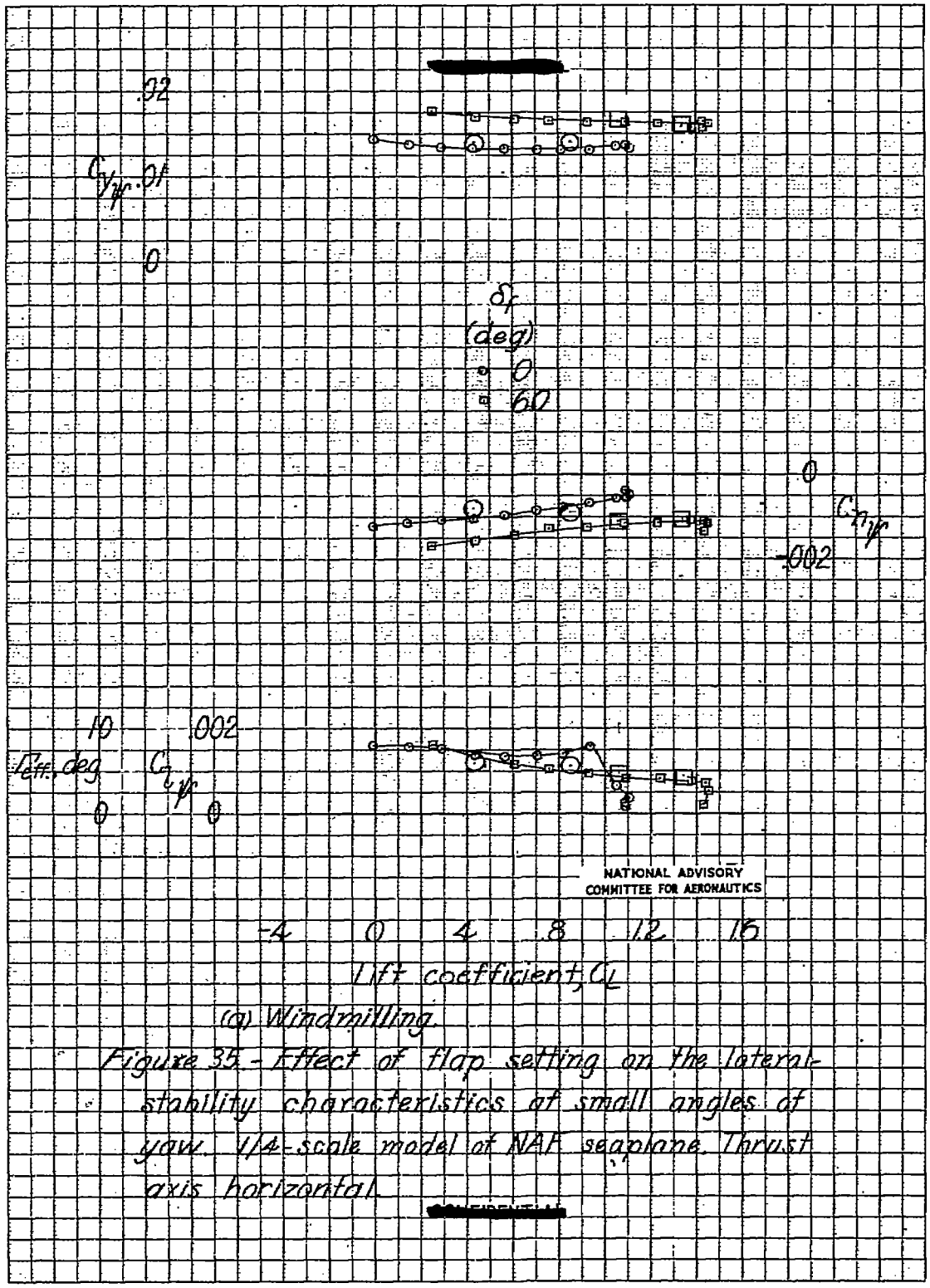

(a) Windmilling.

Figure 35.- Effect of flap setting on the lateral-stability characteristics at small angles of yaw. 1/4-scale model of NAF seaplane. Thrust axis horizontal.

[redacted]

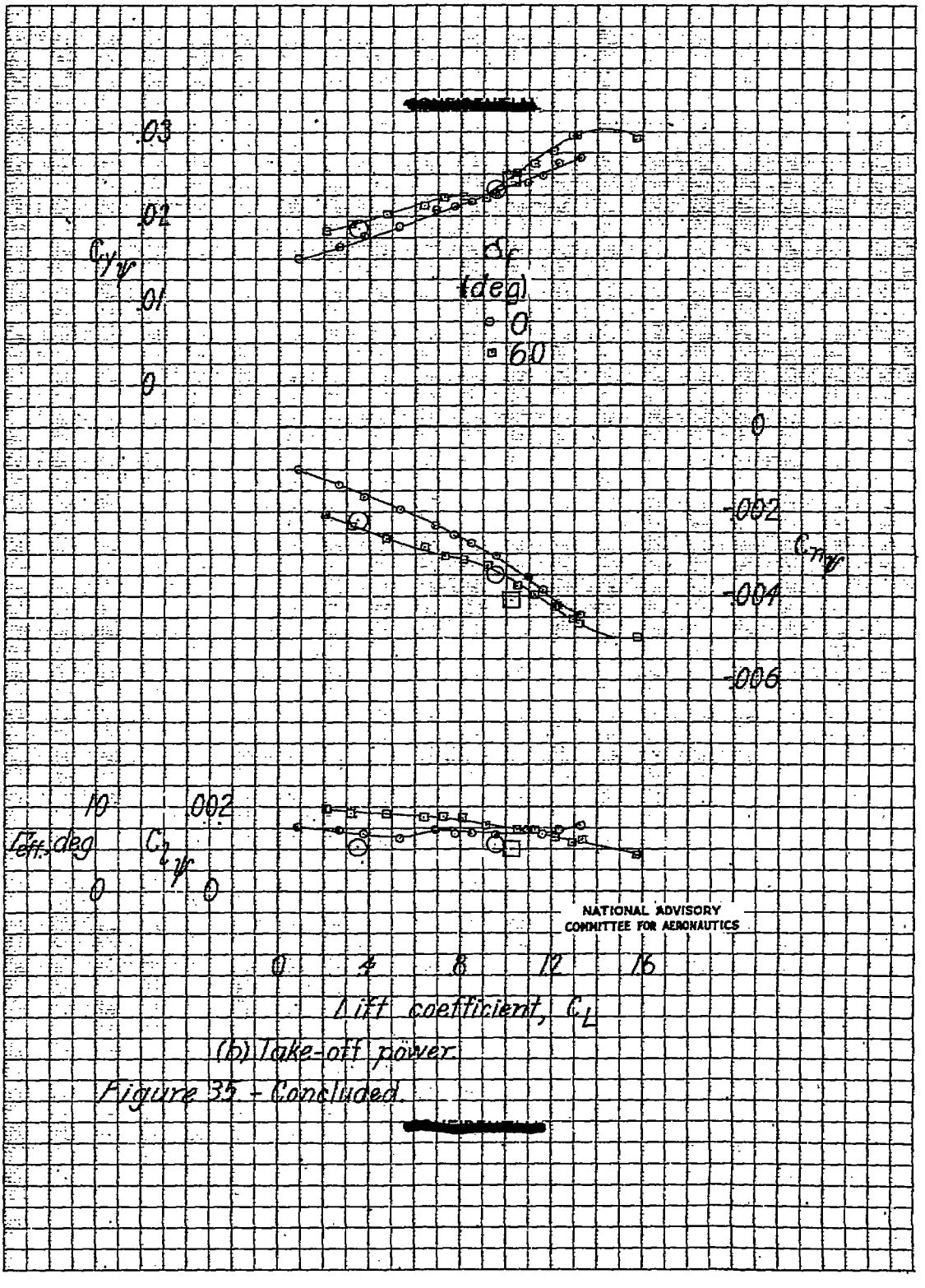

(b) Take-off power.

Figure 35 - Concluded.

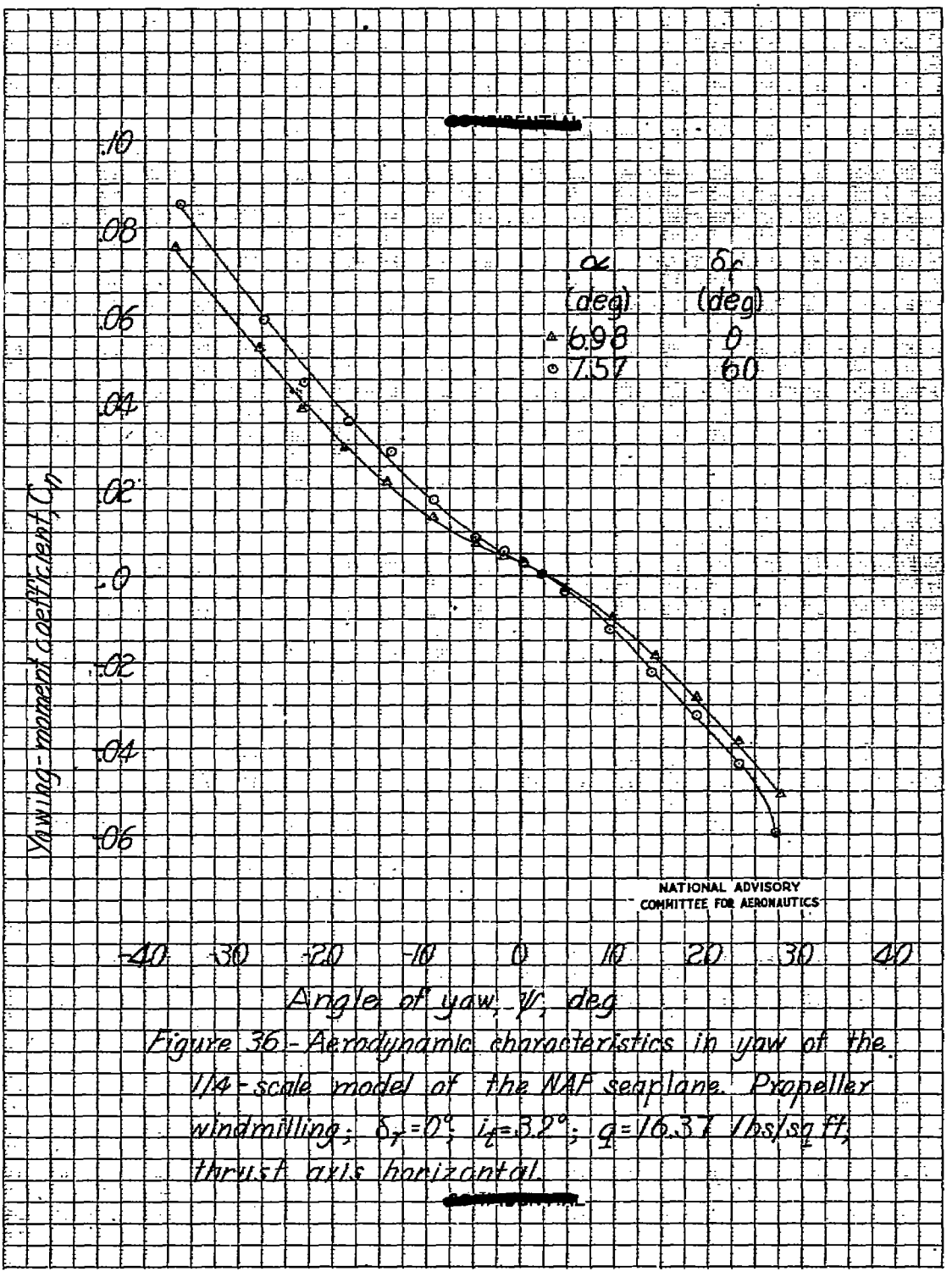

Figure 36.- Aerodynamic characteristics in yaw of the 1/4-scale model of the NAF seaplane. Propeller windmilling; $\delta_f = 0°$; $i_t = 3.2°$; $q = 16.37$ lbs/sq ft; thrust axis horizontal.

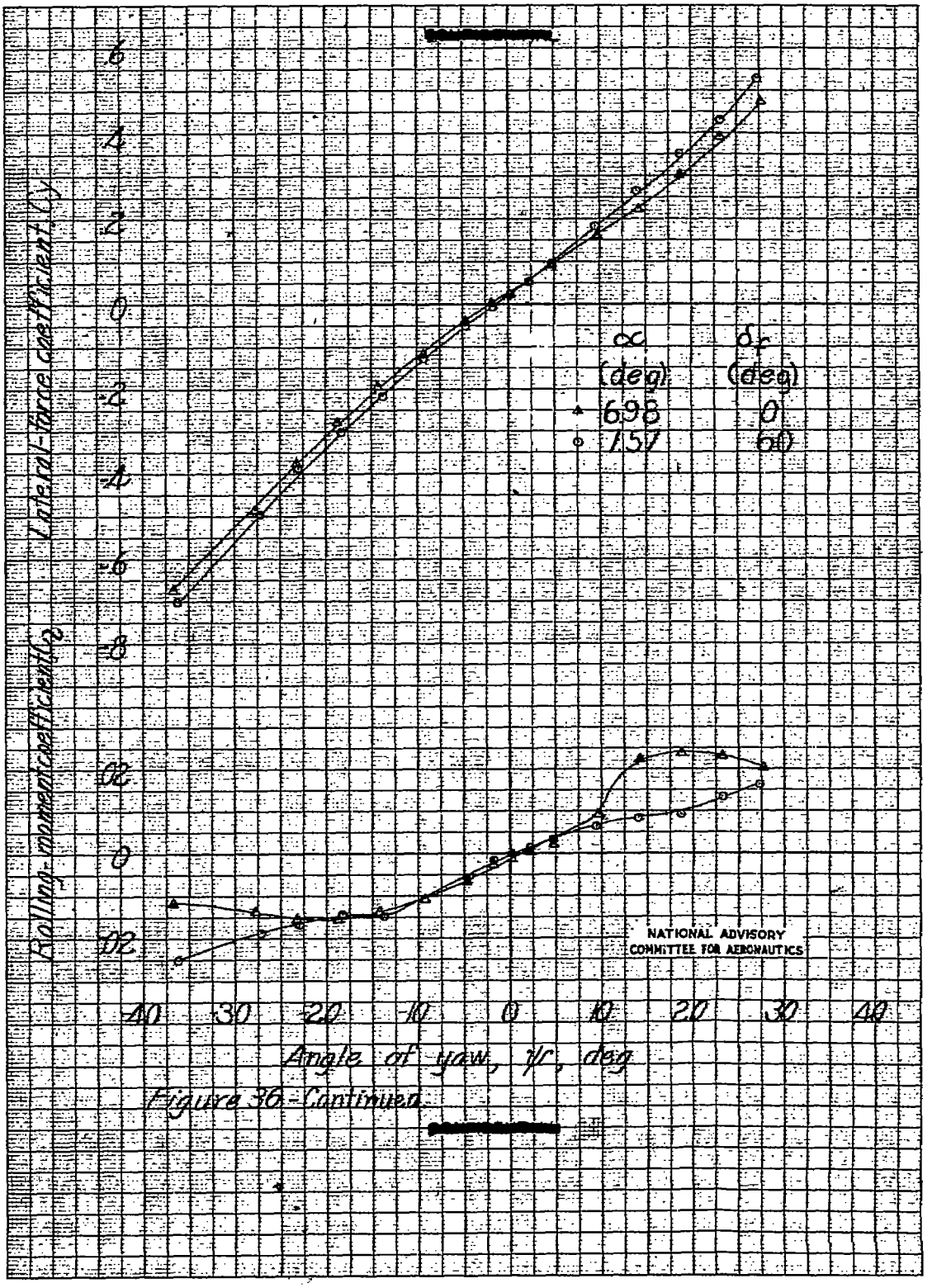

Figure 36.- Continued.

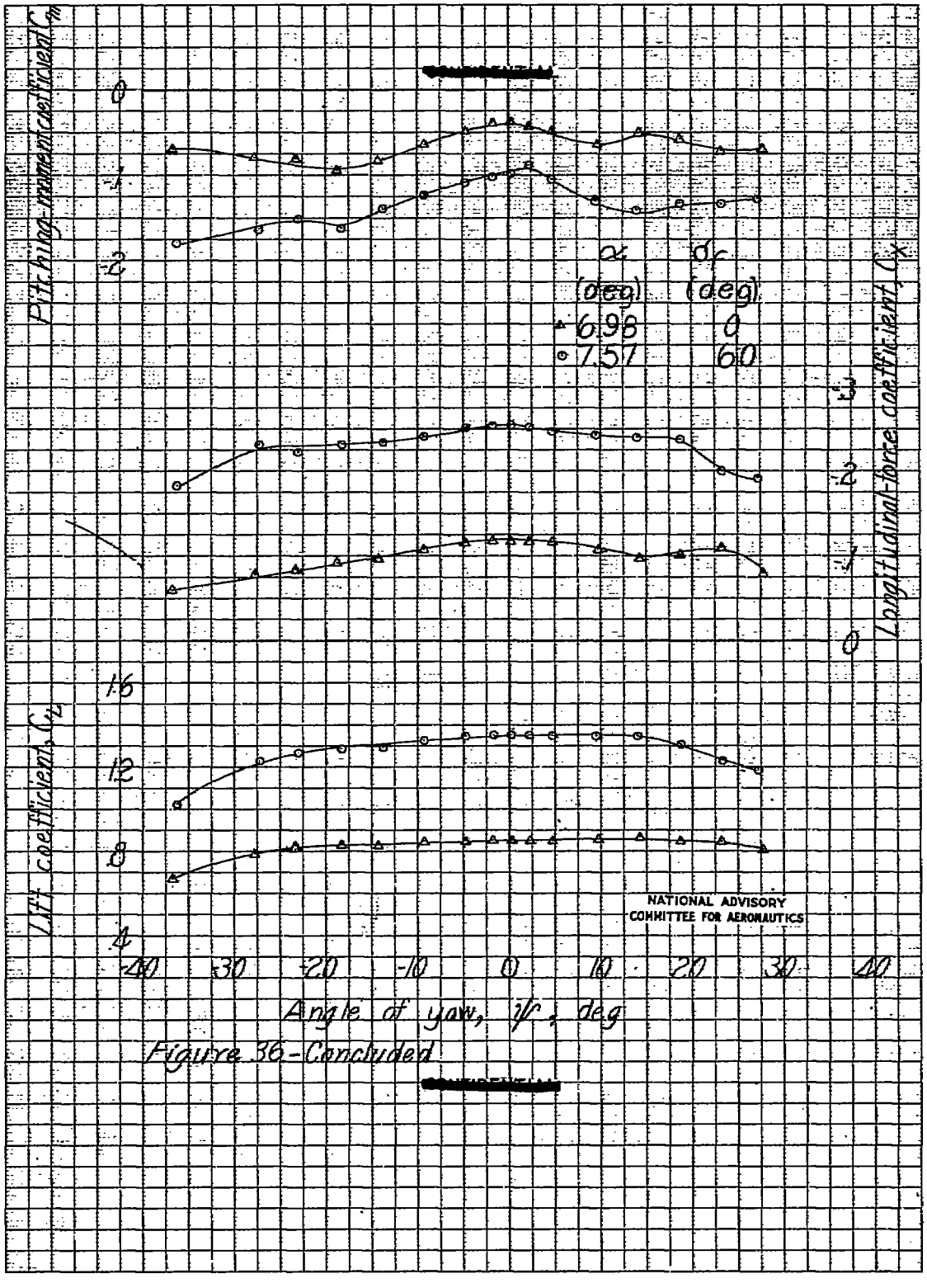

Figure 36.-Concluded

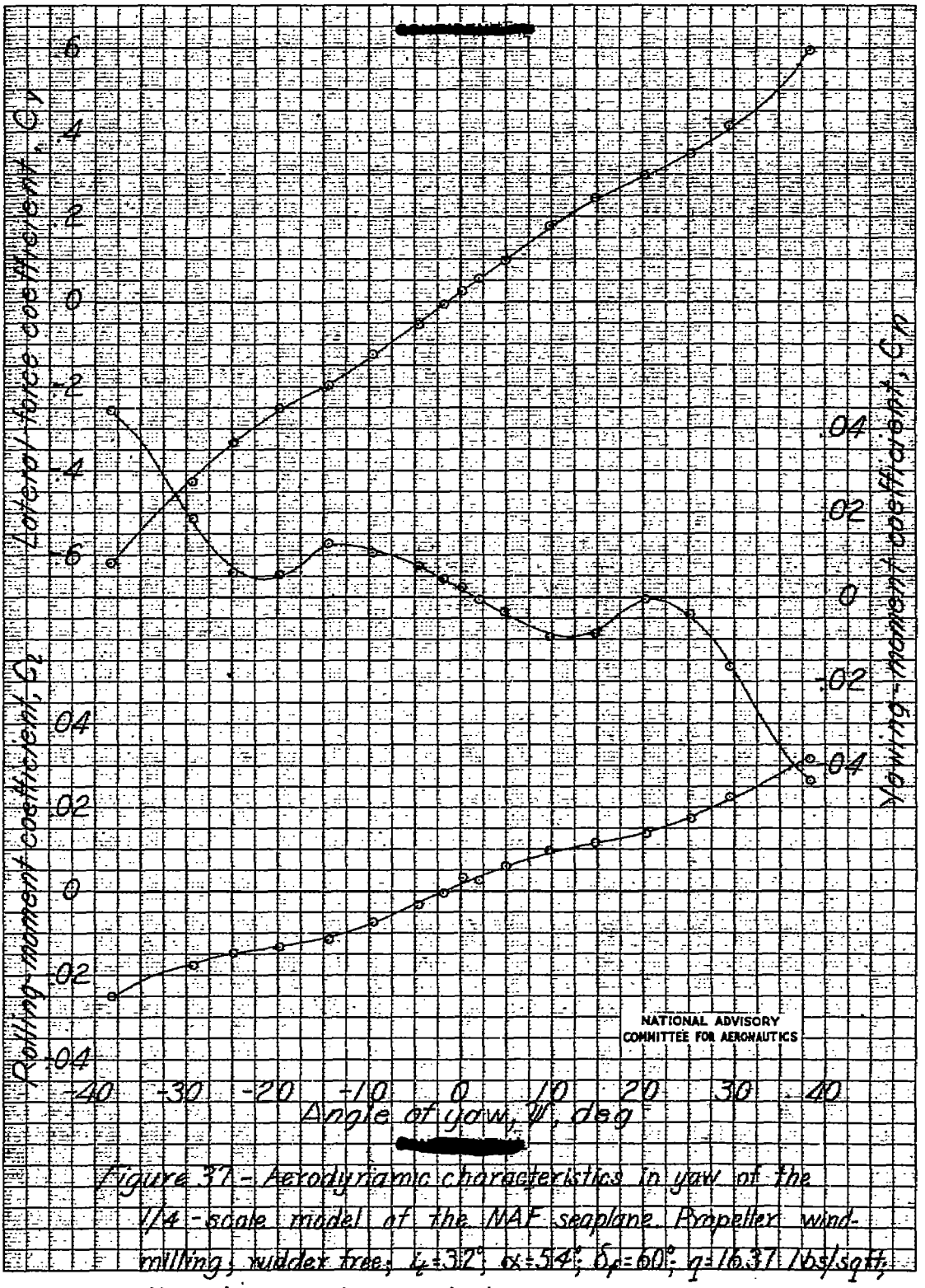

Figure 37 - Aerodynamic characteristics in yaw of the 1/4 - scale model of the MAF seaplane. Propeller windmilling; rudder free; i_t=3.2°; α=5.4°; δ_f=60°; q=16.37 lbs/sq ft; thrust axis horizontal.

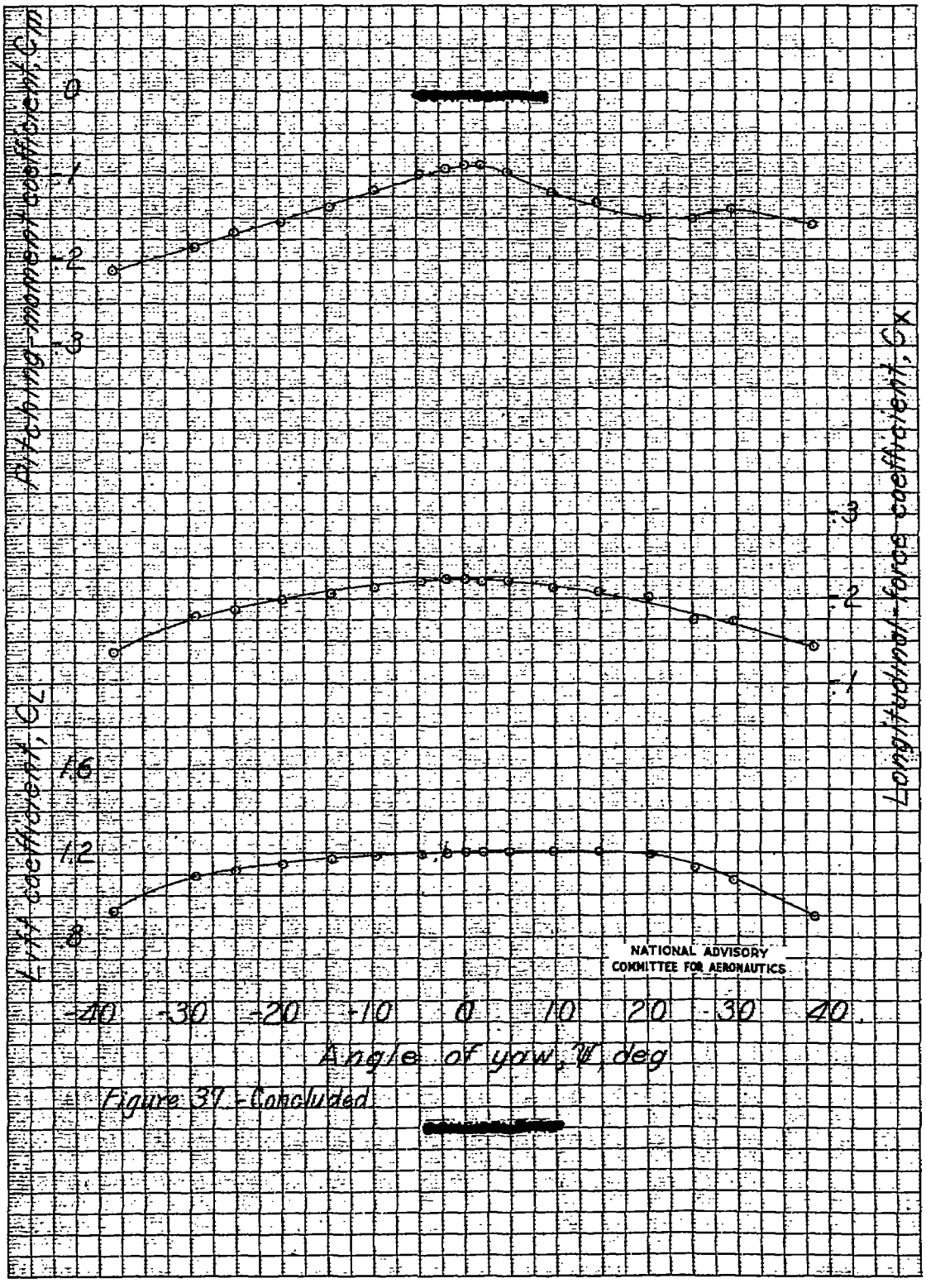

Figure 37.- Concluded

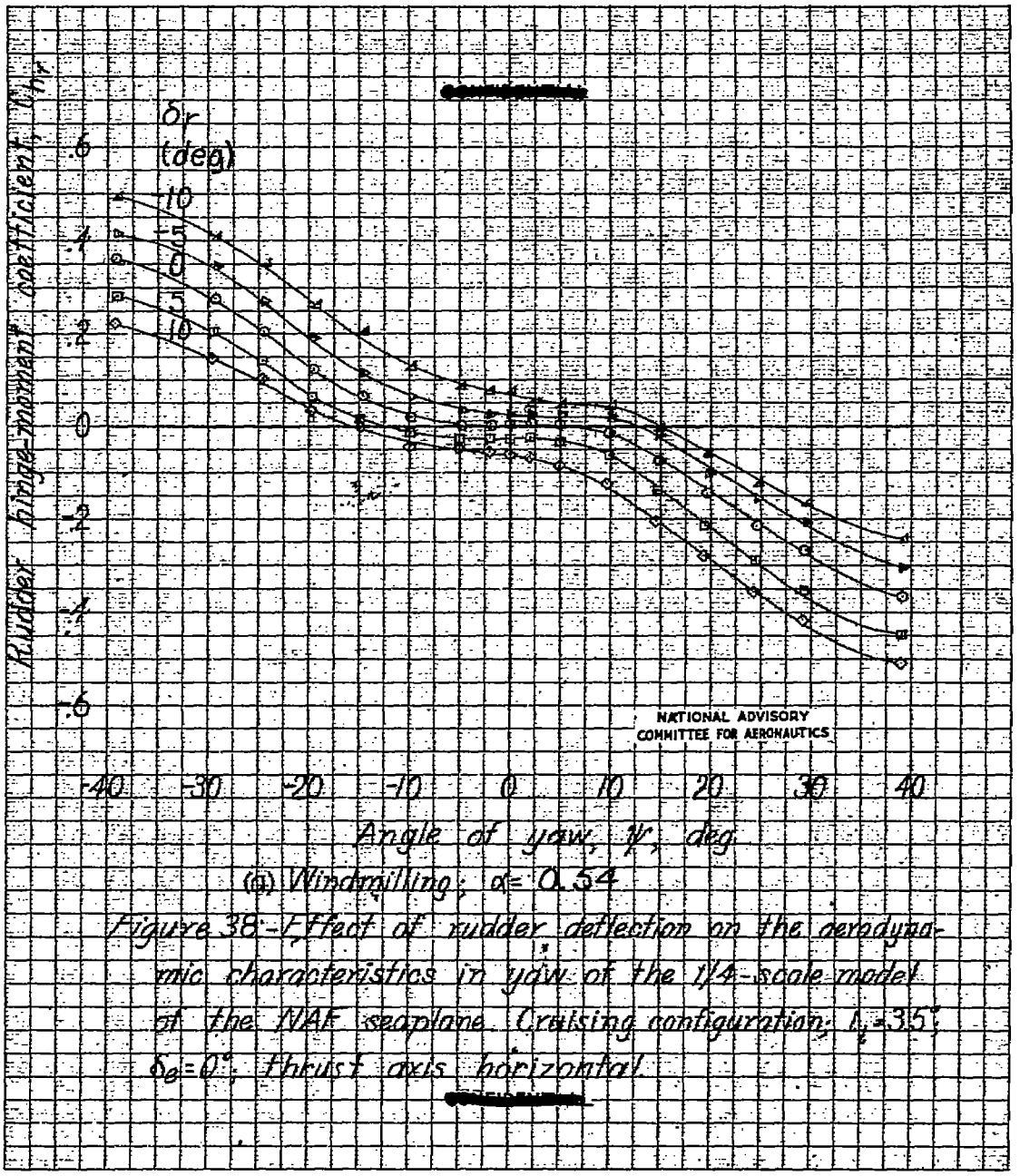

(a) Windmilling; $\alpha = 0.54$

Figure 38.- Effect of rudder deflection on the aerodynamic characteristics in yaw of the 1/4-scale model of the NAF seaplane. Cruising configuration; $i_t = 3.5°$; $\delta_e = 0°$; thrust axis horizontal.

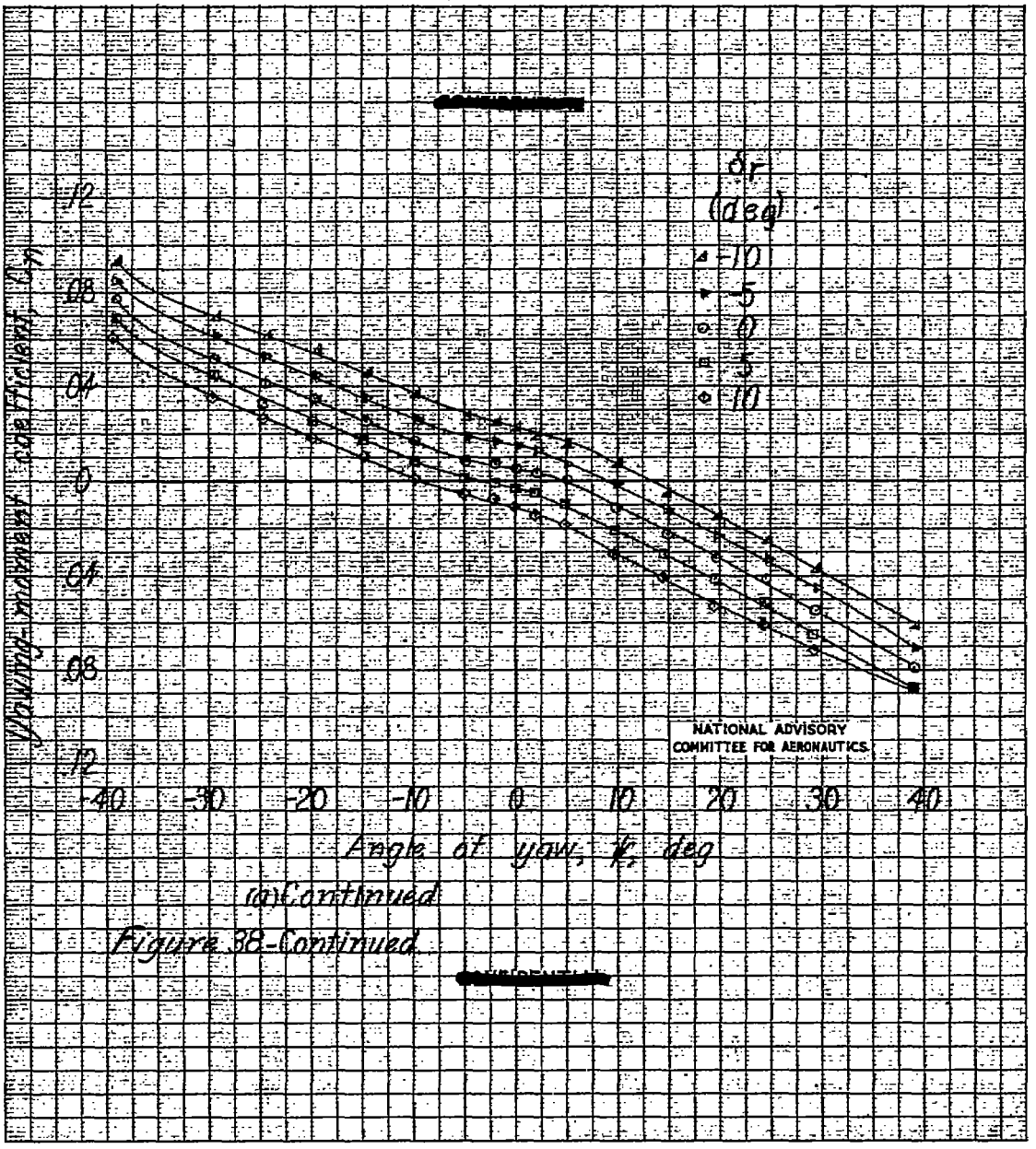

(a) Continued

Figure 38-Continued

CONFIDENTIAL

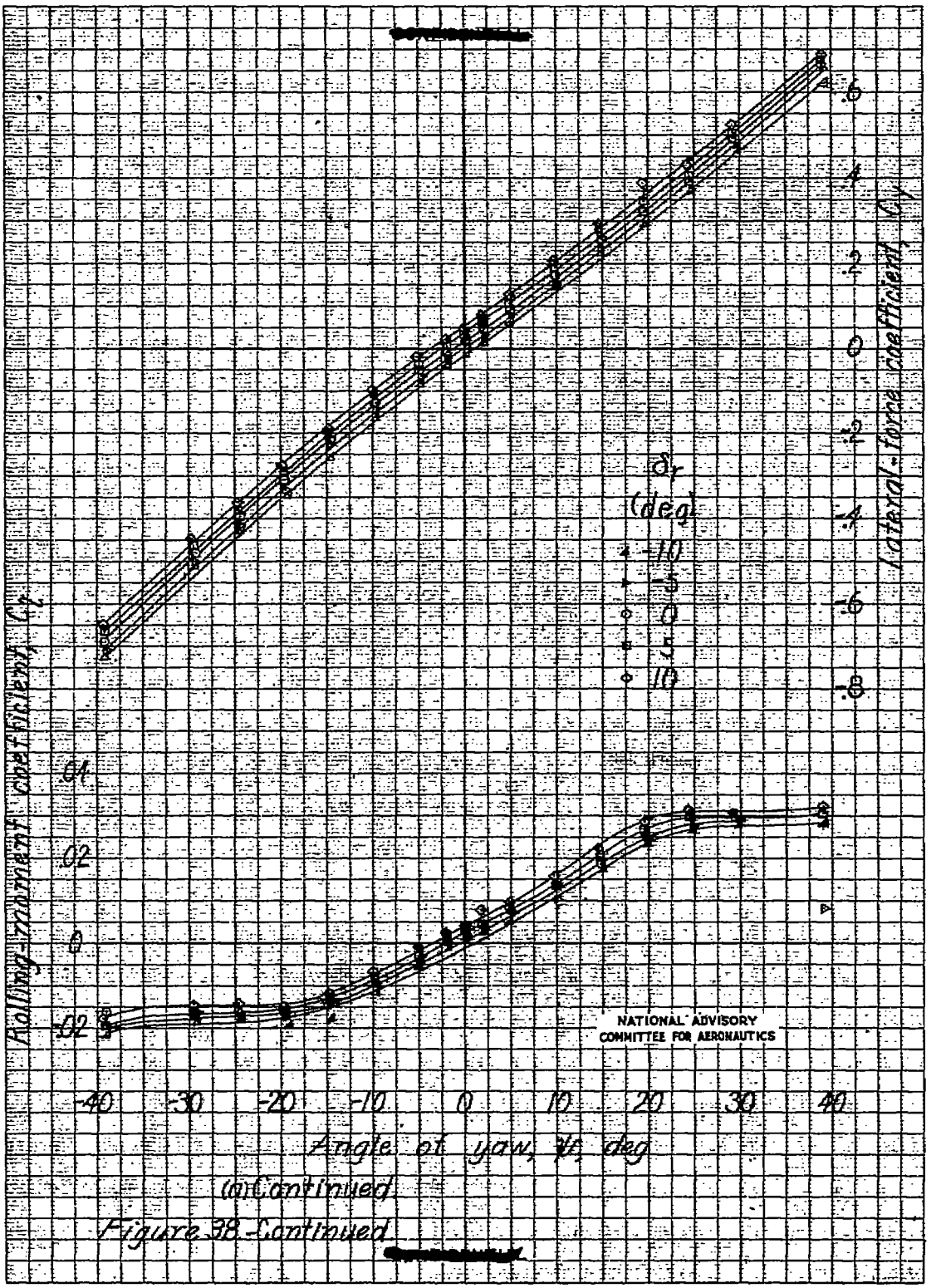

(a)Continued.

Figure 38.-Continued.

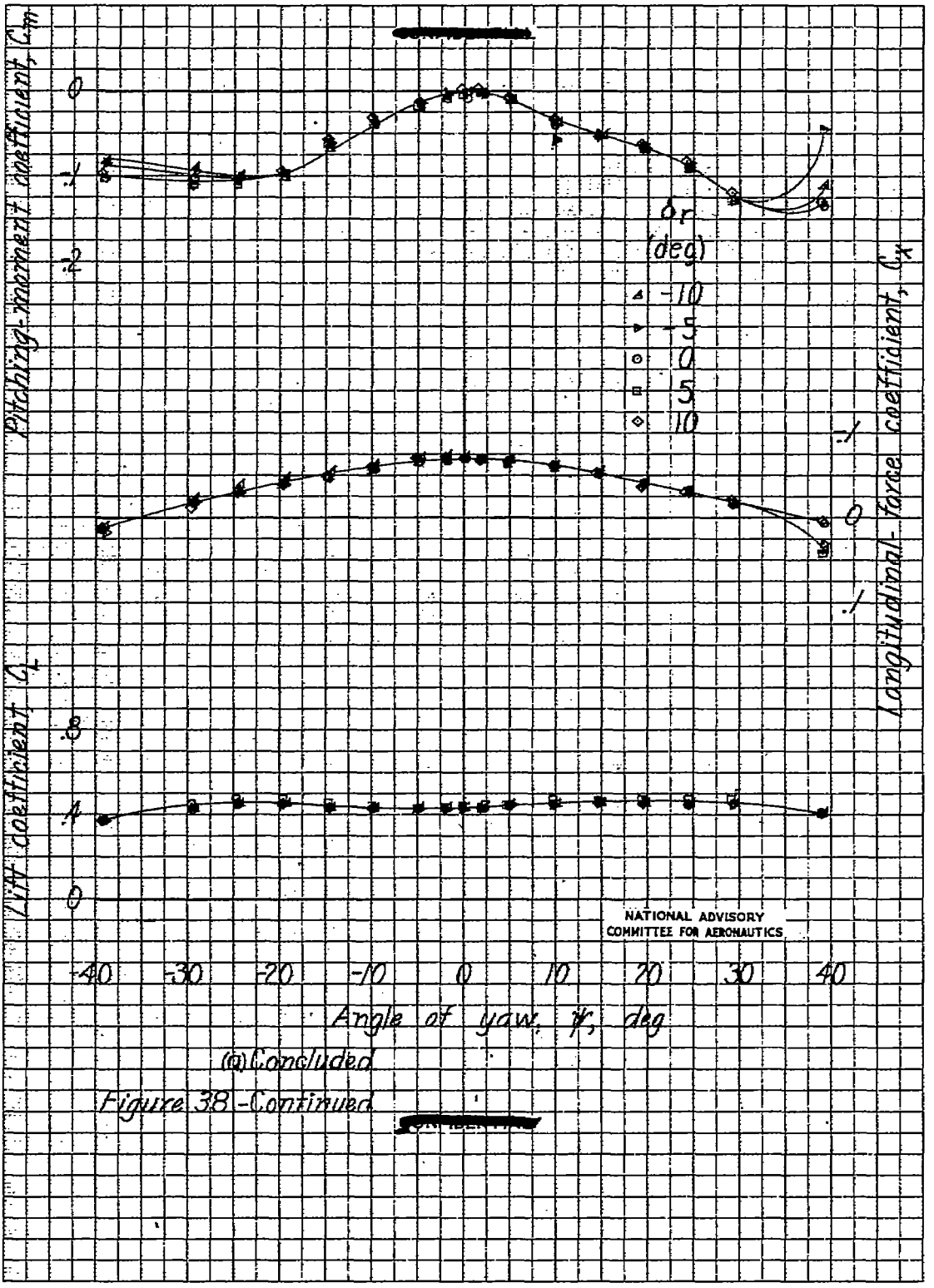

(a) Concluded

Figure 38.-Continued.

CONFIDENTIAL

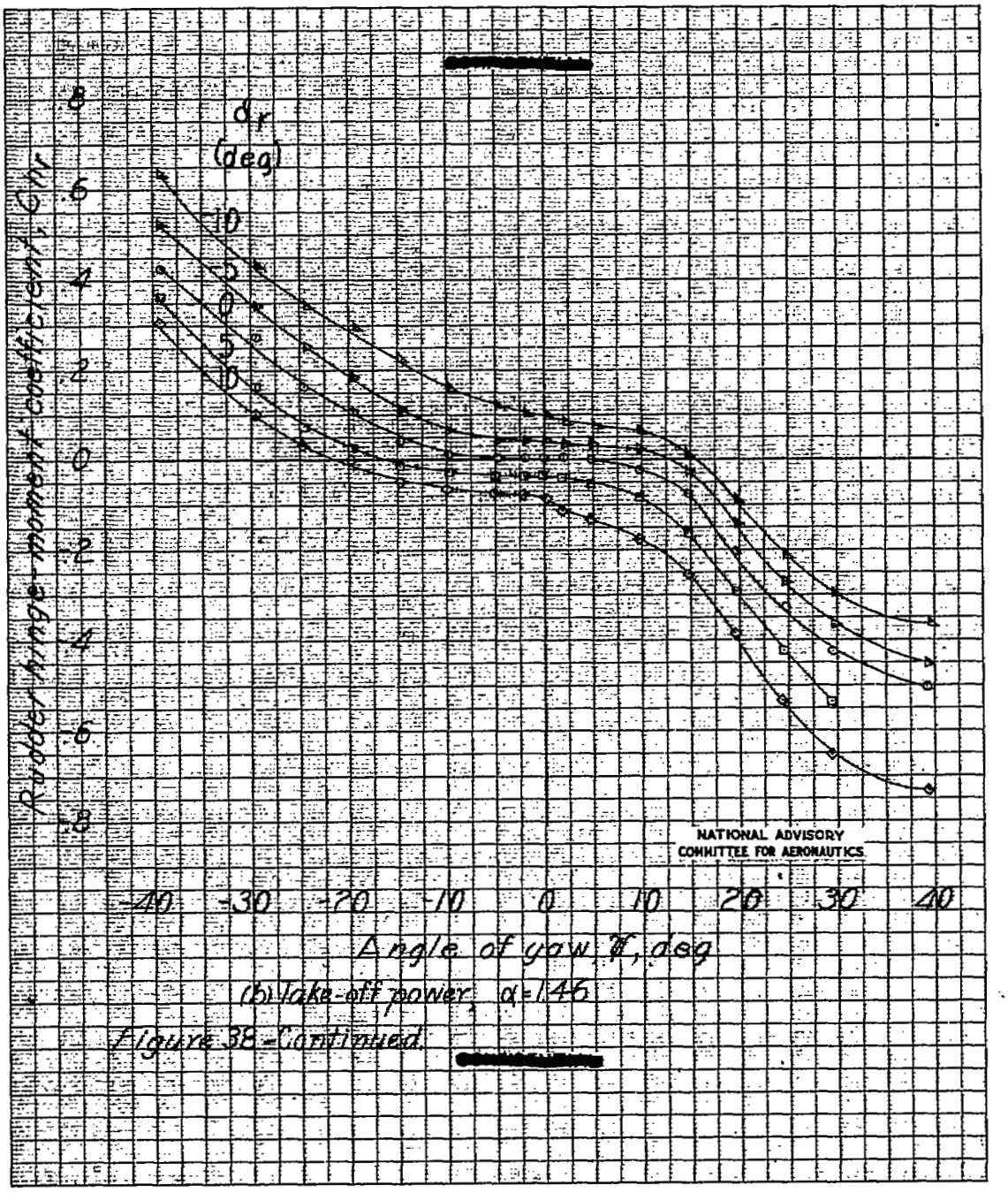

(b) Take-off power, $\alpha = 1.4°$

Figure 38 - Continued.

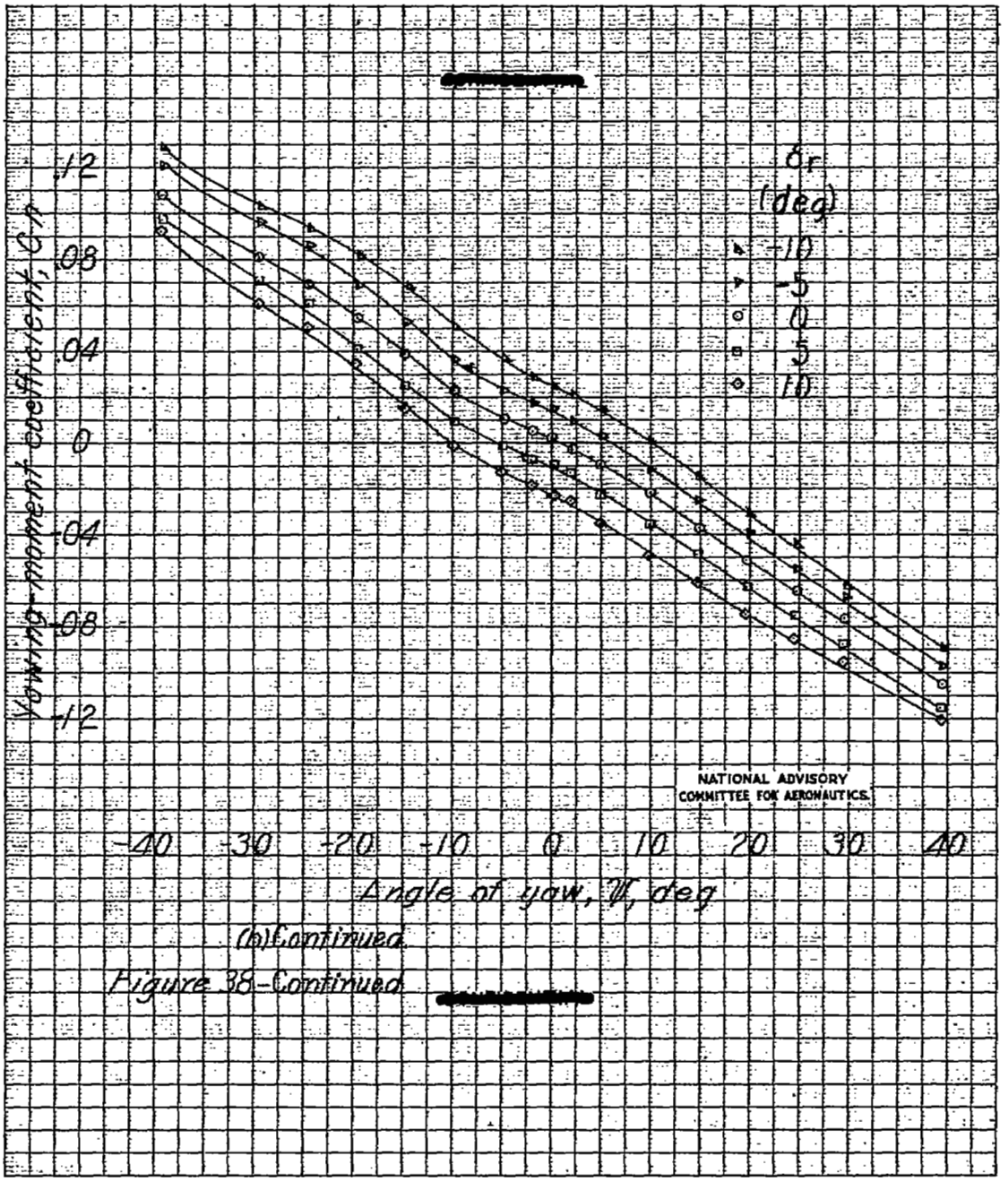

(b) Continued

Figure 38.- Continued

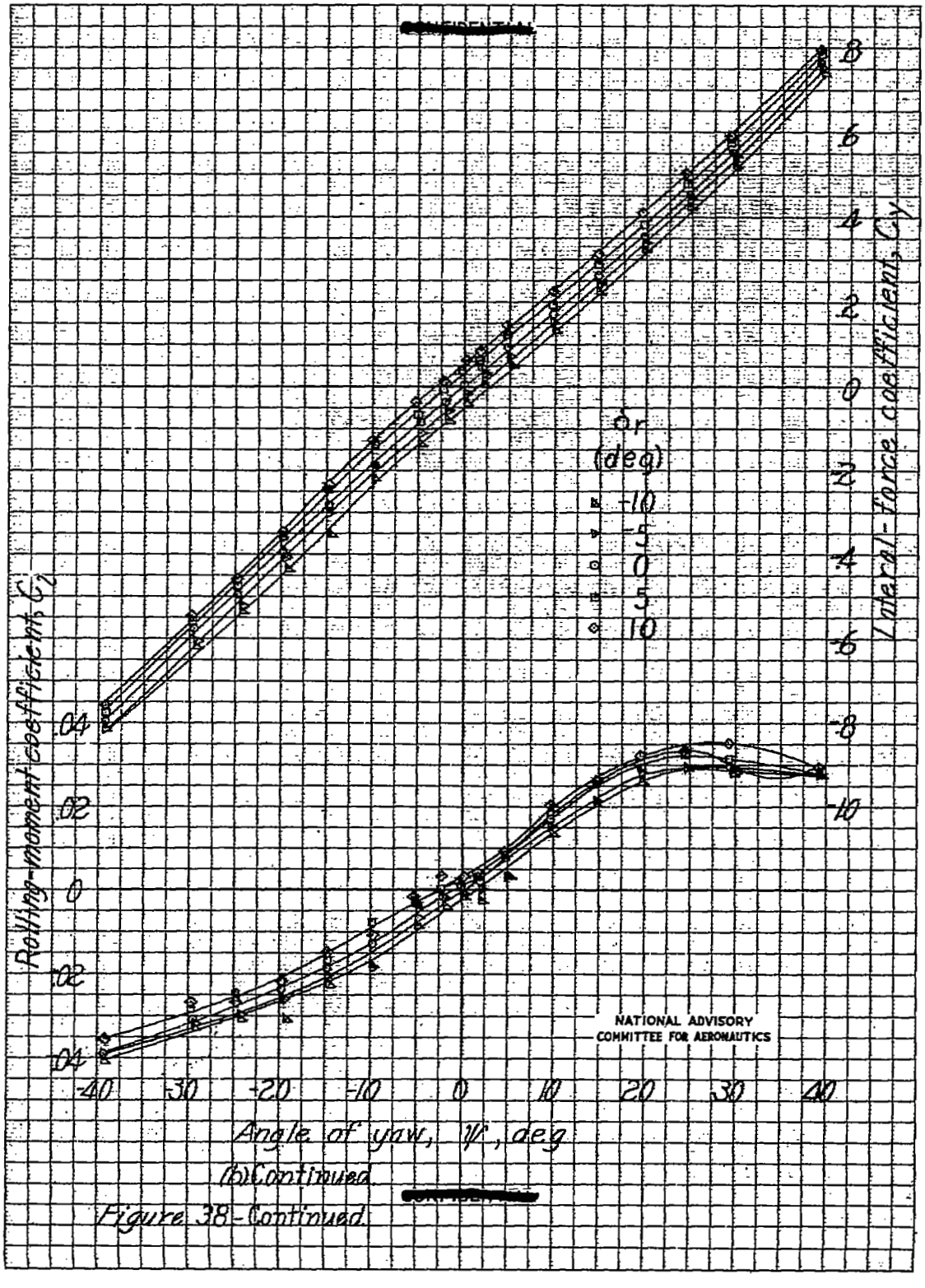

(b) Continued

Figure 38 - Continued

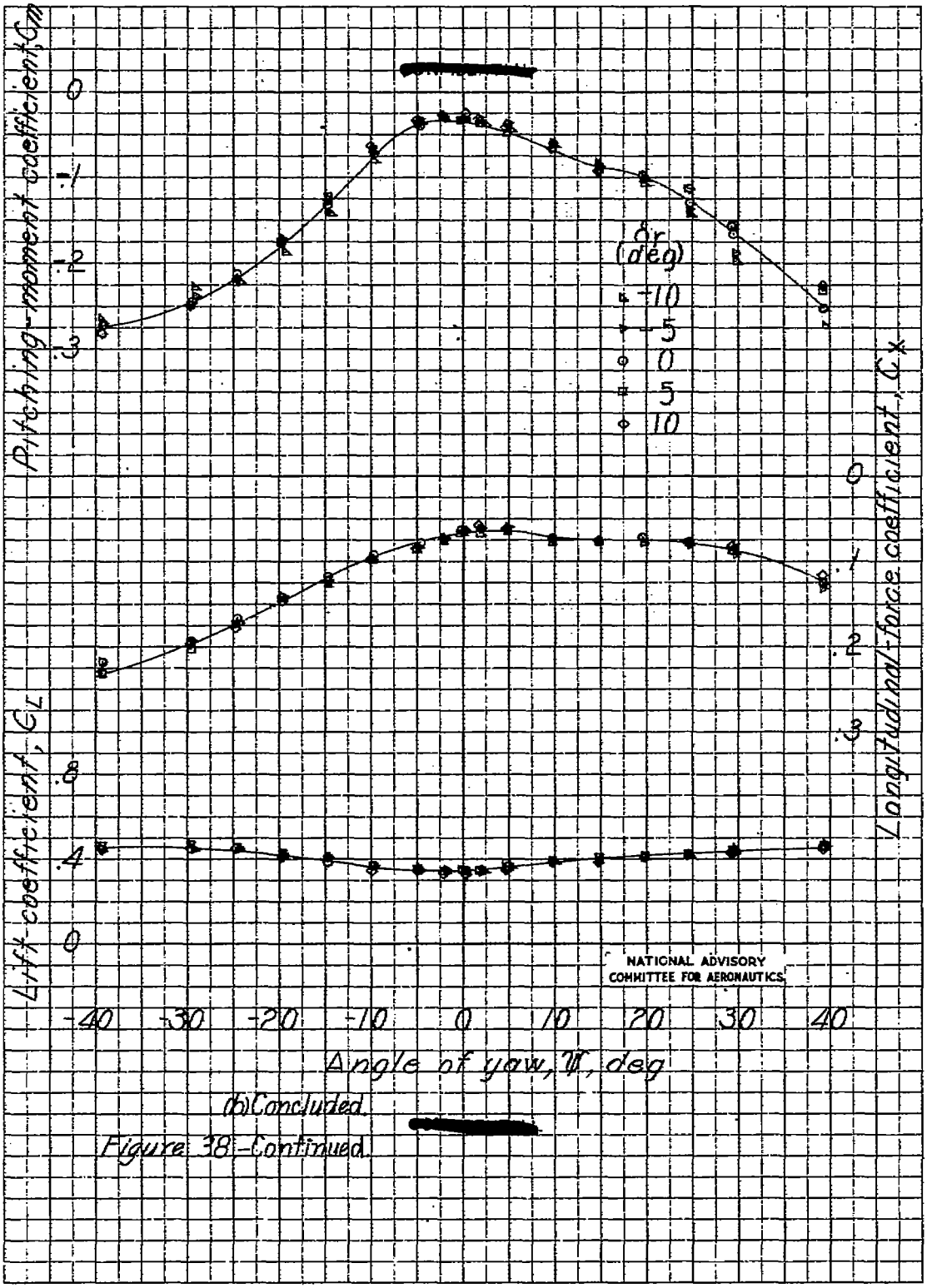

(b) Concluded.

Figure 38.- Continued.

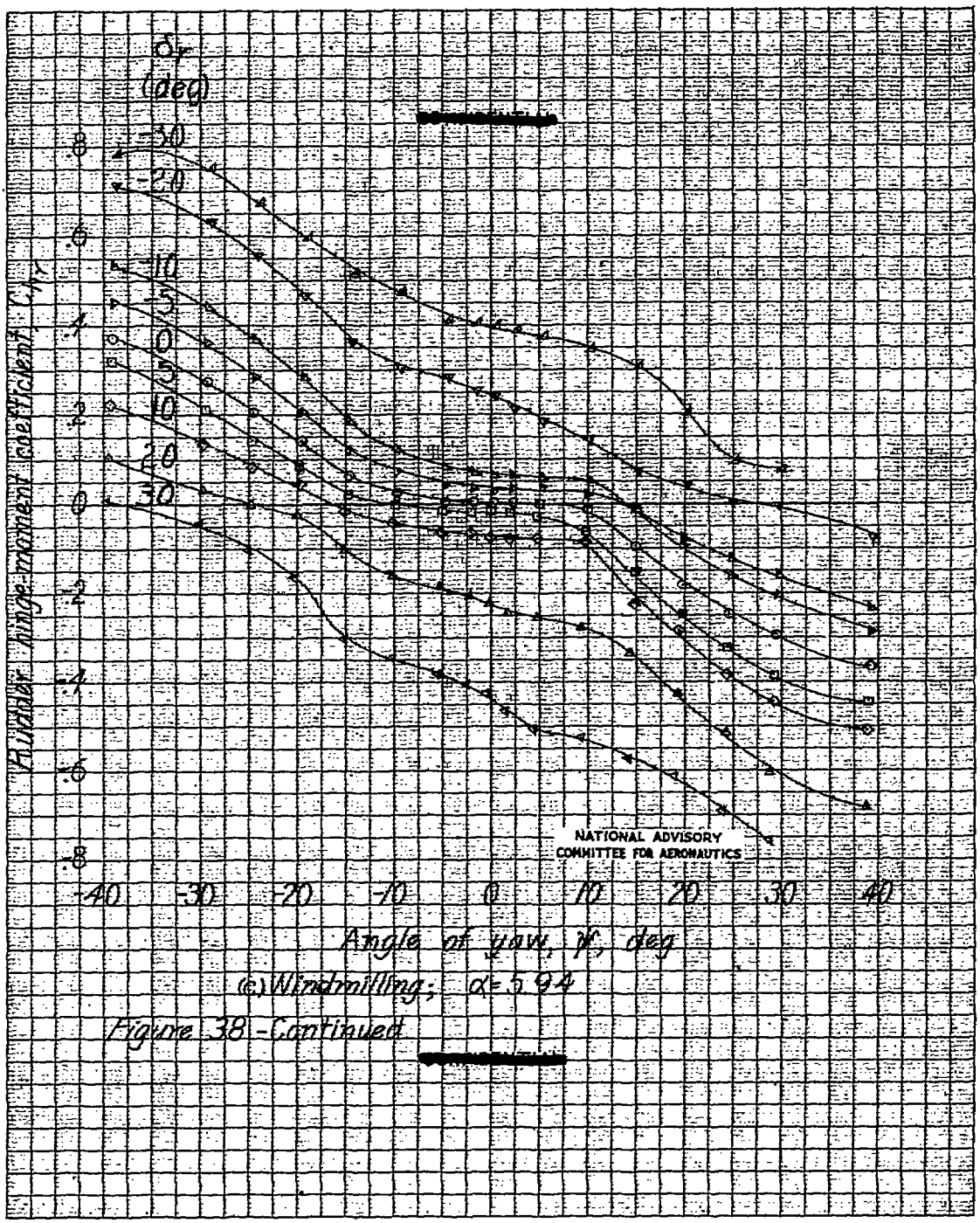

(c) Windmilling; $\alpha = 5.94$

Figure 38 - Continued

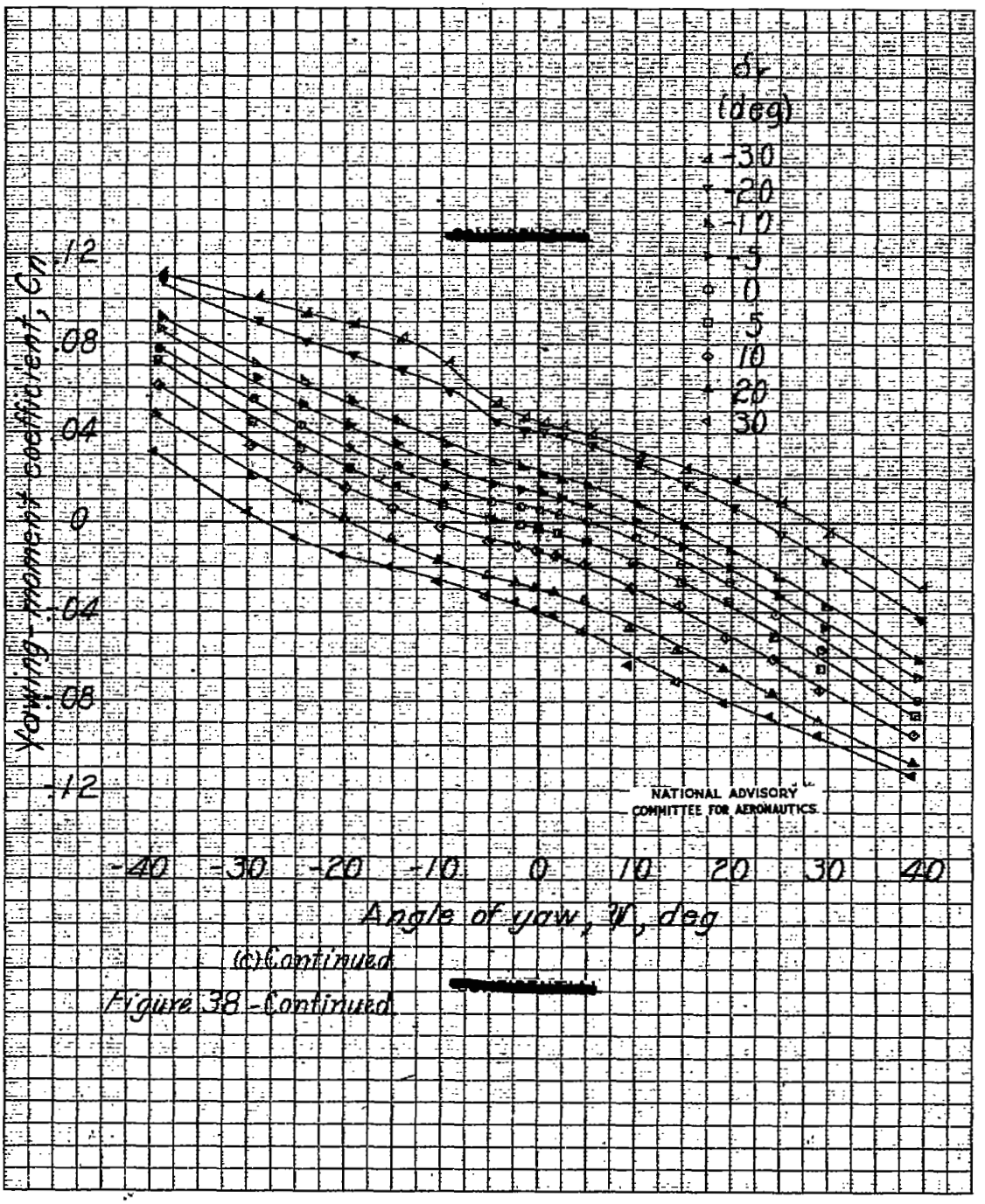

(c) Continued

Figure 38.- Continued.

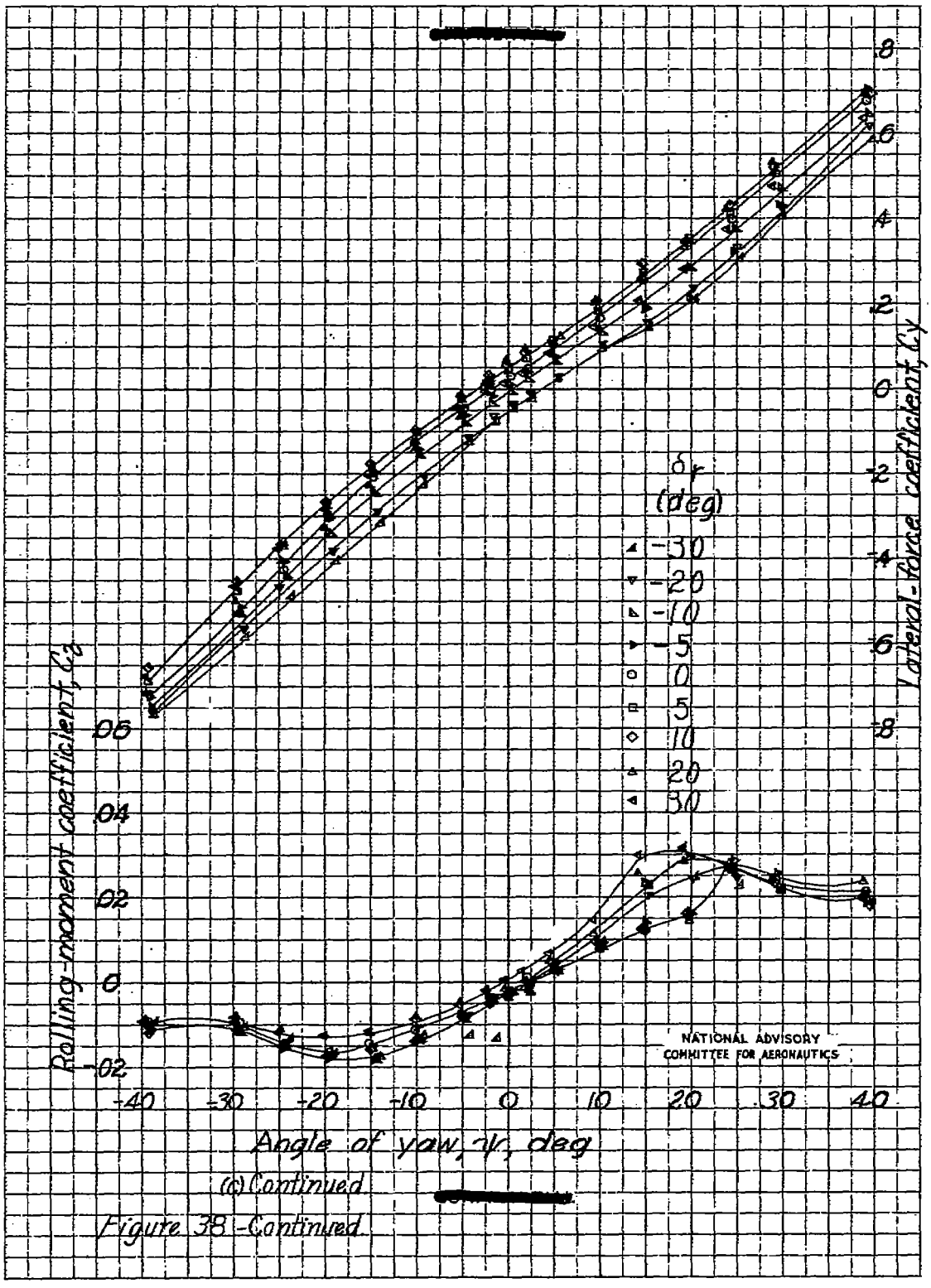

(c) Continued

Figure 38 -Continued

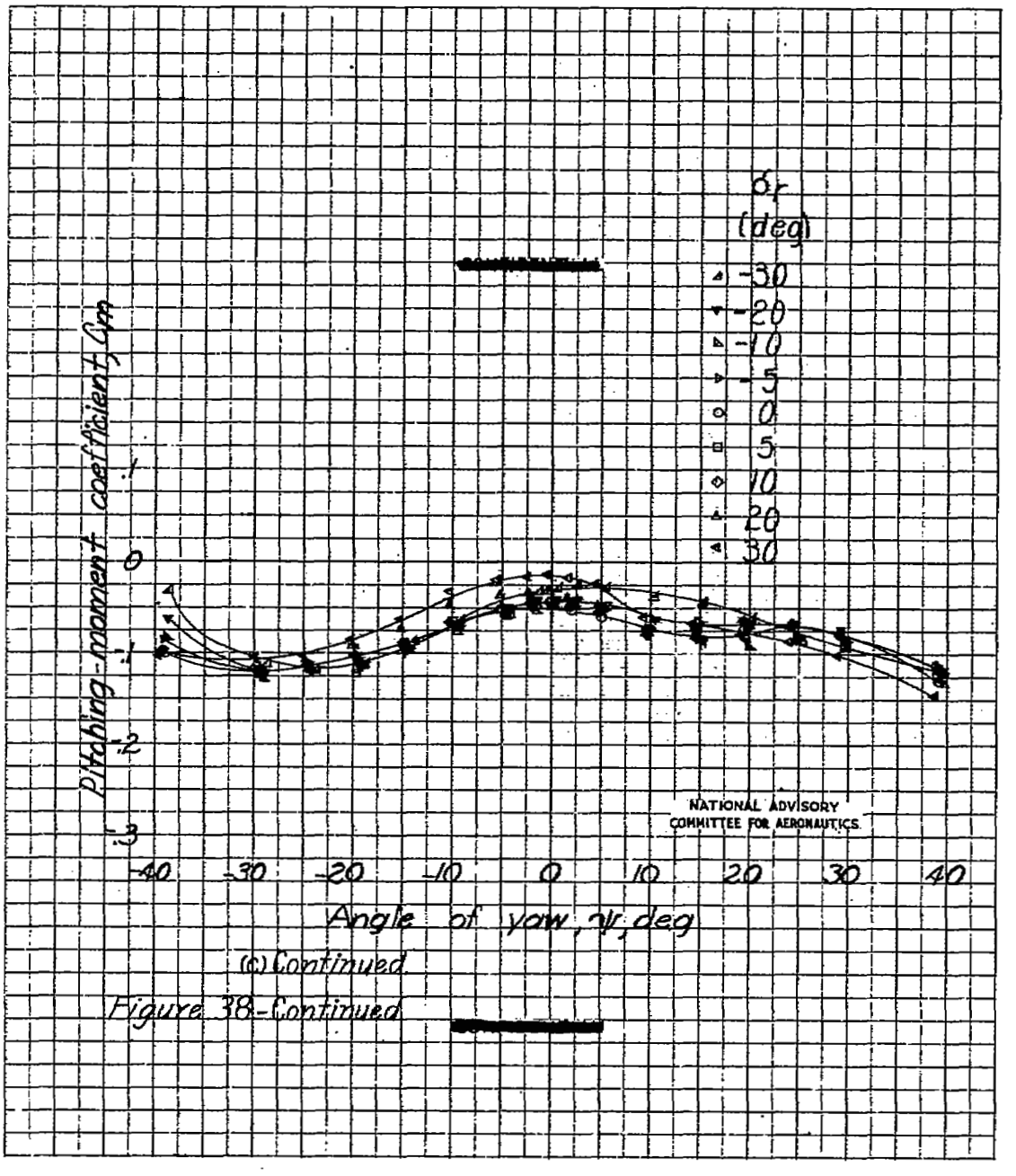

(c) Continued

Figure 38.-Continued

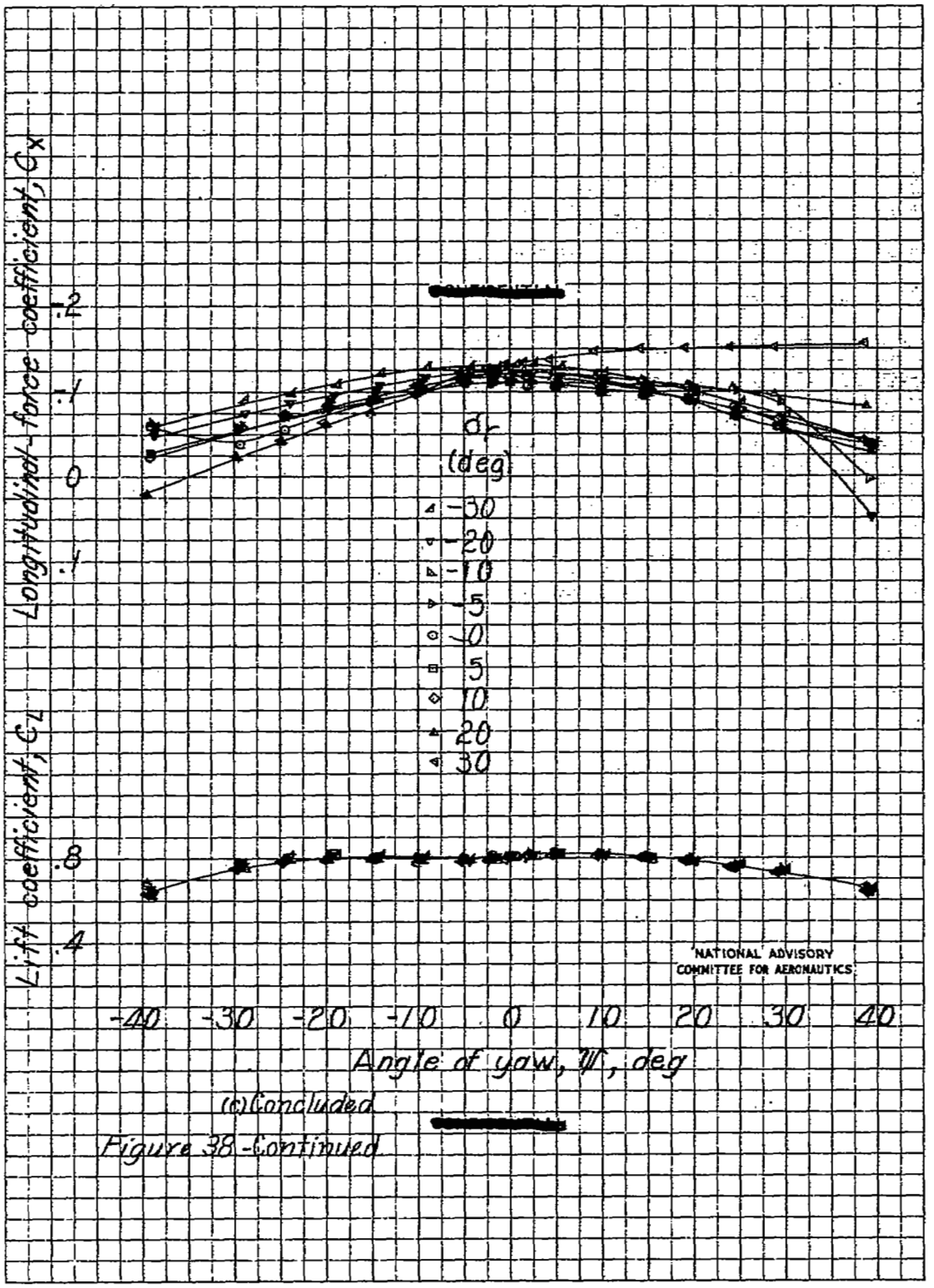

(c) Concluded

Figure 38 - Continued

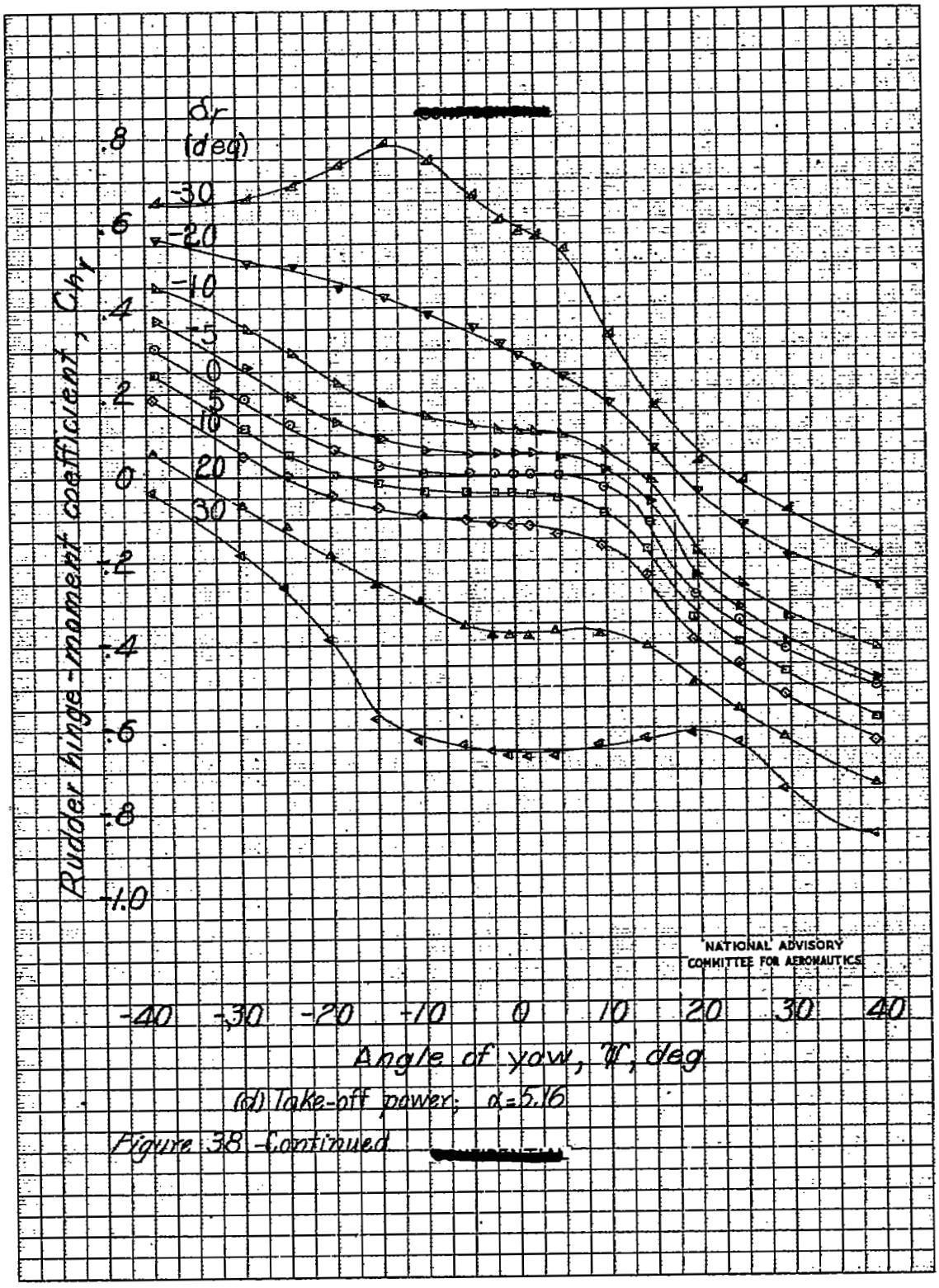

(d) Take-off power; $\alpha = 5.16$

Figure 38.-Continued

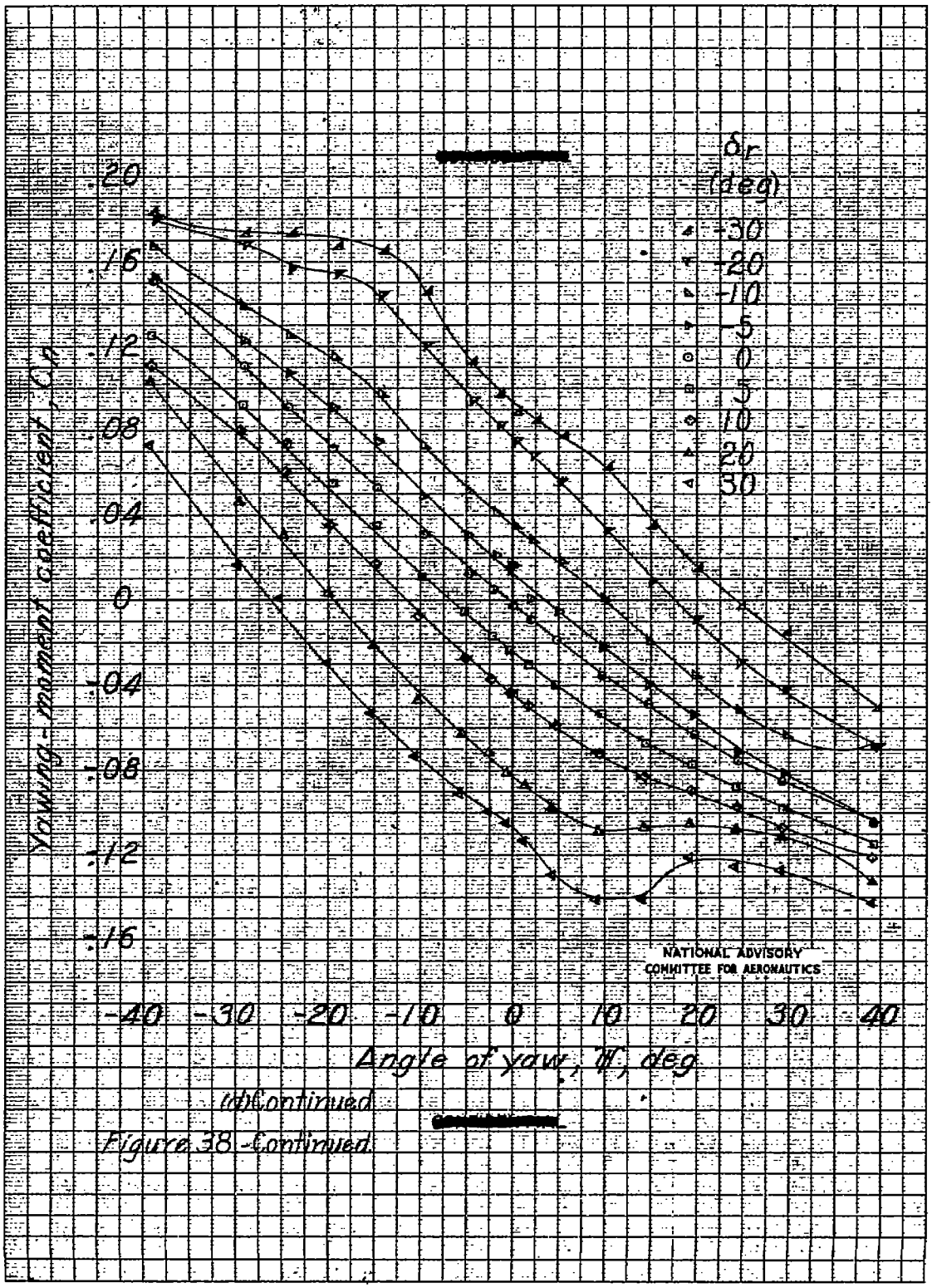

(d) Continued

Figure 38 - Continued

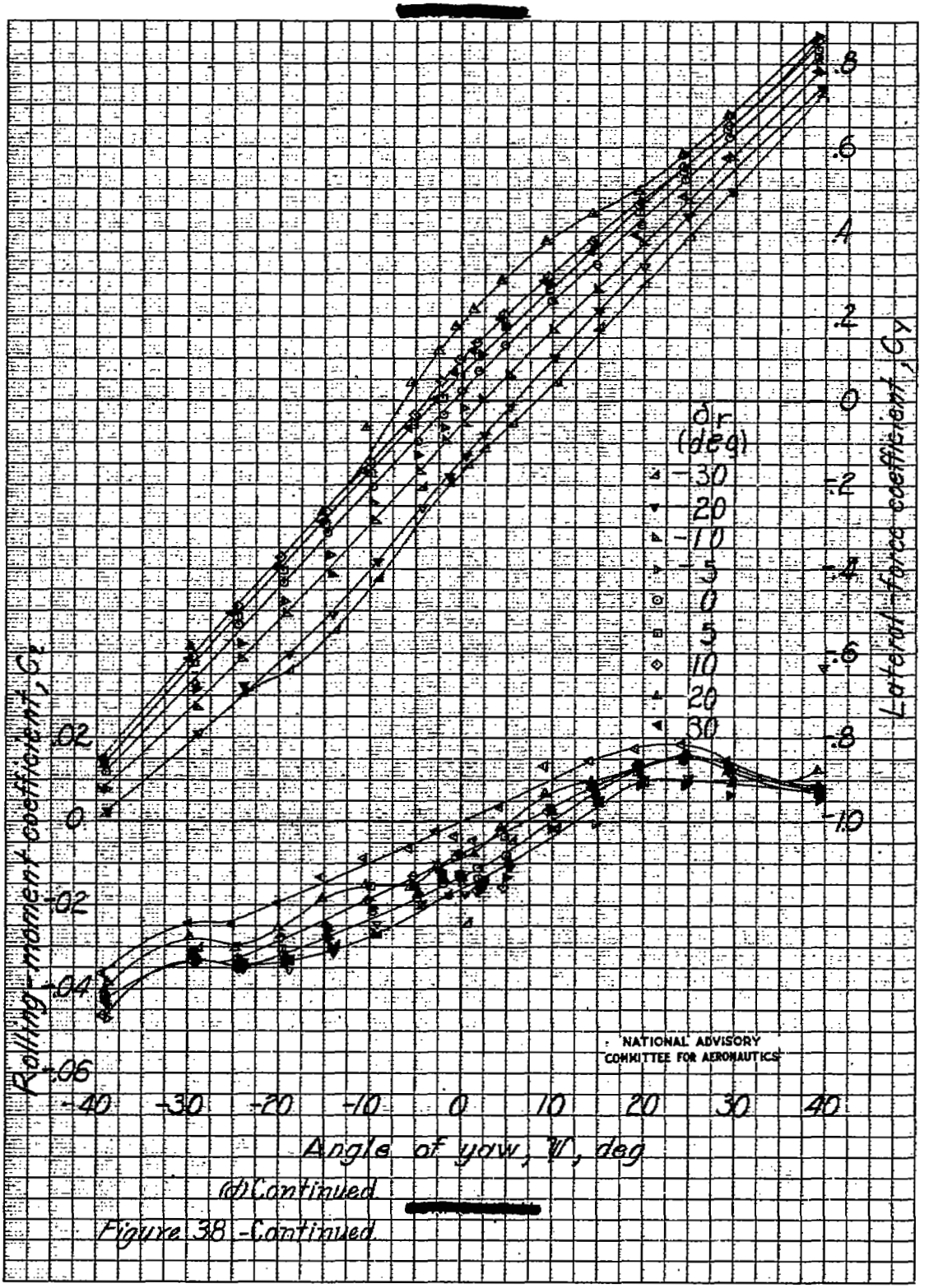

(d) Continued

Figure 38 - Continued

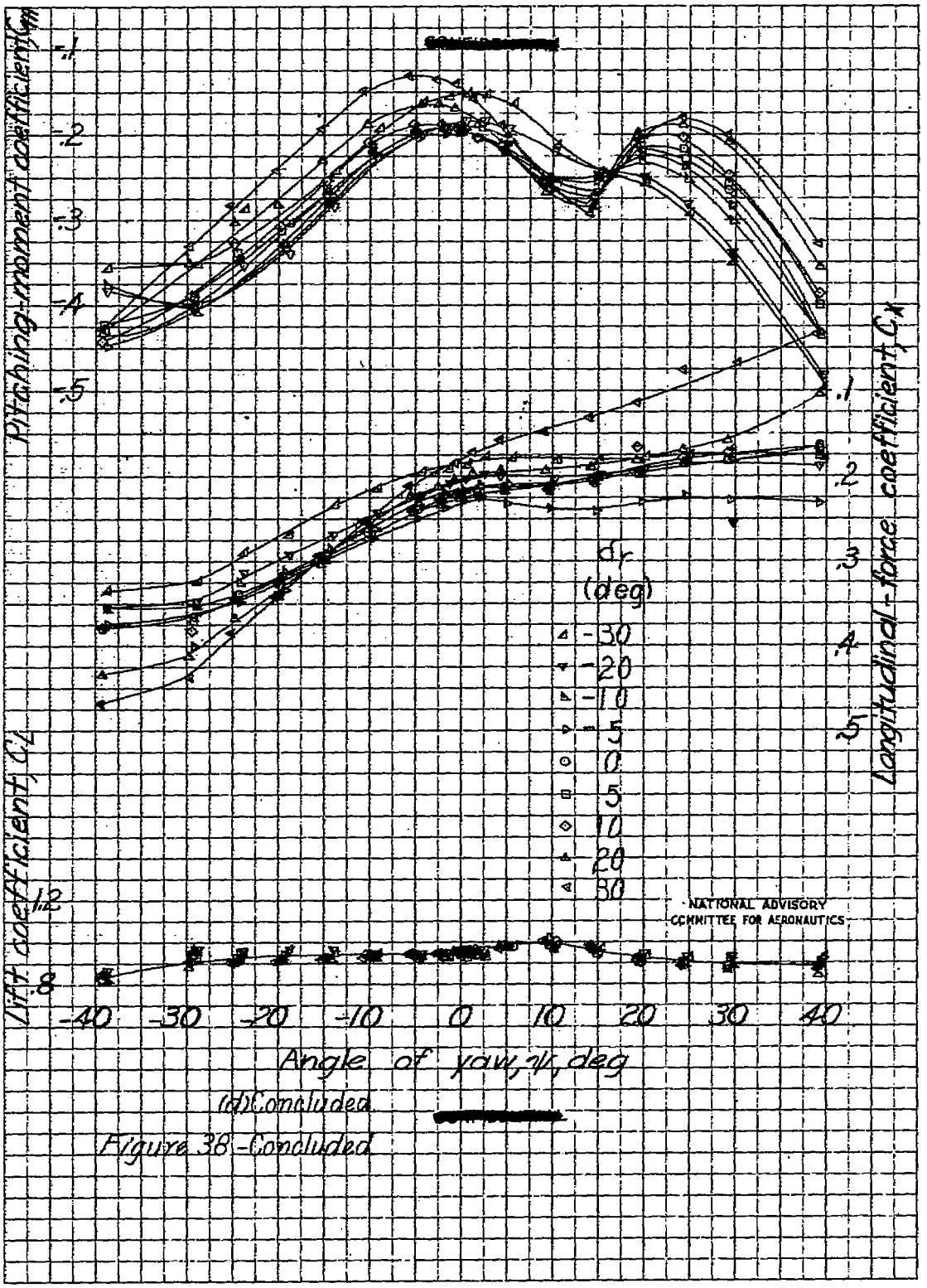

(d) Concluded

Figure 38 - Concluded

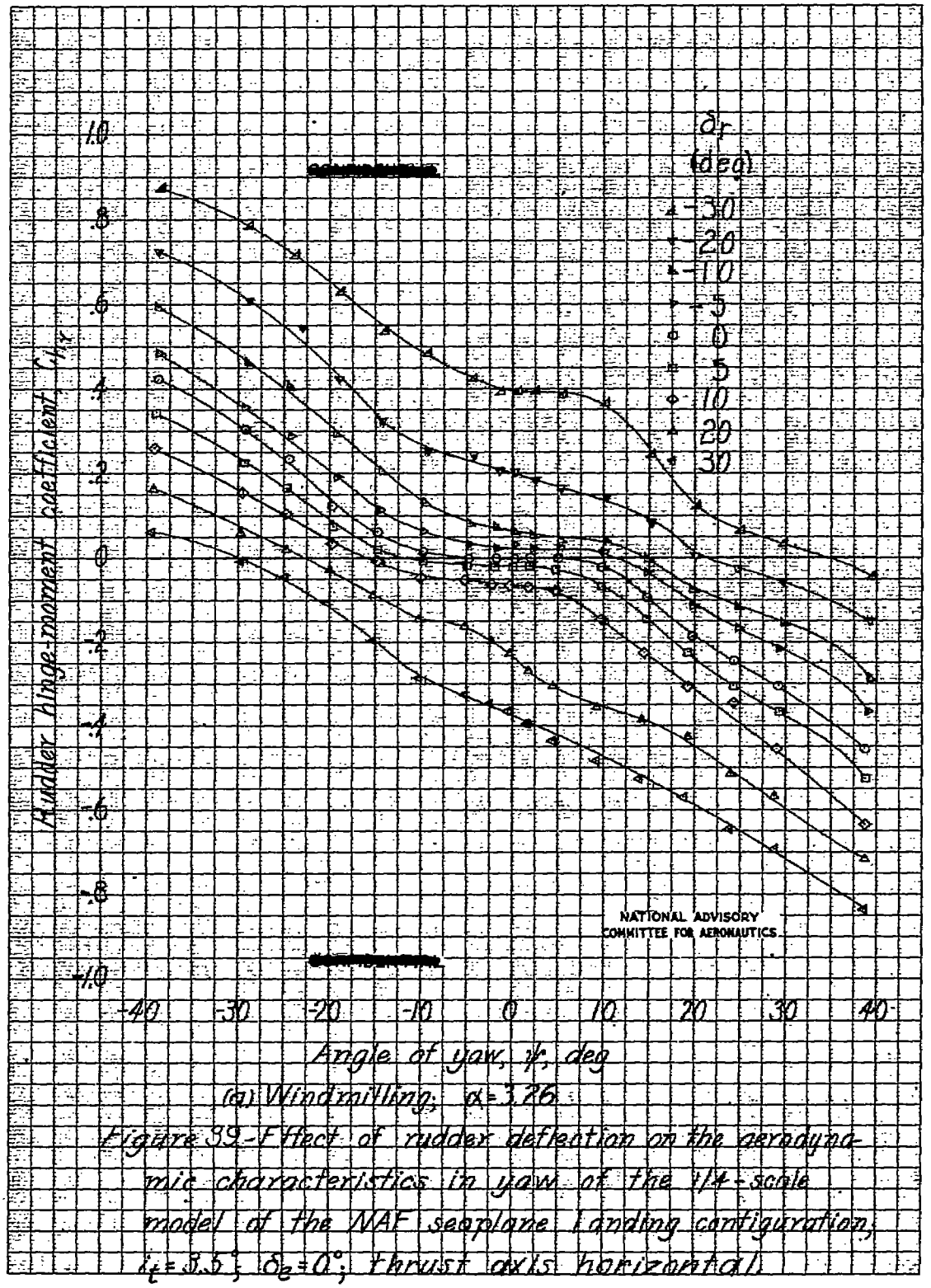

(a) Windmilling; $\alpha = 3.26°$

Figure 39.- Effect of rudder deflection on the aerodynamic characteristics in yaw of the 1/4-scale model of the NAF seaplane landing configuration, $i_t = 3.5°$; $\delta_e = 0°$; thrust axis horizontal

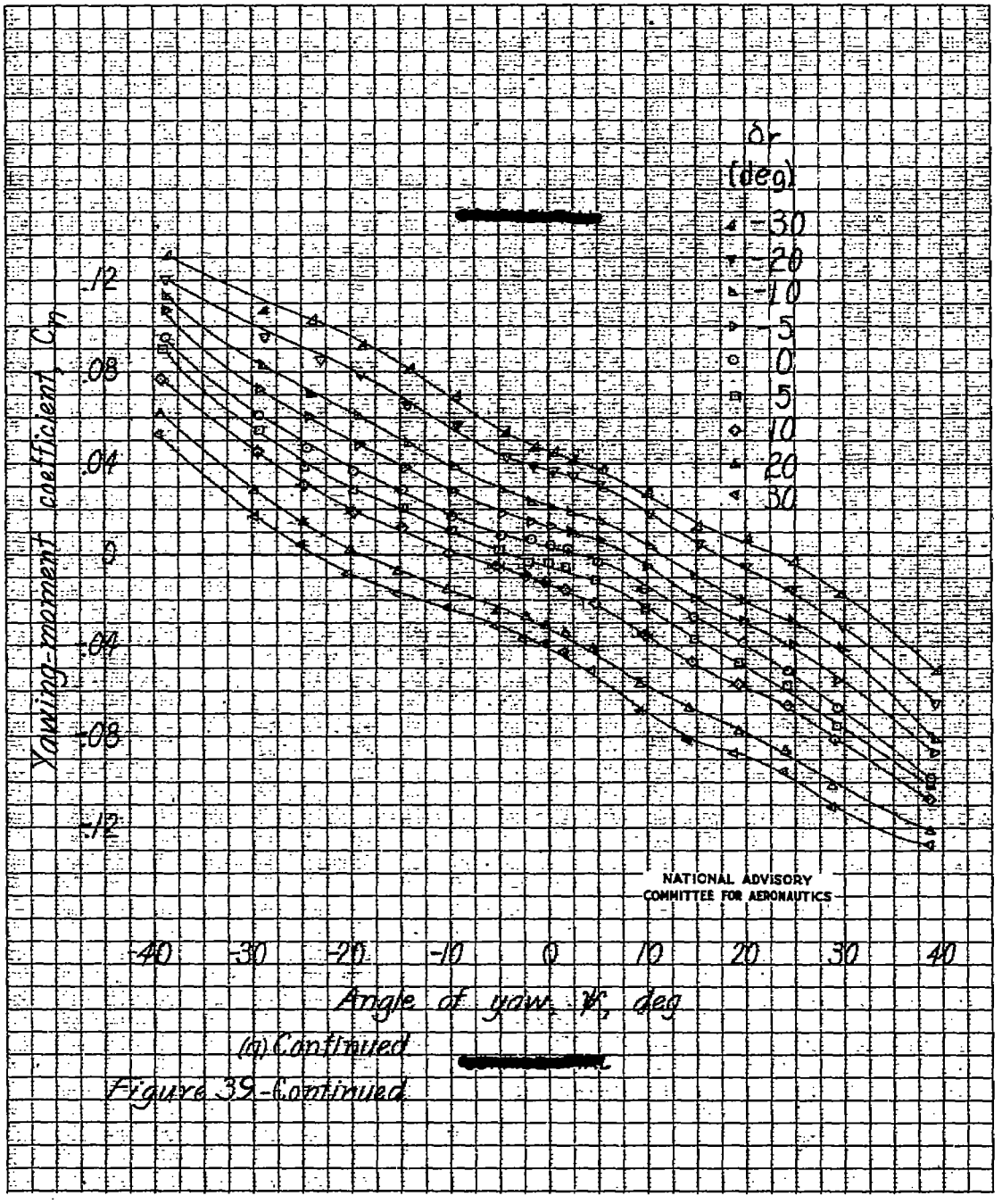

(a) Continued

Figure 39-Continued

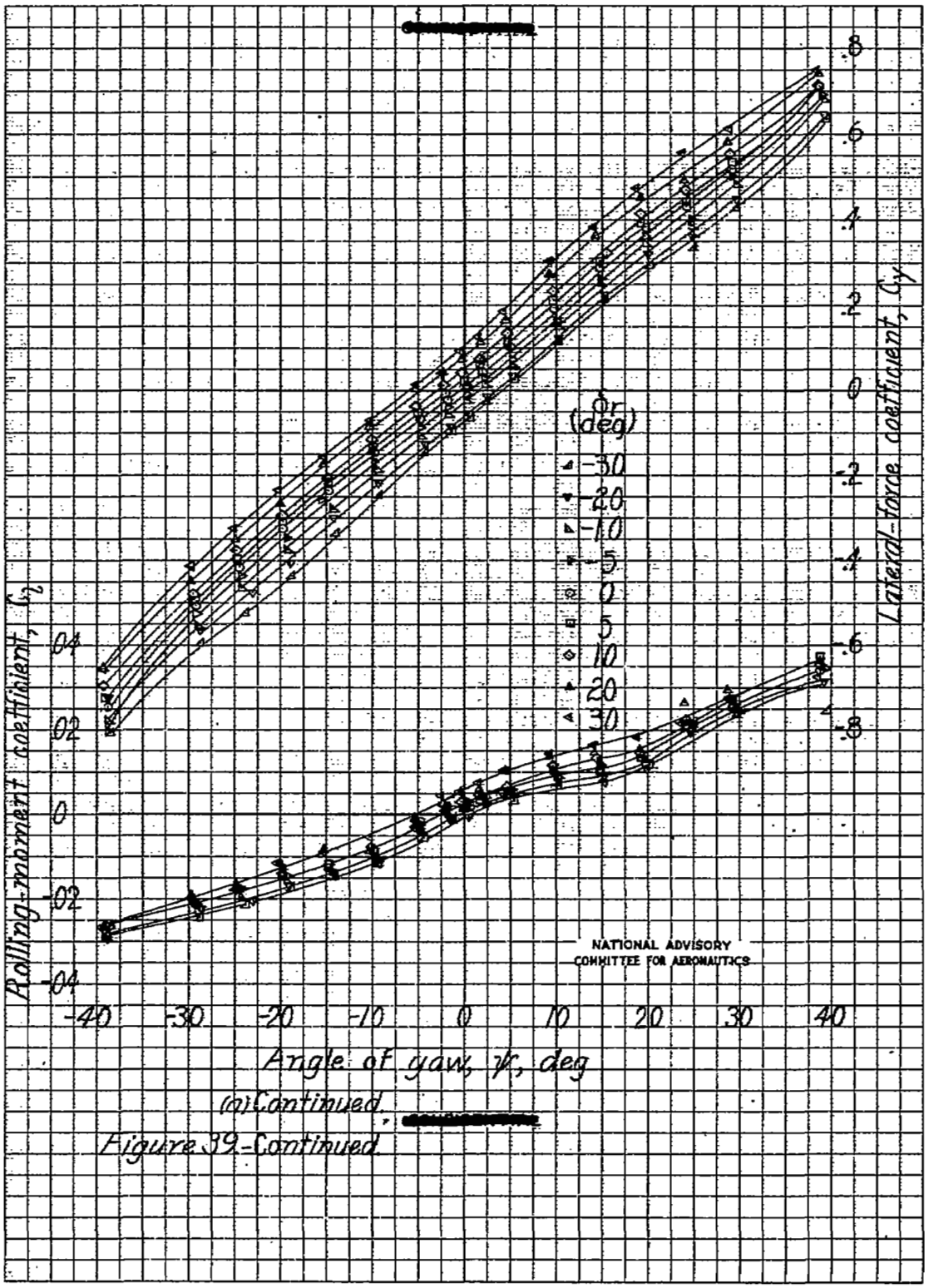

(a) Continued.

Figure 39.-Continued.

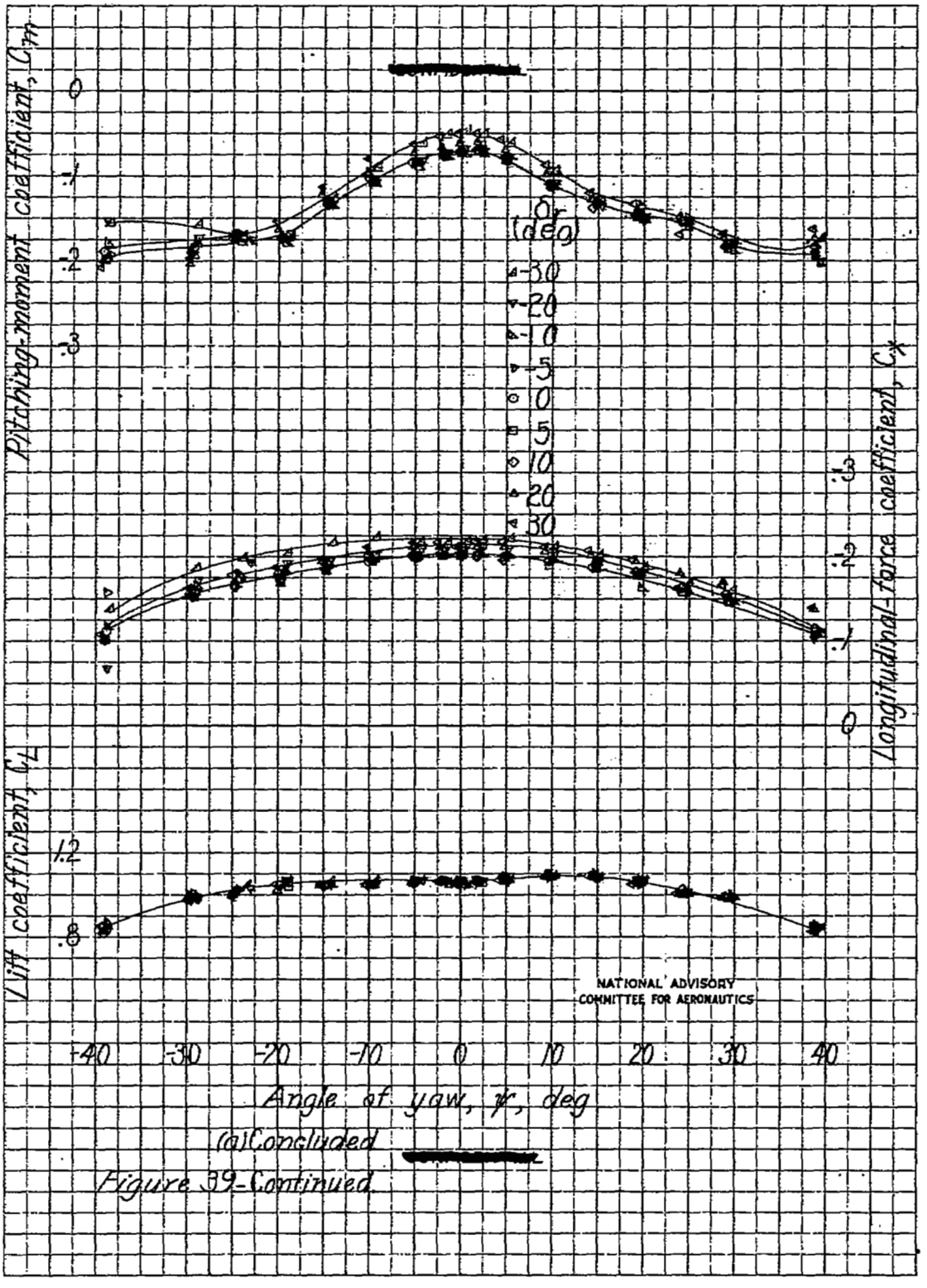

(a) Concluded

Figure 39.- Continued.

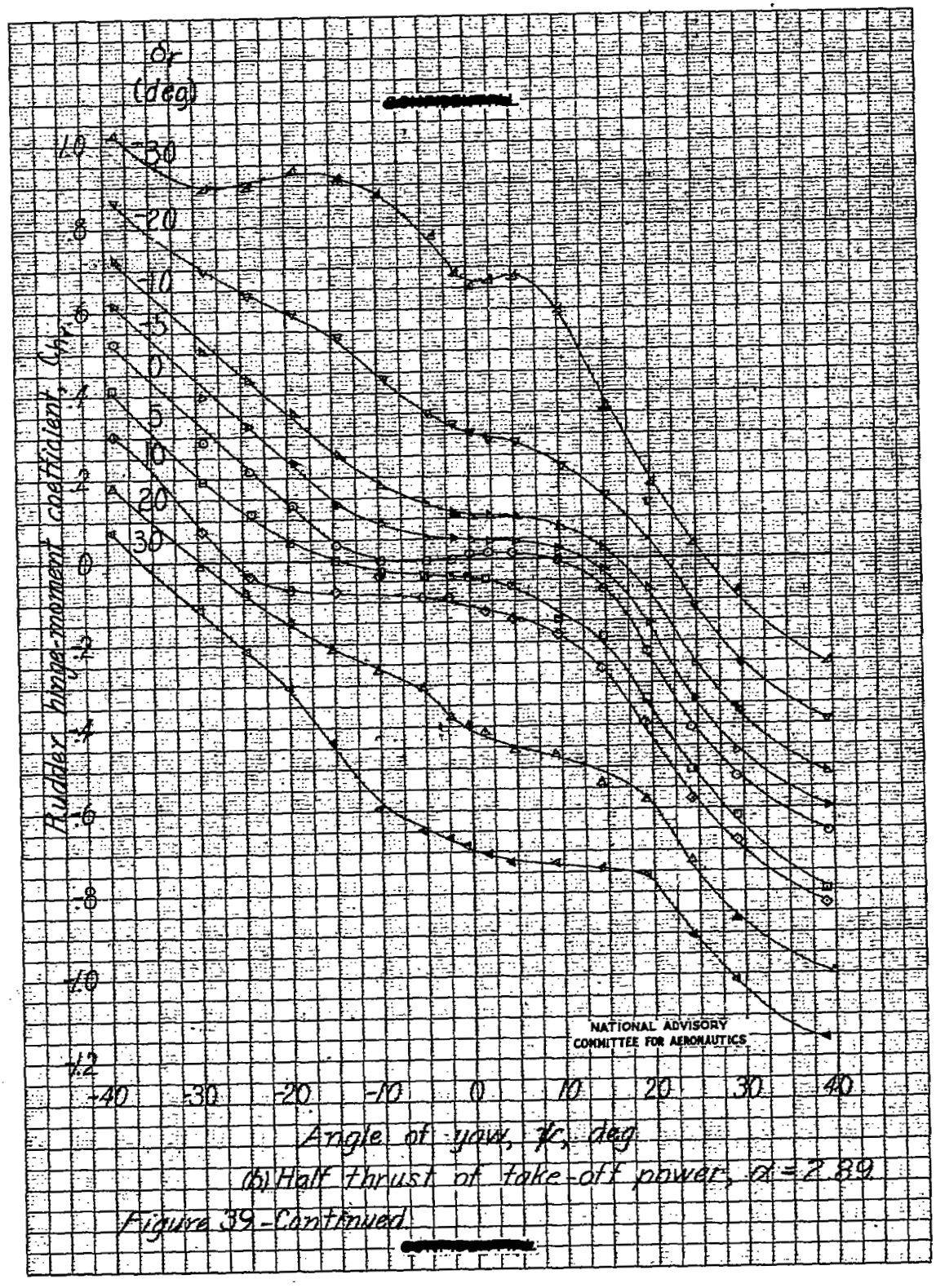

(b) Half thrust of take-off power, $\alpha = 2.8°$

Figure 39.-Continued.

Fig. 39b cont.

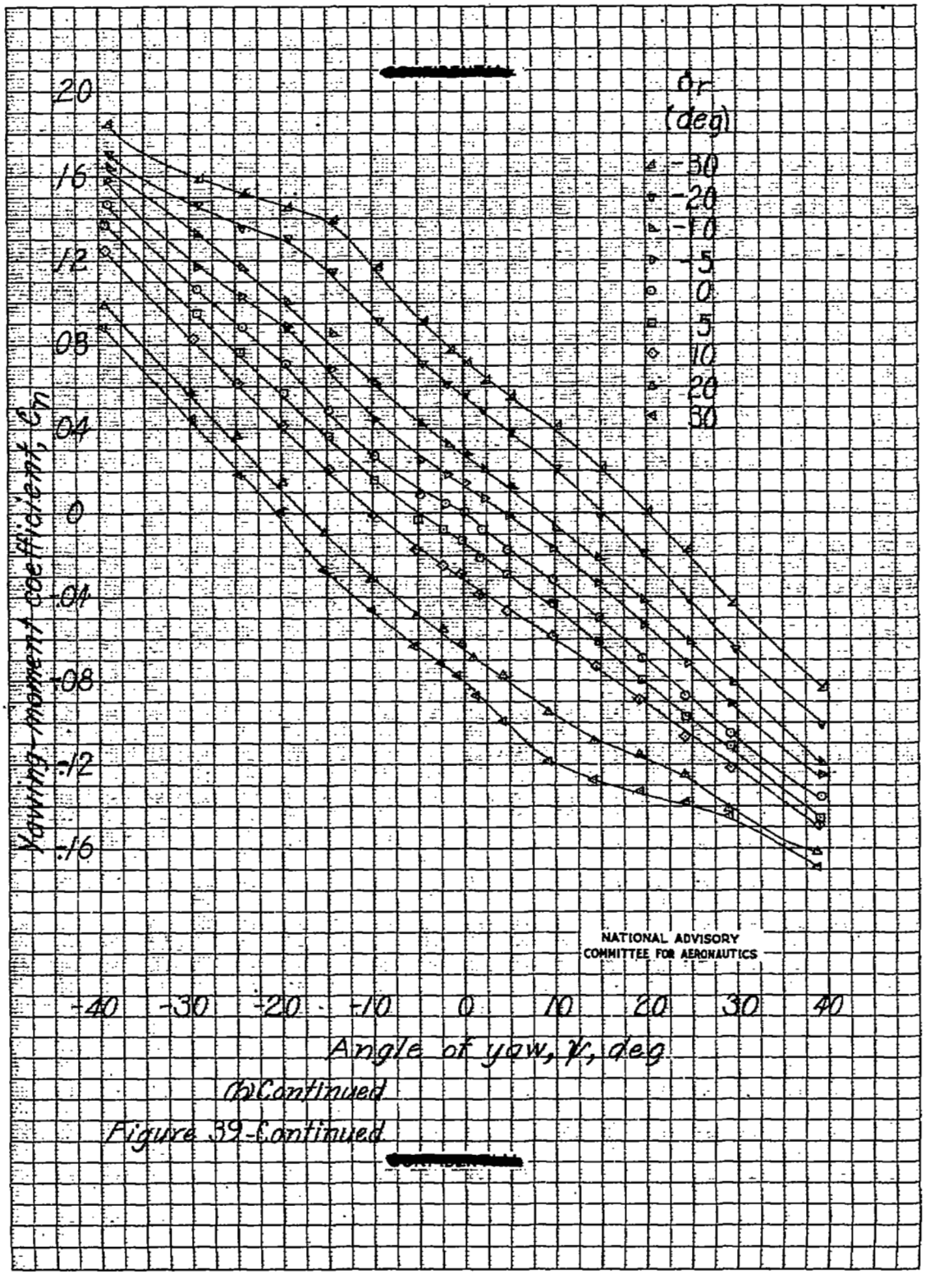

(b) Continued

Figure 39-Continued

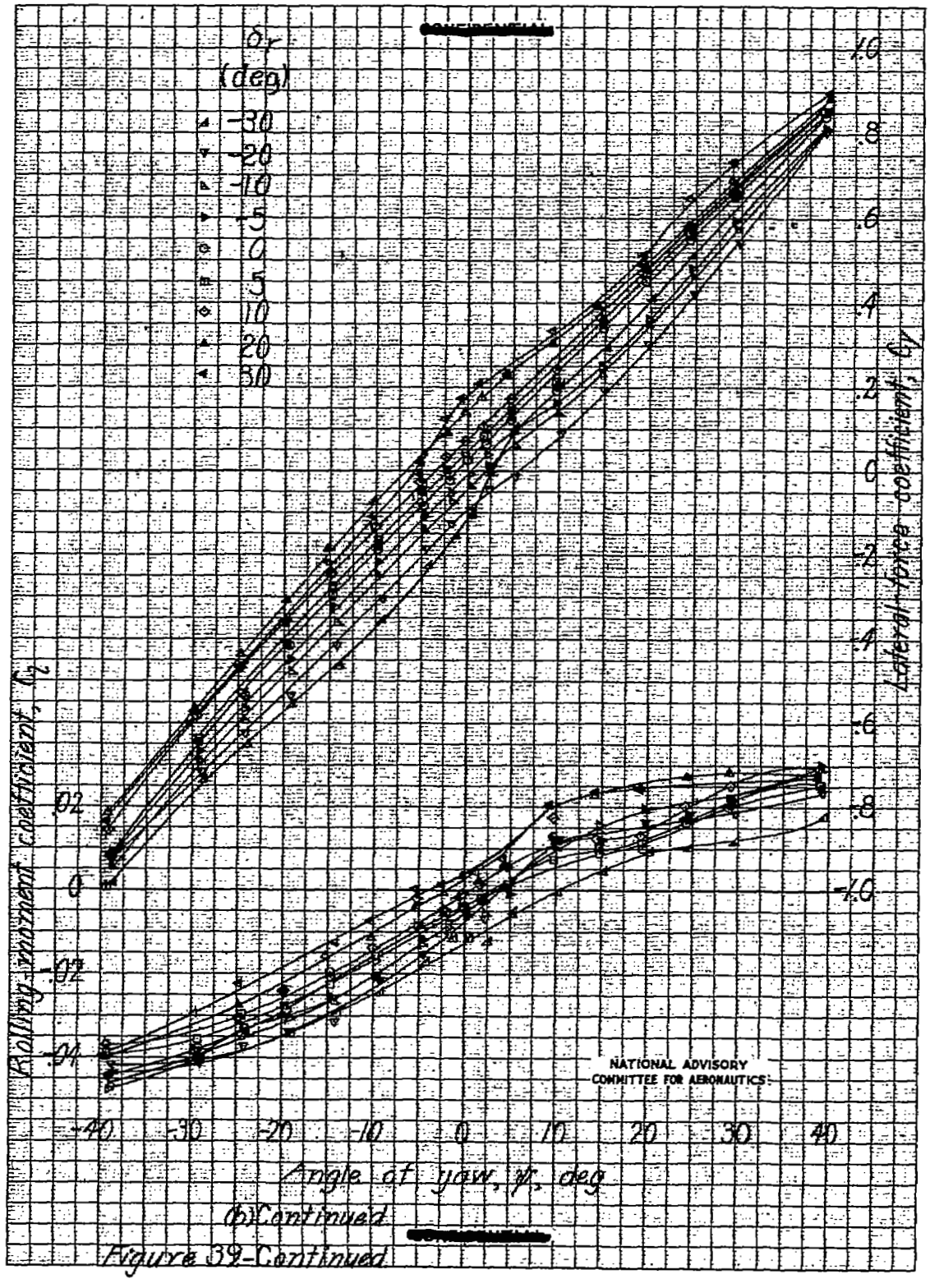

(b) Continued

Figure 39-Continued

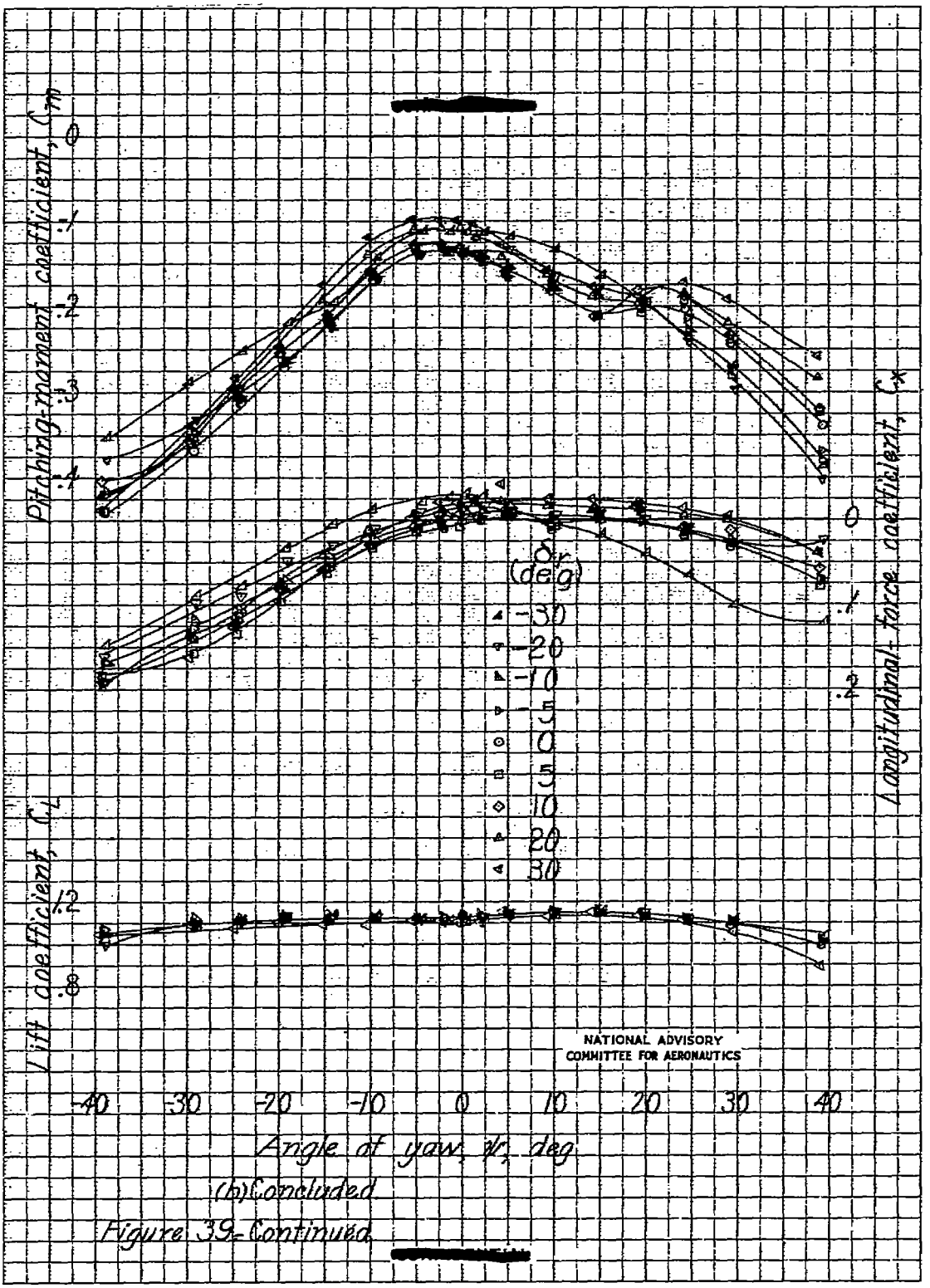

(b) Concluded

Figure 39.- Continued.

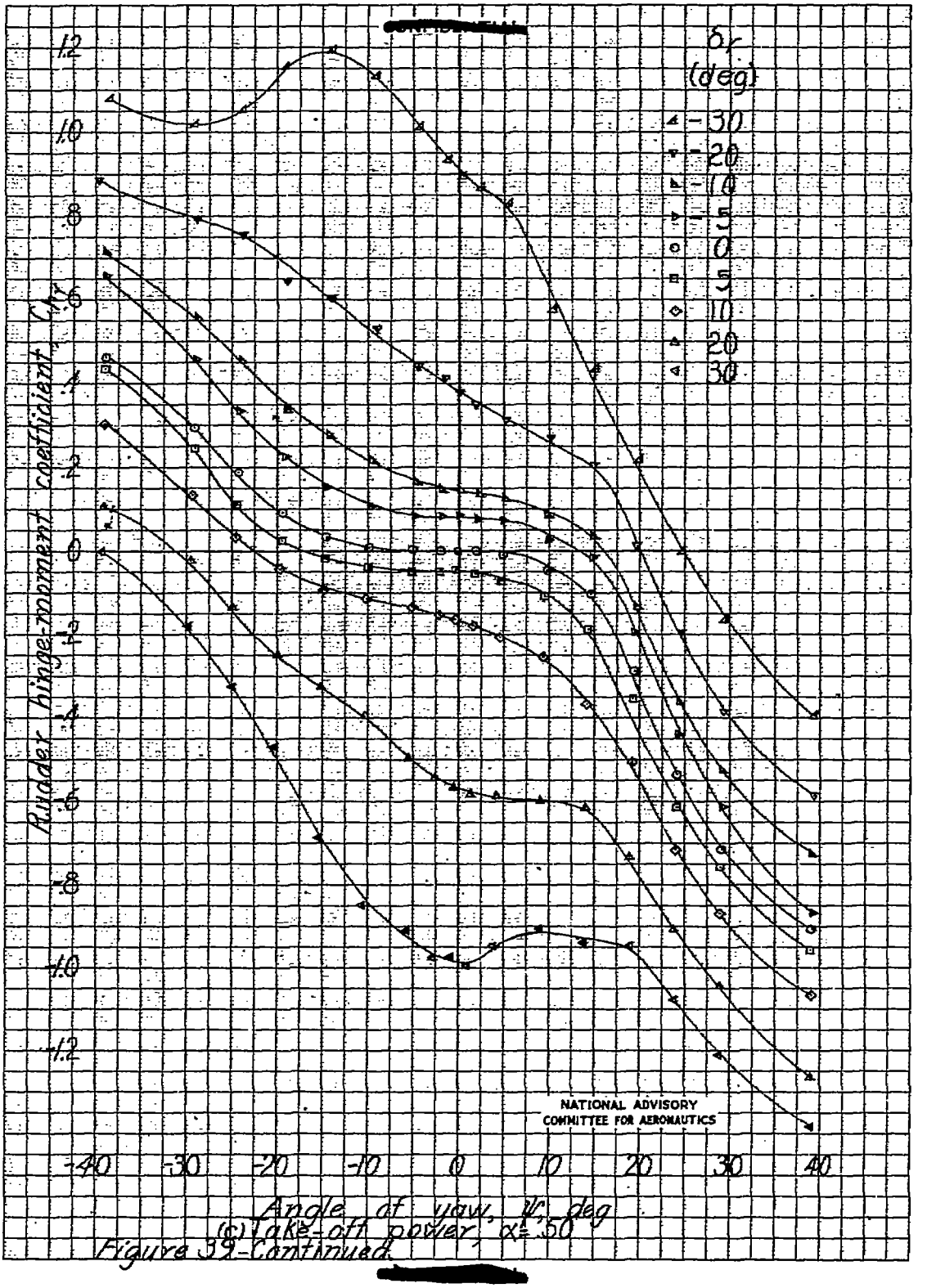

(c) Take-off power, $\alpha = 5°$

Figure 39-Continued

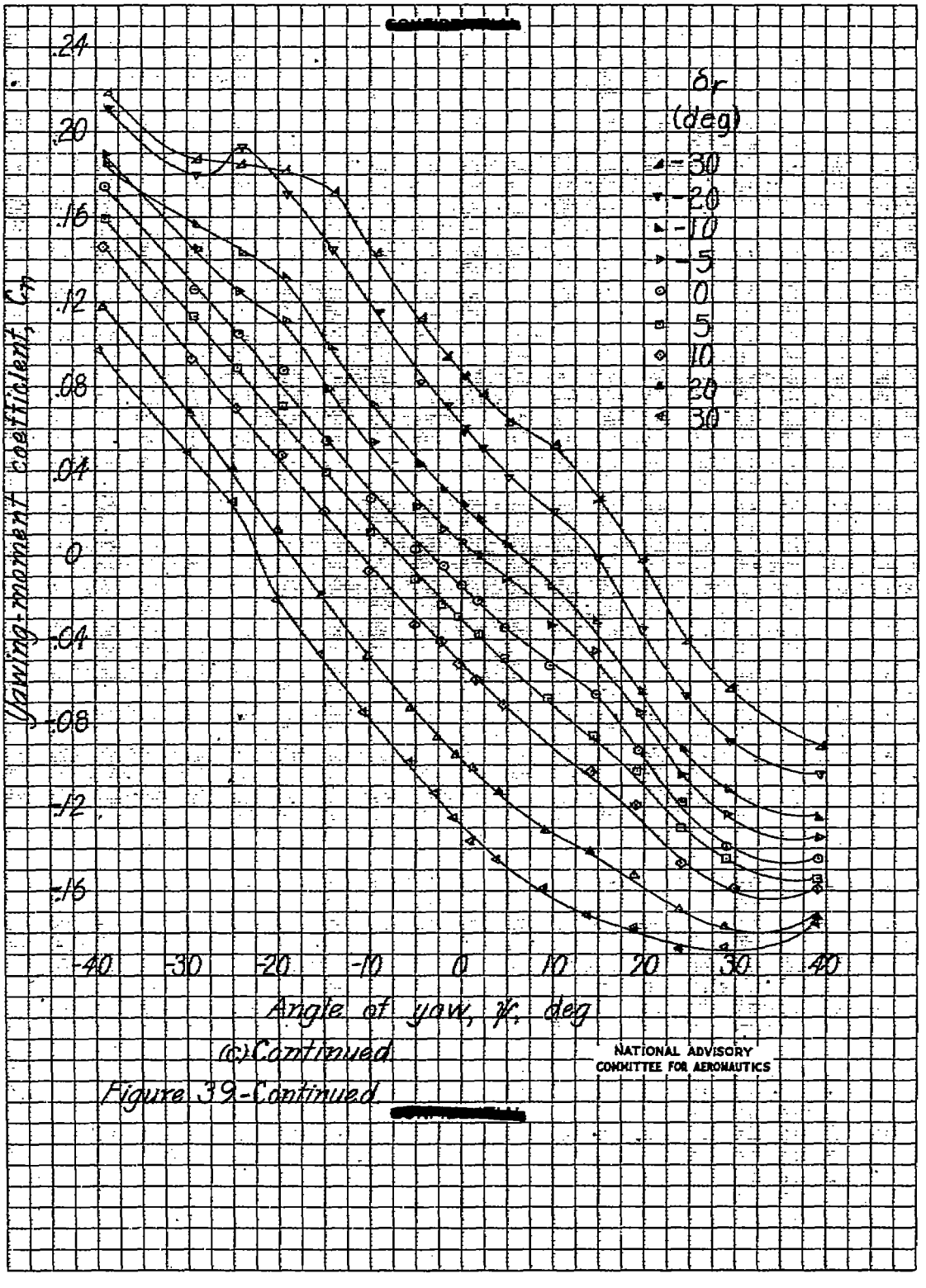

(c) Continued

Figure 39.-Continued

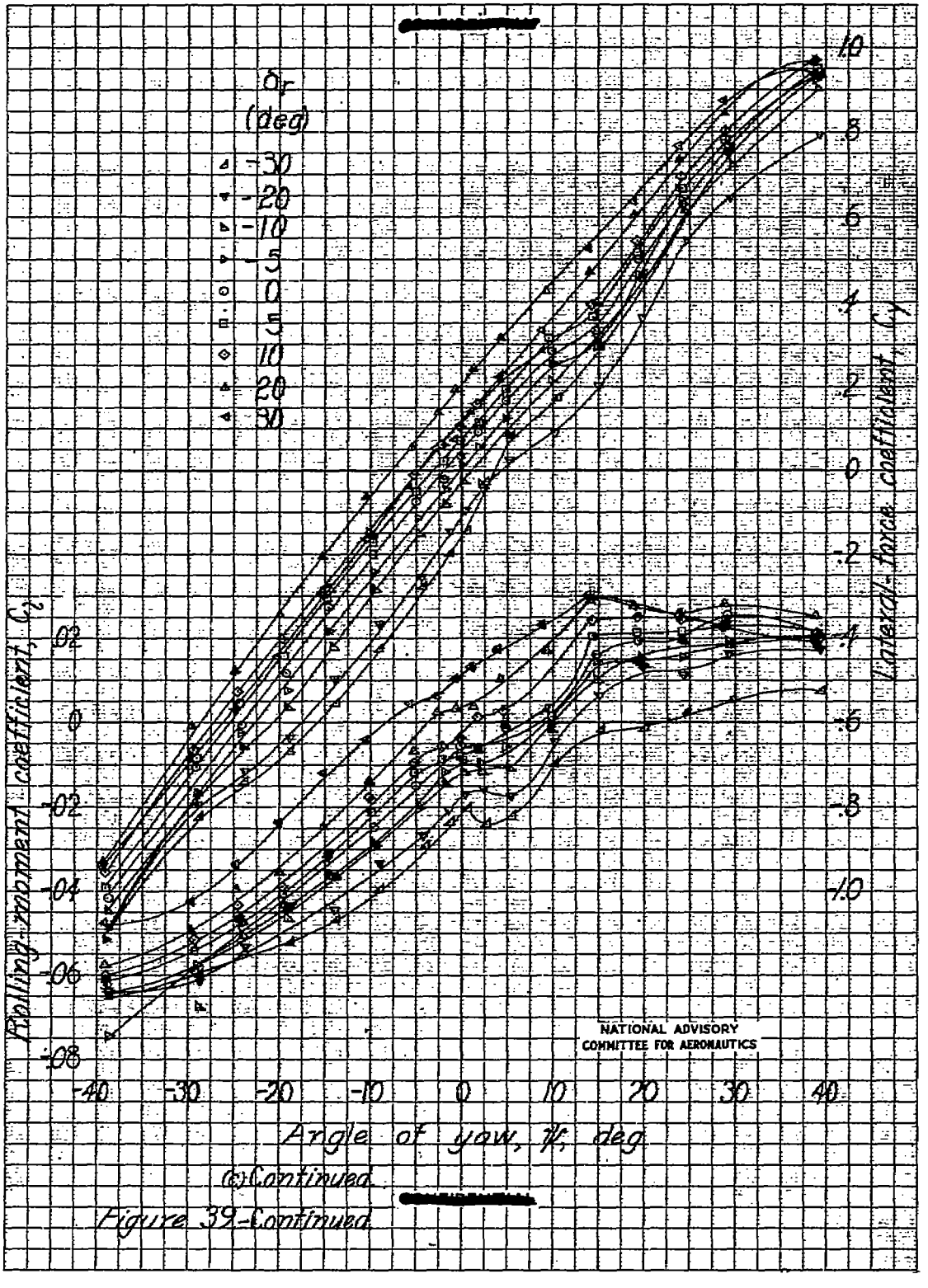

(c) Continued.

Figure 39-Continued.

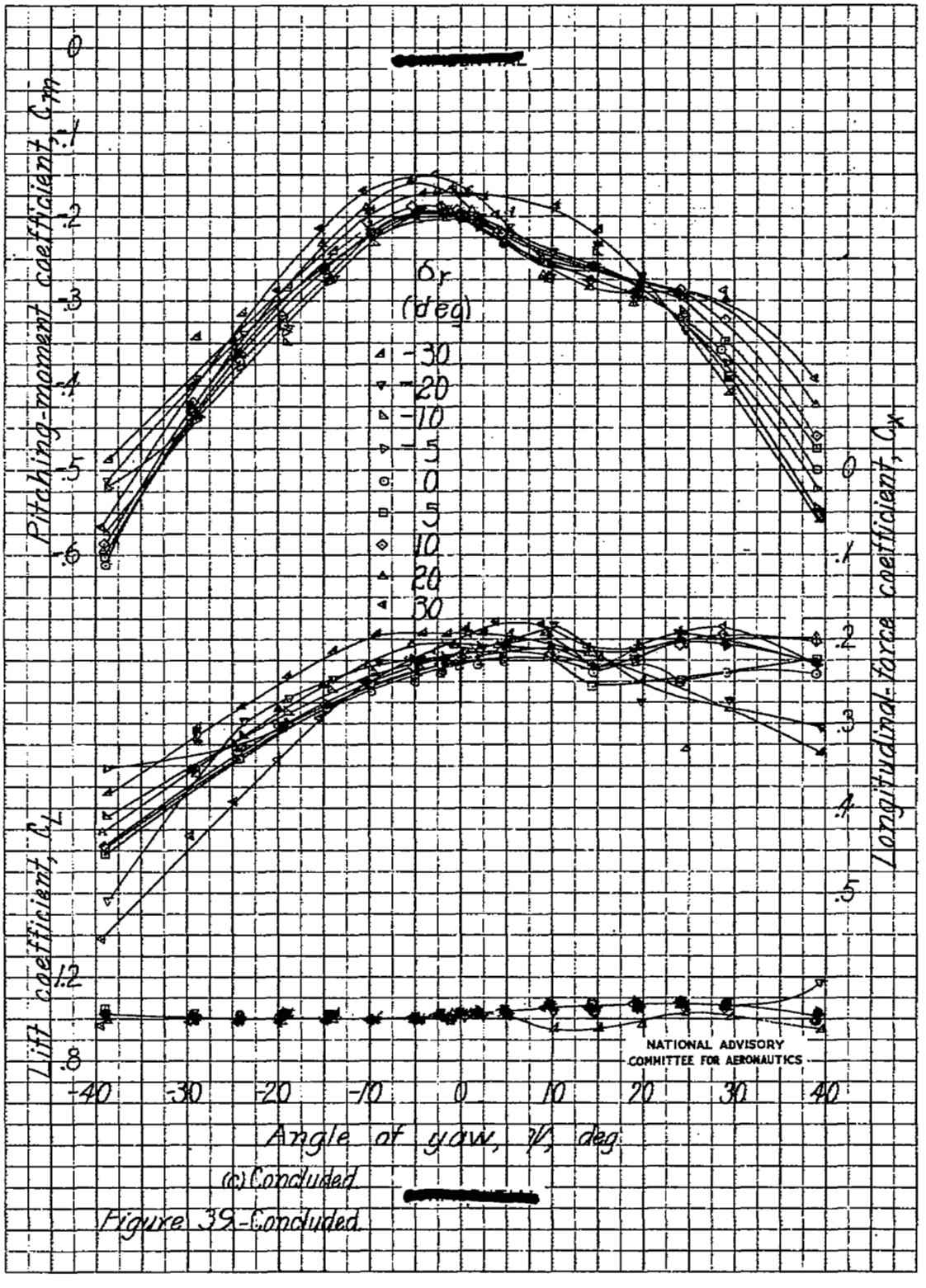

(c) Concluded

Figure 39.-Concluded.

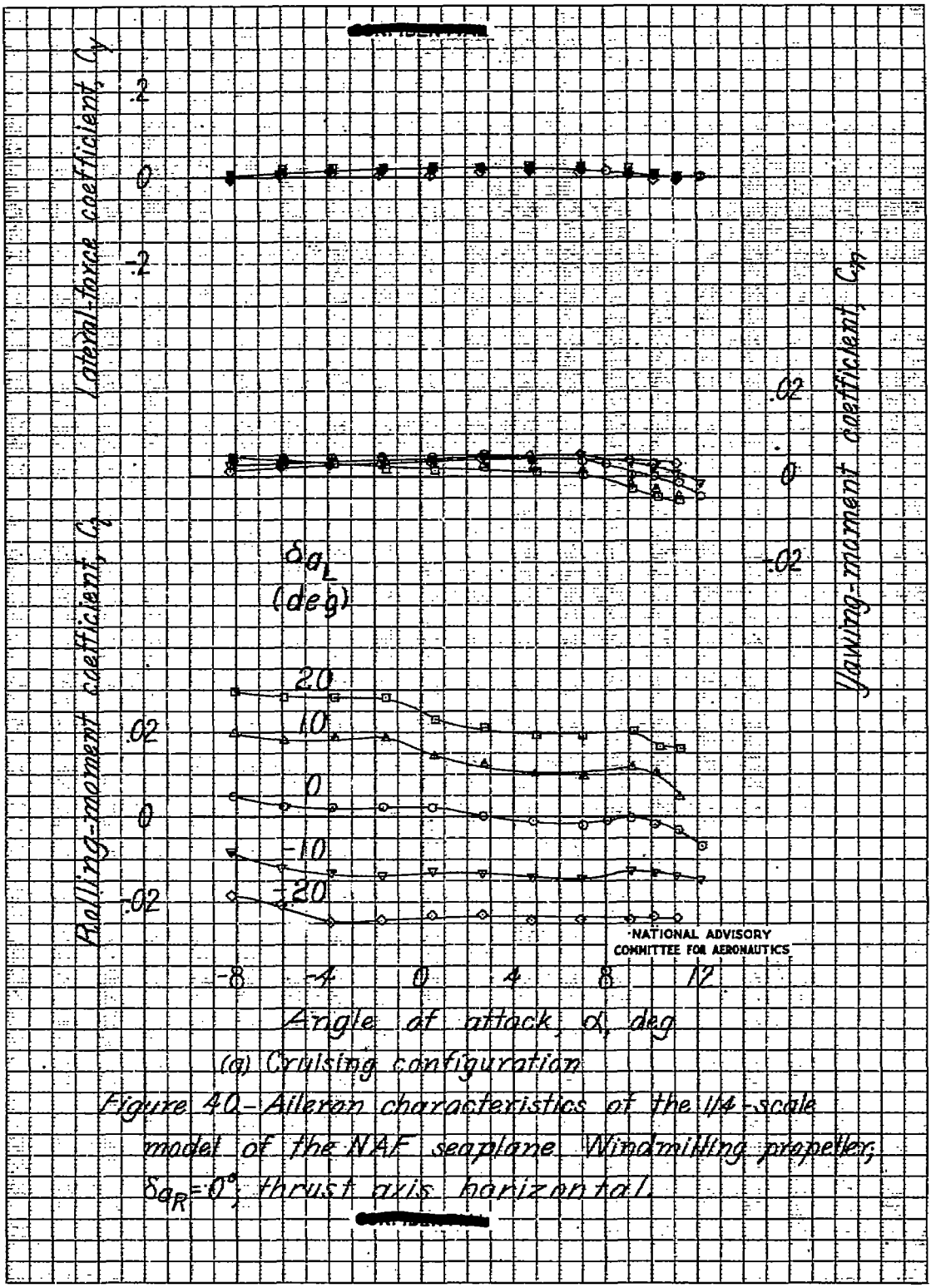

(a) Cruising configuration

Figure 40.- Aileron characteristics of the 1/4-scale model of the NAF seaplane. Windmilling propeller; $\delta a_R = 0°$; thrust axis horizontal.

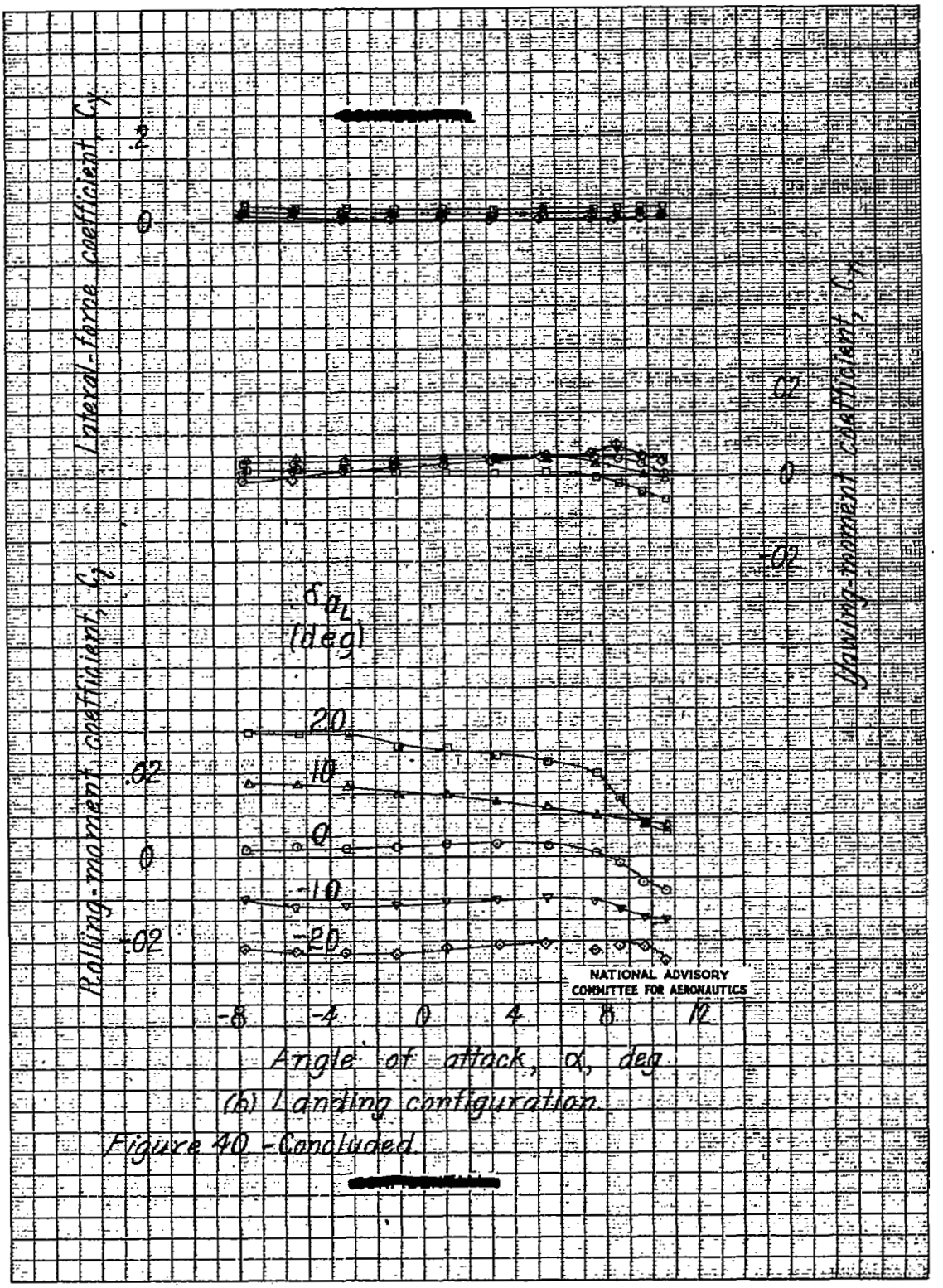

(b) Landing configuration.

Figure 40 - Concluded.